



**MARIA CURIE-SKŁODOWSKA UNIVERSITY
IN LUBLIN**

**Faculty of Chemistry
Institute of Chemical Sciences**

Lukasz Baran

**Computer simulations of the self-assembly
process of various molecules with diverse
architecture on solid surfaces**

Doctoral thesis
conducted in Department of Theoretical Chemistry
under supervision of dr hab. Wojciech Rzyśko
and dr hab. Tomasz Staszewski

Lublin 2022

I would like to thank cordially dr hab. Wojciech Rżysko and dr hab. Tomasz Staszewski for allowing me to perform investigations, scientific collaboration, and tremendous support throughout an entire dissertation. I am also extremely grateful to all other colleagues working in the Department of Theoretical Chemistry.

Contents

1	Introduction	1
1.1	On-surface self-assembly	1
1.2	Concept of the work	5
1.3	Research objectives	6
2	Methodology	7
2.1	Simulation method	7
2.2	Structural parameters	10
2.3	Model and simulation details	14
3	Shortened description of the results	16
3.1	Tetratopic building blocks	16
3.2	Other geometries	22
4	Summary and conclusions	26
5	Record for the doctoral thesis	28
5.1	Publications	28
5.2	Grants	29
6	The remaining record	30
6.1	Publications	30
6.2	Grants	31
6.3	Natonwide awards	31
6.4	Other awards	31
6.5	Internships	31
6.6	Conferences	31
6.7	Bibliometric parameters	32
7	Bibliography	33

Chapter 1

Introduction

1.1 On-surface self-assembly

Self-organization of particles of a different kind leads to systems exhibiting a rich variety and complexity of ordering, phase behavior, and novel, interesting properties that can be important for numerous applications in materials science,^{1,2} medicine,^{3,4} and other fields. Owing to this fact, within the last ten years, a great number of papers devoted to the synthesis of organic chemical compounds possessing the ability to self-assemble into different ordered phases have been published.

One particularly interesting group is formed by organic molecules that undergo on-surface reactions, which often lead to the formation of products different or even not possible to obtain in their bulk counterparts. Two main routes for the fabrication of these novel materials have been established and they are shown in Figure 1.1

The first one is called a top-down approach and one is supposed to exfoliate a layered crystal due to applied external forces to form a single layer of the smallest thickness possible. This has a particular advantage as it benefits from the general knowledge of the three-dimensional (3D) materials such as covalent- or metal-organic frameworks. The second protocol is a bottom-up approach where basic units such as atoms or molecules assemble into larger structures by the means of various physical or chemical forces. This scheme can be applied on the surfaces such as highly oriented pyrolytic graphite (HOPG), coinage metals (Au, Ag, Cu), or in the air/water or liquid/liquid interfaces. Single nanolayers obtained in such a way have been used, *inter alia*, as membranes for the separation of liquid and gas phases,⁵ in batteries,⁶ and in molecular sieves.⁷ The on-surface synthesis performed either in ultrahigh vacuum or liquid conditions generally has proven to be the successful and most conventional routine for the preparation of well-ordered networks.

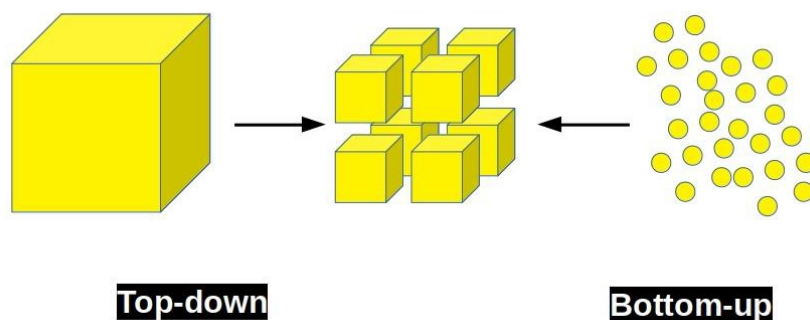


Figure 1.1: Schematic visualization of top-down and bottom-up approaches.

Comprehensive reviews summarizing the findings up to date can be found elsewhere.⁸⁻¹⁰

The chemical compounds of interest will be rigid, polycyclic aromatic hydrocarbons which we will refer to as "building bricks" or tectons. It has been stated that one of the factors influencing the type of ordering being formed is the precursor's architecture.^{11,12} These templates are able to assemble into structures ranging from small clusters¹³ up to extended porous networks,¹⁴ Archimedean tessellations,¹⁵ glasses,¹⁶ *etc.* by the means of directional interactions. Among these, one can distinguish hydrogen¹⁷ and halogen bonds,¹⁸ the metal-organic ligand coordination,¹⁹ as well as van der Waals forces.²⁰

One of the simplest, yet very popular examples of an organic chemical compound that self-assembles on solid surfaces is the benzene-1,3,5-tricarboxylic acid, also known as trimesic acid which forms strong hydrogen bonds.²¹ Another, very similar example is 1,3,5-tris(3-bromophenyl)benzene which due to the interactions with d- and f-block metal atoms forms different ordered structures, depending on the coordination number of metal atoms.²²

Aside from the type of interparticle interactions, the surface nature and symmetry are also important factors in the self-assembly phenomena. For instance, the results of Gutzler *et al.* obtained for tetrabromotetrathienoanthracene, have shown that different supramolecular networks can be formed, depending on the substrate type and the Miller indices of the exposed surface.²³ Moreover, it has recently been reported that the chemical or structural defects in the substrates can deteriorate the formation of supramolecular networks.²⁴ However, the conclusions from these investigations cannot be extracted equivocally. In general, the surface, or more precisely, their periodic properties, can influence the self-assembly if the number of adsorbed molecules is small. Furthermore, for specific cases, it may be a decisive factor that enforces the formation of a given network. This effect, however, decreases with the increase of adsorbed molecules and/or with their size and in such cases can be neglected in the description of the self-assembly process. Apart from the aforementioned factors, the formation of ordered networks can be dependent on the thermodynamic conditions (temperature, density, *etc.*),²⁵ solvent type and its concentration,¹⁷ and the addition of guest molecules.²⁶

The plethora of different molecular architectures has also been a subject of many studies. For instance, tetratopic building blocks have been studied in reference²¹ whereas linear precursors in reference.²⁷⁻²⁹ In this respect, the paper by J. D. Wuest *et al.* is particularly worth highlighting²¹ since they have shown the influence of the number of aromatic rings on the structure of the adsorbed layer. They have studied a series of chemical compounds "originated" from the trimesic acid (**M1**, Fig. 1.2 a) on the HOPG surface. This chemical compound assembles into a planar hexagonal network represented by motif **I**. As the authors state, trimesic acid is a prototypic building block for the study of self-assembly. These molecules are substituted by three carboxylic acid groups and this geometry corresponds to the tripod model studied in paper **PVII**. However, grafting isophthalic acid groups to linear connectors produces tetracarboxylic acids, abbreviated as **M2-M4** as shown in Figure 1.2 a, which are in accordance with our tetratopic model and differ by the length of the segments in "backbone". These molecules form different patterns which can be found in Figure 1.2 b. Adsorption of **M2** and **M4** leads to the formation of open parallel network (motif **II**) and Kagomé pattern (motif **III**). These phases have the same density and create the same number of hydrogen bonds per particle. For **M2** compound, the stable phase is a structure formed with motif **II**, contrary to the **M4** where motif **III** prevails. In the case of **M3** molecules, the simultaneous formation of both phases is observed. It is also worth highlighting that the DFT calculations have shown that the difference between hydrogen bonding energies that molecules **M2** and **M4** form is insignificant. Therefore, the authors stated that the driving force for the

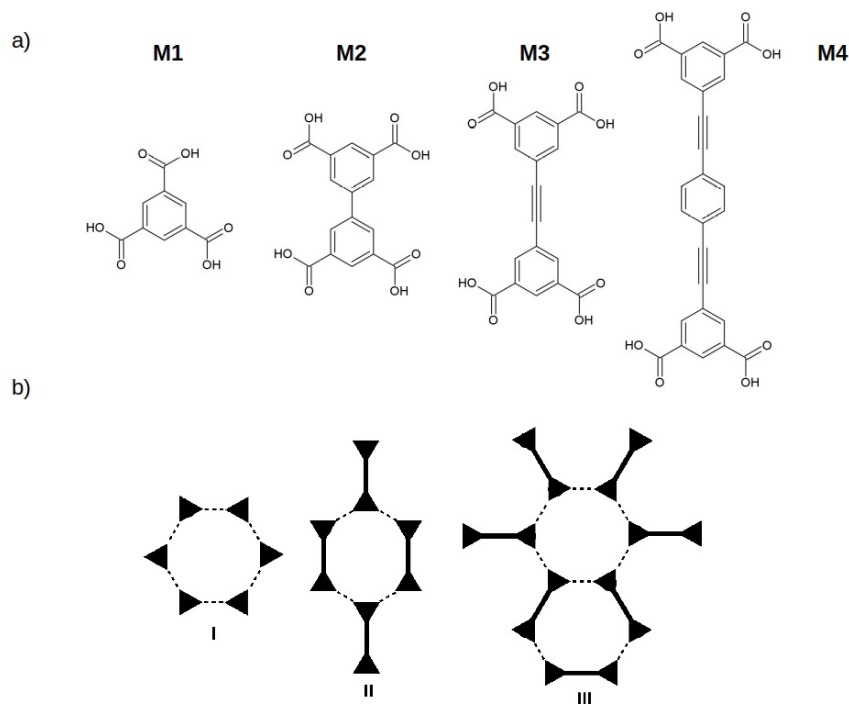


Figure 1.2: Part (a): structural formulas of molecules **M1-M4**. Part (b): fragments of various motifs created by molecules **M1-M4**. 1,3,5-trisubstituted phenyl groups are represented by triangles and hydrogen bonds shown as broken lines. Picture taken from the reference.²¹

formation of ordered structures by these molecules is the difference in the topology of building blocks.

Other noteworthy investigations have been performed for the p-terphenyl-3,5,3',5'-tetracarboxylic acid adsorbed on HOPG surface.^{16,30} This compound also could be described by the tetratopic model proposed in the dissertation. The authors reported the formation of random rhombus tiling which is built of six randomly distributed molecules that adopt one of three possible orientations. In the paper,³¹ it has been found that the chemical modification of the same compound leads to the formation of rhombus networks, corresponding to the dimers that were aligned parallel or at some angle one to another.

Di-substituted polyphenyl molecules have also shown their ability to self-assemble on solid substrates. In paper,²⁹ the study of adsorption of dicyanitriles with a different number of phenyl linkers on Ag(111) surface has been performed. Depending on the number of phenyl linkers ($n = 3, 4, 5$) the formation of diverse supramolecular networks have been observed, i.e. chevron, rhombus, and Kagomé phases have been found for $n = 3, 4$, and 5 , respectively.

Investigations of self-assembly of aforementioned organic chemical compounds have also been thoroughly studied by the means of computer simulations.^{17,32} In these papers, a comparison between molecular simulations and experimental studies have been performed. It is worth highlighting that although the employed models were quite simple, the final agreement between these two approaches was impressive. Studies described in the paper¹⁷ involved the self-assembly of rigid "tripod" molecules with C_3 symmetry adsorbed on HOPG. The authors considered two molecules that differed by the number of aromatic rings in the molecule's "backbone". These building bricks formed molecular networks due to the presence of weak N-H hydrogen bonds. In both cases, they have found two ordered

phases of different densities. By the means of lattice Monte Carlo simulations, they have examined their coexistence in the systems of different total densities.

In the paper,³² computer simulations preceded experimental studies. The authors studied tripod molecules with C_2 symmetry in which one "arm" was significantly larger (was composed of more aromatic rings) than the two remainings. Simulations have been performed for a one-component system and have shown the coexistence between two low-density and one dense ordered phase. According to the Gibbs phase rule $s = \alpha - \beta + 2$, where s , α , and β correspond to the number of degrees of freedom, number of components and phases in the system, respectively, only one low-density structure can be stable. However, if one would examine a binary mixture, both phases could potentially be stable. For this purpose, a series of experimental measurements have been performed where adsorption from solutions of tripod molecules and different solvents have been carried out. Indeed, the authors successfully reported that depending on the type of solution and mixture's concentration, the formation of the first or the second low-density phase has been observed. Moreover, the coexistence of two low-density phases has also been found.

Performing computer simulations requires the evaluation of models of particles of interest. In the dissertation, particular attention will be devoted to coarse-grained models which will be designed in such a way to be simple, yet able to correctly reflect experimental properties of real systems. This choice allows us to conduct simulations of much larger systems, comprising of at least 10^4 "atoms", which is a great advantage given studying the collective phenomena accompanying the self-assembly processes. The selection of proper models and simulation methods is crucial for the evaluation of not only final ordered structures but also allows one to determine their stability and conditions when they can appear. This, in result provides the mechanisms of their formation which are the most important aspect of the self-assembly processes.

It is worth highlighting that for many compounds the quantum calculations such as density functional theory (DFT) have also been successfully used for the investigations of similar processes.²¹ These methods are useful for the evaluation of interaction energies and both "ground-state" and intermediate conformations. These results can be used in our simulations to manipulate the interaction strengths. In principle, the results presented in paper²⁸ concern the behavior of benzonitrile and the authors evaluated the energies of dimers and trimers formed by these molecules in the gas phase and on Au(111) surface. However, one has to note that it usually is used to study from one up to several molecules at solid surfaces due to huge computational cost of such calculations.

Similar limitations concern the use of more "realistic" force fields which would mimic the behavior of a particular chemical compound of interest. However, it is worth stressing that the exact solutions do not exist. Even for a "simple" a molecule like water, plenty of force fields can be distinguished.³³ Depending on the parameterization, they can reflect several quantities correctly and give erroneous values for other which will be dependent on the employed model.³⁴ Therefore, one should not be surprised that the simulations of all-atom models of real chemical compounds, which are even more complex, are also limited. For instance, C. A. Palma *et al.* have conducted a comprehensive experimental and simulation study, where they used molecular dynamics simulations with the MMFF94 force field within the CHARMM package.³⁵ Their results were in a great agreement with these approaches, however due to the more complicated computational approach, they were only able to investigate 80 molecules. Similar investigations have been performed with the Amber99sb force field to study the behavior of perylene-3,4,9,10-tetracarboxylic dianhydride molecules.³⁶ Although the results can be directly converted into the experimental setups, the authors were also able to examine only 60 molecules on a graphene surface due to the computational cost of such simulations.

One can see that even though those approaches are able to compare explicitly all of the properties, such as the strength of the interparticle interactions, measured in experimental studies, they are hardly able to explore structural properties due to the limited amount of molecules in the simulations. Therefore, these methods are not suitable for the study of collective phenomena which are of particular interest here, although it is noteworthy that interaction energies evaluated in this way could be "transferred" into the coarse-grained models.

1.2 Concept of the work

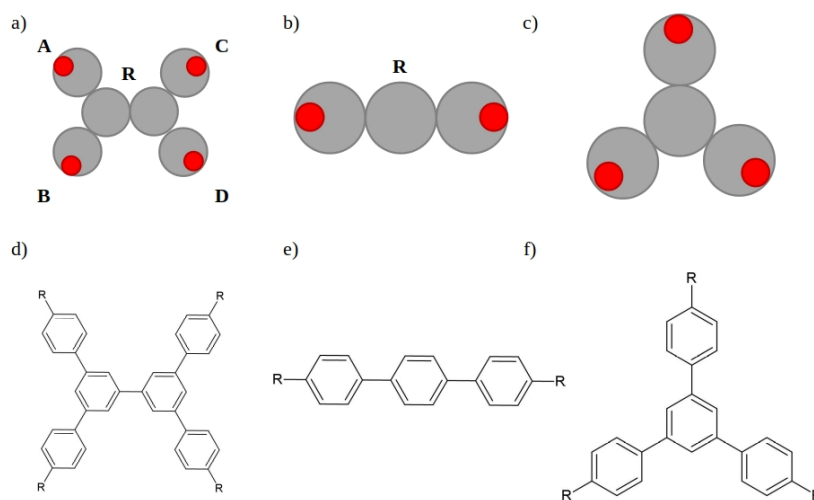


Figure 1.3: Schematic representation of tetratopic (a), linear (b), and tritopic (c) tectons. Parts (d-f) show examples of chemical compounds that could correspond to these models. Confer the text for the description of symbols.

Based on the great experience of the group in this field, we decided to comprehensively study molecular architectures described in the previous section (cf. Sec. 1.1). The examined geometries that have been distinguished involve tetratopic, linear, and tritopic building blocks as shown in Figure 1.3 a, b, and c, respectively. However, in the course of the dissertation, these tectons were not exclusively studied. In Figure 1.3 d, e, and f, one can see the possible chemical compounds that could correspond to these models. The tetra-substituted model can be described as two jointed "Y" letters. These molecules are composed of the "backbone", **R**, and four "arms", abbreviated as **A-D**. The entire architecture of the molecules can be changed, i.e. it can be built of a different number of flat and rigid segments, corresponding to aromatic rings. Moreover, the terminal segment of each arm has been decorated with the so-called "sticky patch", which will be referred to as an active site and can correspond to the presence of functional groups such as -CN, -OH, -B(OH)₂, -COOH, *etc.*

The model of linear building block is much simpler as it is comprised solely of the "backbone" **R**, with active sites embedded at its terminal segments. The segments here also correspond to the number of aromatic rings. In this case, the simulations with the presence of metal atoms both implicitly and explicitly will be performed. In terms of the latter, binary mixtures will be comprised of linear molecules and metal atoms of different size and coordination number. The main idea will be to assess the parameters for both

“single-component” and binary mixture systems which will result in the complementary values of coordination numbers. In such a way one will be able to examine the influence of the mixture composition on the self-assembly process.

In analogy to the tetratopic building blocks, the model of tripods can be described simply as a one “Y” letter. It is composed of the central atom and three “arms” abbreviated as **A-C**. As already mentioned in the previous section (cf. Sec. 1.1) this architecture can correspond to the trimesic acid is considered to be a prototypic building block for self-assembly. In this respect, the existence of a broad variety of experimental findings is available. Given that, one should agree that it is a good benchmark for the verification of the versatility of the model used.

The justification for the choice of the aforementioned tectons is the fact that they can be used for the description of the adsorption of a great number of experimentally investigated molecules. This can be achieved by the manipulation of the molecular topology and the size/energy of active sites.

1.3 Research objectives

Overall, in the course of the analysis of experimental results, questions arise that can not be answered, based on the measurements for that specific system and thermodynamic conditions. One of the usually ignored aspects are *whether the obtained ordered network is stable?* and *whether the system is in equilibrium?* While the synthesis can be tedious and costly, computer modeling can be a very convenient substitute for the exploration of problems of interest and a tool for answering the aforementioned questions. They can also supply experimental studies with the possibility of finding a mechanism of such processes which is not trivial to obtain in the laboratory. Therefore, computer simulations can give valuable insight to experimentalists due to the possibility of examination of the influence of multiple factors, such as particle geometry, under different conditions on the self-assembly process in a reasonable time.

The main goal of the dissertation is to establish the mechanism of the formation of self-assembled supramolecular networks on solid surfaces, by means of computer simulations. Particular attention will be devoted to the tetratopic and linear tectons. For the latter, we will also investigate their binary mixtures of different compositions with metal atoms of different sizes. Studies of other molecular geometries (V-shaped, tri-, penta-, and hexatopic) have been performed to present the versatility of this approach. Proposed models will correspond to the organic compounds composed of aromatic rings with diverse chemically active groups. One example of these are polycyclic aromatic hydrocarbons.

The main objectives are as follows:

1. Verification of the influence of structural parameters such as geometry, type and directions of interparticle interactions on the formation of ordered phases.
2. Determination of the influence of thermodynamic conditions (temperature, density) on the morphology of formed structures.
3. Establishing what parameters (molecular geometry, metal size, and mixture composition) determine the structure of adsorbed layers comprised of binary mixtures.
4. Attempt to evaluate a more “realistic” force-field for tetratopic building blocks.
5. Comparison of available experimental data with computer simulations and suggestions of possible modifications/elucidation of the phenomena.

Chapter 2

Methodology

2.1 Simulation method

Computer simulations can be divided into two categories, namely stochastic and deterministic methods. The former concerns the broad spectrum of Monte Carlo (MC) algorithms whereas the latter refers mainly to the molecular dynamics (MD) method which is the computational technique that will be used throughout the dissertation. In general, molecular dynamics is based on the numerical solutions of Newton's equations of motions which are second-order differential equations. For the N particles interacting one with another we have:

$$\mathbf{F}_i = m_i \frac{d^2 \mathbf{r}_i}{dt^2} \quad (2.1)$$

where m_i ; \mathbf{r}_i are the mass and positions of the i -th atom, respectively and \mathbf{F}_i is the force acting on the i -th atom.

The solution of *N-body problem* in molecular dynamics can be solved with following steps:

1. Assigning initial positions and velocities of all molecules.
2. Assuming an equation for the force vector.
3. Application of algorithm solving equations of motion.

The two first points can be obtained straightforwardly as the boundary conditions can be fulfilled by displacing the positions on a crystal lattice and assigning velocities from, for instance, the Maxwell-Boltzmann distribution. The force vector is also given by:

$$\mathbf{F}_i = -\nabla_{\mathbf{r}_i} u(\mathbf{r}^N) \quad (2.2)$$

where ∇ is the vector differential operator, u is the intermolecular potential and $\mathbf{r}^N = (\mathbf{r}_1, \mathbf{r}_2, \dots, \mathbf{r}_N)$. Hence, one can see that it is sufficient to know a proper intermolecular potential that is suitable to describe the system of interest. The problems, however, arise in the third step. Once we want to investigate the system comprising of more than two interacting atoms which refers to nearly all real systems. In such cases, we need to use numerical methods to solve N non-linear differential equations. One of the most popular and the one used throughout the dissertation is the velocity Verlet algorithm.³⁷ This method allows us to evolve explicitly velocities and positions at the same time step. The positions are evolved in the following way:

$$\mathbf{r}_i(t + \Delta t) = \mathbf{r}_i(t) + \Delta t \mathbf{v}_i(t) + \frac{\Delta t^2}{2m_i} \mathbf{F}_i(t) \quad (2.3)$$

and velocities

$$\mathbf{v}_i(t + \Delta t) = \mathbf{v}_i(t) + \frac{\Delta t}{2m_i} [\mathbf{F}_i(t) + \mathbf{F}_i(t + \Delta t)] \quad (2.4)$$

This method has a particular advantage over other numerical solvers as it possess two properties that are crucial for the long-time stability of numerical solvers. The first one is time-reversibility which means that if we take initial conditions $\mathbf{r}_i(t + \Delta t), \dots, \mathbf{r}_N(t + \Delta t), \mathbf{v}_i(t + \Delta t), \dots, \mathbf{v}_N(t + \Delta t)$ and use time step $-\Delta t$ we will arrive at the state $\mathbf{r}_i(t), \dots, \mathbf{r}_N(t), \mathbf{v}_i(t), \dots, \mathbf{v}_N(t)$. The second property is the symplecticity which means that the algorithm maps the initial phase space point \mathbf{r}_0 into \mathbf{r}_t without destroying the symplectic properties of classical mechanics.

Variations of molecular dynamics

By the definition, Newton's equations of motion give us the trajectories evolved in an isolated system composed of N particles in a container of volume V and a total energy E corresponding to a Hamiltonian \mathcal{H} . These conditions are known as a microcanonical ensemble, NVE . On the other hand, the majority of real systems' conditions are such that we control the temperature and pressure instead of energy. This is also possible to do in molecular dynamics simulations, however, one needs to perturb the classical dynamics with the use of thermostats and/or barostats to sample, for instance, the canonical NVT or isothermal-isobaric NpT ensembles. It is also important to note that in such a way we do not have a constant temperature which would result in having constant kinetic energy, but rather we can change the dynamics to have a constant average temperature.

In the course of the simulations, we have used two algorithms allowing us to control the temperature. The first one is the Berendsen thermostat³⁸ which assumes that the system at temperature T is in contact with a heat bath at a temperature T_0 . Therefore, the temperature is controlled in the following way:

$$\frac{dT}{dt} = \frac{T_0 - T(t)}{\tau_B} \quad (2.5)$$

where τ_B is a damping factor that determines the coupling of a system with the heat bath. The choice of this parameter is crucial as it regulates the order of thermal fluctuations in the system. It is also worth highlighting that this thermostat has been used solely for the initial equilibration as it does not sample the canonical distribution properly. Due to this fact, we have employed another algorithm which is the Martyna, Tuckermann, and Klein (commonly known as Nosé-Hoover chains) thermostat.^{39,40} This is an extension of the original equations of motion proposed by Nosé⁴¹ and Hoover.⁴²

The idea is to scale particle velocities by an additional dimensionless friction factor p_η . The equations of motion are then given by:

$$\begin{aligned}
 \dot{\mathbf{r}} &= \frac{\mathbf{p}_i}{m_i} \\
 \dot{\mathbf{p}}_i &= \mathbf{F}_i - \frac{p_{\eta_1}}{Q_1} \mathbf{p}_i \\
 \dot{\eta}_j &= \frac{p_{\eta_j}}{Q_j} \\
 \dot{p}_{\eta_1} &= \left[\sum_{i=1}^N \frac{p_i^2}{m_i} - N_f k_B T \right] - p_{\eta_1} \frac{p_{\eta_2}}{Q_2} \\
 \dot{p}_{\eta_j} &= \left[\frac{p_{\eta_{j-1}}^2}{Q_{j-1}} - kT \right] - p_{\eta_j} \frac{p_{\eta_{j+1}}}{Q_{j+1}} \\
 \dot{p}_{\eta_M} &= \left[\frac{p_{\eta_{M-1}}^2}{Q_{M-1}} - kT \right]
 \end{aligned} \tag{2.6}$$

where $j = 1, \dots, M$, Q_j are the masses of particle thermostats that determine the time scale of thermal fluctuations, k_B is the Boltzmann constant, and N_f is the number of degrees of freedom. For $M = 1$ the equations reduce to the Nosé-Hoover (NH) equations of motion. A good choice of parameter Q_j will support the dynamics achieving canonical distribution. It has been shown³⁹ that the optimal choice should be:

$$\begin{aligned}
 Q_1 &= \frac{N_f k_B T}{\tau_{NH}^2} \\
 Q_j &= \frac{k_B T}{\tau_{NH}^2}
 \end{aligned} \tag{2.7}$$

where τ_{NH} is the frequency at which particle thermostats fluctuate. The algorithm presented in equations 2.6 has a great advantage over the regular NH method as it is able to sample correctly a canonical ensemble for small or constrained systems.

To control the pressure in the initial steps of the simulations, devoted to attaining the desired density we have simulated the NpT ensemble with the use of Berendsen barostat.³⁸ The idea is similar to Berendsen's thermostat and the system at pressure p is coupled to the "pressure bath" at pressure p_0 . Therefore, the pressure is rescaled in the following way:

$$\frac{dp}{dt} = \frac{p_0 - p(t)}{\tau_B} \tag{2.8}$$

where τ_B has the same meaning as in equation 2.5. At every time step, the volume is scaled by the factor χ

$$\chi = 1 - \beta_T \frac{\Delta t}{\tau_B} (p - p_0) \tag{2.9}$$

where Δt is a timestep, β_T is the isothermal compressibility which can be fixed and included into τ_B factor. Aside from the volume, positions of center of mass \mathbf{r}_{COM} of all molecules are rescaled by:

$$r' = \frac{\chi^{1/D}}{\mathbf{r}_{\text{COM}}} \tag{2.10}$$

where r' are new positions after the change of systems' volume and D is the dimensionality of the system.

2.2 Structural parameters

To attain a deeper insight into the self-assembly processes, a variety of different parameters have been defined. These quantities are useful for the description of both local and global ordering. While computer simulation data tend to be reflected by experiments and *vice versa*, the analysis can be inaccessible by the available experimental methods.

The benefit of the former method is the possibility to divide the analysis with respect to particular components or even atom types, present in the system with relative ease. Moreover, one can employ structural parameters that are immeasurable or extremely hard to measure.

Radial distribution function

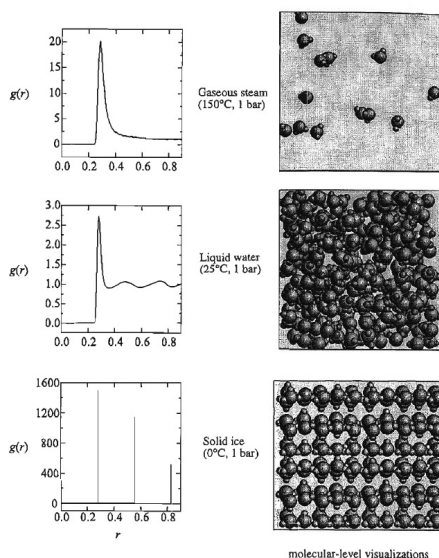


Figure 2.1: Radial distribution functions for gas, liquid and solid phases of water and their relationship to molecular-level visualizations. Picture taken from the reference.⁴³

The function devoted to measure the probability of finding two particles a distance r apart is a radial distribution function which in three-dimensional system can be defined as:

$$g(r) = \frac{1}{4\pi r^2 \rho} \left\langle \sum_{i < j} \delta(\mathbf{r} - \mathbf{r}_{ij}) \right\rangle \quad (2.11)$$

where δ is the Dirac delta and ρ is the system's density. For gases and liquids, correlations vanish with the distance, hence:

$$\lim_{r \rightarrow \infty} g(r) = 1 \quad (2.12)$$

Another valuable information that can be extracted from this quantity is the *coordination number*, z . It can be defined as the average number of molecules in the first coordination shell of the radial distribution function, given by:

$$z = 4\pi\rho \int_{r_1}^{r_2} g(r)r^2 dr \quad (2.13)$$

where $r_2 - r_1$ is the width of the first coordination shell.

Structure factor

The structure factor is the quantity closely related to the radial distribution function defined by equation 2.11. This property, however, possesses one particular advantage, namely, it can be directly compared with the intensity of scattering radiation in experiments. In general, it can be defined as:

$$S(\mathbf{k}) = \frac{1}{n_\alpha} \langle g(\mathbf{k})g(-\mathbf{k}) \rangle \quad (2.14)$$

where n_α is the number of scattering points, $g(\mathbf{k})$ is a Fourier transform of a radial distribution function defined as:

$$g(\mathbf{k}) = \sum_{n=1} n_\alpha \exp(i\mathbf{k}\mathbf{r}_n) \quad (2.15)$$

Since our systems possess the ability to self assemble into nanostructures, we need to reformulate the equation 2.14 for the anisotropic cases which is given by:

$$S(\mathbf{k}) = \frac{1}{n_\alpha} \langle g(\mathbf{k}) \rangle \quad (2.16)$$

and from the properties of modulus of complex number we have:

$$S(\mathbf{k}) = \frac{1}{n_\alpha} \left\langle \left(\sum_{n=1} n_\alpha \cos(\mathbf{k}\mathbf{r}_n) \right)^2 + \left(\sum_{n=1} n_\alpha \sin(\mathbf{k}\mathbf{r}_n) \right)^2 \right\rangle \quad (2.17)$$

Multiple-angle formulas were calculated from the recurrence relations:

$$\begin{aligned} \sin(kx) &= 2 \sin[(k-1)x] \cos(x) - \sin[(k-2)x] \\ \cos(kx) &= 2 \cos[(k-1)x] \cos(x) - \cos[(k-2)x] \end{aligned} \quad (2.18)$$

The final structure factor $S(k)$ was obtained as an average over all $S(\mathbf{k})$ where $|k|$ is equal k .

Bond-orientational order parameter

To analyze the 2D crystalline phases, we used the global 2D bond-orientational order parameter Q_k ,^{44,45} defined as:

$$Q_k = \frac{1}{N_{\text{bond}}} \left| \sum_i \sum_{j \neq i} \exp(ki\phi_{ij}) \right| \quad (2.19)$$

where i runs over all particles of the system, j runs over all neighbours of i , ϕ_{ij} denotes the angle between the bond connecting particles i and j and an arbitrary but fixed reference axis, N_{bond} denotes the number of bonds in the system, and $k = 1, 2, \dots, 6$. This parameter can take values between 0 and 1 for the disordered and ordered phases of k -symmetry, respectively.

Nematic order parameter

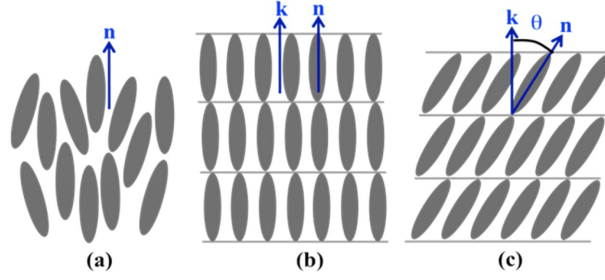


Figure 2.2: Schematic representation of the nematic (a), smectic A (b), and smectic C (c) phases of rod-like molecules. Here, n and k are the director and layer normal, respectively, and θ is the (tilt) angle between n and k . Picture taken from the reference.⁴⁶

In order to quantify whether a given phase possesses an orientational (cf. Fig. 2.2 a-c) but not necessarily a positional order (cf. Fig. 2.2 b, c), one can use the nematic order parameter^{47,48} given by:

$$Q_{\alpha\beta} = \sum_i^N \left[\frac{D \times b_\alpha(i)b_\beta(i) - \delta_{\alpha\beta}}{D - 1} \right] \quad (2.20)$$

where D is the dimensionality of the system, $b_\alpha(i)$ is the α -th coordinate of the unit vector b , specifying the orientation of the molecule i , and δ is the Kronecker delta function. The corresponding eigenvalues of Q are $\pm S$, however, it has to be noted that the absolute values of S tend to 1 in a perfectly ordered phase, and is expected to vanish in a disordered phase when $N \rightarrow \infty$.

Relative shape anisotropy

Another quantity that allows determining the symmetry of a given structure is relative shape anisotropy⁴⁹ given by:

$$\kappa = \frac{1}{D - 1} \left[\frac{D(\lambda_x^4 + \lambda_y^4 + \lambda_z^4)}{(\lambda_x^2 + \lambda_y^2 + \lambda_z^2)^2} - \delta_{ij} \right] \quad (2.21)$$

where D is the dimensionality of the system, λ_x , λ_y , λ_z are eigenvalues of the gyration tensor in x , y , and z directions, respectively, and δ_{ij} is the Kronecker delta. The gyration tensor, R_g^2 can be defined as:

$$R_g^2 = \frac{1}{N} \sum_{i=1}^N (r_i - r_{\text{COM}})^2 \quad (2.22)$$

where r_{COM} and r_i are the geometric center and the position of the i -th molecule, respectively. The gyration tensor components for 3D systems are defined as:

$$M = \frac{1}{N} \begin{bmatrix} \sum_i (x_i - x_{\text{COM}})^2 & \sum_i (x_i - x_{\text{COM}})(y_i - y_{\text{COM}}) & \sum_i (x_i - x_{\text{COM}})(z_i - z_{\text{COM}}) \\ \sum_i (x_i - x_{\text{COM}})(y_i - y_{\text{COM}}) & \sum_i (y_i - y_{\text{COM}})^2 & \sum_i (y_i - y_{\text{COM}})(z_i - z_{\text{COM}}) \\ \sum_i (x_i - x_{\text{COM}})(z_i - z_{\text{COM}}) & \sum_i (y_i - y_{\text{COM}})(z_i - z_{\text{COM}}) & \sum_i (z_i - z_{\text{COM}})^2 \end{bmatrix} \quad (2.23)$$

Moreover, the gyration radius can be defined as $R_g^2 = \lambda_x^2 + \lambda_y^2 + \lambda_z^2$. Relative shape anisotropy, in analogy to previous order parameters, takes values between 0 and 1, when the system is spherically symmetric or the molecules lie along a straight line, respectively.

Block density distribution method

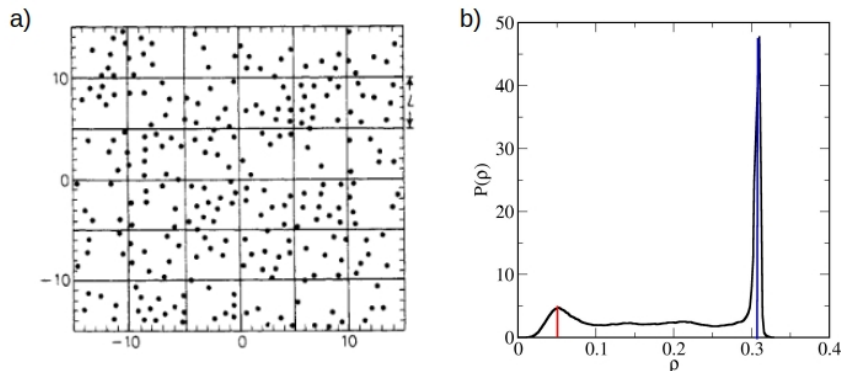


Figure 2.3: Part a) displays a schematic representation of the simulation cell divided into blocks. Picture taken from.⁵⁰ Part b) shows an example of distribution function.

One of the possible methods to evaluate the phase diagrams involves analysis of the density distribution function in blocks.⁵⁰ Although this distribution does not describe the structural parameters, it is a convenient tool to detect phase separation in the system. The algorithm is as follows, the simulation cell is divided into smaller blocks (cf. Fig. 2.3 a) and the distribution of the density probability $P(\rho)$ is estimated for all blocks. Figure 2.3 b displays an example of the function $P(\rho)$ that exhibits a double-peak behavior corresponding to the two-phase coexistence. From the distributions $P(\rho)$ the densities of coexisting phases are determined from the maxima of the peaks (red and blue lines in Fig. 2.3 b).

Other quantities

Aside from the parameters described above, a number of other quantities devoted to the description of structural order have been reported. Probably one of the most popular is the Steinhardt order parameter^{51,52} and its variations,⁵³⁻⁵⁵ however, none of those have been used in this dissertation. In these papers, it has been shown that they are extremely useful for the description of both the local and global order.

In this respect, in our group, it was possible to determine the type of ordering for Janus particles in 2D confinement solely because of the use of the Steinhardt and 2D bond-orientational order parameters (cf. Eq. 2.19). It has been found that the presence of external field resulted in (i) the two-dimensional crystallization of nanoclusters, (ii) the surface-induced formation of “levitating” slabs, and (iii) “inverted” adsorption in Janus-like pores.⁵⁶ The first case is particularly interesting since those nanoclusters locally possess three-dimensional crystal ordering of hexagonal close-packed structure. On top of that, due to the confining forces, these nanoclusters “levitate” in the middle of a slit-like pore and center of masses of each nanocluster are arranged into two-dimensional hexagonal structure.

2.3 Model and simulation details

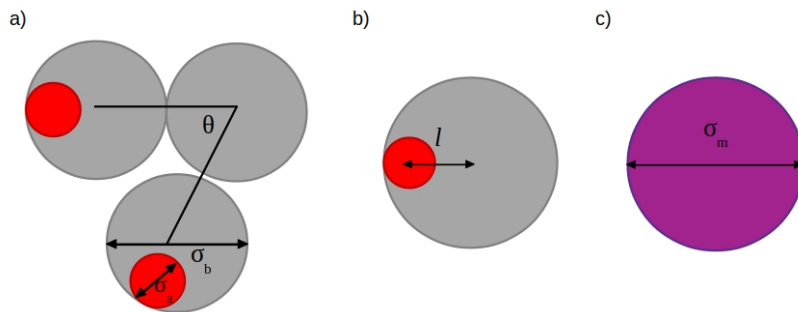


Figure 2.4: Schematic representation of parameters of the model used in the course of the simulations.

Schematic representation and corresponding chemical compounds of a few molecules studied have been shown in Figure 1.3. In this section, the parameters of the model used will be described in more detail (cf. Fig 2.4). The segments in the main framework (both backbone and arms) were of identical size equal to $\sigma_b = \sigma$ whereas active sites were five times smaller $\sigma_a = 0.2\sigma$ (unless specified otherwise). The angle θ between neighboring arms has been changed and set to different values depending on the studied molecular architecture. The bonding distance between the terminal arms' segment and the active site was abbreviated as l and depending on the embedment it determined the interaction zone size (cf. Fig. 3.2). As already specified, for chosen systems, we have also examined binary mixtures of linear linkers with metal atoms of size σ_m .

In molecular dynamics simulations, all of the molecules have been treated as flat, rigid objects. To maintain the molecular geometry, we have used harmonic binding potentials:

$$u_{bb} = k(r - \sigma_{bb})^2 \quad (2.24)$$

and

$$u_{ab} = k(r - \sigma_{ab})^2 \quad (2.25)$$

Likewise, all of the necessary angles have been preserved:

$$u(\theta_{bb}) = k_\theta(\theta_{bb} - \theta_{0,bb})^2 \quad (2.26)$$

and

$$u(\theta_{ab}) = k_\theta(\theta_{ab} - \theta_{0,ab})^2 \quad (2.27)$$

The interparticle potential employed in the simulations was (12,6) Lennard-Jones potential which has been truncated but appropriately shifted to ensure its continuity, as well as its first derivative:⁵⁷

$$U_{SF} = \begin{cases} U_{LJ}(r) - U_{LJ}(r_{cut}) + U'_{LJ}(r_{cut})(r - r_{cut}) & r < r_{cut} \\ 0 & \text{otherwise} \end{cases} \quad (2.28)$$

where

$$U_{LJ}(r) = 4\epsilon_{kl} \left[\left(\frac{\sigma_{kl}}{r} \right)^{12} - \left(\frac{\sigma_{kl}}{r} \right)^6 \right] \quad (2.29)$$

and $U'_{LJ}(r_{cut})$ is the first derivative of the energy $U_{LJ}(r)$ at $r = r_{cut}$.

The interparticle interactions have been designed in such a way that the only attraction in the system is due to the association between active sites. In other words, all of the cutoff distances have been set to $r_{cut,ij} = \sigma_{ij}$ where $ij = ab, bb$ and $r_{cut,aa} = 2\sigma_{aa}$. This should result in the vanishing of a critical point of liquid-vapor condensation and possible liquid phases due to an insufficient range of attractive forces.^{58,59} In consequence, the phase diagrams should be of swan-neck type.

All of the molecular dynamics simulations have been performed in the NVT ensemble, using the LAMMPS simulation package.⁶⁰ The velocity Verlet³⁷ integration scheme has been used with the reduced time step of the order of $t = 0.001\tau$. The number of molecules varied from 2500 to 8100. However, one has to note that the total number of “atoms” varied depending on the molecular architecture. This amount is sufficient for most self-assembly systems, which are simultaneously large enough to form ordered networks and small enough to form those structures in a reasonable time frame. The simulation scheme involved preliminary runs in the NpT ensemble to establish the desired density. Next, equilibration runs for around $10^6 - 10^7$ time steps using Berendsen thermostat³⁸ with the damping constant equal to $\tau_B = 10\tau$ have been performed. Further equilibration for around $10^7 - 10^8$ time steps as well as production runs have been performed using the Nosé-Hoover chain algorithm,³⁹ with the damping constant equal to $\tau_{NH} = 10\tau$ and the number of chains set to $M = 3$. Every system has been cooled down from temperatures where we did not observe any order, up to the point where self-assembled networks have been distinct.

Chapter 3

Shortened description of the results

The foundation of the presented doctoral thesis is a series of eight publications, abbreviated hereafter as **PI-PVIII**.

3.1 Tetratopic building blocks

In the first paper **PI**, we have examined the behavior of the simple tetratopic molecules. The main idea of the paper was to determine the influence of the system's density and temperature on the formation of ordered phases. It has been shown that in the density $\rho^* = 0.25$, molecules assemble simultaneously into "parallel" and Kagomé networks, as expected based on the paper.²¹ However, the coexistence of two ordered and a gas phases is inconsistent with the Gibbs phase rule for one-component systems as investigated in our case. Based on that, we know that only one of these networks can be stable. Similar cases have already been described in Section 1.1.

To assess which one, we have performed the simulations at two distinct densities. For the higher density $\rho^* = 0.4$, solely the parallel network was present, while for the lower density $\rho^* = 0.1$, the obtained configurations still correspond to the behavior observed in $\rho^* = 0.25$. As already mentioned, in such a case, one of the phases has to be metastable, and we conclude that this situation refers to the Kagomé. It is worth highlighting that the origin of why these networks can be observed simultaneously is the same potential energy and that the density of ideal networks is only slightly different.

Other molecular architectures have also been examined. The building block with two segments in the backbone **R** and every arm **A-D** form solely the Kagomé network. On the other hand, elongation of the backbone **R**, does not lead to the stabilization of the parallel network but results in the formation of a completely different phase with hexagonal symmetry. Moreover, we have observed quite unusual ordering of the active sites which has not been found for any other system examined here. It resembled "glassy-like" patterns where long-range ordering is not present and a single unit cell could not be discriminated. Owing to that, we have proposed a methodology for the calculation of two-dimensional structure factors. We have found that this parameter describing the order in the system should not be averaged if more than one domain is present. Other than that, we are tracking trajectories where differently oriented clusters are present which can lead to a completely incorrect interpretation of the results. An example of this can be found in Figure 3.1. Theoretically evaluated diffraction pattern for segments of an entire framework proves the hexagonal symmetry of the network (Fig. 3.1 a). Surprisingly, active sites exhibit similar symmetry (Fig. 3.1 b), however, a deeper analysis has shown that the final pattern is an overlap of at least two unit cells, namely, rhombic and rectangular, which imitates the hexagonal arrangement of the molecules. As already stressed, if one would

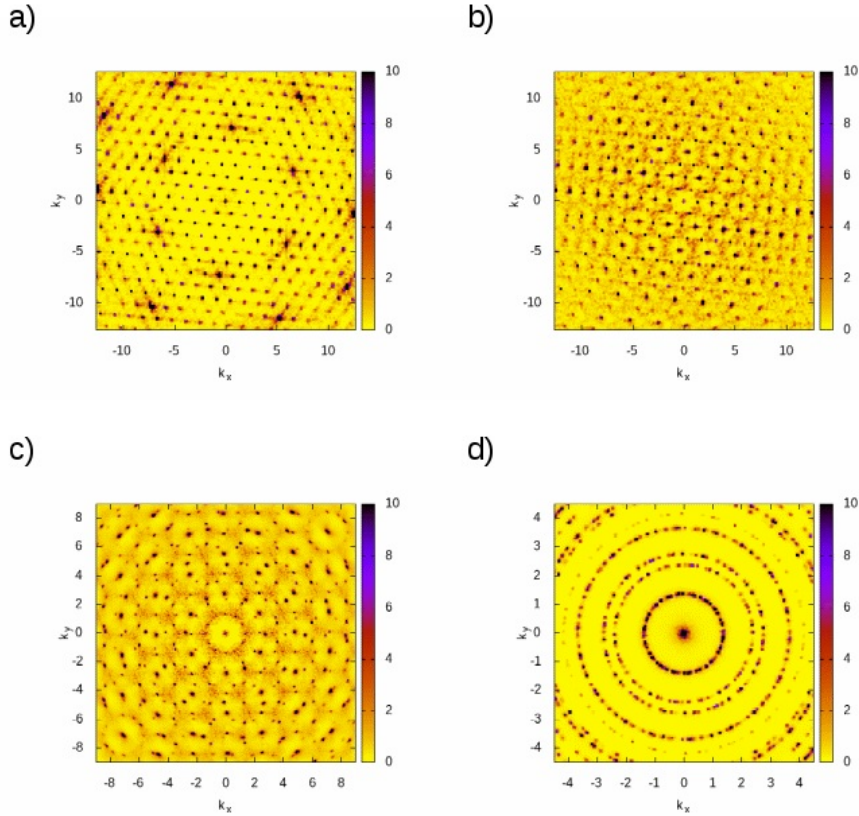


Figure 3.1: Part (a) represents the diffraction patterns for a fragment of frameworks' segments. (b-d) Display diffractograms for a part of one configuration and averaged over 500 and 5000 configurations of the entire system for active sites, respectively.

calculate this parameter for the entire system as a time average when differently oriented domains are present, a diffraction pattern, similar to quasicrystals 12-fold noncrystallographic diffraction symmetries can be obtained simply due to the rotation of clusters in time (cf. Fig 3.1 c). This conclusion can be proven by prolonging the calculations as shown in Figure 3.1 d where the diffraction peaks became diffused. Therefore, it is readily visible that the best diffraction patterns are available from a fragment of only one configuration because such methodology is not exposed on perturbations induced by rotation of differently oriented domains.

The next papers (**PII-PIV**) are the extension of the same tetratopic model aiming at the verification of the use of other directions of interparticle interactions. In the first one (**PII**), we have found that with the increase of the backbone length \mathbf{R} , the density of the forming phases decreases as the voids in the networks' structure increase, due to the change of the molecular architecture. This has been shown on the schematic phase diagrams which turned out to be qualitatively the same and invariant of the molecular geometry. The only difference that is pronounced is the gradual decrease of the density with the increase of backbone or arm length. This behavior may be related to the increase in the cavity sizes observed in these structures. It also has been shown that these diagrams are of swan-neck type which corroborates that the manipulation with attractive forces will result in solely gas-solid transitions, as described in Section 2.3.

A deeper insight into the behavior of the studied system has been gained due to the calculation of the nematic order parameter (cf. Eq. 2.20). It has shown that the backbones are aligned in the same direction in these phases. Moreover, this behavior was invariant of

l	σ_a	$r_{cut,aa}$	CN
0.4	0.2	0.4	2
0.45	0.2	0.4	3
0.6	0.2	0.4	4
0.65	0.3	0.6	5
0.7	0.4	0.8	6

Table 3.1: Model interaction parameters used in the paper **PIII** resulting in a particular coordination number (CN).

the molecular topology. Temperature dependence of this parameter exhibited a hysteresis which may indicate a first-order phase transition. However, finite-size scaling analyses have not been performed to verify its presence in the thermodynamic limit.

On top of that, a comparison with an off-lattice Monte Carlo simulations has been performed and a reasonable agreement has been attained for interaction zone size $\gamma = 10^\circ$. On the other hand, the increase of this parameter to $\gamma = 76^\circ$ resulted in the formation of “ladder-like” networks. Although the parameter γ was sufficiently large to allow for a simultaneous interaction of a single active site with two other molecules, this was not the case in the present situation and each tetratopic building block associated with only one molecule.

A comprehensive study on the influence of the interaction zone size ($\alpha = \gamma/2$) was the subject of the following papers presented in **PIII** and **PIV**. Subsequent simulations (**PIII**) have shown that different directions of interparticle interactions result in the formation of a broad variety of ordered networks. Among those we can distinguish (i) linear structures in which length increased together with the length of the backbone **R**, (ii) rotated parallel and Kagomé networks, similar to those as in paper **PI**. For the latter phases, different ratios of one or the other have been observed, depending on the manipulation of building block architecture.

Additionally, we have established the parameters of the Lennard-Jones potential for the interactions between the active sites that could mimic (i) different chemically active groups or (ii) the implicit presence of metal atoms. The parameters can be found in table 3.1.

As already specified in Section 2.3, we embedded the terminal arms’ segments by the “phantom site” to achieve the “directionality” of spherically symmetric Lennard-Jones potential. In previous papers, only two molecules were allowed to interact one with another. Currently, the idea of the manipulation of the active site size σ_a or/and the bonding distance l is to decrease the directionality of the interparticle potential, hence allowing more particles to interact with each other.

Using this information, we have checked the behavior of the tetratopic molecules with the same direction of interparticle interactions as in the paper **PI**. In such a case, the formation of different phases compared to previous studies can be observed. Similarly to all molecular architectures, we manipulated the building blocks geometry and the most interesting finding could be observed for the tecton with four segments in the backbone and one in every of the **A-D** arms. Within this structure three distinct sizes of cavities can be distinguished and it is worth highlighting that the almost identical structures have been observed experimentally by J. Li, *et al.* for relatively similar compound.⁶¹

The last stage of studying a coarse-grained model for tetratopic molecules was described in the paper **PIV**. The main goal was to assess the influence of the change of the molecular architecture (angle θ , cf. Fig. 2.4 a) in the molecules of this kind on the

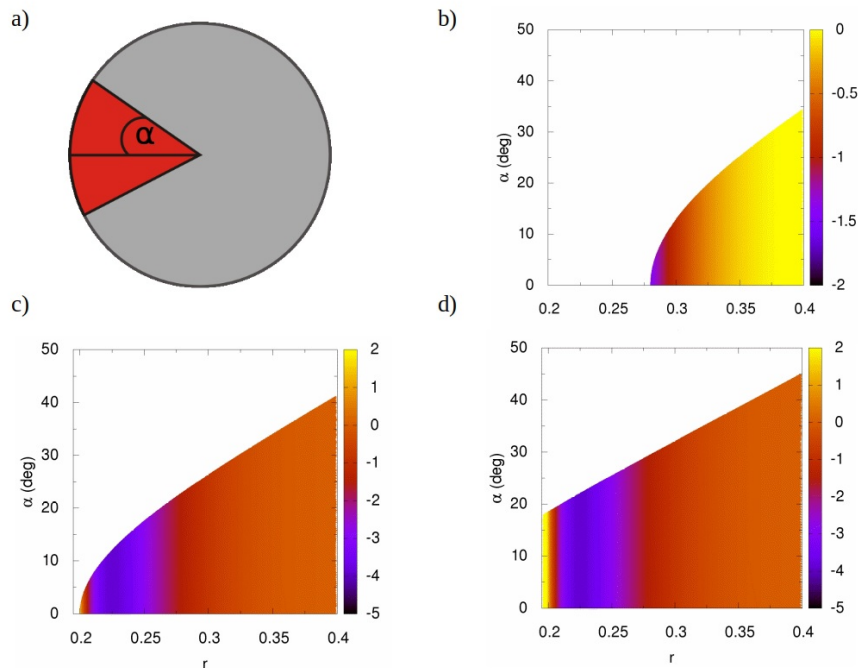


Figure 3.2: Schematic representation of the interaction zone (a). Parts (b-d) present the angular dependence of the Lennard-Jones potential with respect to the separation distance between active sites for $l = 0.36\sigma$ (b), $l = 0.4\sigma$ (c), and $l = 0.44\sigma$ (d).

self-assembly process, in comparison to the geometry shown in paper **PI**. Moreover, we wanted to examine in a more precise way how we can manipulate the models' parameters, similarly to what has been already shown in table 3.1, for the target design of supramolecular networks. In analogy to the previous paper (**PIII**), we have changed the bonding distance l , to which we will refer as an "interaction zone" α (cf. Fig. 3.2). Parts b-d of Fig. 3.2 demonstrate the influence of the bonding distance l on the angular behavior of the employed Lennard-Jones potential. We have estimated that the maximum size of the interaction zone changes with l and is equal to 34.6° and 45.2° for $l = 0.36\sigma$ and $l = 0.44\sigma$, respectively. This corresponded to the formation of pairs ($l = 0.36\sigma$) or triplets ($l = 0.44\sigma$) whereas in the case of intermediate bonding length $l = 0.4\sigma$, depending on the molecular architecture, association of both two and three molecules was possible. These results have been validated with available literature data. Kalyuzhnyi and Cummings⁶² have shown the ranges of the interaction zone size α allowing for the connections between two ($30^\circ < \alpha \leq 35.3^\circ$), three ($35.3^\circ < \alpha \leq 45^\circ$), *etc.*, "patchy particles", due to geometrical constraints. It is worth stressing that although these authors used a relatively short-ranged square-well potential and the above ranges of α are expected to vary depending on the form of interparticle potential, we observe a quite similar tendency in the case of Lennard Jones potential used in this work.

Another interesting feature is that solely for this molecular architecture, the formation of triplets for intermediate bonding ($l = 0.4\sigma$) distance was observed. This should emphasize how the self-assembly process can be sensitive to such subtle changes which are not invariant on the molecule's topology.

For currently studied molecular geometry (paper **PIV**), we have found the rules governing the formation of, *inter alia*, the Sierpinski triangles, Archimedean tessellations, Kagomé, and ladder networks. The most prominent result of this work is that one can attain a desired ordered structure by the manipulation of the interaction zone α . In Fig-

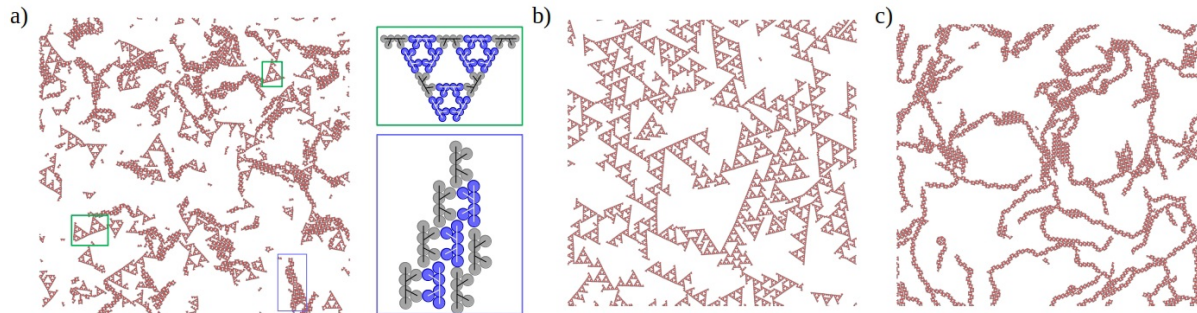


Figure 3.3: Parts (a-c) display the configurations at the same density for tetratopic building blocks for separation distance $l = 0.4\sigma$, $l = 0.36\sigma$, and $l = 0.44\sigma$, respectively. Schematically drawn association paths are shown on the right-hand side of panel (a).

ure 3.3 a, one can see the simultaneous formation of Sierpinski triangles and a dense phase for $l = 0.4\sigma$. By the change of this parameter, one can selectively obtain either one phase or the other as shown in parts (b) and (c) of Figure 3.3. This is particularly important, because the same effect can be observed in experimental system where, for instance, the same molecular architecture can exhibit distinct behavior depending on the substitution with different chemically active groups (e.g. $-\text{B}(\text{OH})_2$, $-\text{OH}$, $-\text{COOH}$, $-\text{Br}$, *etc.*) which would promote the formation of dimers, trimers, *etc.*

On top of that, the appearance of Sierpinski triangles is rather surprising, since the majority of papers report the formation of such structures in completely different systems. The only general rule that has been established and proved experimentally is that the so-called “V-shaped” molecules are able to order into Sierpinski triangles.^{18,63} To date, we could not find any experimental findings that exhibit similar behavior for relatively small tetratopic tectons which would correspond to the results presented in paper **PIV**. Therefore, we believe that due to this quite unexpected outcome, the possibility for further studies is open.

Another remarkable finding is the formation of ladder networks. As shown in Figure 3.4 a, for the $l = 0.4\sigma$, these wires align in one direction, however, small patches of a dense phase, similar to those displayed on the right-hand side of Figure 3.3 a can also be spotted. It is also noteworthy that the increase of the system’s density does not result in the gluing of these “lines” one with another but the structure rearranges into a denser phase, instead.

In analogy to the previous building block that formed Sierpinski triangles, we can achieve the selectivity of the formation of either of these networks by the change of parameter l and it can be seen that two phases are no longer present in Figure 3.4 b, d, but their assembly is steered by the value of l . When embedment is changed to $l = 0.36\sigma$, the formation of wires is only observed as in the case of $l = 0.4\sigma$. However, it is worth highlighting that the increase of the system’s density results in the wires starting to glue laterally one to another. This resembles the behavior of liquid crystals which, even without the presence of attractive interactions, tend to form densely-packed, ordered structures. Two-dimensional structure factors calculated with respect to the backbone \mathbf{R} which are given in the insets to parts b, c of Figure 3.4 corroborate with these observations. The former is diffused and the distances in reciprocal space are small which means that those wires are separated (large distance in real space). For a higher density system (Figure 3.4 c) the structure factor shows the opposite. On the other hand, an increase of the bonding distance to $l = 0.44\sigma$ leads to the emergence of a more dense phase in systems at both low and high densities and the ladder networks have not been observed at all (Fig. 3.4 d).

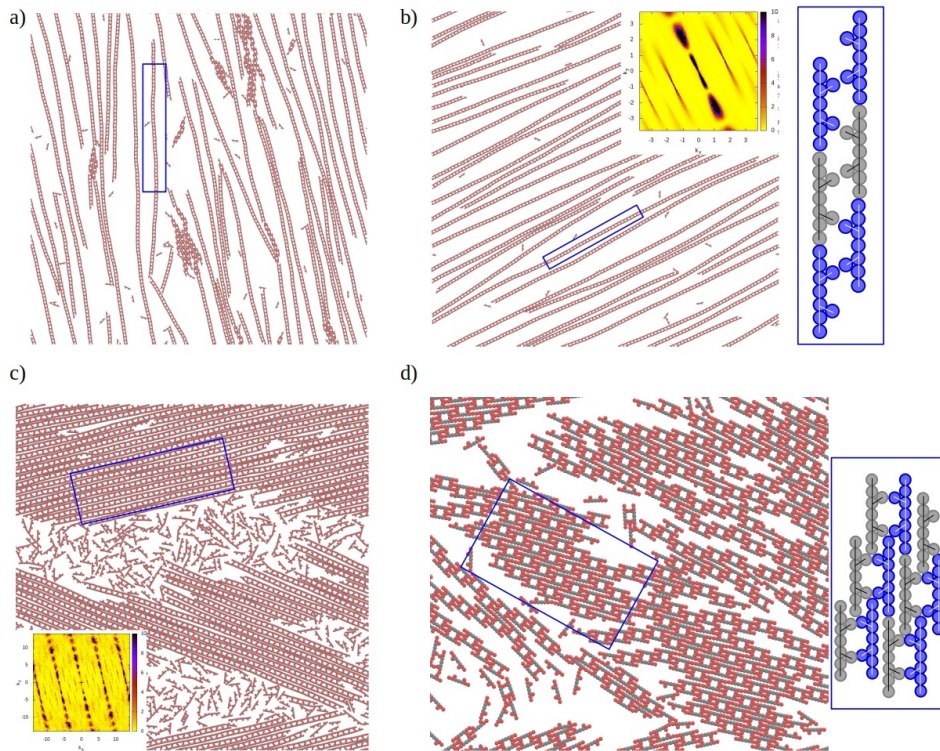


Figure 3.4: Parts (a, c, d) display the configurations at the same density for tetratopic building blocks for separation distance $l = 0.4\sigma$, $l = 0.36\sigma$, and $l = 0.44\sigma$, respectively. Part (c) presents the configuration recorded at density $\rho^* = 0.5$ and $l = 0.36\sigma$. 2-D structure factors are shown in the insets to parts (b, c). Schematically drawn association paths are shown on the right-hand side of panels (b, d).

3.2 Other geometries

To verify the versatility of the employed model we wanted to simulate molecular architectures other than tetratopic building blocks. The first one studied was linear tecton. In the paper **PIII**, one-component systems have been examined and the metal atoms of different coordination numbers have been treated implicitly, due to the change of the model's parameters as shown in Table 3.1. The formation of square and triangular lattices was reported, however, the most intriguing structure was found for the "crossover" parameters resulting in the coordination number $CN=5$. This network is called $3^2.4.3.4$ Archimedean tessellation and is composed of different polygons (squares and triangles) where one, distinct unit cell cannot be distinguished. Moreover, we conducted the simulations for V-shaped molecules and with the choice of parameters allowing the formation of triplets, Sierpinski triangles have been observed. It has to be emphasized that these results for both linear and V-shaped molecules are consistent with the literature data.^{15,18,63,64}

Although the aforementioned studies for one-component systems turned out to be a quite successful tool for the description of experimental findings, they possess one relatively important flaw. Such an approach lacks the possibility to change the concentration of the mixtures since the second component has been treated implicitly. Hence, in the paper **PV** we wanted to validate the importance of the mixture composition. We have found the formation of disordered, square (SN1, SN2), and parallel (PN) networks depending on the metal atoms' size when the mixture was composed of an equal number of the linear linker and metal atoms. Moreover, increasing the number of linker molecules resulted in the formation of $3^2.4.3.4$ Archimedean tiling (AT1, AT2), structure of triangular symmetry (TN) and "spaghetti" wires (SW). Schematic phase diagram for different mixture composition χ and metal atom size σ_m can be found in Figure 3.5.

Other molecular geometries have been examined in the paper **PVI**. The building blocks proposed were tetra-, penta-, and hexatopic molecules and their behavior in single-component systems as well as in binary mixtures with either linear or V-shaped molecules to which we will refer as linkers. The motivation of the former was to assess the influence of the addition of a second component on the self-organization process we need to know their behavior in such conditions. We benefit from the knowledge of linkers self-assembly resulting from the investigations described in paper **PIII**.

The results for tetra- and hexatopic molecules in single-component systems were as expected as the symmetry of the ordered phase resulted from the precursor's symmetry.

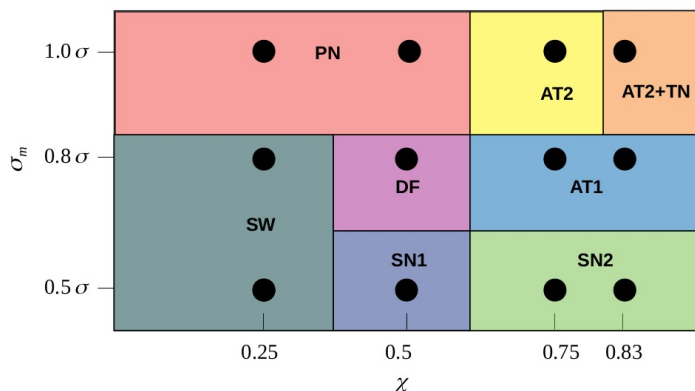


Figure 3.5: Schematic overview of structures formed in the binary mixtures. For the abbreviations confer the text. Black circles refer to simulation results; structure boundaries are drawn arbitrarily to guide the eye.

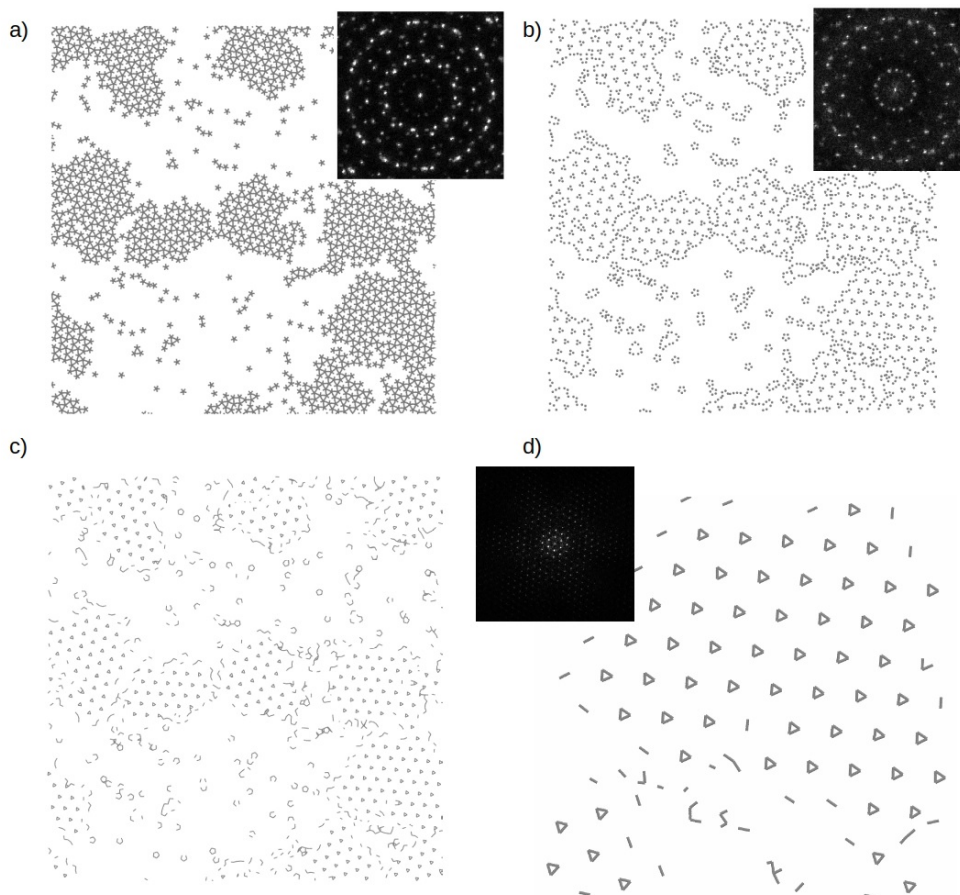


Figure 3.6: Parts (a) and (b) show configurations of the entire system for pentavalent molecules and non-associated terminal segments, respectively. Part (c) represents different graphical representations of part (b) whereas part (d) shows the magnified fragment. Diffraction patterns corresponding to each configurations are given in the insets.

However, in the case of a molecule with five arms, the behavior was completely different and the formation of a few differently oriented domains has been found. The obtained structure could only be characterized by the void analysis. It has shown that the cavities are arranged in a specific way. It could be observed that within the hollow space, triplets of non-associated arms were present and their center of mass formed a network of triangular symmetry (cf. Fig. 3.6).

The behavior of binary mixtures of tetra- and hexatopic precursors with linear linkers was nearly identical, compared to one-component systems, and the only differences were (i) increase of the cavity sizes and (ii) imperfections of the network, increasing with the number of linear molecules in the mixture.

In analogy to a single-component system, binary mixtures of pentavalent molecules with linear linkers are particularly worth highlighting. These systems form a unique network that resembles $3^2.4.3.4$ Archimedean tessellation. Since the structure is completely different we wanted to assess the origin of this behavior. We have changed the length of the linear linker to verify whether this structure emerges solely due to the presence of a second component or is caused by the increased interparticle distance. To inspect the latter, we have created also a pentatopic molecule with elongated arms and simulated it in a one-component system. As shown in Figure 3.7, for all linker lengths the same

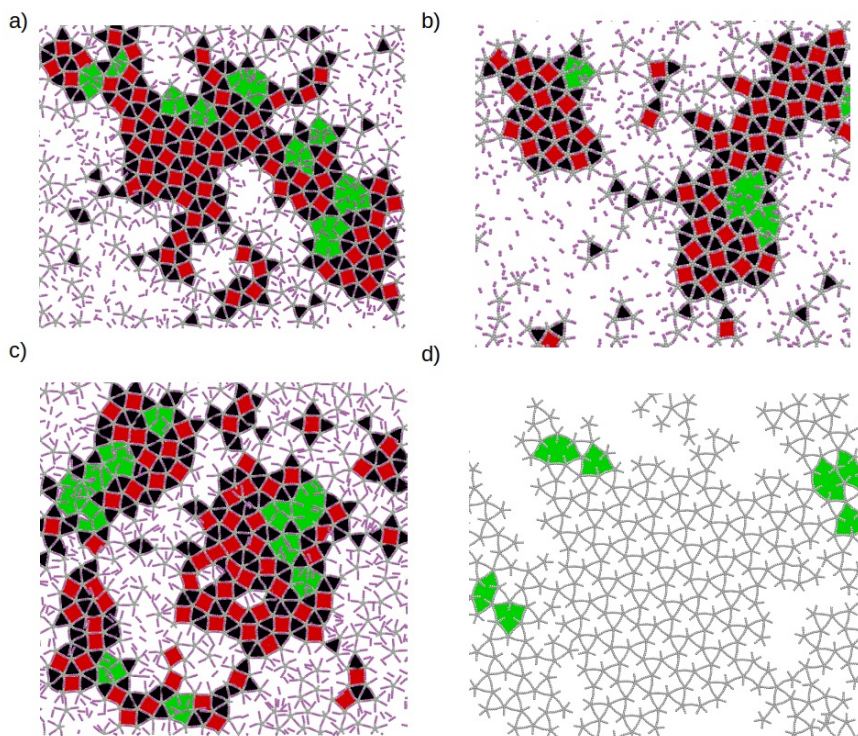


Figure 3.7: Parts (a-c) display configurations of binary mixtures for pentavalent molecules with linear linkers of 3 (a), 2 (b), and 4 (c) segments in backbone \mathbf{R} , respectively. Part (d) shows the fragment of configuration for a one-component system comprised of pentatopic molecules with elongated arms. Particular polygons belonging to Archimedean tiling are colored in red (squares) and black (triangles). The reminiscence of the one-component system is marked in green.

Archimedean tiling is present whereas a single-component system with longer arms still exhibits the same behavior as previously (cf. Fig. 3.6). Owing to the lack of qualitative difference between obtained structures in binary mixtures (Fig. 3.7a-c), the conclusion which naturally arises is that the length of the linker does not affect the formation of such an ordered phase and it is formed strictly due to the presence of the second component. Moreover, it can be assumed, that the linkers' mobility drives the self-assembly of the Archimedean tiling-like network in this system.

In the following paper **PVII**, simulations of tritopic molecules have been performed. Two molecular topologies have been studied, *i.e.* (i) with the same angle between all of the \mathbf{A} - \mathbf{C} arms ($\theta = 120^\circ$) and (ii) with angle $\theta = 60^\circ$ between \mathbf{A} , \mathbf{C} arms. Different directions of interparticle interactions as well as the number of segments in the arms have also been examined.

The formation of various ordered networks has been reported, depending on the molecular architecture. It has been shown that for the molecules with $\theta = 60^\circ$, the structures formed are almost identical and invariant of the topology or direction of interparticle interactions. However, for the molecules with $\theta = 120^\circ$ a variety of different phases have been observed and the rules governing the formation of distinct ordered networks have not been found due to the complexity of the phenomena.

For given cases, lattice Monte Carlo simulations have also been performed to check the compatibility of these methods. Unfortunately, in several situations, triangular lattice enforced the formation of other structures. Although the results were congruent with its symmetry they were not reproducible with the currently used molecular dynamics model.

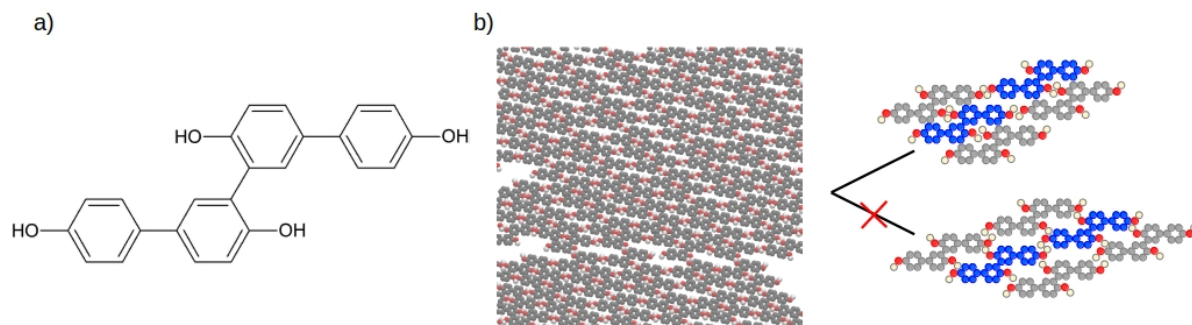


Figure 3.8: Part a) and b) display structural formula and fragment of configuration formed by compound **M1**, respectively. Schematically drawn association paths are shown on the right-hand side of panel b).

This situation should be particularly emphasized that lattice simulations should be only used as a preliminary tool for the investigation of any problem of interest.

The last stage of the investigations was devoted to extending the currently used coarse-grained model to the one that will be able to reflect molecular architectures of compounds of interest to a higher extent. In this respect, another model has been introduced. Briefly, in this representation, every atom has been distinguished, apart from -CH groups of benzene aromatic rings which were unified. The influence of both substitution position and the type of active groups on self-assembly has been assessed. Each of the four aromatic rings has been substituted by either -OH or -COOH groups. A more detailed description of the model can be found in Section 2 of **PVIII**.

Compound abbreviated as **M1** (cf. Fig. 3.8 a) have been already synthesized and crystal structure have been determined in our group (cf. paper 6 in Section 6.1). Therefore, the initial idea of the current study was to combine experimental and computer simulation results. Unfortunately, we did not manage to attain the results from scanning tunneling microscope in ultra-high vacuum conditions (UHV-STM) during the course of the dissertation, however the group of prof. M. Jałochowski from the Institute of Physics, UMCS is currently performing this kind of measurement on metallic surfaces. In this respect, we wanted to gain a preliminary insight into the possible on-surface behavior of the compound of interest as well as its derivatives. The first step involved quantum mechanic calculations which have shown that some of the model compounds could exist in the form of either of the two conformations. Specifically, the **M1** molecule was found to preferentially occur solely in one conformation named “zigzag”. Based on that, complementary molecular dynamics simulations have been performed. It turned out that the molecule **M1** forms solely one ordered network (cf. Fig 3.8 b) which is quite densely packed. On the right-hand side of this Figure, one can see a schematic representation of the ordering within this network. It can be seen that the resulting ordered phase forms dimers of hydroxyl groups of the same type (inner -Y and external -X substitution positions, cf. Fig. 1 in **PVIII**). Even though an alternate arrangement with disparately connected X-Y hydroxyl group types is also possible, it is not the case that has been demonstrated in radial distribution functions.

Chapter 4

Summary and conclusions

The dissertation concerned the study of various building blocks, possessing the ability to form self-assembled nanostructures by the means of computer simulations. The main method used was molecular dynamics, however, several complementary simulations using both lattice and off-lattice Monte Carlo have been performed.

A series of molecular architectures, as well as model parameters, have been introduced. Models proposed in the course of the dissertation proved to be able to both reflect already existing data and predict possible novel structures of potential interest. To gain a deeper insight into the self-organization process, a variety of structural parameters have been used to quantify given networks.

It has been proposed how a spherically-symmetric Lennard-Jones potential can be mapped onto an angular-dependent one just by the manipulation of the active site size and bond length l . We report that it can be reflected in the substitution of chemical compounds of similar geometry by such a group that is able to form dimers, trimers, etc. Due to this approach, the target design of desired ordered supramolecular networks can be performed in a much easier way and with a closer relation to the experimental findings. It is particularly worth highlighting that in the case of the simultaneous occurrence of two ordered phases a selectivity can be attained due to the procedure used.

Another noteworthy result is the introduction of a specific methodology on how to evaluate two-dimensional structure factors that correspond to the experimentally obtained diffraction patterns. It has been found that in the presence of more than one ordered network of the same kind but with different orientations, averaging of this parameter may result in the wrong interpretation of the outcome.

To summarize, the most pronounced results, found in the course of the dissertation studies are:

1. Presentation of the model for tetratopic building blocks which allows one to reflect experimental data as well as predict the existence of new ones.
2. Evaluation of the methodology for the analysis of two-dimensional structure factors to assess the type of order.
3. Display of how a spherically-symmetric Lennard-Jones potential can be mapped onto an angular-dependent one just by the manipulation of the active site size and bond length l .
4. Demonstration by the means of computer simulations that the tetratopic building blocks can form fractal networks (Sierpiński triangles) and structures resembling liquid crystals.

-
5. Presentation of two versions of the model for linear molecules which are (i) steering of the active site size/embedment and (ii) binary mixtures with “metal” atoms of different sizes.
 6. Extension of these models for other molecular geometries, *inter alia* V-shaped, penta-, hexatopic and their mixtures.
 7. Demonstration that the hollow spaces can be arranged in a specific manner that facilitates analysis of obtained ordered network.
 8. Evidence that the presence of the second component (linear linker) can be a driving force for the formation of Archimedean tessellation.
 9. A trial for the evaluation of a more “realistic” force field for tetratopic building blocks.

Chapter 5

Record for the doctoral thesis

5.1 Publications

PI **L. Baran**, D. Nieckarz, P. Szabelski, W. Rżysko, “*Controlling of the 2D Self-Assembly Process by the Variation of Molecular Geometry*”, Journal of Physical Chemistry C, 2019, **123**, 19549-19556.

IF₂₀₁₉=4.189, MEiN₂₀₁₉=140 pkt

PII **L. Baran**, “*Influence of the molecular geometry on the formation of the self-assembled structures*”, Journal of Molecular Liquids, 2019, **294**, 111627.

IF₂₀₁₉=5.065, MEiN₂₀₁₉=100 pkt

PIII **L. Baran**, W. Rżysko, “*Application of a coarse-grained model for the design of complex supramolecular networks*”, Molecular Systems Design & Engineering, 2020, **5**, 484-492.

IF₂₀₂₀=4.935, MEiN₂₀₂₀=20 pkt

PIV **L. Baran**, W. Rżysko, D. Tarasewicz, “*Variation of interaction zone size for the target design of 2D supramolecular networks*”, Molecular Systems Design & Engineering, 2021, **6**, 805-816.

IF₂₀₂₀=4.935, MEiN₂₀₂₀=20 pkt

PV **L. Baran**, *Coarse-Grained Modeling of On-Surface Self-Assembly of Mixtures Comprising Di-Substituted Polyphenyl-Like Compounds and Metal Atoms of Different Sizes*“, ACS Omega, 2021, **6**, 25193-25200.

IF₂₀₂₀=3.512, MEiN₂₀₂₀=70 pkt

PVI **L. Baran**, W. Rżysko, S. Szajnar, “*Archimedean Tessellation Found by the Variation of Building Blocks’ and Linkers’ Geometry: In Silico Investigations*“, Journal of Physical Chemistry C, 2020, **124**, 20101-20108.

IF₂₀₂₀=4.126, MEiN₂₀₂₀=140 pkt

PVII L. Baran, W. Rżysko, E. Słyk, "Simulations of the 2D self-assembly of tripod-shaped building blocks", Beilstein Journal of Nanotechnology, 2020 **11**, 884-890.

IF₂₀₂₀=2.612, MEiN₂₀₂₀=70 pkt

PVIII L. Baran, K. Dyk, D. M. Kamiński, M. Stankevič, W. Rżysko, D. Tarasewicz, T. Zientarski, "Influence of the substitution position in the tetratopic building blocks on the self-assembly process", Journal of Molecular Liquids, 2022, **346** 117074.

IF₂₀₂₀=6.165, MEiN₂₀₂₀=100 pkt

5.2 Grants

1. "Diamentowy Grant" funded by Polish Ministry of Science and Higher Education, **DI 2017 001147**

The person responsible: Łukasz Baran

Title: "Computer simulations of the self-assembly process of various molecules with diverse architecture on solid surfaces".

Total funding: 159 442 PLN

Supervisor: dr hab. Wojciech Rżysko

Realization time: 09.2018-09.2021

Chapter 6

The remaining record

6.1 Publications

1. **L. Baran**, S. Sokołowski, "A comparison of molecular dynamics results for two models of nanoparticles with fixed and mobile ligands in two-dimensions", Applied Surface Science, 2017, **396**, 1343-1351.

IF₂₀₁₇=5.155, MNiSW₂₀₁₇=35 pkt, MEiN₂₀₂₁=140 pkt

2. **L. Baran**, S. Sokołowski, "Effective interactions between a pair of particles modified with tethered chains", Journal of Chemical Physics, 2017, **147**, 044903.

IF₂₀₁₇=2.991, MNiSW₂₀₁₇=35 pkt, MEiN₂₀₂₁=140 pkt

3. **L. Baran**, M. Borówko, W. Rżysko, S. Sokołowski, "Self-organisation in two dimensional system involving patchy and isotropic disks", Molecular Physics, 2018, **117** 2802-2813.

IF₂₀₁₈=1.571, MNiSW₂₀₁₈=20 pkt, MEiN₂₀₂₁=70 pkt

4. **L. Baran**, M. Borówko, W. Rżysko, A. Patrykiewicz, "Self assembly of Janus disks confined in a slit", Journal of Chemical Physics, 2019, **151**, 104703.

IF₂₀₁₉=2.991, MEiN₂₀₁₉=100 pkt

5. **L. Baran**, M. Borówko, W. Rżysko, "Self-Assembly of Amphiphilic Janus Particles Confined between Two Solid Surfaces", Journal of Physical Chemistry C, 2020, **124**, 17556- 17565.

IF₂₀₂₀=4.126, MEiN₂₀₂₀=140 pkt

6. K. Dyk, **L. Baran**, W. Rżysko, M. Stankevic, D. M. Kamiński, "Interplay between the crystal stability and the energy of the molecular conformation", CrystEngComm, 2021, **23**, 2683-2694.

IF₂₀₂₀=3.545, MEiN₂₀₂₀=100 pkt

7. **L. Baran**, K. Dąbrowska, W. Rżysko, S. Sokołowski, "Molecular Dynamic study of model two-dimensional systems involving Janus dumbbells and spherical particles", Condensed Matter Physics 2021, **24**, 33401.

IF₂₀₂₀=1.128, MEiN₂₀₂₀=40 pkt

6.2 Grants

1. *PRELUDIUM 20* funded by National Science Centre, Poland, **2021/41/N/ST4/00437**
The person responsible: Łukasz Baran
Title: "Self-assembly of patchy nanoparticles under confinement"
Total funding: 146 400 PLN
Supervisor: Supervisor: dr hab. Wojciech Rżysko
Realization time: 01.2022-01.2025

6.3 Natonwide awards

1. Winner of Foundation for Polish Science START 2020 competition.
2. Polish Ministry of Science and Higher Education scholarship - 2017/2018.
3. Finalist of "Złoty Medal Chemii" competition organized by IChF PAN in Warsaw.

6.4 Other awards

1. Rector scholarship for the best doctoral candidates obtained in 2018/2019; 2019/2020; 2020/2021; 2021/2022.
2. Scholarship from the Own Scholarship Fund obtained in 2018/2019; 2019/2020; 2020/2021; 2021/2022.

6.5 Internships

1. Internship at the Faculty of Chemistry, Complutense University in Madrid, Spain, in the group "Computer Simulations of Interfaces" led by prof. Luis G. MacDowell.
Period: 21.06-20.12.2021

6.6 Conferences

1. Oral presentation "Variation of interaction zone size for the target design of 2D supramolecular networks" at VI Workshop Red Espanola de Simulacion Molecular, Baiona, Spain 4-6th of October 2021.
2. Poster presentation "Hierarchical self-assembly of tetratopic building blocks" at 11th Liquid Matter Conference 2020/2021, Online Conference, 19th-23rd of July 2021.

3. Poster presentation "*Formation of Archimedean Tessellation Found in the Mixtures of Pentatopic and Linear Molecules*" at SmallChem2021 International Online Conference, 17-18th of February 2021.
4. Poster presentation "*Prediction of self-assembled structures by means of off- lattice Monte Carlo and Molecular Dynamics methods*" at 39th International Conference and CCP5 Annual General Meeting 2019. Advances in Simulations and Theory of Matter, London, United Kingdom 16-18 of September 2019.
5. Poster presentation "*Molecular networks formed on the solid surfaces - insight from computer simulations*" at CCP5 Summer School, Durham, United Kingdom, 8-18th of July 2019.
6. Poster presentation "*Formation of self-assembled structures on solid surfaces - insights from molecular dynamics simulations*" at European Student Colloid Conference, Varna, Bulgaria, 18th-22nd of June 2019.
7. Poster presentation "*The self-assembly process of organic compounds with different architecture in two-dimensional systems*" at Sixteenth Polish-Ukrainian Symposium on Theoretical and Experimental Studies of Interfacial Phenomena and Their Technological Applications, Lublin, Poland, 28th-31st of August 2018.
8. Oral presentation "*Zastosowanie dynamiki molekularnej w symulacjach nanocząstek*" at 60th Zjeździe Naukowym Polskiego Towarzystwa Chemicznego, Wrocław, Poland, 17th-21st of September 2017.

6.7 Bibliometric parameters

	Number of citations	Number of citations (no autocitations)	Hirsch index
Scopus	60	36	5
Web of Science	59	35	5

Chapter 7

Bibliography

- ¹ S. R. White, N. R. Sottos, P. H. Geubelle, J. S. Moore, M. R. Kessler, S. R. Sriram, E. N. Brown, and S. Viswanathan, “Autonomic healing of polymer composites,” *Nature*, vol. 409, pp. 794–797, Feb 2001.
- ² V. L. Colvin, “From opals to optics: Colloidal photonic crystals,” *MRS Bulletin*, vol. 26, pp. 637–641, Aug 2001.
- ³ H. Stoyanov, M. Kolloosche, S. Risse, R. Waché, and G. Kofod, “Soft conductive elastomer materials for stretchable electronics and voltage controlled artificial muscles,” *Advanced Materials*, vol. 25, no. 4, pp. 578–583, 2013.
- ⁴ M. D. Lima, N. Li, M. J. de Andrade, S. Fang, J. Oh, G. M. Spinks, M. E. Kozlov, C. S. Haines, D. Suh, J. Foroughi, S. J. Kim, Y. Chen, T. Ware, M. K. Shin, L. D. Machado, A. F. Fonseca, J. D. W. Madden, W. E. Voit, D. S. Galvão, and R. H. Baughman, “Electrically, chemically, and photonically powered torsional and tensile actuation of hybrid carbon nanotube yarn muscles,” *Science*, vol. 338, no. 6109, pp. 928–932, 2012.
- ⁵ C. Zhang, B.-H. Wu, M.-Q. Ma, Z. Wang, and Z.-K. Xu, “Ultrathin metal/covalent–organic framework membranes towards ultimate separation,” *Chem. Soc. Rev.*, vol. 48, pp. 3811–3841, 2019.
- ⁶ S. Wang, Q. Wang, P. Shao, Y. Han, X. Gao, L. Ma, S. Yuan, X. Ma, J. Zhou, X. Feng, and B. Wang, “Exfoliation of covalent organic frameworks into few-layer redox-active nanosheets as cathode materials for lithium-ion batteries,” *Journal of the American Chemical Society*, vol. 139, no. 12, pp. 4258–4261, 2017. PMID: 28316238.
- ⁷ G. Li, K. Zhang, and T. Tsuru, “Two-dimensional covalent organic framework (cof) membranes fabricated via the assembly of exfoliated cof nanosheets,” *ACS Applied Materials & Interfaces*, vol. 9, no. 10, pp. 8433–8436, 2017. PMID: 28248482.
- ⁸ J. V. Barth, “Molecular architectonic on metal surfaces,” *Annual Review of Physical Chemistry*, vol. 58, no. 1, pp. 375–407, 2007. PMID: 17430091.
- ⁹ S. Clair and D. G. de Oteyza, “Controlling a chemical coupling reaction on a surface: Tools and strategies for on-surface synthesis,” *Chemical Reviews*, vol. 119, no. 7, pp. 4717–4776, 2019. PMID: 30875199.
- ¹⁰ W. Auwärter, D. Écija, F. Klappenberger, and J. V. Barth, “Porphyrins at interfaces,” *Nature Chemistry*, vol. 7, pp. 105–120, Feb 2015.

-
- ¹¹ X. Zhang, Q. Zeng, and C. Wang, "Molecular templates and nano-reactors: two-dimensional hydrogen bonded supramolecular networks on solid/liquid interfaces," *RSC Adv.*, vol. 3, pp. 11351–11366, 2013.
- ¹² X. Zhang, Q. Zeng, and C. Wang, "On-surface single molecule synthesis chemistry: a promising bottom-up approach towards functional surfaces," *Nanoscale*, vol. 5, pp. 8269–8287, 2013.
- ¹³ D. Heim, K. Seufert, W. Auwärter, C. Aurisicchio, C. Fabbro, D. Bonifazi, and J. V. Barth, "Surface-assisted assembly of discrete porphyrin-based cyclic supramolecules," *Nano Letters*, vol. 10, no. 1, pp. 122–128, 2010. PMID: 19888718.
- ¹⁴ T. Kudernac, S. Lei, J. A. A. W. Elemans, and S. De Feyter, "Two-dimensional supramolecular self-assembly: nanoporous networks on surfaces," *Chem. Soc. Rev.*, vol. 38, pp. 402–421, 2009.
- ¹⁵ D. Ćija, J. I. Urgel, A. C. Papageorgiou, S. Joshi, W. Auwärter, A. P. Seitsonen, S. Klyatskaya, M. Ruben, S. Fischer, S. Vijayaraghavan, J. Reichert, and J. V. Barth, "Five-vertex archimedean surface tessellation by lanthanide-directed molecular self-assembly," *Proceedings of the National Academy of Sciences*, vol. 110, no. 17, pp. 6678–6681, 2013.
- ¹⁶ J. P. Garrahan, A. Stannard, M. O. Blunt, and P. H. Beton, "Molecular random tilings as glasses," *Proceedings of the National Academy of Sciences*, vol. 106, no. 36, pp. 15209–15213, 2009.
- ¹⁷ A. Ciesielski, P. J. Szabelski, W. Rzyśko, A. Cadeddu, T. R. Cook, P. J. Stang, and P. Samorì, "Concentration-dependent supramolecular engineering of hydrogen-bonded nanostructures at surfaces: Predicting self-assembly in 2d," *Journal of the American Chemical Society*, vol. 135, no. 18, pp. 6942–6950, 2013. PMID: 23590179.
- ¹⁸ J. Shang, Y. Wang, M. Chen, J. Dai, X. Zhou, J. Kuttner, G. Hilt, X. Shao, J. M. Gottfried, and K. Wu, "Assembling molecular sierpiński triangle fractals," *Nature Chemistry*, vol. 7, pp. 389–393, May 2015.
- ¹⁹ Q. Fan, C. Wang, Y. Han, J. Zhu, J. Kuttner, G. Hilt, and J. M. Gottfried, "Surface-assisted formation, assembly, and dynamics of planar organometallic macrocycles and zigzag shaped polymer chains with c–cu–c bonds," *ACS Nano*, vol. 8, no. 1, pp. 709–718, 2014. PMID: 24328267.
- ²⁰ K. Tahara, C. A. Johnson, T. Fujita, M. Sonoda, F. C. De Schryver, S. De Feyter, M. M. Haley, and Y. Tobe, "Synthesis of dehydrobenzo[18]annulene derivatives and formation of self-assembled monolayers: implications of core size on alkyl chain interdigitation," *Langmuir*, vol. 23, no. 20, pp. 10190–10197, 2007. PMID: 17760473.
- ²¹ H. Zhou, H. Dang, J.-H. Yi, A. Nanci, A. Rochefort, and J. D. Wuest, "Frustrated 2d molecular crystallization," *Journal of the American Chemical Society*, vol. 129, no. 45, pp. 13774–13775, 2007. PMID: 17948995.
- ²² M. Ammon, T. Sander, and S. Maier, "On-surface synthesis of porous carbon nanoribbons from polymer chains," *Journal of the American Chemical Society*, vol. 139, no. 37, pp. 12976–12984, 2017. PMID: 28820266.

-
- ²³ R. Gutzler, L. Cardenas, J. Lipton-Duffin, M. El Garah, L. E. Dinca, C. E. Szakacs, C. Fu, M. Gallagher, M. Vondráček, M. Rybachuk, D. F. Perepichka, and F. Rosei, “Ullmann-type coupling of brominated tetrathienoanthracene on copper and silver,” *Nanoscale*, vol. 6, pp. 2660–2668, 2014.
- ²⁴ A. M. Bragança, B. E. Hirsch, A. Sanz-Matias, Y. Hu, P. Walke, K. Tahara, J. N. Harvey, Y. Tobe, and S. De Feyter, “How does chemisorption impact physisorption? molecular view of defect incorporation and perturbation of two-dimensional self-assembly,” *The Journal of Physical Chemistry C*, vol. 122, no. 42, pp. 24046–24054, 2018.
- ²⁵ Z. Tao, T. Wang, D. Wu, L. Feng, J. Huang, X. Wu, and J. Zhu, “Construction of molecular regular tessellations on a cu(111) surface,” *Chem. Commun.*, vol. 54, pp. 7010–7013, 2018.
- ²⁶ M. O. Blunt, J. C. Russell, M. d. C. Gimenez-Lopez, N. Taleb, X. Lin, M. Schröder, N. R. Champness, and P. H. Beton, “Guest-induced growth of a surface-based supramolecular bilayer,” *Nature Chemistry*, vol. 3, pp. 74–78, Jan 2011.
- ²⁷ S. Stepanow, N. Lin, D. Payer, U. Schlickum, F. Klappenberger, G. Zoppellaro, M. Ruben, H. Brune, J. Barth, and K. Kern, “Surface-assisted assembly of 2d metal–organic networks that exhibit unusual threefold coordination symmetry,” *Angewandte Chemie International Edition*, vol. 46, no. 5, pp. 710–713, 2007.
- ²⁸ Y. Okuno, T. Yokoyama, S. Yokoyama, T. Kamikado, and S. Mashiko, “Theoretical study of benzonitrile clusters in the gas phase and their adsorption onto a au(111) surface,” *Journal of the American Chemical Society*, vol. 124, no. 24, pp. 7218–7225, 2002. PMID: 12059248.
- ²⁹ U. Schlickum, R. Decker, F. Klappenberger, G. Zoppellaro, S. Klyatskaya, W. Auwärter, S. Neppel, K. Kern, H. Brune, M. Ruben, and J. V. Barth, “Chiral kagomé lattice from simple ditopic molecular bricks,” *Journal of the American Chemical Society*, vol. 130, no. 35, pp. 11778–11782, 2008. PMID: 18693686.
- ³⁰ M. O. Blunt, J. C. Russell, M. del Carmen Giménez-López, J. P. Garrahan, X. Lin, M. Schröder, N. R. Champness, and P. H. Beton, “Random tiling and topological defects in a two-dimensional molecular network,” *Science*, vol. 322, no. 5904, pp. 1077–1081, 2008.
- ³¹ A. Stannard, J. C. Russell, M. O. Blunt, C. Salesiotis, M. d. C. Giménez-López, N. Taleb, M. Schröder, N. R. Champness, J. P. Garrahan, and P. H. Beton, “Broken symmetry and the variation of critical properties in the phase behaviour of supramolecular rhombus tilings,” *Nature Chemistry*, vol. 4, pp. 112–117, Feb 2012.
- ³² J. Adisojojoso, K. Tahara, S. Lei, P. Szabelski, W. Rzyśko, K. Inukai, M. O. Blunt, Y. Tobe, and S. De Feyter, “One building block, two different nanoporous self-assembled monolayers: A combined stm and monte carlo study,” *ACS Nano*, vol. 6, no. 1, pp. 897–903, 2012. PMID: 22206261.
- ³³ M. A. González and J. L. F. Abascal, “The shear viscosity of rigid water models,” *The Journal of Chemical Physics*, vol. 132, no. 9, p. 096101, 2010.
- ³⁴ C. Vega and E. de Miguel, “Surface tension of the most popular models of water by using the test-area simulation method,” *The Journal of Chemical Physics*, vol. 126, no. 15, p. 154707, 2007.

-
- ³⁵ C.-A. Palma, P. Samorì, and M. Cecchini, “Atomistic simulations of 2d bicomponent self-assembly: From molecular recognition to self-healing,” *Journal of the American Chemical Society*, vol. 132, no. 50, pp. 17880–17885, 2010. PMID: 21114285.
- ³⁶ Y. Zhao and J. Wang, “How to obtain high-quality and high-stability interfacial organic layer: Insights from the ptcda self-assembly,” *The Journal of Physical Chemistry C*, vol. 121, no. 8, pp. 4488–4495, 2017.
- ³⁷ W. C. Swope, H. C. Andersen, P. H. Berens, and K. R. Wilson, “A computer simulation method for the calculation of equilibrium constants for the formation of physical clusters of molecules: Application to small water clusters,” *The Journal of Chemical Physics*, vol. 76, no. 1, pp. 637–649, 1982.
- ³⁸ H. J. C. Berendsen, J. P. M. Postma, W. F. van Gunsteren, A. DiNola, and J. R. Haak, “Molecular dynamics with coupling to an external bath,” *The Journal of Chemical Physics*, vol. 81, no. 8, pp. 3684–3690, 1984.
- ³⁹ G. J. Martyna, M. L. Klein, and M. Tuckerman, “Nosé–hoover chains: The canonical ensemble via continuous dynamics,” *The Journal of Chemical Physics*, vol. 97, no. 4, pp. 2635–2643, 1992.
- ⁴⁰ G. J. Martyna, M. E. Tuckerman, D. J. Tobias, and M. L. Klein, “Explicit reversible integrators for extended systems dynamics,” *Molecular Physics*, vol. 87, no. 5, pp. 1117–1157, 1996.
- ⁴¹ S. Nosé, “A unified formulation of the constant temperature molecular dynamics methods,” *The Journal of Chemical Physics*, vol. 81, no. 1, pp. 511–519, 1984.
- ⁴² W. G. Hoover, “Canonical dynamics: Equilibrium phase-space distributions,” *Phys. Rev. A*, vol. 31, pp. 1695–1697, Mar 1985.
- ⁴³ J. W. Tester and M. Modell, *Thermodynamics and Its Applications, 3rd Edition*. New Jersey: Prentice Hall, 1997.
- ⁴⁴ H. Weber, D. Marx, and K. Binder, “Melting transition in two dimensions: A finite-size scaling analysis of bond-orientational order in hard disks,” *Phys. Rev. B*, vol. 51, pp. 14636–14651, May 1995.
- ⁴⁵ B. I. Halperin and D. R. Nelson, “Theory of two-dimensional melting,” *Phys. Rev. Lett.*, vol. 41, pp. 121–124, Jul 1978.
- ⁴⁶ G. Singh, M. Fisch, and S. Kumar, “Emissivity and electrooptical properties of semi-conducting quantum dots/rods and liquid crystal composites: a review,” *Reports on Progress in Physics*, vol. 79, p. 056502, apr 2016.
- ⁴⁷ D. Frenkel and R. Eppenga, “Evidence for algebraic orientational order in a two-dimensional hard-core nematic,” *Phys. Rev. A*, vol. 31, pp. 1776–1787, Mar 1985.
- ⁴⁸ U. Fabbri and C. Zannoni, “A monte carlo investigation of the lebwohl-lasher lattice model in the vicinity of its orientational phase transition,” *Molecular Physics*, vol. 58, no. 4, pp. 763–788, 1986.
- ⁴⁹ D. N. Theodorou and U. W. Suter, “Shape of unperturbed linear polymers: polypropylene,” *Macromolecules*, vol. 18, no. 6, pp. 1206–1214, 1985.

-
- ⁵⁰ M. Rovere, D. W. Hermann, and K. Binder, “Block density distribution function analysis of two-dimensional lennard-jones fluids,” *Europhysics Letters (EPL)*, vol. 6, pp. 585–590, aug 1988.
- ⁵¹ P. J. Steinhardt, D. R. Nelson, and M. Ronchetti, “Bond-orientational order in liquids and glasses,” *Phys. Rev. B*, vol. 28, pp. 784–805, Jul 1983.
- ⁵² P. Rein ten Wolde, M. J. Ruiz-Montero, and D. Frenkel, “Numerical calculation of the rate of crystal nucleation in a lennard-jones system at moderate undercooling,” *The Journal of Chemical Physics*, vol. 104, no. 24, pp. 9932–9947, 1996.
- ⁵³ W. Lechner and C. Dellago, “Accurate determination of crystal structures based on averaged local bond order parameters,” *The Journal of Chemical Physics*, vol. 129, no. 11, p. 114707, 2008.
- ⁵⁴ F. Romano, E. Sanz, and F. Sciortino, “Crystallization of tetrahedral patchy particles in silico,” *The Journal of Chemical Physics*, vol. 134, no. 17, p. 174502, 2011.
- ⁵⁵ A. H. Nguyen and V. Molinero, “Identification of clathrate hydrates, hexagonal ice, cubic ice, and liquid water in simulations: the chill+ algorithm,” *The Journal of Physical Chemistry B*, vol. 119, no. 29, pp. 9369–9376, 2015. PMID: 25389702.
- ⁵⁶ Ł. Baran, M. Borówko, and W. Rżysko, “Self-assembly of amphiphilic janus particles confined between two solid surfaces,” *The Journal of Physical Chemistry C*, vol. 124, no. 32, pp. 17556–17565, 2020.
- ⁵⁷ S. Toxvaerd and J. C. Dyre, “Communication: Shifted forces in molecular dynamics,” *The Journal of Chemical Physics*, vol. 134, no. 8, p. 081102, 2011.
- ⁵⁸ W. Rżysko and A. Trokhymchuk, “Vapor-liquid coexistence in 2d square-well fluid with variable range of attraction: Monte carlo simulation study,” *The Journal of Chemical Physics*, vol. 137, no. 22, p. 224505, 2012.
- ⁵⁹ P. Bolhuis, M. Hagen, and D. Frenkel, “Isostructural solid-solid transition in crystalline systems with short-ranged interaction,” *Phys. Rev. E*, vol. 50, pp. 4880–4890, Dec 1994.
- ⁶⁰ A. P. Thompson, H. M. Aktulga, R. Berger, D. S. Bolintineanu, W. M. Brown, P. S. Crozier, P. J. in ’t Veld, A. Kohlmeyer, S. G. Moore, T. D. Nguyen, R. Shan, M. J. Stevens, J. Tranchida, C. Trott, and S. J. Plimpton, “LAMMPS - a flexible simulation tool for particle-based materials modeling at the atomic, meso, and continuum scales,” *Comp. Phys. Comm.*, vol. 271, p. 108171, 2022.
- ⁶¹ J. Li, B. Tu, X. Li, C. Ma, C. Chen, W. Duan, X. Xiao, and Q. Zeng, “Self-assembled flower structures formed by c3-symmetric aromatic carboxylic acids with meta-carboxyl groups,” *Chem. Commun.*, vol. 55, pp. 11599–11602, 2019.
- ⁶² Y. V. Kalyuzhnyi and P. T. Cummings, “Two-patch colloidal model with re-entrant phase behaviour,” *The Journal of Chemical Physics*, vol. 139, no. 10, p. 104905, 2013.
- ⁶³ Y. Mo, T. Chen, J. Dai, K. Wu, and D. Wang, “On-surface synthesis of highly ordered covalent sierpiński triangle fractals,” *Journal of the American Chemical Society*, vol. 141, no. 29, pp. 11378–11382, 2019. PMID: 31288514.
- ⁶⁴ J. I. Urgel, D. Écija, G. Lyu, R. Zhang, C.-A. Palma, W. Auwärter, N. Lin, and J. V. Barth, “Quasicrystallinity expressed in two-dimensional coordination networks,” *Nature Chemistry*, vol. 8, pp. 657–662, Jul 2016.

Attachments

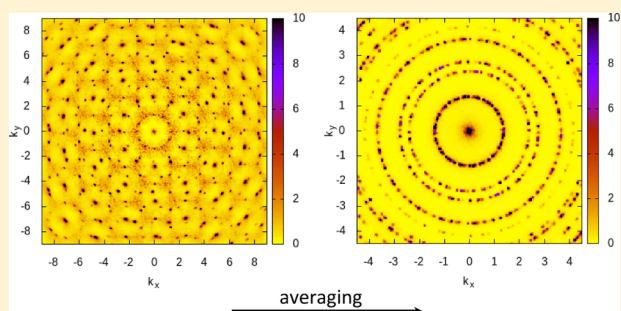
Controlling of the 2D Self-Assembly Process by the Variation of Molecular Geometry

L. Baran,^{*,†} D. Nieckarz,[‡] P. Szabelski,^{‡,§} and W. Rzyśko[†]

[†]Department for the Modelling of Physico-Chemical Processes and [‡]Department of Theoretical Chemistry, Maria Curie Skłodowska University, Lublin 20-031, Poland

Supporting Information

ABSTRACT: In this paper, we check how the molecular architecture influences the self-assembly process of tetrapod molecules. These particles were built of the linear core and four attached arms. For this purpose, we employ molecular dynamics simulation together with the lattice Monte Carlo method to investigate the formation of supramolecular networks. To characterize them, we evaluated structure parameters such as distribution of the core–core angle, average degree of association, and theoretical diffractograms. Moreover, we conclude that for the latter parameter, the influence of the rotation of differently oriented domains may lead to wrong interpretation of results.



INTRODUCTION

Directed self-assembly of functional molecular units has been recently recognized as a promising method to fabricate low-dimensional structures with tunable architectures and functions. In this field, the on-surface self-assembly involving weak molecular interactions, such as hydrogen^{1,2} and halogen bonding,^{3,4} metal–organic ligand coordination,^{5,6} and van der Waals forces⁷ has been frequently used to create diverse supramolecular structures, ranging from small-molecular aggregates⁸ to extended porous networks.⁹ This synthetic approach has been also adopted in the polymerization of functional monomers adsorbed on⁸ catalytically active metallic supports (Cu, Ag, and Au), where covalent bonding results in persistent molecular constructs, including carbon nanoribbons, nanoflakes, wires, and cyclic polymers.^{10–12} The methods of creation of the surface-confined molecular connections have been particularly attractive, as they often produce new nanostructures which are hardly or not obtainable with bulk synthesis. Moreover, those nanostructures can have special electronic, optical, catalytic, and so forth properties which increase their application potential in nanotechnology and material engineering.

An important factor which facilitates the self-assembly in adsorbed overlayers is the spatial confinement reducing substantial translational and rotational freedom of the admolecules. In this case, effective intermolecular contacts, resulting in a stabilizing interaction or a covalent bond, are enhanced, as the molecules can easily position/orient appropriately, required for the interaction or bonding. To create an adsorbed molecular structure using this beneficial effect, it is thus necessary to select a molecular building block having suitable structural features and functionality. This refers

especially to molecular size, shape, and intramolecular distribution of functional groups (active centers). As it has been demonstrated in numerous experimental studies, manipulation of these factors is an useful way to direct the self-assembly/polymerization toward molecular superstructures with predefined properties.^{1–12}

Among various functional building blocks used in the 2D self-assembly, the star-shaped molecules bearing terminal active centers have been recently used to create on-surface structures with diverse geometry and connectivity, in ultrahigh vacuum and at the liquid/solid interface. One of such building blocks is the tetrapod functional units equipped with arms having terminal aldehyde and carboxylic groups.^{13–15} In the case of the on-surface polymerization, the molecular arms have been usually terminated with halogen atoms, so that the tetrapod monomers were covalently bonded via the Ullmann coupling reaction.¹⁶ As it has been observed in the experiment, molecules such as >-<-shaped tetracarboxylic acids are able to form extended porous networks with diverse morphologies. For example, dichotomous self-assembly producing Kagomé and brickwall porous phases has been observed for tetracarboxylic acid molecules adsorbed at the liquid phase/graphite interface.^{13,14} Moreover, when analogous building blocks with an altered aspect ratio (shorter linear core) were used, the self-assembly produced one glassy network with regular hexagonal pores but with aperiodic spatial distribution of the interacting molecules.^{13,14} These findings highlight the role of shape and size of a tetrapod functional unit in the

Received: May 1, 2019

Revised: July 20, 2019

Published: July 22, 2019

creation of the corresponding low-dimensional structures. Careful tuning of the structural molecular parameters is thus an efficient way to direct the 2D self-assembly of organic tectons such as the tetrapod molecules.

As test 2D self-assembly experiments usually require probe tetrapod units differing in size/shape/functionality, these molecules have to be synthesized, and the corresponding STM imaging has to be performed in each case. An useful way to reduce time and resources associated with these efforts has been the computer simulations. In the computer-based modeling techniques molecular parameters can be easily modified, so that a large pool of candidate building blocks can be screened, aiming at the selection of the optimal molecule able to form the 2D superstructure with presumed properties (porosity, periodicity, etc.). This refers to the Monte Carlo (MC) calculations^{2,17–21} and molecular dynamics (MD) simulations^{22–25} which have been successfully used to model the self-assembly of functional molecules on solid substrates. In our previous studies, we used first of these methods to predict the structure formation in the overlayers comprising tripod and tetrapod tectons with different sizes²⁶ and backbone aspect ratio.²⁷ Our studies demonstrated the formation of diverse 2D superstructures ranging from chains, ladders, clusters, and porous periodic and aperiodic networks comprising void spaces whose size and shape was determined by the intrinsic structural properties of the building blocks at play.

To further explore the possibility of tuning the structure of 2D networks by manipulating properties of the contributing molecular tectons, in this study, we use MD simulations and compare the predicted assemblies with their selected counterparts obtained with the MC method. To that end, a series of tetrapod molecular building blocks with adjustable shape proportions is studied, and the obtained superstructures are characterized in detail using distribution functions of selected structural parameters. Moreover, theoretically predicted diffraction patterns of these 2D assemblies are provided to refine and complement the gathered structural information.

METHODS

The molecules used in this study comprised a few interconnected segments (disks) forming the tetrapod planar structures, of which one example is shown in Figure 1. The contributing backbone segments, N_b , of diameter $\sigma_b = \sigma$ with σ being the unit length, were tangentially joined, and their number was selected based on the assumed molecular size and aspect ratio. Specifically, in these building blocks, two main structural elements can be distinguished, namely, the linear molecular core and four attached arms of equal length, with the side arms meeting at an angle of $\theta = 120^\circ$ (see Figure 1). The size of these elements can be expressed in the number of segments of the core (N_C) and the arm (N_A), or alternatively described by the distances, d_1 and d_2 shown in Figure 1. In the latter case, d_2 , we are dealing with the sum of lengths of two collinearly aligned molecular arms and the distance between the contacting terminal arm segments. As we will show later, using the adjustable parameters, d_1 and d_2 are particularly convenient to establish the structure–property in the modeled systems.^{13,14} To encode intermolecular interactions in the tetrapod tectons, we assumed that the terminal arm segments were active, that is, they were equipped with discrete interaction centers (active centers), denoted by a (Figure 1c). This approach corresponds, for example, to the end-functionalization of the arms of a polyaromatic tetrapod

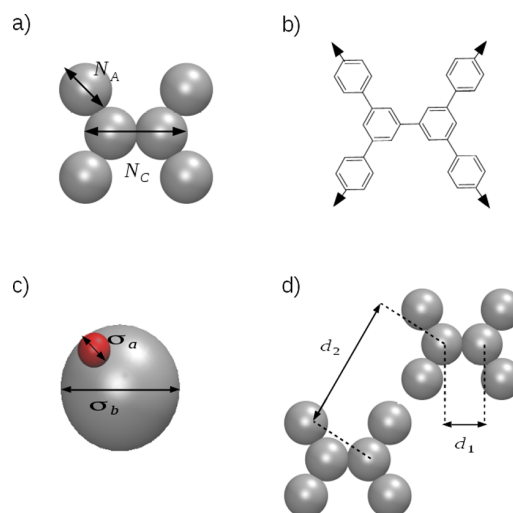


Figure 1. Part (a) displays the tetrapod molecule, where N_C and N_A are equal to the length of the core and arm respectively. Part (b) shows a schematic representation of the chemical compound, which could correspond to our model. The arrows show the terminal direction of interparticle interactions. Part (c) displays the terminal arm segment (silver) and entirely embedded active site (red). The diameter of the backbone and active sites were equal to σ_b and σ_a , respectively. Finally, part (d) displays how the d_1 and d_2 distances were evaluated.

backbone using chemically different groups, including carboxylic, aldehyde, and others.^{13–15} In this view, each benzene segment of the model tecton can represent one benzene ring and the functional groups; according to the assumed interaction pattern, it was attached in the para position (see Figure 1b). The interaction centers, mimicking the presence of the functional para substituents, were represented by small circular zones of diameter $\sigma_a = 0.2\sigma$ buried inside the terminal segments at the distance $l = 0.4\sigma$ from the segment center (see Figure 1c). The abovementioned condition means that the active centers are entirely embedded in the terminal segments, and the main purpose for this assumption was the reduction of the angular diameter of the effective interaction zone. In this way, it was possible to model highly directional intermolecular interactions, such as, for example, the hydrogen bonding between terminal functional groups of tetrapod tetracarboxylic acids.

All of the intermolecular interactions were modeled using the Lennard-Jones (12,6) potential

$$u_{kl}(r) = \begin{cases} 4\epsilon_{kl}[(\sigma_{kl}/r)^{12} - (\sigma_{kl}/r)^6] & r < r_{\text{cut},kl} \\ 0 & \text{otherwise} \end{cases} \quad (1)$$

where $kl = bb, ab, aa$; r is the distance between interacting species. The parameters σ in the above equation were calculated using the conventional Lorentz–Berthelot mixing rule, that is, $\sigma_{kl} = (\sigma_k + \sigma_l)/2$, while the energy parameters were $\epsilon_{bb} = \epsilon_{ab} = \epsilon$ and $\epsilon_{aa} = 5\epsilon$, where ϵ is the unit of energy. The increased value of the energy of interaction between the active centers (5ϵ) was assumed to reflect the dominant role of the terminal functional groups in the formation of short-range directional bonds between the adsorbed tetrapods. The cut-off parameters $r_{c,ij}$ were equal to σ_{ij} for $ij = ab, bb$, meaning a simple size-exclusion condition and to $2\sigma_{aa}$ in the case of the interaction between a pair of the active sites. To maintain rigidity of the model tetrapod building blocks, distances

between the composite segments (and the active site) were fixed by imposing the harmonic potentials:

$$u_{bb} = k_{bb}(r - \sigma_{bb})^2 \quad (2)$$

and

$$u_{ab} = k_{ab}(r - \sigma_{ab})^2 \quad (3)$$

and similarly for the angles between these components

$$u_{ij}(\theta_{ij}) = k_{\theta}(\theta_{ij} - \theta_{0,ij})^2 \quad (4)$$

where $\theta_{0,ij}$ is an actual angle between segments i and j , and θ_{ij} is the reference angle corresponding to the assumed molecular geometry (see Figure 1). The values of the potential constants in eqs 2–4 were set large enough to make the molecules stiff, namely, k_{bb} and k_{ab} were both set equal to $1000\epsilon/\sigma^2$, and k_{θ} was equal to $1000\epsilon/(\text{radian}^2)$. Each of the backbone segments (N_b) had unit mass m , and the reduced time, density, and temperature were expressed as $\tau^* = t\sqrt{\epsilon/m\sigma^2}$, $\rho^* = \rho\sigma^2/\epsilon$, $T^* = kT/\epsilon_{aa}$. The meaning of the latter is that we wanted to employ the temperature scale, which is independent on the energy of association ϵ_{aa} . The mass of the small active center was assumed to be five times smaller than m .

All of the MD simulations described in this work were performed using the LAMMPS package.^{28,29} Starting molecular configurations were prepared by distributing 2500 tetrapod tectons in a square lattice in the simulation box, size of which was adjusted using the Berendsen barostat to obtain the assumed reduced density. Accordingly, the total number of segments in the simulation box varied depending on the size/shape of the tetrapod tecton. The simulations were run using the Berendsen thermostat with the damping constant $\tau_B^* = 10\tau^*$ along with the isokinetic temperature rescaling ($\tau_{ik}^* = 1000\tau^*$) to eliminate the temperature drift. The reduced time step was of the order of $0.001\tau^*$, and the equilibration was carried out for at least 10^8 time steps. Additionally, at least 20 replicas of each modeled system were produced for averaging purposes, differing by the starting configuration. The modeled molecular assemblies were gradually heated up and subsequently cooled down to obtain representative results. Production runs lasted for at least 10^7 time steps. During this final stage, various structural parameters were calculated, including distributions of molecular orientation and diffraction patterns for each well-defined phase. Additionally, the average association number and radial distribution functions were determined.

RESULTS AND DISCUSSION

To study the 2D self-assembly of the tetrapod molecules, we first tested the smallest tecton sketched in Figure 1a and characterized by the parameters $d_1 = 1$ ($N_C = 2$) and $d_2 = 3$ ($N_A = 1$). This building block is further called 1|3, and similar abbreviation ($d_1|d_2$) is consequently used for the larger molecules. Figure 2 shows two extended porous phases which were observed in the simulations with the 1|3 building block at $T^* = 0.1$ and $\rho^* = 0.2591$. In the case of the first phase, the molecules form brickwall-like network in which they are fully coordinated, that is, each molecule has four interacting neighbors. A closer inspection of this phase reveals that it is aperiodic and comprises tetragonal pores differing in shape. The possible shapes of these pores are dictated by the relative orientation of the four contributing molecules. The resulting

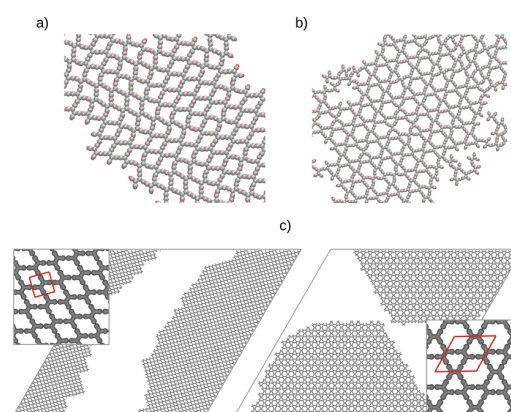


Figure 2. Part (a) brickwall phase, part (b) Kagomé network, and (c) lattice MC results. Snapshots are obtained in the density $\rho^* = 0.25907$ at temperature $T^* = 0.1$.

network is a collection of (randomly) interconnected pores of the four types (see Figure S1 in the Supporting Information). Interestingly, this brickwall-type structure is continuous, and no vacancy defects were observed. The second structural type shown in Figure 2b corresponds to the trihexagonal tiling called also the Kagomé network. In this case, we are dealing with pores of two types, including the smaller triangular-shaped and larger hexagonal-shaped void spaces. An interesting property of the Kagomé type-networks has been the magnetic frustration and long-range antiferromagnetism at low temperatures.^{30,31} Similarly, for the brickwall-type phase, we can observe the creation of pores whose rims comprise differently oriented molecules producing a few variants of the hexagonal and triangular pore (see Figure S2 in the Supporting Information). The increased diversity of structural motifs observed for the Kagomé and brickwall phases results from the presence of the interaction centers which, albeit small in size, offer the possibility of (slightly) noncollinear alignment of a pair of interacting arms of neighboring molecules. If the geometric condition for the intermolecular interaction is stricter, as imposed, for example, in the lattice modeling, the molecules create perfectly ordered networks.²⁶ To show this, for comparative purposes, in the bottom part of Figure 2, we presented snapshots of the analogous brickwall and Kagomé structures simulated for the same average adsorbate density $\rho^* = 0.26$. These results were obtained assuming that each segment of 1|3 occupies one vertex of a triangular 200×200 lattice, and the interaction between terminal arm segments occurs only when the neighboring arms are collinear ($\rightarrow\leftarrow$), resulting in $\epsilon = -1$ energy contribution. Comparing the predictions of the MD and the MC lattice modeling, we observe small difference in the structure formation; however, one can see that the underlying lattice enforces the creation of networks with the corresponding symmetry. To examine the structure formation in the systems comprising 1|3 in more detail, we performed additional calculations at relatively high and low adsorbate densities. In the first case, for $\rho^* = 0.4016$ and $T^* = 0.12$, one extended domain of the brickwall phase emerged. However, at low density, $\rho^* = 0.1002$ and $T^* = 0.086$, a collection of smaller domains of both types (Kagomé and brickwall) was usually observed. The systematic inspection we performed using twenty system replicas at $\rho^* = 0.2591$ cooled down to $T^* = 0.1$ and revealed the occurrence of the Kagomé and brickwall phases in various proportions. In most

of the replicas, the brickwall phase dominated (Figure 3b); however, in one case, the ratio of the coexisting phases was close to unity, as it is seen in Figure 3a.

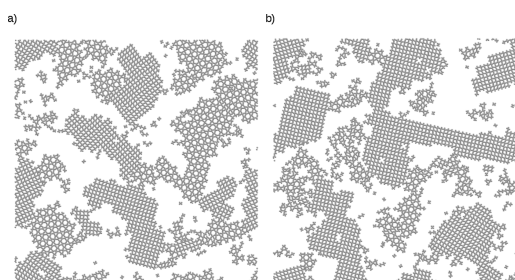


Figure 3. Part (a) configuration with the proportion of the Kagomé and brickwall phases close to unity, (b) snapshot of the system in which the formation of the brickwall phase was more favorable.

To quantify the observed effects, we calculated the distribution of the angle, θ , between molecular cores belonging to a pair of neighboring molecules of 113. The resulting normalized distribution function, $p(\theta)$, defines the probability of finding a molecular core of a neighboring molecule that is oriented at $0 < \theta < 180^\circ$ relative to the selected molecular core. This parameter describes well the Kagomé and brickwall phases, as it should take increased values at the angles which are characteristic for the Kagomé-type: 60° and for the brickwall-type: 0° and 90° . To demonstrate this, we first calculated the function $p(\theta)$ for the reference one-phase system comprising the brickwall network formed by 113 at the high density $\rho^* = 0.4016$ ($T^* = 0.12$). In the case of the

reference Kagomé-type network, we used the results simulated for the molecule 115 ($N_C = 2$, $N_A = 2$) which was found to create extended phase of this structural type at $T^* = 0.088$ and $\rho^* = 0.19599$. The corresponding distributions are shown in Figure 4a and they, as expected, differ in the position of maxima being footprints of the two phases. Taking into account the most probable values of the angle, θ , observed in each case, that is, 60° for the Kagomé and 0° and 90° for the brickwall phase, we used them to analyze the results obtained for the systems in which domains of both types are mixed at different proportions. Figure 4b presents the results calculated for the systems 1 and 2, whose snapshots are shown in Figure 3. In the first case (1, black line), it is clearly visible that the proportions of the coexisting phases are very close to each other, whereas the second curve (red) confirms that the brickwall phase prevails the Kagomé network, which agrees with the configurations from Figure 3. Moreover, we can observe that, contrary to the reference system 115, a small peak around 30° occurs. Closer inspection of the Kagomé network reveals the structural perturbations caused by the different arrangement of the 113 tectons (see Figure S2 in the Supporting Information). Additional characteristics which we showed in the inset to Figure 4b are the associated radial distribution functions, where r is the distance $g(r)$ between centers of mass of the tectons. The different shapes of the curves calculated for the systems 1 and 2 also reflect the structural differences in these molecular assemblies, and they are correlated with the corresponding distributions $p(\theta)$. Specifically, for both systems, the highest maximum in $g(r)$ (first sharp peak) occurs at $r \approx 3.7$ which equals to the smallest intermolecular distance between interacting molecules forming the Kagomé and brickwall networks. Moreover, the second

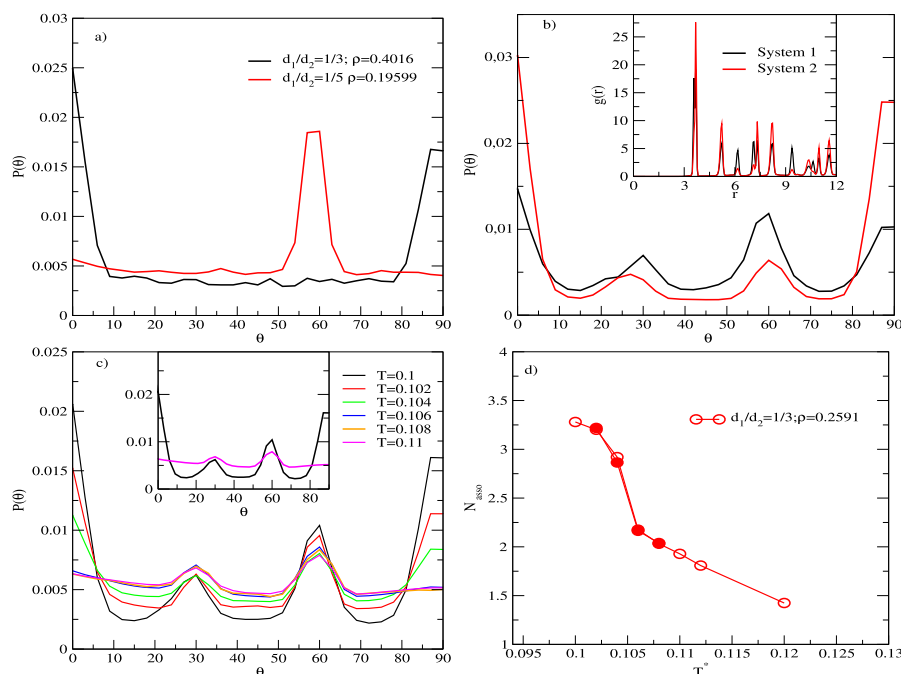


Figure 4. Part (a) distribution of the angles for reference systems and (b) for the adsorbed configurations from Figure 3. The inset to part (b) displays the center of mass radial distribution functions, $g(r)$. Part (c) shows the variation of the probability function with temperature—the inset shows two extreme temperature cases, and part (d) displays the average association number as a function of temperature obtained for the model $d_1/d_2 = 1/3$ at $\rho^* = 0.25907$. Empty circles represent cooling of the system down, while the filled were obtained for heating the adsorbed overlaid up -see the text for details.

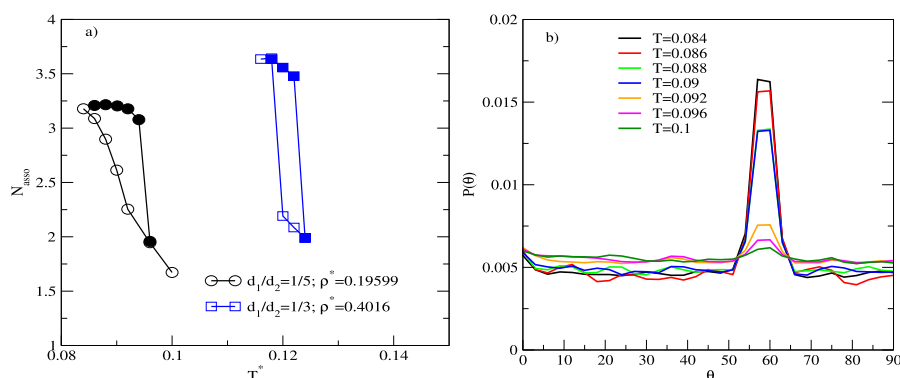


Figure 5. Part (a) shows the association number for the reference systems. Open and closed symbols refer to cooling and heating of the adsorbed monolayer, respectively. Part (b) influence of the temperature on the distribution of the probability of the angles calculated for 115 at $\rho^* = 0.19599$.

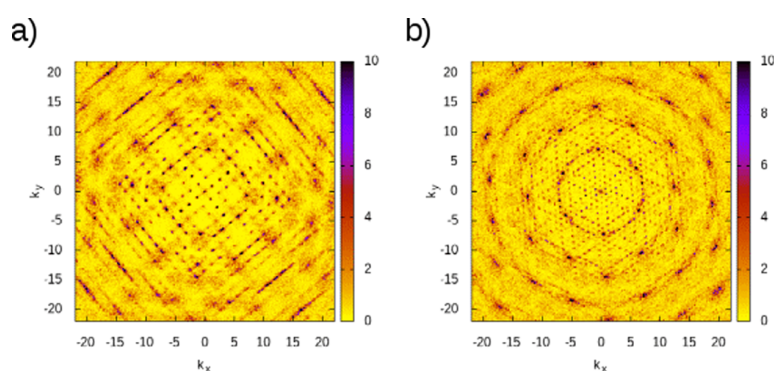


Figure 6. Diffraction patterns calculated for (a) the brickwall phase and (b) the Kagomé phase for the molecules $d_1/d_2 = 1/3$ at $\rho^* = 0.25907$ and $T^* = 0.1$.

peak at $r \approx 5.7$ and third at $r \approx 6.2$ are helpful in distinguishing these phases. Namely, the second and third peaks correspond to the distance in the linear arrangement of molecules in the brickwall and Kagomé phases, respectively (see Figure S3 in the Supporting Information).

To assess the influence of temperature on the phase coexistence in the overlayer comprising 113, we calculated the corresponding functions $p(\theta)$ and plotted them in Figure 4c. These results were obtained by averaging twenty system replicas at each T . Taking into account the magnitude of the characteristic peaks from Figure 4c, it can be concluded that at low temperatures (black line, $T = 0.1$), the content of the brickwall phase (peaks at 0 and 90°) is about twice higher than for the Kagomé phase (peaks at 60 and 30°). An important effect which can be clearly seen in Figure 4c is that the relative content of the brickwall phase decreases strongly with increasing temperature. Specifically, at the temperatures higher than $T^* = 0.104$, the peaks representing the brickwall phase decay to the base line (≈ 0.005 – 0.006), whereas the peaks of the Kagomé phase are still present on the plot, even though their magnitude decreases noticeably when T grows. The changes in $p(\theta)$ observed for the decreasing temperature are consistent with the ordering transition occurring within the range of $T^* = 0.106$ – 0.104 . Additionally, at higher temperatures, the disordered fluid still creates several smaller clusters, which is reflected in the increased values of the function $p(\theta)$ for the angles centered around $\theta = 30^\circ$ and $\theta = 60^\circ$.

The results shown in Figure 4c indicate that for $\rho^* = 0.2591$ and below $T^* = 0.104$, we are dealing with the coexistence of the brickwall and Kagomé phases. To prove this, we performed

additional calculations of the average association number, N_{asso} as a function of temperature. This structural parameter measures the average number of neighboring molecules within the interaction zone of the active sites of a selected molecule. It can take values from zero to four, and the association was counted when active sites of neighboring molecules were in the distance smaller than $r_{\text{cut,aa}}$. The parameter N_{asso} was calculated in both heating and cooling protocols, and the corresponding results are shown in Figure 4d. As it can be seen there, the curves obtained for both temperature scans coincide, and no hysteresis is observed which demonstrates that the system is approximately in the middle of the gas and ordered phase coexistence. As we observe gas and two ordered phases, this type of behavior is possible when a system is close to the triple point, but it is not consistent with the Gibbs phase rule. Otherwise, two ordered phases could not be observed at the same time. To check this, we performed the simulations at two distinct densities as mentioned previously, that is, $\rho^* = 0.1002$ and $\rho^* = 0.4016$. For the higher density, we observed only the brickwall phase, while for the lower density, the obtained configurations still correspond to the behavior as in the triple point, which as already mentioned is impossible to observe in the thermodynamic limit. In such a case, one of the phases has to be metastable, and we conclude that this situation refers to the Kagomé. To prove this, we also examined these contrary systems in the temperature plane, which confirms our statement. However, one has to note that in our case, both of the ordered phases (Kagomé and brickwall) have the same potential energy, and the densities of the ideally packed structures slightly differs (ratio of densities of Kagomé and of

brickwall phases equals to 0.92). Hence, those two phases can be simultaneously observed in both the experiment¹³ and our simulations.

A significantly different result was obtained for the one-phase reference systems discussed previously (113—brickwall and 115—Kagomé phase, see Figure 5). The corresponding functions $N_{\text{asso}}(T)$ are shown in Figure 5a, and in both cases, we can observe hysteresis loops when the heating and cooling protocol was used, being evidence for the formation of the ordered phase of one type (Kagomé for 115 and brickwall for 113) in these reference systems. The latter effect is the final proof for the stability for the brickwall phase. However, one has to note that the occurrence of metastable phases such as the Kagomé phase in our case has been a frequent effect observed experimentally.

To illustrate the effect of temperature in a one-phase system, we used the overlayer comprising 115 at $\rho^* = 0.19599$ as an example. Figure 5b shows the probability functions $p(\theta)$ calculated for this system for the different temperatures T^* , ranging from 0.084 to 0.1. As before, we can estimate that the ordering transition occurs within the range of $T^* = 0.094$ –0.09, which coincides with the association degree plot from Figure 5a. Additional structural characteristics that we provide here are the theoretical diffraction patterns calculated for the brickwall and Kagomé phases using the method described in detail elsewhere.³² The patterns displayed in Figure 6 correspond to the molecular orientations as shown in Figure 2a,b. These results prove the existence of highly ordered, solid-like structures, which exhibit long-range correlations. Similar calculations were performed for the reference systems 113 at $\rho^* = 0.4016$ and $T^* = 0.12$ and 115 at $\rho^* = 0.19599$ and $T^* = 0.088$, but they lead to comparable results, which are omitted for the sake of brevity.

We also examined the self-assembly of the tectons characterized by the ratios d_1/d_2 close to the values considered previously (113 and 115), however, having different geometries. The types of structures obtained for these molecules (brick and Kagomé) were identical as for 113 and 115 tectons and are presented in the Supporting Information in Figure S4.

Let us now proceed to the system built of molecules comprising four segments ($N_C = 4$) in the core and one segment in each arm ($N_A = 1$), abbreviated hereafter as 313. For this tecton, the simulations performed for $\rho^* = 0.2601$ and $T^* = 0.1$ revealed the formation of the hexagonal network as shown in Figure 7a. Although the distribution of the hexagonal pores occurring therein is periodic, there are a few different ways in which the pore rims can be formed (see Figure S5 in the Supporting Information). These different rim configurations are responsible for the irregular (aperiodic) molecular pattern which can be clearly seen when, for example, the position of the active centers is considered. Such visualization is presented in Figure 7b, and it demonstrates the emergence of the glassy-like disordered molecular overlayer. This result is qualitatively similar to the glassy pattern obtained using the lattice modeling for the molecule 313. For comparative purposes, in Figure 7c, we presented the snapshot obtained for molecules of this type (corresponding to $\rho^* = 0.26$) adsorbed on the 200×200 triangular lattice at $T^* = 0.1$. The left part of Figure 7c shows the obtained hexagonal network, while the right part presents only terminal (active) segments of the adsorbed molecules. As it can be seen in these panels, the results obtained with the MC lattice model are very similar to their MD counterparts. This refers especially to the molecular

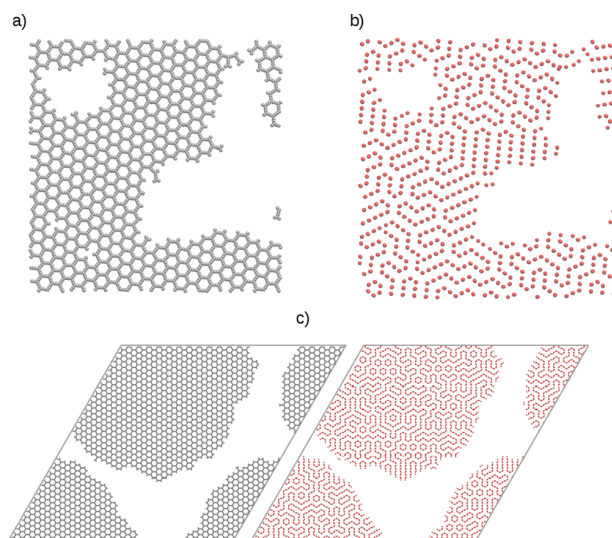


Figure 7. Fragments of the configurations simulated for the molecules with the ratio $d_1/d_2 = 1$ at $\rho^* = 0.2601$ and $T^* = 0.1$. Part (a) shows all of the molecular segments, while part (b) presents only the active interaction centers. Part (c) shows the results of the complementary lattice MC results.

configurations of the molecules forming rims of hexagonal pores, which are identical for both MC and MD results. This result differs from the previous MD case of tecton 113 which due to the more compact shape was able to create deformed nanocavities (see Figure 2) not occurring in the MC simulations. For tecton 313, due to a special aspect ratio, that is $d_1 = d_2$, the different molecular configurations forming the hexagonal pore are possible to occur in the MD modeling as well as in the lattice and off-lattice MC approach. To show this, we performed additional calculations for molecule 515 equipped with six core segments ($N_C = 6$) and two segments in each arm ($N_A = 2$). As expected, the simulations run for $\rho^* = 0.1603$, and $T^* = 0.072$ revealed the hexagonal ordering observed already for 313 and characterized by the analogous aperiodic distribution of molecules; these are not shown for brevity. The above observations will apply to any tetrapod molecule characterized by the ratio d_1/d_2 equaling to one. As we demonstrated, this quantity plays an essential role in the formation of the glassy network structures comprising the functional tetrapod building blocks.

To gain a deeper insight into the structure, we calculated the corresponding diffraction patterns. Analysis of the data revealed that while for the hexagonal structure, the diffraction patterns correspond perfectly to the observed configuration, the one for active sites exhibits long-range order as well. It can be seen that the final pattern is an overlap of at least two unit cells, namely, rhombic and rectangular, which imitates the hexagonal arrangement of the molecules in two-dimensional structure factors. For a better understanding, we have also computed the diffractogram for 500 configurations of the entire system. It is interesting that this diffraction pattern exhibits similarity to the one observed in quasi-crystals, namely, it displays the noncrystallographic 12-fold rotational symmetry.³³ It is most likely interconnected with the rotation of domains in time. To prove this, we have prolonged our computations for 5000 configurations, and the results are shown in Figure 8d. It is readily visible that the best diffraction patterns are available from a fragment of only one

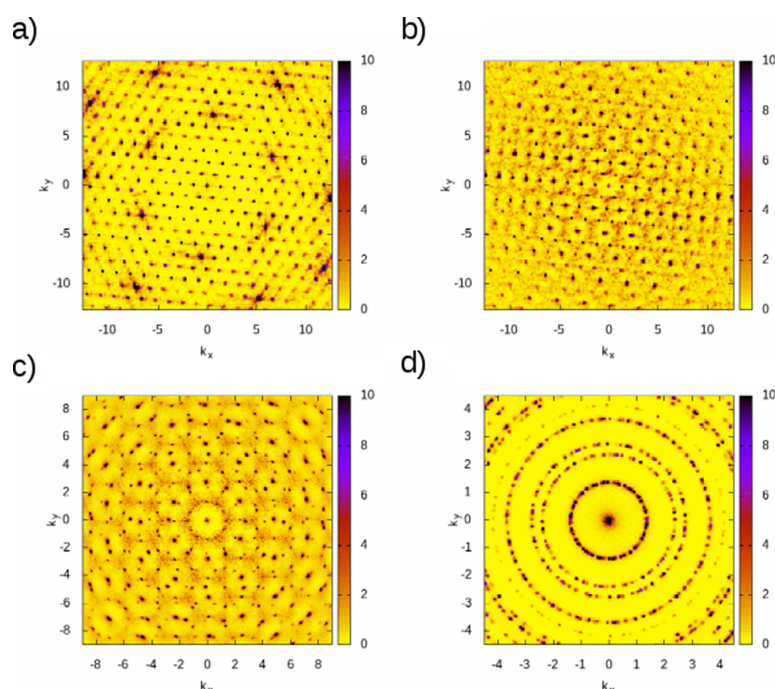


Figure 8. Part (a) represents the diffraction patterns for a fragment of frameworks' segments. (b–d) Display diffractograms for a part of one configuration and averaged over 500 and 5000 configurations of the entire system for active sites, respectively.

configuration because such methodology is not exposed on perturbations induced by rotation of differently oriented domains.

CONCLUSIONS

In this paper, using the MD modeling, we demonstrated the ways in which the molecular self-assembly on surfaces can be directed by tuning the geometry of tetrapod functional units. Even though, in real situations, the chemical mechanisms governing the self-assembly can be very complex; our results obtained with the simplified coarse-grained approach indicate clearly that molecular geometry plays the decisive role in the structure formation. Specifically, our calculations revealed that the structural descriptor d_1/d_2 is primarily responsible for the creation of the brickwall and Kagomé networks and the porous glassy superstructures. Moreover, to assess the effect of the surface corrugation on the self-assembly, we compared the results obtained from the lattice MC modeling and the MD calculations. This analysis revealed that the adsorbing surface with high triangular symmetry can effectively eliminate defective molecular connections producing 2D pores with imperfect shapes. On the other hand, the connectivity of the networks predicted by both methods (MC and MD) was found to be identical, highlighting the less important influence of the surface on the molecular coordination. Apart from these findings, we also calculated additional structural characteristics, including the distributions of the core–core angles and the radial distribution functions which facilitated identification of the ordered porous phases emerging in the simulated assemblies and prediction of their stability. An additional comprehensive information about the simulated structures was obtained with the 2D structure factors which can correspond to the X-ray scattering patterns in the experiment. As we demonstrated, the differently rotated molecular domains of the same type can produce apparent symmetry elements which are

not present in these adsorbed systems. To avoid this discrepancy, one can, for example, analyze reoriented clusters to achieve one common orientation direction instead of averaging over the directions in the entire system. The result of our simulations refers to the tetrapod molecules with one particular set of the assigned interaction directions, but the model can be easily extended to cover tectons with differently encoded interaction patterns. These possibilities are currently the subject of our further simulation studies. The findings reported herein can be useful in designing and fabrication of 2D molecular architectures with application potential in nanotechnology and material engineering.

ASSOCIATED CONTENT

Supporting Information

The Supporting Information is available free of charge on the ACS Publications website at DOI: 10.1021/acs.jpcc.9b04108.

Diverse pores forming the brickwall network, comparison of Kagomé pores, distances in brickwall and Kagomé networks, additional snapshots, and diverse pores forming the hexagonal network (PDF)

AUTHOR INFORMATION

Corresponding Author

*E-mail: lukasz.baran95@gmail.com.

ORCID

Ł. Baran: 0000-0003-1777-1998

P. Szabelski: 0000-0002-3543-9430

Notes

The authors declare no competing financial interest.

ACKNOWLEDGMENTS

We would like to thank Daniel Kamiński for the fruitful discussions. Ł.B. acknowledges support from the Polish

Ministry of Science and Higher Education under grant no. DI2017 001147.

REFERENCES

- (1) Dienstmaier, J. F.; Mahata, K.; Walch, H.; Heckl, W. M.; Schmittl, M.; Lackinger, M. On the Scalability of Supramolecular Networks – High Packing Density vs Optimized Hydrogen Bonds in Tricarboxylic Acid Monolayers. *Langmuir* **2010**, *26*, 10708–10716.
- (2) Ciesielski, A.; Szabelski, P. J.; Rzyzko, W.; Cadeddu, A.; Cook, T. R.; Stang, P. J.; Samori, P. Concentration-Dependent Supramolecular Engineering of Hydrogen-Bonded Nanostructures at Surfaces: Predicting Self-Assembly in 2D. *J. Am. Chem. Soc.* **2013**, *135*, 6942–6950.
- (3) Silly, F. Concentration-Dependent Two-Dimensional Halogen-Bonded Self-Assembly of 1,3,5-Tris(4-iodophenyl)benzene Molecules at the Solid-Liquid Interface. *J. Phys. Chem. C* **2017**, *121*, 10413–10418.
- (4) Shang, J.; Wang, Y.; Chen, M.; Dai, J.; Zhou, X.; Kuttner, J.; Hilt, G.; Shao, X.; Gottfried, J. M.; Wu, K. Assembling molecular Sierpiński triangle fractals. *Nat. Chem.* **2015**, *7*, 389–393.
- (5) Shi, Z.; Lin, N. Structural and Chemical Control in Assembly of Multicomponent Metal–Organic Coordination Networks on a Surface. *J. Am. Chem. Soc.* **2010**, *132*, 10756–10761.
- (6) Fan, Q.; Wang, C.; Han, Y.; Zhu, J.; Kuttner, J.; Hilt, G.; Gottfried, J. M. Surface-Assisted Formation, Assembly, and Dynamics of Planar Organometallic Macrocycles and Zigzag Shaped Polymer Chains with C–Cu–C Bonds. *ACS Nano* **2014**, *8*, 709–718.
- (7) Tahara, K.; Johnson, C. A.; Fujita, T.; Sonoda, M.; De Schryver, F. C.; De Feyter, S.; Haley, M. M.; Tobe, Y. Synthesis of Dehydrobenzo[18]annulene Derivatives and Formation of Self-Assembled Monolayers: Implications of Core Size on Alkyl Chain Interdigitation. *Langmuir* **2007**, *23*, 10190–10197.
- (8) Heim, D.; Seufert, K.; Auwärter, W.; Aurisicchio, C.; Fabbro, C.; Bonifazi, D.; Barth, J. V. Surface-Assisted Assembly of Discrete Porphyrin-Based Cyclic Supramolecules. *Nano Lett.* **2010**, *10*, 122–128.
- (9) Kudernac, T.; Lei, S.; Elemans, J. A. A. W.; De Feyter, S. Two-dimensional supramolecular self-assembly: nanoporous networks on surfaces. *Chem. Soc. Rev.* **2009**, *38*, 402–421.
- (10) Lipton-Duffin, J. A.; Ivasenko, O.; Perepichka, D. F.; Rosei, F. Synthesis of polyphenylene molecular wires by surface-confined polymerization. *Small* **2009**, *5*, 592–597.
- (11) Cai, J.; Ruffieux, P.; Jaafar, R.; Bieri, M.; Braun, T.; Blankenburg, S.; Muoth, M.; Seitsonen, A. P.; Saleh, M.; Feng, X.; et al. Atomically precise bottom-up fabrication of graphene nanoribbons. *Nature* **2010**, *466*, 470–473.
- (12) Simonov, K. A.; Vinogradov, N. A.; Vinogradov, A. S.; Generalov, A. V.; Zagrebina, E. M.; Svirskiy, G. I.; Cafolla, A. A.; Carpy, T.; Cunniffe, J. P.; Taketsugu, T.; et al. From Graphene Nanoribbons on Cu(111) to Nanographene on Cu(110): Critical Role of Substrate Structure in the Bottom-Up Fabrication Strategy. *ACS Nano* **2015**, *9*, 8997–9011.
- (13) Zhou, H.; Dang, H.; Yi, J.-H.; Nanci, A.; Rochefort, A.; Wuest, J. D. Frustrated 2D Molecular Crystallization. *J. Am. Chem. Soc.* **2007**, *129*, 13774–13775.
- (14) Blunt, M. O.; Russell, J. C.; Gimenez-Lopez, M. d. C.; Garrahan, J. P.; Lin, X.; Schroder, M.; Champness, N. R.; Beton, P. H. Random Tiling and Topological Defects in a Two-Dimensional Molecular Network. *Science* **2008**, *322*, 1077–1081.
- (15) Mo, Y.-P.; Liu, X.-H.; Wang, D. Concentration-Directed Polymorphic Surface Covalent Organic Frameworks: Rhombus, Parallelogram, and Kagome. *ACS Nano* **2017**, *11*, 11694–11700.
- (16) Gutzler, R.; Cardenas, L.; Lipton-Duffin, J.; El Garah, M.; Dinca, L. E.; Szakacs, C. E.; Fu, C.; Gallagher, M.; Vondráček, M.; Rybachuk, M.; et al. Ullmann-type coupling of brominated tetrathienoanthracene on copper and silver. *Nanoscale* **2014**, *6*, 2660–2668.
- (17) Misūnäs, T.; Tornau, E. E. Ordered Assemblies of Triangular-Shaped Molecules with Strongly Interacting Vertices: Phase Diagrams for Honeycomb and Zigzag Structures on Triangular Lattice. *J. Phys. Chem. B* **2012**, *116*, 2472–2482.
- (18) Szabelski, P.; Rzyzko, W.; Nieckarz, D. Directing the Self-Assembly of Tripod Molecules on Solid Surfaces: A Monte Carlo Simulation Approach. *J. Phys. Chem. C* **2016**, *120*, 13139–13147.
- (19) Fortuna, S.; Cheung, D. L.; Troisi, A. Hexagonal Lattice Model of the Patterns Formed by Hydrogen-Bonded Molecules on the Surface. *J. Phys. Chem. B* **2010**, *114*, 1849–1858.
- (20) van der Lit, J.; Marsman, J. L.; Koster, R. S.; Jacobse, P. H.; den Hartog, S. A.; Vanmaekelbergh, D.; Klein Gebbink, R. J. M.; Filion, L.; Swart, I. Modeling the Self-Assembly of Organic Molecules in 2D Molecular Layers with Different Structures. *J. Phys. Chem. C* **2016**, *120*, 318–323.
- (21) Nieckarz, D.; Szabelski, P. Simulation of the self-assembly of simple molecular bricks into Sierpiński triangles. *Chem. Commun.* **2014**, *50*, 6843–6845.
- (22) El Garah, M.; Dianat, A.; Cadeddu, A.; Gutierrez, R.; Cecchini, M.; Cook, T. R.; Ciesielski, A.; Stang, P. J.; Cuniberti, G.; Samori, P. Atomically Precise Prediction of 2D Self-Assembly of Weakly Bonded Nanostructures: STM Insight into Concentration-Dependent Architectures. *Small* **2016**, *12*, 343–350.
- (23) Copie, G.; Cleri, F.; Makoudi, Y.; Krzeminski, C.; Berthe, M.; Cherioux, F.; Palmino, F.; Grandidier, B. Surface-Induced Optimal Packing of Two-Dimensional Molecular Networks. *Phys. Rev. Lett.* **2015**, *114*, 066101. DOI: 10.1103/physrevlett.114.066101
- (24) Palma, C.-A.; Samori, P.; Cecchini, M. Atomistic Simulations of 2D Bicomponent Self-Assembly: From Molecular Recognition to Self-Healing. *J. Am. Chem. Soc.* **2010**, *132*, 17880–17885.
- (25) Zhao, Y.; Wang, J. How To Obtain High-Quality and High-Stability Interfacial Organic Layer: Insights from the PTCCA Self-Assembly. *J. Phys. Chem. C* **2017**, *121*, 4488–4495.
- (26) Nieckarz, D.; Rzyzko, W.; Szabelski, P. On-surface self-assembly of tetrapod molecular building blocks. *Phys. Chem. Chem. Phys.* **2018**, *20*, 23363–23377.
- (27) Rzyzko, W.; Nieckarz, D.; Szabelski, P. Modeling of the 2D self-assembly of tripod-shaped functional molecules with patchy interaction centers. *Adsorption* **2019**, *25*, 75–85.
- (28) Plimpton, S.; et al. *Large-scale Atomic/Molecular Massively Parallel Simulator*. lammmps.sandia.gov, 1995 [Online; accessed April 29, 2019].
- (29) Plimpton, S. Fast Parallel Algorithms for Short-Range Molecular Dynamics. *J. Comput. Phys.* **1995**, *117*, 1–19.
- (30) Wills, A. S.; Harrison, A.; Ritter, C.; Smith, R. I. Magnetic properties of pure and diamagnetically doped jarosites: Modelkagoméantiferromagnets with variable coverage of the magnetic lattice. *Phys. Rev. B: Condens. Matter Mater. Phys.* **2000**, *61*, 6156–6169.
- (31) Rao, C. N. R.; Sampathkumaran, E. V.; Nagarajan, R.; Paul, G.; Behera, J. N.; Choudhury, A. Synthesis, Structure, and the Unusual Magnetic Properties of an Amine-Templated Iron(II) Sulfate Possessing the Kagomé Lattice. *Chem. Mater.* **2004**, *16*, 1441–1446.
- (32) Borówko, M.; Rzyzko, W.; Sokolowski, S.; Staszewski, T. Phase behavior of decorated soft disks in two dimensions. *J. Chem. Phys.* **2016**, *145*, 224703.
- (33) Fischer, S.; Exner, A.; Zielske, K.; Perlich, J.; Deloudi, S.; Steurer, W.; Lindner, P.; Förster, S. Colloidal quasicrystals with 12-fold and 18-fold diffraction symmetry. *Proc. Natl. Acad. Sci. U.S.A.* **2011**, *108*, 1810–1814.

lic. Łukasz Baran
Katedra Chemii Teoretycznej
Instytut Nauk Chemicznych
Wydział Chemii UMCS
Pl. Marii Curie-Skłodowskiej 3
20-031 Lublin

Lublin, 16.05.2022

OŚWIADCZENIE

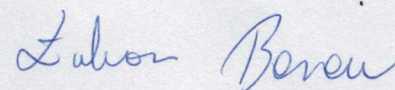
Oświadczam, że mój wkład w niniejszej pracy:

[PI] Ł. Baran*, D. Nieckarz, P. Szabelski, W. Rżysko, "Controlling of the 2D Self-Assembly Process by the Variation of Molecular Geometry", Journal of Physical Chemistry C, 2019, **123**, 19549-19556.

polegał na przeprowadzeniu symulacji metodą dynamiki molekularnej, napisaniu manuskryptu i przeprowadzeniu analizy części wyników

Udział ten szacuję na 75 %.

lic. Łukasz Baran



PI

dr Damian Nieckarz
Katedra Chemii Teoretycznej
Instytut Nauk Chemicznych
Wydział Chemii UMCS
Pl. Marii Curie-Skłodowskiej 3
20-031 Lublin

Lublin, 15.05.2022

OŚWIADCZENIE

Oświadczam, że mój wkład w niniejszej pracy:

[PI] **Ł. Baran***, D. Nieckarz, P. Szabelski, W. Rżysko, "Controlling of the 2D Self-Assembly Process by the Variation of Molecular Geometry", Journal of Physical Chemistry C, 2019, **123**, 19549-19556.

polegał na interpretacji otrzymanych wyników teoretycznych.

Udział ten szacuję na 5 %.

dr Damian Nieckarz

Damian Nieckarz

prof. dr hab. Paweł Szabelski
Katedra Chemii Teoretycznej
Instytut Nauk Chemicznych
Wydział Chemii UMCS
Pl. Marii Curie-Skłodowskiej 3
20-031 Lublin

Lublin, 15.05.2022

OŚWIADCZENIE

Oświadczam, że mój wkład w niniejszej pracy:

[PI] **L. Baran***, D. Nieckarz, P. Szabelski, W. Rzyśko, "Controlling of the 2D Self-Assembly Process by the Variation of Molecular Geometry", Journal of Physical Chemistry C, 2019, **123**, 19549-19556.

polegał na

opracowaniu koncepcji obliczeń w ramach siatkowego modelu Monte Carlo dla samoorganizacji cząsteczek funkcjonalnych

Udział ten szacuję na 10 %.



prof. dr hab. Paweł Szabelski

PI

dr hab. Wojciech Rzyśko, prof. UMCS
Katedra Chemii Teoretycznej
Instytut Nauk Chemicznych
Wydział Chemii UMCS
Pl. Marii Curie-Skłodowskiej 3
20-031 Lublin

Lublin, 16.05.2022

OŚWIADCZENIE

Oświadczam, że mój wkład w niniejszej pracy:

[PI] Ł. Baran*, D. Nieckarz, P. Szabelski, W. Rzyśko, "Controlling of the 2D Self-Assembly Process by the Variation of Molecular Geometry", Journal of Physical Chemistry C, 2019, **123**, 19549-19556.

polegał na koordynowaniu merytorycznym badań i analizie wyników

Udział ten szacuję na 10 %.

dr hab. Wojciech Rzyśko, prof. UMCS





Influence of the molecular geometry on the formation of the self-assembled structures



Ł. Baran

Department for Modelling of Physicochemical Processes, Maria Curie-Skłodowska University, Lublin 20-031, Poland

ARTICLE INFO

Article history:

Received 16 May 2019

Received in revised form 20 July 2019

Accepted 24 August 2019

Available online 28 August 2019

Keywords:

Self-assembly

Molecular simulations

Order parameters

Supramolecular chemistry

ABSTRACT

This paper presents simulations of the molecular dynamics and off-lattice Monte Carlo devoted to investigate self-assembly process of molecules with tetrapod architecture. Formation of diverse supramolecular networks were found, which were characterized by several structure and order parameters, such as two-dimensional structure factors and nematic order parameters. Moreover, it follows from the aforementioned functions that one of the most important factors driving the self-assembly phenomena is the molecular architecture and the presence of directional interactions.

© 2019 Elsevier B.V. All rights reserved.

1. Introduction

Construction of novel self-assembled, supramolecular networks has been of particular interest over several decades, for both experimental and theoretical investigations. The above statement is supported by a large number of papers devoted to the synthesis of new chemical compounds having the ability to self-assemble, and attempting to elucidate the mechanism of already known processes or to propose the new ones. One of the most promising fields is the new and rapidly developing method of “on-surface synthesis”, aiming at the use of solid substrates to initiate chemical reactions, which would not occur at all or would be very hard to perform in bulk systems. There are several factors that allow to control the self-assembly processes, such as the precursor architecture [1,2], the substrate nature and symmetry [3,4].

The molecules that can be used as the templates for self-assembly include, for instance, linear [5-8], tripod [9,10] and tetrapod molecules [11-16]. The chemical compounds assemble into the structures ranging from small clusters [17] up to the extended porous networks [18] by means of directional interactions. These interactions involve the hydrogen [19,20] and halogen [21,22] bonding, the metal-organic ligand coordination [23, 24] as well as the van der Waals forces [25]. Additionally, the surface nature and symmetry are also important factors in the self-assembly phenomena. For instance, the results of Gutzler et al. obtained

for tetrabromotetrathienoanthracene, have shown that different supramolecular networks can be formed, depending on the substrate type and the Miller indices of the exposed surface [3]. Moreover, it has recently been reported that the chemical or structural defects in the substrates can deteriorate the formation of supramolecular networks [26].

Apart from the employed template molecules or substrates, there are also other factors influencing the self-assembly processes. Among them we should mention, the guest molecules [13,14,27], the concentration dependent self-assembly [28,29] and the type of the solvent used [30]. Comprehensive reviews that elucidate the effects of the aforementioned factors can be found in Refs. [31,32].

Since the tendency towards self-assembly and the formation of the desired supramolecular structures by real molecules is rather hard to predict *a priori*, the synthesis of appropriate molecules may be difficult and costly. Therefore, computer simulations seem to be a convenient tool to investigate the effects of multiple factors on the self assembly of the molecules of different structure and chemical composition. Computer modelling allows to easily change the system parameters so that the large number of molecules, characterized by different shape, symmetry and intermolecular interactions, can be examined. The results of computer modelling may be very important, allowing to select the molecules, which self assemble into the supramolecular structures of desired properties, such as the porosity and periodicity. In this way, the results of computer simulations may be a valuable guide for experimentalists.

There are two basic computer simulation methods, Monte Carlo (MC) and molecular dynamics (MD), which can be used. In the case

E-mail address: lukasz.baran95@gmail.com.

of Monte Carlo method, either lattice [33,34] or off-lattice [35] methods can be used to model self-assembly of the molecules of various architecture. The molecular dynamics simulations have also been successfully used to model the self-assembly process of molecules on solid surfaces [36–39].

In this study, the molecular dynamics and the off-lattice Monte Carlo simulations, have been used to investigate self-assembly of model molecules. Examination of diverse architectures of the tectons possessing ability to form supramolecular networks has revealed that the molecular geometry itself may be one of the most important factors. The obtained structures have been characterized by various distribution functions and order parameters. Additionally, the diffraction patterns have been computed to complete the description of the emerging superstructures.

2. The model and simulation details

The main goal of this study has been to model the tetra-substituted chemical compounds where, for instance, isophthalic or halogen groups are attached to the terminal phenyl rings. As already mentioned, these types of molecules are likely to self-assemble on solid surfaces. Therefore, the particles used in this work have been treated as flat, rigid objects, which consisted of the rod-like “core” of the length N_C , and four arms, of the length N_A , attached to it. The angle between two arms at each side of the core has been set to $\theta = 120^\circ$. The sizes of the segments forming the arms and the core have been set to be the same, and equal to σ_b . In the following will

be referred to as the components of the backbone. The bonding distance between particular entities in the main structure has also been assumed to be equal to σ_b .

The active sites, each of size σ_a , have been defined as the regions entirely embedded into the terminal arms, and the backbone-site bonding distance has been abbreviated as l . The inclusion of the site into the disk defining the terminal arm has been done in order to make the models used in molecular dynamics and Monte Carlo simulations compatible.

The molecular architecture used in this work has been schematically represented in Fig. 1a. However, in the case of Monte Carlo simulations, the description of directional interactions has been done using a different model of active sites at the surface of patchy arms [40,41] (Fig. 1d). In this case, the interparticle potential has been the truncated and shifted Lennard-Jones (12-6) potential [42], instead of the square well potential. Moreover, each Monte Carlo step consisted of translation, with orientational bias, and reorientation of randomly chosen molecule [43]. The simulation cell has been a square of the linear size L . The box size has varied between $L_x = 96$ and 140, depending on the molecular architecture, allowing to keep the same number of molecules.

In the case of molecular dynamics simulations, the backbone-backbone (bb) and the backbone-site (ab) bond lengths have been allowed to relax by imposing the harmonic binding potentials

$$u_{bb}(r) = k_{bb}(r - \sigma_{bb})^2 \quad (1)$$

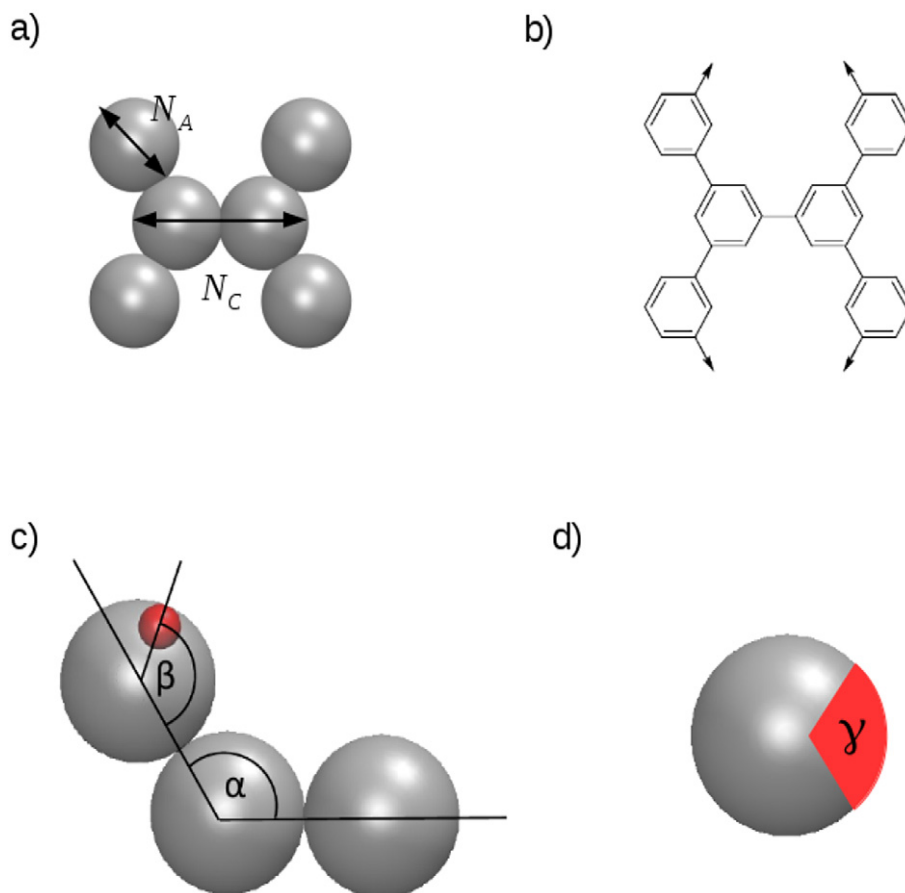


Fig. 1. Schematic representation of a molecule with $N_C = 2$ and $N_A = 1$ used in this paper. Part b) displays an example of the chemical compound, which can be described by our model. Part c) defines angles in the model, and we have assumed that both α and β are the same and equal to 120° . Part d) shows the terminal arm in model used in the Monte Carlo simulations. The angle γ determines the size of interaction zone.

and

$$u_{ab}(r) = k_{ab}(r - l)^2 \quad (2)$$

Similarly, the angles between the backbone-backbone (bb) and the backbone-site (ab) bonds have also been allowed to fluctuate, owing to the applied angular-harmonic potentials

$$u_{bb}(\theta_{bb}) = k_{\theta}(\theta_{bb} - \theta_{0,bb})^2 \quad (3)$$

$$u_{ab}(\theta_{ab}) = k_{\theta}(\theta_{ab} - \theta_{0,ab})^2 \quad (4)$$

To ensure the continuity of the truncated (12,6) Lennard-Jones potential, necessary in the case of molecular dynamics simulations, it has been appropriately shifted [42],

$$U_{SF} = \begin{cases} U_{LJ}(r) - U_{LJ}(r_{cut}) + U'_{LJ}(r_{cut})(r - r_{cut}) & r < r_{cut} \\ 0 & \text{otherwise} \end{cases} \quad (5)$$

where $U_{LJ}(r) = 4\epsilon_{kl}[(\sigma_{kl}/r)^{12} - (\sigma_{kl}/r)^6]$ and $U'_{LJ}(r_{cut})$ is the derivative of $U_{LJ}(r)$ at $r = r_{cut}$. Thus, the total potential energy of the system has been defined as

$$U_{total} = U_{SF} + u_{kl}(r) + u_{kl}(\theta) \quad (6)$$

where $kl = aa, ab, bb$

The backbone Lennard-Jones parameters $\sigma \equiv \sigma_{bb}$ and $\epsilon \equiv \epsilon_{bb}$ have been set at the units of length and energy, respectively, and the reduced time and temperature are equal to $\tau^* = t\sqrt{\epsilon/m\sigma^2}$, $T^* = kT/\epsilon_{aa}$. The latter definition has been used in order to keep the temperature scale independent of the association energy. Additionally, the number density has been defined as $\rho^* = \frac{N_C + 4 \cdot N_A}{L_x \cdot L_y}$. The mass of the backbone entities, as well as of the active sites have been both set to unity, although their diameters have not been assumed to be equal. The core and the arm segments diameters are equal to $\sigma_{bb} = \sigma$, while the active sites diameter is equal to $\sigma_{aa} = 0.2\sigma$. The energies of the backbone-backbone and the backbone-active site interactions have been fixed and equal to $\epsilon_{bb} = \epsilon$ and $\epsilon_{aa} = 5.0\epsilon$, respectively. One should note that this kind of screened interparticle interactions is characteristic of various chemical compounds in solutions. However, in our model the solvent molecules have not been treated explicitly, since our main aim has been to investigate the interactions between active sites of different molecules, which can be treated as, for example, corresponding to the formation of hydrogen bonds between the molecules. The backbone-site diameter and the energy of backbone-site interaction have been assumed to be equal to $\sigma_{ab} = (\sigma_{bb} + \sigma_{aa})/2$ and $\epsilon_{ab} = \epsilon$ respectively. The distance between the terminal arm segment and the active site has been set as equal to $l = 0.4\sigma$. The cut-off distance of the interaction between two active sites has been set as equal to $r_{cut,aa} = 2\sigma_{aa}$. On the other hand, we have assumed that $r_{cut,kl} = \sigma_{kl}$, for $kl = bb, ab$, ensuring that bb and ab interactions are non-attractive. The harmonic potential constants $k_{bb} \equiv k_{ab}$ have been set as equal to $1000\epsilon/\sigma^2$, and $k_{\theta} = 1000\epsilon/(\text{radian}^2)$.

All molecular dynamics simulations have been performed in the NVT ensemble using the LAMMPS package [44, 45]. The velocity Verlet integration scheme with the time step equal to $t = 0.001\tau$ has been used. In every system the number of particles has been the same and equal to 2500. However, the total number of ‘‘atoms’’ has been depending on the particular architecture.

As already mentioned, the size of simulation cells has been appropriately adjusted to keep the density and the particles number constant. The preliminary equilibration has been performed using the Berendsen thermostat [46], with the dampening constant

$\tau_B = 10\tau$ for 5×10^6 time steps, and further equilibration has been performed for 5×10^7 time steps, using the Nosé-Hoover chains approach [47] with $N_{chain} = 3$, and with the dampening constant equal to $\tau_{chain} = 10\tau$. Each system has been slowly cooled down, with the temperature grid $\Delta T^* = 0.002$, from the temperature at which the system has been disordered, to sufficiently low temperatures, at which the self-assembled structures developed. In order to ensure that the self-assembled networks are stable, we have performed several heating up and cooling down runs for every system.

The production runs have been carried out using the Nosé-Hoover chain thermostat. The number of time steps required to obtain sufficiently accurate results has been observed to vary from 2×10^7 to 5×10^8 . During the production runs, the calculation of two-dimensional structure factor for well-defined structure has been performed. This corresponds to the X-ray scattering patterns in experimental data, and can be treated as the ‘‘theoretical diffractograms’’. Moreover, for each system, the evaluation of various parameters to determine the structure of molecular networks, such as the nematic order parameter, and the core-core angle distribution has been performed.

The phase diagrams have been determined using finite size scaling of the block density distribution functions following the method proposed by Binder [48]. We have also investigated, how the structure of applied molecules influence the shape of phase diagrams.

3. Results and discussion

The discussion begins with the presentation of results obtained for different systems presented in Table 1. In Fig. 2, we have presented the examples of snapshots of the systems M_{21} , M_{41} , M_{22} and M_{42} , obtained from molecular dynamics simulations, which demonstrate the influence of the tetrapod geometry on the formation of molecular networks.

The complementary results of Monte Carlo simulations, for the interaction zone $\gamma = 10^\circ$ have shown the formation of exactly the same networks (see Fig. S1 in the supplementary material). These highly ordered structures form different types of porous networks, depending on the molecular architecture, and resemble those presented in the recent paper published by S. Xing et al. [11]. In order to get a deeper insight into the structure of the adsorbed overlayers, the calculations of different structure parameters are needed. For this purpose, we have calculated the core-core angle (θ) distributions between the neighbouring molecular cores, for the systems given in Table 1. The resulting normalized distribution function, $p(\theta)$, which gives the probability of finding a molecular core of adjacent tetrapod oriented with respect to the selected molecular core with the angle θ , from the interval between 0 and 180° .

The distribution functions $p(\theta)$ for the systems M_{21} , M_{41} , M_{22} and M_{42} have been presented in Fig. 3, and demonstrate that in all the cases, the distributions reach rather high maxima for $\theta = 0^\circ$. This allows to conclude that all networks are identical with respect to their core-core orientations. Thus, the final structure is determined by the entire architecture, i.e., by the numbers of arm's and core's segments, leading to locally different ordering. On the other hand,

Table 1
Abbreviations for the systems studied in this work.

M_{CA}	N_C	N_A
M_{21}	2	1
M_{31}	3	1
M_{41}	4	1
M_{22}	2	2
M_{32}	3	2
M_{42}	4	2

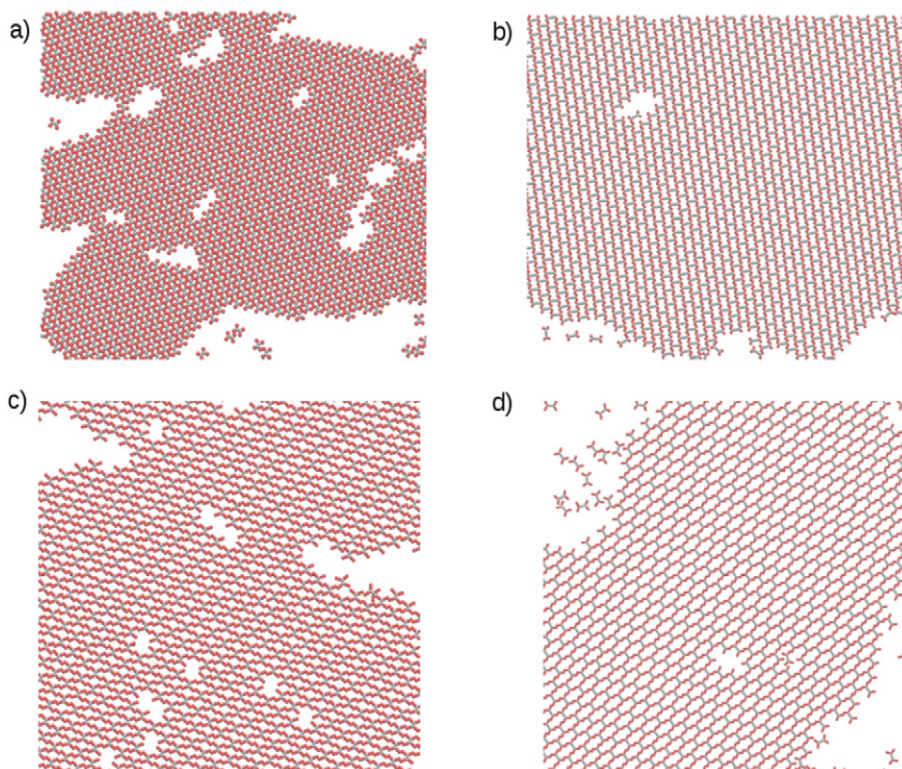


Fig. 2. Parts of the configurations for the systems M_{21} (a) and M_{41} (b) at $T^* = 0.092$ in $\rho^* = 0.25$, M_{22} (c) and M_{42} (d) at $T^* = 0.088$ in $\rho^* = 0.2$. Silver and red disks mark the core and arms segments, respectively.

the global order has been found to be of nematic type, and entirely determined of the orientations of cores.

The appearance of small and rather diffused maxima around 30° and 50° , for the M_{42} and M_{41} systems, respectively, has been found to be due to two reasons. The inspection of snapshots has revealed the presence of gas-like regions, in which the molecules can freely rotate, and lead to the appearance of perturbations in the calculated distribution function. In order to demonstrate this, we have performed the calculations at higher density, equal to $\rho^* = 0.45$, and the

resulting distribution of core-core angle functions has not shown any trace of those diffused maxima. This is demonstrated by the results given in the inset to Fig. 3. The second reason for the appearance of those additional peaks may be associated to the presence of differently oriented clusters. In such a case, the perturbation in $p(\theta)$ results from the presence of interfaces between differently oriented clusters. When the orientation of the clusters is the same, these extra peaks at $p(\theta)$ have not been observed.

The finding that the structures observed in hitherto investigated systems exhibit a pseudo long range order [49] and similar ordering relative to their core orientations, has been supported by the calculations of the two-dimensional centres of mass structure factors. As already mentioned, the structure factor corresponds to the X-ray scattering patterns and considered as “theoretical diffractograms”. The results given in Fig. 4 demonstrate that the structure factors correspond to the rhombic symmetry for all the networks considered. One should note, that the only difference between the particular architectures, is due to different elementary cells parameters, which coincide with the distances between reflexes observed in structure factors. Complementary results for the cores and the segments are presented in Figs. S2 and S3 in the supplementary material.

Another function characterizing the structure is the nematic order parameter defined as

$$Q_{\alpha\beta} = N^{-1} \sum_i [2b_{\alpha}(i)b_{\beta}(i) - \delta_{\alpha\beta}] \quad (7)$$

where $b_{\alpha}(i)$ is the α -th coordinate of the unit vector b , specifying the orientation of the molecule i , and $\delta_{\alpha\beta}$ is the Kronecker delta function. The corresponding eigenvalues of Q are $\pm S$. This function takes on the values between 0 and 1 in disordered and perfectly ordered phases, respectively. In real systems, it is very difficult to reach the value of Q equal to 1, due to possible imperfections of the ordered structure.

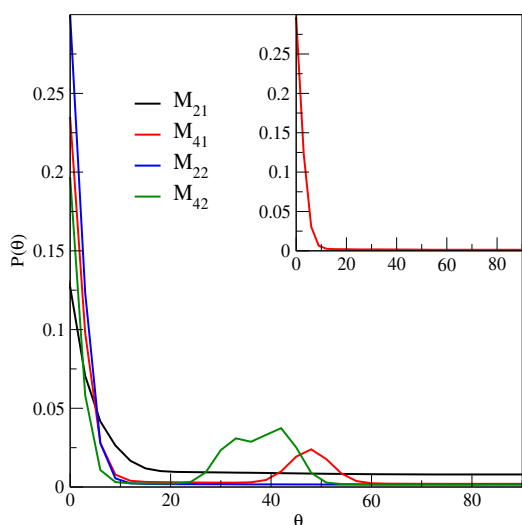


Fig. 3. The core-core angle distributions for the systems M_{21} , M_{41} , M_{22} and M_{42} . The diagrams are shown over the range of $0^\circ < \theta < 90^\circ$, since the distributions are symmetric with respect to $\theta = 90^\circ$.

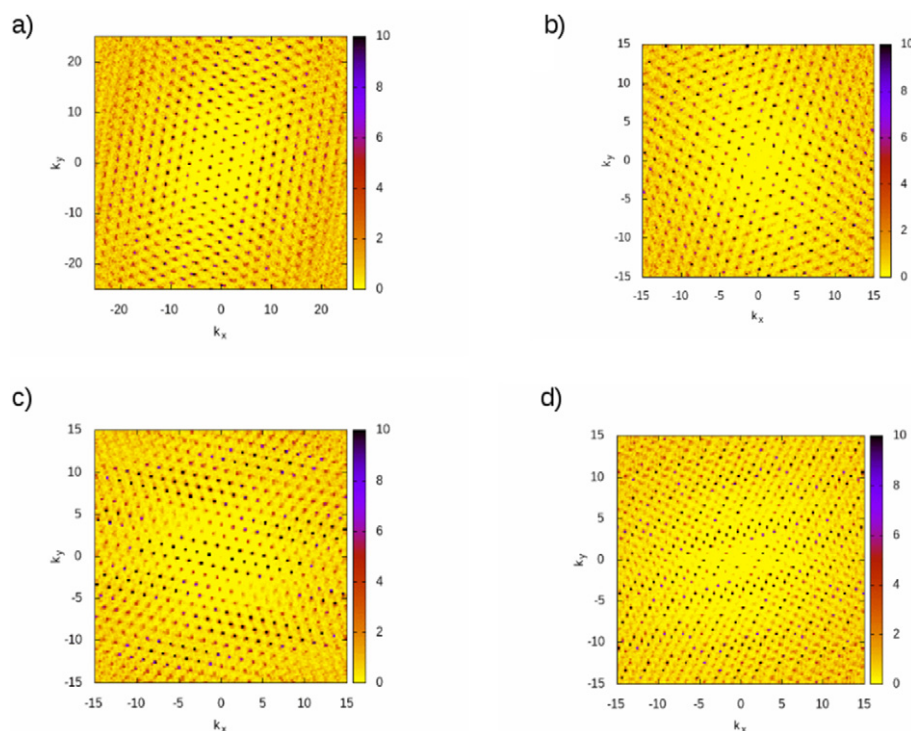


Fig. 4. 2-Dimensional centre of mass structure factors for the molecules M_{21} (a) and M_{41} (b) at $T^* = 0.092$ in $\rho^* = 0.25$, M_{22} (c) and M_{42} (d) at $T^* = 0.088$ in $\rho^* = 0.2$.

Fig. 5(a) displays the temperature changes of the nematic order parameter for different systems. In the case of the systems M_{41} and M_{22} , the order parameter increases above 0.8 when the temperature is lowered, indicating the formation of highly ordered structure. These results are in agreement with the behaviour of structure factors presented in Fig. 4. On the other hand, in the case of M_{21} and M_{42} molecules, the values of the order parameter reach the values about $S = 0.5$, at the lowest temperature used here, suggesting that the structures are less ordered than the structures of M_{41} and M_{22} molecules. It is not the case, however, since lower values of the order parameter are due to the presence of two perfectly ordered domains of opposite orientations. In such cases, the averaged values of the nematic order parameter would be zero, despite that the local value in each cluster may be very close to unity. Indeed, the inspection of configurations has revealed that this is the case in our systems. Fig. 5 (b) presents the snapshot for the molecule M_{42} , in which two differently oriented domains are well seen. Very similar results have been

obtained for the molecule M_{21} , but they are omitted for the sake of brevity.

The above results are of particular importance, because the formation of differently oriented domains may lead to wrong interpretation of the temperature changes of the orientation-dependent order parameters, such as the nematic order parameter, and the two-dimensional structure factors. The influence of differently oriented clusters on the behaviour of the two-dimensional structure factor is now under study. The inset to Fig. 5(a) shows the hysteresis loop obtained during cooling down and heating up runs. The appearance of hysteresis loops suggests that the formation of supramolecular networks occurs via the first-order phase transition.

Now, we proceed to the discussion of phase diagrams. Following the Binder's block analysis method [48], the simulation cell has been divided into blocks of different sizes. Then, the density probability distributions for the segments of backbone, $P(\rho^*)$, have been estimated for each block. The inset to Fig. 6 (b) presents an example

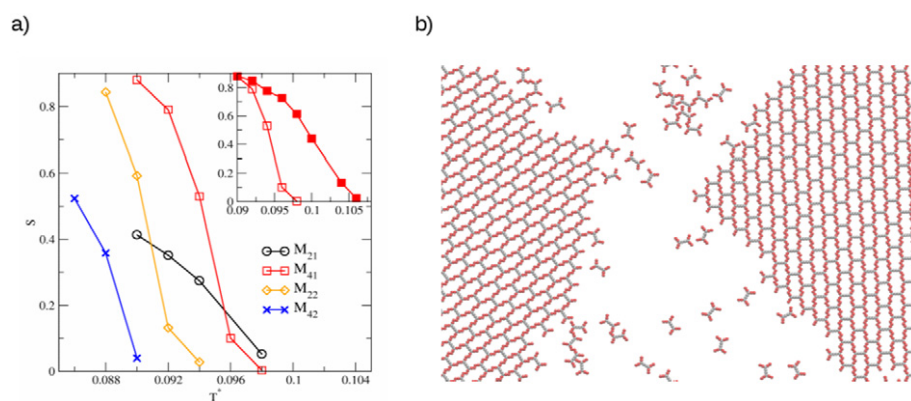


Fig. 5. Part (a) shows the temperature changes of the nematic order parameter for different systems, while the inset shows the hysteresis of the nematic order parameter (see text for more details). Part (b) presents a fragment of the configuration for the molecule M_{42} , which leads to the perturbations in the order parameter.

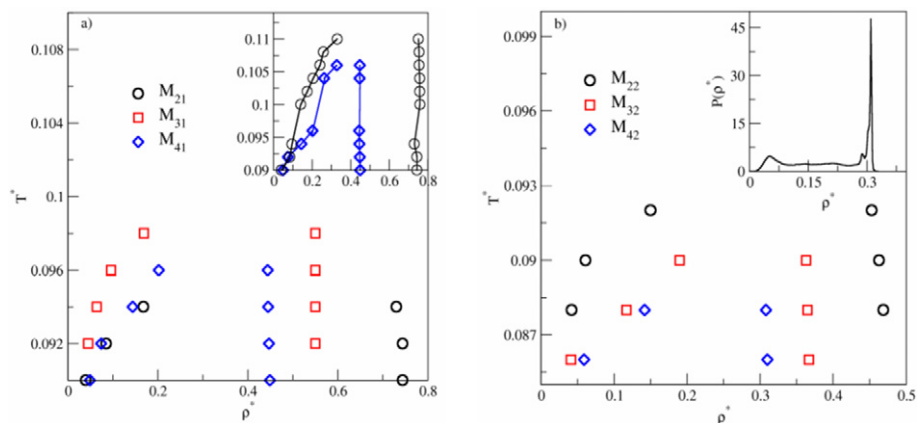


Fig. 6. Parts (a) and (b) show the phase diagrams for different systems. The inset to part (b) shows an example of the density distribution function recorded for the system M_{42} , at the temperature $T^* = 0.086$ and the block size equal to $L_x = L_y = 55$.

of the normalized $P(\rho^*)$, which exhibits double-peak behaviour corresponding to the two phase-coexistence. From these distributions, the densities of coexisting phases have been determined from the locations of maxima of the peaks.

From the results presented in Fig. 6 it follows that the phase diagrams are qualitatively the same and independent of the molecular geometry. The main difference between the phase diagrams for different systems is a gradual decrease of density of the condensed phase, when the core and arms length increases. This behaviour may be related to a gradual increase of the porosity. This finding is supported by the snapshots presented in Fig. 2. It has been presumed that the phase diagrams are of the “swan-neck” type. In order to confirm this prediction, we have performed the calculations of density probability functions for several systems at slightly higher density. The results have been then used to estimate the locations of coexistence points at higher temperatures, shown in the inset of Fig. 6a. We should note that the investigation of phase behaviour at

high temperature and at high densities has not been the aim of this work.

Then, we have used Monte Carlo method to study the model system with rather large angle $\gamma = 76^\circ$. This value of γ is sufficiently large to allow for a simultaneous interaction of a single active site with two other molecules. In the previously considered situations, each active site could interact with only one active site located on another molecule. Thus, the coordination number in the presently considered case is larger.

Surprisingly, we have found the formation of structures involving tetrapods, in which each molecule interacts with only two other molecules. Fig. 7, shows the examples of configurations recorded for different model molecules. One can see that these networks form ladder-like structures of different porosity

and one has to note that similar tendency than for the lower value of the angle can be seen. With the increase of the number of core’s and arm’s segments, the increase of empty spaces can be seen. This

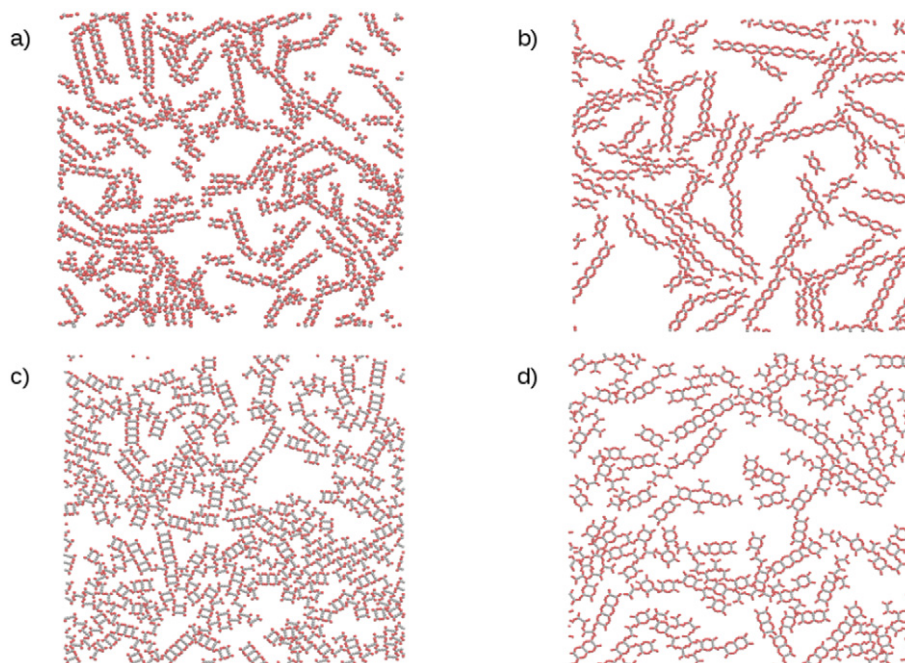


Fig. 7. Configurations recorded during the off-lattice Monte Carlo runs for a) M_{21} at $T^* = 0.1$, b) M_{22} at $T^* = 0.08$, c) M_{41} at $T^* = 0.1$ and d) M_{42} at $T^* = 0.08$ in $\rho^* = 0.2$ for every system.

can be interconnected with the decrease of ordered phases density and thus, increase of porosity of the system.

4. Conclusions

We have presented the results of self-assembly and the formation of supramolecular networks, obtained by means of molecular dynamics and Monte Carlo simulations. The latter were used to investigate the influence of the interaction zone on the formation of diverse phases. It has been shown that the employed model leads to qualitatively the same results as obtained experimentally [11], and is able to predict novel structures. This suggests that the key factor, driving the self-assembly processes, is the molecular architecture and the presence of directional interactions. This finding is consistent with the experimental data presented in Refs. [12,13]. Of course, the structure of the underlying surface and the type of solvent used may both considerably alter the structure of dense phases. In our study these effects have not been considered, since the surface was a uniform plane and the solvent was not taken into account. However, the influence of the surface structure and symmetry on self-assembly, as well as the effects resulting from the presence of explicit solvents of different properties is presently under study in our laboratory.

The ability of the studied molecules to form the structures described in this work seems to be of importance, because it might be helpful for experimentalists, working with similar systems, capable to self-assembly on the solid surfaces. Our study has shown that the application of simplified models, which are able to mimic a variety of architectures and types of interparticle interactions allows to find structures of the presumed symmetry.

Moreover, various parameters characterizing the structure of obtained supramolecular networks were employed. It has been shown that the quantities, such as the nematic order parameter, the core-core angle distribution functions, and the two-dimensional structure factors are particularly sensitive to the imperfections of the ordered phases. In particular, we have demonstrated that the presence of differently oriented clusters leads to the appearance of extra peaks on the core-core angle distribution functions and to considerably lower values of the nematic order parameter. Therefore, such side effects have to be taken into account, to avoid a wrong interpretation of simulation results.

Declaration of Competing Interest

There are no conflicts of interests.

Acknowledgements

I would like to thank Wojciech Rzyśko and Andrzej Patrykiewicz for their helpful suggestions.

This study has been supported by the Polish Ministry of Science and Higher Education, under grant no. DI2017 001147.

Appendix A. Supplementary data

Supplementary data to this article can be found online at <https://doi.org/10.1016/j.molliq.2019.111627>.

References

- [1] X. Zhang, Q. Zeng, C. Wang, On-surface single molecule synthesis chemistry: a promising bottom-up approach towards functional surfaces, *Nanoscale* 5 (2013) 8269–8287.
- [2] X. Zhang, Q. Zeng, C. Wang, Molecular templates and nano-reactors: two-dimensional hydrogen bonded supramolecular networks on solid/liquid interfaces, *RSC Adv.* 3 (2013) 11351–11366.
- [3] R. Gutzler, L. Cardenas, J. Lipton-Duffin, M. El Garah, L.E. Dinca, C.E. Szakacs, C. Fu, M. Gallagher, M. Vondráček, M. Rybachuk, D.F. Perepichka, F. Rosei, Ullmann-type coupling of brominated tetrathienoanthracene on copper and silver, *Nanoscale* 6 (2014) 2660–2668.
- [4] L. Cardenas, R. Gutzler, J. Lipton-Duffin, C. Fu, J.L. Brusso, L.E. Dinca, M. Vondráček, Y. Fagot-Revurat, D. Malterre, F. Rosei, D.F. Perepichka, Synthesis and electronic structure of a two dimensional -conjugated polythiophene, *Chem. Sci.* 4 (2013) 3263–3268.
- [5] Y.-Q. Zhang, T. Lin, B. Cirera, R. Hellwig, C.-A. Palma, Z. Chen, M. Ruben, J.V. Barth, F. Klappenberger, One-dimensionally disordered chiral sorting by racemic tiling in a surface-confined supramolecular assembly of achiral tectons, *Angew. Chem. Int. Ed.* 56 (2017) 7797–7802.
- [6] J. Ren, E. Larkin, C. Delaney, Y. Song, X. Jin, S. Amirjalayer, A. Bakker, S. Du, H. Gao, Y.-Y. Zhang, S.M. Draper, H. Fuchs, Chemistry of 4-((4-bromophenyl)ethynyl)pyridine at metal surfaces studied by STM, *Chem. Commun.* 54 (2018) 9305–9308.
- [7] D. Ćija, J.I. Urgel, A.C. Papageorgiou, S. Joshi, W. Auwärter, A.P. Seitsonen, S. Klyatskaya, M. Ruben, S. Fischer, S. Vijayaraghavan, J. Reichert, J.V. Barth, Five-vertex Archimedean surface tessellation by lanthanide-directed molecular self-assembly, *Proc. Natl. Acad. Sci.* 110 (2013) 6678–6681.
- [8] J.I. Urgel, D. Ćija, G. Lyu, R. Zhang, C.-A. Palma, W. Auwärter, N. Lin, J.V. Barth, Quasicrystallinity expressed in two-dimensional coordination networks, *Nat. Chem.* 8 (2016) 657–662. Article.
- [9] J. Liu, T. Lin, Z. Shi, F. Xia, L. Dong, P.N. Liu, N. Lin, Structural transformation of two-dimensional metal-organic coordination networks driven by intrinsic in-plane compression, *J. Am. Chem. Soc.* 133 (46) (2011) 18760–18766. PMID: 21985163.
- [10] M. Ammon, T. Sander, S. Maier, On-surface synthesis of porous carbon nanoribbons from polymer chains, *J. Am. Chem. Soc.* 139 (2017) 12976–12984. PMID: 28820266.
- [11] S. Xing, Z. Zhang, X. Fei, W. Zhao, R. Zhang, T. Lin, D. Zhao, H. Ju, H. Xu, J. Fan, J. Zhu, Y.-q. Ma, Z. Shi, Selective on-surface covalent coupling based on metal-organic coordination template, *Nat. Commun.* 10 (2019) 70.
- [12] H. Zhou, H. Dang, J.-H. Yi, A. Nanci, A. Rochefort, J.D. Wuest, Frustrated 2d molecular crystallization, *J. Am. Chem. Soc.* 129 (2007) 13774–13775. PMID: 17948995.
- [13] A. Stannard, J.C. Russell, M.O. Blunt, C. Salesiotis, M. d. C. Giménez-López, N. Taleb, M. Schröder, N.R. Champness, J.P. Garrahan, P.H. Beton, Broken symmetry and the variation of critical properties in the phase behaviour of supramolecular rhombus tilings, *Nat. Chem.* 4 (2011) 112–117. Article.
- [14] M. Blunt, X. Lin, M. d. C. Gimenez-Lopez, M. Schröder, N.R. Champness, P.H. Beton, Directing two-dimensional molecular crystallization using guest templates, *Chem. Commun.* (2008) 2304–2306.
- [15] H. Zhou, T. Maris, J.D. Wuest, Using systematic comparisons of 2d and 3d structures to reveal principles of molecular organization. Tetraesters of linear bisisophthalic acids, *J. Phys. Chem. C* 116 (2012) 13052–13062.
- [16] J.-F. Zhao, Y.-B. Li, Z.-Q. Lin, L.-H. Xie, N.-E. Shi, X.-K. Wu, C. Wang, W. Huang, Molecule length directed self-assembly behavior of tetrapotic oligomeric phenyleneethylenes end-capped with carboxylic groups by scanning tunneling microscopy, *J. Phys. Chem. C* 114 (2010) 9931–9937.
- [17] D. Heim, K. Seufert, W. Auwärter, C. Aurisicchio, C. Fabbro, D. Bonifazi, J.V. Barth, Surface-assisted assembly of discrete porphyrin-based cyclic supramolecules, *Nano Lett.* 10 (2010) 122–128. PMID: 19888718.
- [18] T. Kudernac, S. Lei, J.A.A.W. Elemans, S. De Feyter, Two-dimensional supramolecular self-assembly: nanoporous networks on surfaces, *Chem. Soc. Rev.* 38 (2009) 402–421.
- [19] J.F. Dienstmaier, K. Mahata, H. Walch, W.M. Heckl, M. Schmittel, M. Lackinger, On the scalability of supramolecular networks high packing density vs optimized hydrogen bonds in tricarboxylic acid monolayers, *Langmuir* 26 (2010) 10708–10716.
- [20] A. Ciesielski, P.J. Szabelski, W. Rzyśko, A. Cadetdu, T.R. Cook, P.J. Stang, P. Samorì, Concentration-dependent supramolecular engineering of hydrogen-bonded nanostructures at surfaces: predicting self-assembly in 2d, *J. Am. Chem. Soc.* 135 (2013) 6942–6950. PMID: 23590179.
- [21] F. Silly, Concentration-dependent two-dimensional halogen-bonded self-assembly of 1,3,5-tris(4-iodophenyl)benzene molecules at the solid-liquid interface, *J. Phys. Chem. C* 121 (2017) 10413–10418.
- [22] J. Shang, Y. Wang, M. Chen, J. Dai, X. Zhou, J. Kuttner, G. Hilt, X. Shao, J.M. Gottfried, K. Wu, Assembling molecular Sierpinski triangle fractals, *Nat. Chem.* 7 (2015) 389–393. Article.
- [23] Z. Shi, N. Lin, Structural and chemical control in assembly of multicomponent metalorganic coordination networks on a surface, *J. Am. Chem. Soc.* 132 (2010) 10756–10761. PMID: 20681708.
- [24] Q. Fan, C. Wang, Y. Han, J. Zhu, J. Kuttner, G. Hilt, J.M. Gottfried, Surface-assisted formation, assembly, and dynamics of planar organometallic macrocycles and zigzag shaped polymer chains with c-cu-c bonds, *ACS Nano* 8 (2014) 709–718. PMID: 24328267.
- [25] K. Tahara, C.A. Johnson, T. Fujita, M. Sonoda, F.C. De Schryver, S. De Feyter, M.M. Haley, Y. Tobe, Synthesis of dehydrobenzo[18]annulene derivatives and formation of self-assembled monolayers: implications of core size on alkyl chain interdigitation, *Langmuir* 23 (2007) 10190–10197. PMID: 17760473.
- [26] A.M. Bragança, B.E. Hirsch, A. Sanz-Matias, Y. Hu, P. Walke, K. Tahara, J.N. Harvey, Y. Tobe, S. De Feyter, How does chemisorption impact physisorption? Molecular view of defect incorporation and perturbation of two-dimensional self-assembly, *J. Phys. Chem. C* 122 (2018) 24046–24054.
- [27] M.O. Blunt, J.C. Russell, M. d. C. Gimenez-Lopez, N. Taleb, X. Lin, M. Schröder, N.R. Champness, P.H. Beton, Guest-induced growth of a surface-based supramolecular bilayer, *Nat. Chem.* 3 (2010) 74–78. Article.

- [28] A. Ciesielski, A. Cadeddu, C.-A. Palma, A. Gorczyński, V. Patroniak, M. Cecchini, P. Samorì, Self-templating 2d supramolecular networks: a new avenue to reach control over a bilayer formation, *Nanoscale* 3 (2011) 4125–4129.
- [29] M.E. Garah, T.R. Cook, H. Sepehrpour, A. Ciesielski, P.J. Stang, P. Samorì, Concentration-dependent supramolecular patterns of c3 and c2 symmetric molecules at the solid/liquid interface, *Colloids Surf. B: Biointerfaces* 168 (2018) 211–216. Honoring Piero Baglioni.
- [30] I. Cebula, E.F. Smith, M. d. C. Gimenez-Lopez, S. Yang, M. Schröder, N.R. Champness, P.H. Beton, Packing of isophthalate tetracarboxylic acids on au(111): rows and disordered herringbone structures, *J. Phys. Chem. C* 117 (2013) 18381–18385. PMID: 24163714.
- [31] S. Clair, D.G. de Oteyza, Controlling a chemical coupling reaction on a surface: tools and strategies for on-surface synthesis, *Chem. Rev.* 119 (2019) 4717–4776. PMID: 30875199.
- [32] L. Dong, Z. Gao, N. Lin, Self-assembly of metal–organic coordination structures on surfaces, *Prog. Surf. Sci.* 91 (2016) 101–135.
- [33] D. Nieckarz, W. Rżysko, P. Szabelski, On-surface self-assembly of tetrapotic molecular building blocks, *Phys. Chem. Chem. Phys.* 20 (2018) 23363–23377.
- [34] W. Rżysko, D. Nieckarz, P. Szabelski, Modeling of the 2d self-assembly of tripod-shaped functional molecules with patchy interaction centers, *Adsorption* 25 (2019) 75–85.
- [35] T.A. Maula, H.W. Hatch, V.K. Shen, S. Rangarajan, J. Mittal, Designing molecular building blocks for the self-assembly of complex porous networks, *Mol. Syst. Des. Eng.* (2019)–.
- [36] M. El Garah, A. Dianat, A. Cadeddu, R. Gutierrez, M. Cecchini, T.R. Cook, A. Ciesielski, P.J. Stang, G. Cuniberti, P. Samorì, Atomically precise prediction of 2d self-assembly of weakly bonded nanostructures: STM insight into concentration-dependent architectures, *Small* 12 (2016) 343–350.
- [37] G. Copie, F. Cleri, Y. Makoudi, C. Krzeminski, M. Berthe, F. Cherioux, F. Palmino, B. Grandidier, Surface-induced optimal packing of two-dimensional molecular networks, *Phys. Rev. Lett.* 114 (2015) 066101.
- [38] C.-A. Palma, P. Samorì, M. Cecchini, Atomistic simulations of 2d bicomponent self-assembly: from molecular recognition to self-healing, *J. Am. Chem. Soc.* 132 (2010) 17880–17885. PMID: 21114285.
- [39] Y. Zhao, J. Wang, How to obtain high-quality and high-stability interfacial organic layer: insights from the PTCDA self-assembly, *J. Phys. Chem. C* 121 (8) (2017) 4488–4495.
- [40] Y.V. Kalyuzhnyi, P.T. Cummings, Two-patch colloidal model with re-entrant phase behaviour, *J. Chem. Phys.* 139 (2013) 104905.
- [41] W. Rżysko, S. Sokołowski, T. Staszewski, Monte Carlo simulations of a model two-dimensional, two-patch colloidal particles, *J. Chem. Phys.* 143 (2015) 064509.
- [42] S. Toxvaerd, J.C. Dyre, Communication: shifted forces in molecular dynamics, *J. Chem. Phys.* 134 (2011) 081102.
- [43] D. Frenkel, B. Smit, Chapter 1 - introduction, in: D. Frenkel, B. Smit (Eds.), *Understanding Molecular Simulation* (Second Edition), Academic Press, San Diego, 2002, pp. 1–6. <http://www.sciencedirect.com/science/article/pii/B9780122673511500031>. <https://doi.org/10.1016/B978-012267351-1/50003-1>.
- [44] Steve Plimpton, Large-Scale Atomic/Molecular Massively Parallel Simulator, (1995) [Online; accessed 29-April-2019]. lammps.sandia.gov.
- [45] S. Plimpton, Fast parallel algorithms for short-range molecular dynamics, *J. Comput. Phys.* 117 (1995) 1–19.
- [46] H.J.C. Berendsen, J.P.M. Postma, W.F. van Gunsteren, A. DiNola, J.R. Haak, Molecular dynamics with coupling to an external bath, *J. Chem. Phys.* 81 (1984) 3684–3690.
- [47] G.J. Martyna, M.L. Klein, M. Tuckerman, Nosé-Hoover chains: the canonical ensemble via continuous dynamics, *J. Chem. Phys.* 97 (1992) 2635–2643.
- [48] K. Binder, Finite size scaling analysis of Ising model block distribution functions, *Z. Phys. B: Condens. Matter* 43 (1981) 119–140.
- [49] N.D. Mermin, H. Wagner, Absence of ferromagnetism or antiferromagnetism in one- or two-dimensional isotropic Heisenberg models, *Phys. Rev. Lett.* 17 (1966) 1133–1136.



Cite this: *Mol. Syst. Des. Eng.*, 2020, 5, 484

Application of a coarse-grained model for the design of complex supramolecular networks†

Ł. Baran * and W. Rżysko 

We introduce a coarse-grained model, which allows us to understand the self-assembly behavior of complex chemical compounds on solid surfaces. It has been shown that such a simplified approach can be used for various molecular architectures, such as tetratopic, V-shape and linear molecules. Moreover, different directions of interparticle interactions, as well as the size of the interaction zone have been taken into account. In such a way we can estimate the influence of the shape of the molecule and the direction of the interparticle interactions on the formation of various molecular networks. By avoiding the full-atom representation and complexity of chemical interactions, our coarse-grained model is able to reproduce experimental data. It follows from this that the shape of the molecules and the directional interactions between them are the driving force for the self-assembly phenomena investigated in the course of the study. In our opinion the method presented here can be very helpful for the design of supramolecular networks and can give insight for the preparation of experimental studies.

Received 14th September 2019,
Accepted 20th November 2019

DOI: 10.1039/c9me00122k

rsc.li/molecular-engineering

Design, System, Application

The manuscript presents the results of molecular dynamics simulations devoted to investigate the influence of the molecular geometry on the self-assembly process in two-dimensional systems. Additionally, examination of the influence of the size of the interaction zone on the formation of self-assembled structures were taken into account. Our results demonstrate how the architecture of molecules can be controlled to create supramolecular networks of desired morphology. It follows from the work that the molecular architecture and the presence of directional interactions are two of the most important factors driving the self-assembly process. Since we have examined various geometries of the molecules we conclude that extension of the model to diverse architectures is obvious. The findings presented in this paper can be helpful for scientists working on such systems, as they can help select a building block that is able to create a 2D network with predefined topology.

1 Introduction

Development of novel supramolecular networks has gained a broad interest over past years. This was followed by a vast amount of papers of both experimental and theoretical findings. Experimentalists are mainly interested in the synthesis of new chemical compounds, which are able to self-assemble on solid surfaces or to find applications for already existing ones. On the other hand, theoretical predictions are devoted mainly to the elucidation of already known phenomena, or to predict novel supramolecular networks, which could be further investigated experimentally. Recently, several factors have been established that could be helpful to allow the control of the self-assembly process, such as the

precursor architecture^{1,2} or the substrate nature and symmetry.^{3,4}

The templates which are of particular interest involve building blocks of linear,^{5–9} V-shape,^{10,11} tripod^{12,13} and tetrapod^{14–19} molecules. Moreover, there is a lot of interest devoted to investigation of porphyrins^{20,21} and tetraphenylethylene derivatives (TPE).^{22–25} The chemical compounds assemble on solid surfaces by means of highly directional interactions, such as hydrogen^{26,27} and halogen^{28,29} bonding, metal–organic ligand coordination^{30–32} as well as van der Waals forces.³³ Besides that, the formation of highly ordered structures is dependent on the temperature,³⁴ solvent type and its concentration.

Since increasing attention can be observed for the investigation of such phenomena, development of supramolecular networks with desired properties may be of interest, however it is also hard to predict. Because of that, the synthesis of such chemical compounds can be tedious and costly. Therefore, the need for the application of computer simulations seems to be an obvious and

Department for Theoretical Chemistry, Institute of Chemical Sciences, Faculty of Chemistry, Maria Curie-Skłodowska University in Lublin, Poland.

E-mail: lukasz.baran95@gmail.com

† Electronic supplementary information (ESI) available. See DOI: 10.1039/c9me00122k

convenient tool to investigate the effects of multiple factors on the self-assembly process. Computer modelling allows us to change various parameters so that a vast range of both molecules of different geometry and different conditions can be examined. Therefore, such an approach can give very valuable insight for experimentalists.

The most commonly used methods involve lattices with triangular symmetry^{35,36} and off-lattice³⁷ Monte Carlo, where for the first one interactions only between the nearest neighbors have been taken into account, while for the latter square-well potentials have been employed. Another approach was to use the model of so-called patchy rhombi particles,^{38,39} which were supposed to reflect the behavior of tetracarboxylic acids, forming random and ordered structures. Additionally, very recently, we have also shown that the application of the Lennard-Jones (12,6) potential using the molecular dynamics method^{40,41} is a suitable tool for the reproduction of the behavior of real experimental data.

One can obviously say that the form of the interparticle potential determines the behavior of the system. However, it is important to note that the evaluation of the approximate realistic force field, which would mimic the behavior of a particular chemical compound, is very tedious and time consuming. Moreover, exact solutions for complex molecules do not exist. Even for a simple molecule like water, there are plenty of force fields which display only several quantities correctly and others which do not, dependent on the employed model.⁴² Thus it is not surprising that the approaches for simulation of all-atom models of real chemical compounds, which are more complex, are limited. There have been several approaches that were able to reflect the exact behavior of particular experimental systems.^{43,44} For instance, C. A. Palma *et al.* have performed a comprehensive experimental and simulation study, where they used MD simulations with the MMFF94 force field within the CHARMM package.⁴⁵ They obtained results which corroborated for both methods, however, it is not surprising that due to the more complicated computational approach, they were only able to investigate 80 molecules. Very similar simulations have been performed with the Amber99sb force field to reflect the behavior of perylene-3,4,9,10-tetracarboxylic dianhydride molecules.⁴⁶ They were also able to investigate only 60 molecules on a graphene surface. One can see that even though those approaches are able to compare explicitly all of the properties, such as the strength of the interparticle interactions, measured in experimental studies, they are hardly able to investigate structural properties due to the limited amount of molecules in the simulations. It is well known that to study collective phenomena such as, for example, self-assembly, which is a phase transition of a different order, depends on the investigated system. In such a case many more molecules should be considered due to finite size effects.⁴⁷ For instance, Fig. 18b of ref. 48 shows that for smaller systems, a phase transition occurs, which is only an artifact of the finite size system and will never be observed in the thermodynamic limit. In these cases the coarse-grained

simulations provide an effective research tool. Moreover, the use of coarse-grained models can be necessary to predict numerous specific properties of materials, *e.g.*, elasticity, viscosity, *etc.* All-atom approaches are also computationally more expensive in contrast to coarse-grained modelling.

Hence, the need for simplified approaches is very important to complement the methodology of analysis of structural properties. Our intention then, was to create a model that would be able to both reflect experimental data and to predict novel supramolecular structures. Moreover, such an approach can help us to understand which factor plays the key role in self-assembly phenomena. The main reason that this is important is that it is a cheaper and a faster way to examine a vast space of different conditions, of which only the most interesting cases can be further investigated experimentally. Therefore, in this study we propose a molecular dynamics (MD) technique suitable for representation of various molecular architectures. The reason for such an approach is mainly the facility of its implementation (LAMMPS package)^{49,50} and the possibility of investigation of quite complex systems in a reasonable time and their dynamical properties.

The outline of this paper is as follows. In section 2 we describe the model and simulation details used in the course of our study. Section 3.1 presents molecular dynamics results, which show possibilities of this approach for various directions of interparticle interactions of tetratopic molecules. Finally 3.2 presents an extension of the model, which allows us to mimic completely different architectures of chemical compounds.

2 Model and simulation details

The model proposed was chosen so that it could reproduce tetra substituted chemical compounds. Besides that, we wanted to examine whether our model is suitable for investigation of different molecular architectures, such as linear and V-shape tectons. We also propose a model of decorated disks,^{51,52} which can mimic the behavior of TPE and porphyrins.

All of the molecules used in the course of the simulations are shown in Fig. 1. They were treated as flat rigid bodies.

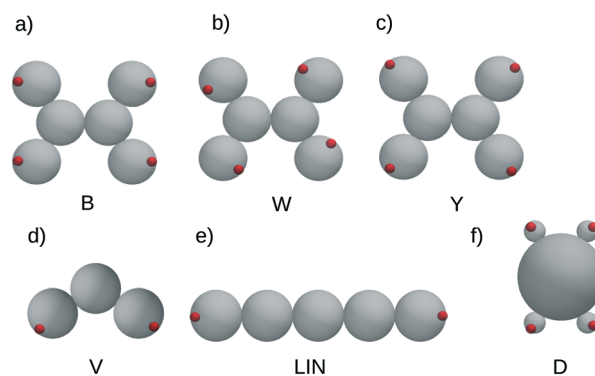


Fig. 1 Schematic representation of the tetratopic models (parts a–c) used in this work. Parts d–f show diverse geometries inspected in the course of this study. Silver and red circles correspond to the components of the backbone and “phantom” active sites, respectively.

The tetratopic particles consisted of a rod-like “core” of length N_C and four “arms”, each of length N_A , attached to it (see Fig. 2a). The angle between the arms at each side was set to $\theta = 120^\circ$. The size of the components of both core and arms was set to be equal and abbreviated as σ_b . Because of this, we will not distinguish them one from another and they will be referred to as the components of the backbone. The bonding distance between these entities was also set to σ_b . The active sites, each of size σ_a , have been settled into the terminal arm's segment, and the backbone-site bonding distance is abbreviated hereafter as l . In the case of linear and V-shape molecules, both the bonding distance l , and the active site size σ_a changed, however the size of the backbone constituents remained equal to σ_b . In the case of the model of decorated particles, we had only one core of size $\sigma_c = 4\sigma_b$ and four arms of size σ_b , defined as in the previous tetratopic model. Additionally, we have also changed the angle, α , between arms at each side – see Fig. 2c.

In the case of molecular dynamics simulations, to ensure distances between particular entities in the entire framework, we have employed harmonic binding potentials

$$u_{bb}(r) = k_{bb}(r - \sigma_{bb})^2 \quad (1)$$

and

$$u_{ab}(r) = k_{ab}(r - l)^2. \quad (2)$$

In a similar manner, the angles have also been allowed to fluctuate, by application of angular-harmonic potentials

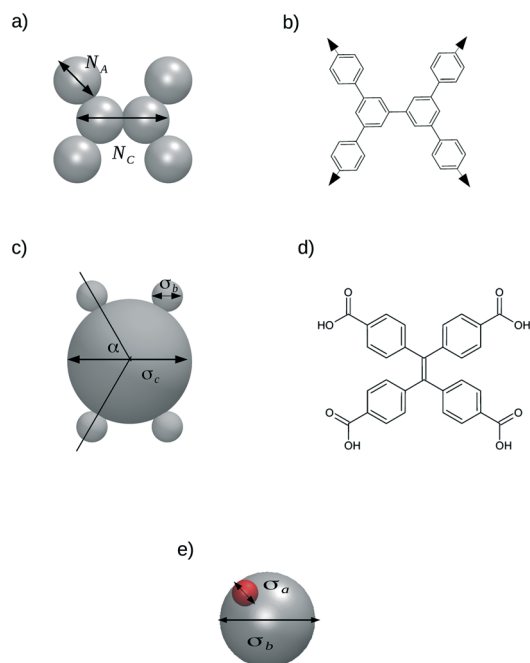


Fig. 2 a) Schematic representation of a tetratopic molecule – see the text for the meanings of the abbreviations. b) and d) show the chemical compounds which could correspond to the employed model. The arrows denote the direction of the interactions. c) and e) explain the parameters of the model used.

$$u_{bb}(\theta_{bb}) = k_{\theta}(\theta_{bb} - \theta_{0,bb})^2 \quad (3)$$

and

$$u_{ab}(\theta_{ab}) = k_{\theta}(\theta_{ab} - \theta_{0,ab})^2. \quad (4)$$

To ensure the continuity of the truncated (12,6) Lennard-Jones potential, necessary in the case of molecular dynamics simulations, it has been appropriately shifted,⁵³

$$U_{SF} = \begin{cases} U_{LJ}(r) - U_{LJ}(r_{cut}) + U'_{LJ}(r_{cut})(r - r_{cut}) & r < r_{cut} \\ 0 & \text{otherwise} \end{cases} \quad (5)$$

where $U_{LJ}(r) = 4\epsilon_{kl}[(\sigma_{kl}/r)^{12} - (\sigma_{kl}/r)^6]$ and $U'_{LJ}(r_{cut})$.

The backbone Lennard-Jones parameters $\sigma \equiv \sigma_b$ and $\epsilon \equiv \epsilon_{bb}$ have been set to be the units of length and energy, respectively. The reduced time and temperature are equal to $\tau^* = t\sqrt{\epsilon/m\sigma^2}$, $T^* = kT/\epsilon_{aa}$. The latter definition has been used in order to keep the temperature scale independent of the association energy. Additionally, the number density has been defined as $\rho^* = \frac{N_C \cdot \sigma_b^2 + X \cdot N_A \cdot \sigma_a^2}{L_x \cdot L_y}$, where X means the

number of “arms”, which for the models **Y**, **B**, and **W**, $X = 4$, for the model **V**, $X = 2$ and for the **LIN**, $X = 0$ – see Fig. 1. However, for the decorated particle (molecule **D**), in the following formula σ_b was replaced by σ_c , and $X = 4$. In the molecular dynamics simulations the mass of the backbone entities, as well as of the active sites have been both set to unity, although their diameters have not been assumed to be equal. The core and the arm segment diameters are equal to $\sigma_b = \sigma$, while the active site diameter is equal to $\sigma_a = 0.2\sigma$ for the V-shape and tetratopic molecules, and the active site-terminal arm's bonding was set to $l = 0.4$ or $l = 0.45$ if we assumed that two or three particles can associate, respectively. However, for the linear molecules the active site diameter was set to $\sigma_a = 0.2\sigma, 0.3\sigma$, and 0.4σ , and in such a case l was set so that the active sites were tangentially jointed into the terminal segment of the molecule. It has been done in order to increase even further the maximum amount of molecules which can associate.

The energies of the backbone–backbone and the backbone-active site interactions have been fixed and are equal to $\epsilon_{bb} = \epsilon$ and $\epsilon_{aa} = 5.0\epsilon$. It is important to note that this kind of screened interparticle interactions can reflect diverse chemical compounds in solutions. Nevertheless, in our systems solvent molecules have not been treated explicitly, because we were mainly interested in the interactions between active sites of different molecules, which can be treated as, for instance, corresponding to the formation of hydrogen bonds between the molecules, as mentioned above. The mixtures of such molecules with solvent particles are currently being thoroughly investigated in our laboratory.

The backbone-site diameter and the energy of the backbone-site interaction have been assumed to be equal to $\sigma_{ab} = (\sigma_{bb} + \sigma_{aa})/2$ and $\epsilon_{ab} = \epsilon$, respectively. The cut off distance of the interaction between two active sites has been

set as equal to $r_{\text{cut,aa}} = 2\sigma_{\text{aa}}$, on the other hand, we have assumed that $r_{\text{cut,kl}} = \sigma_{\text{kl}}$, for $\text{kl} = \text{bb}, \text{ab}$, ensuring that bb and ab interactions are non-attractive. The harmonic potential constants $k_{\text{bb}} \equiv k_{\text{ab}}$ have been set as equal to $1000\epsilon/\sigma^2$, and $k_{\theta} = 1000\epsilon/(\text{radian}^2)$.

For the sake of brevity all of the model parameters are listed in Table 1.

All of the molecular dynamics simulations have been performed in the NVT ensemble using the LAMMPS simulation package.^{49,50} The velocity Verlet integration algorithm has been used. The reduced time step was equal to $t = 0.001\tau$. In the molecular dynamics simulations the number of molecules was set to 2500. However, one has to note that the total amount of “atoms” varied with the molecular architecture.

The preliminary equilibration runs were performed using a Berendsen thermostat with the damping constant equal to $\tau_{\text{B}} = 10\tau$ for 5×10^6 time steps. Further equilibration for 5×10^7 time steps, as well as the production runs, were performed by Nosé–Hoover chains algorithm. The number of chains used was set to $N_{\text{chain}} = 3$ with the dampening constant $\tau_{\text{NH}} = 10\tau$. Each system (Table 2) has been slowly cooled down from temperatures at which the system was disordered to temperatures where the formation of self-assembled structures was observed, with the temperature grid equal to $\Delta T = 0.002$.

3 Results and discussion

3.1 Application for tetratopic molecules

We start with a description of the chemical compounds, which were experimentally investigated by S. Xing. *et al.*¹⁴ The authors presented the self-assembly of 1,4-bis(6,6'-dibromo-[2,2':6',2''-terpyridin]-4'-yl)benzene on the Au(111) surface. They showed that a mixture of this compound with Fe atoms (template atoms) leads to selectivity of the on-surface reactions, which introduces highly directional interactions, resulting in the formation of nanoribbons.

We propose a simplified model, which is shown in Fig. 1a, which should reproduce their results. The reason for choosing this particular direction of interparticle interactions was to mimic the structures which have been obtained in the mixture of tetrapod tectons with metal atoms. However, we did not want to include additional atoms explicitly, because we did not want to exactly reflect any real chemical compound nor their interaction, but to reproduce an approximate form of the effective interactions observed in

Table 1 List of interaction parameters for all models

Model	σ_{b}	σ_{a}	l	X	$r_{\text{cut,aa}}$
B	1	0.2	0.4	4	0.4
W	1	0.2	0.4	4	0.4
Y	1	0.2	0.45	4	0.4
V	1	0.2	0.45	2	0.4
LIN	1	0.2; 0.3; 0.4	0.6; 0.65; 0.7	0	0.4; 0.6; 0.8
D	$1; \sigma_{\text{c}} = 4\sigma_{\text{b}}$	0.2	0.4	4	0.4

Table 2 The systems investigated in the course of our simulations. *P* means different models (a–c), as shown in Fig. 1. For abbreviations of *d* and *e* see the text

P_{CA}	N_{C}	N_{A}
P_{21}	2	1
P_{31}	3	1
P_{41}	4	1
P_{22}	2	2
P_{32}	3	2
P_{42}	4	2

the systems. Besides that, we wanted to further extend their work to study the influence of molecular geometry, that is the core and the arm length.

Fig. 3 and 4 show the formation of the bead-like structures of different sizes, depending on the molecular architecture. One can see in the case of particles \mathbf{B}_{21} to \mathbf{B}_{41} that the increase of the core length, N_{C} , causes an increase of the cluster length. This statement has been proven by the cluster analysis procedure, described in ESI† and the results of average cluster sizes are shown in Fig. S1.† In Fig. 4 even for a short core size we observe very long clusters. This means that the length of the arms allows formation of bigger structures. Moreover, those long beads tend to “glue” one with another to minimize the empty spaces. This results in a structure where the cores of one cluster are alternately arranged with respect to another cluster. It is marked in the red ellipse – see Fig. 4. Of course, the length of the beads is temperature and density dependent and for some conditions, we could obtain similar results for every system. However, our intention was to estimate the influence of molecular geometry for the stabilization of longer clusters.

Since our model reflects the behavior of quite complex experimental systems consisting of tetratopic molecules, we wanted to check the possibility of including other directions of interactions, not investigated yet, to the best of our knowledge. Results for molecules \mathbf{W}_{21} to \mathbf{W}_{41} (Fig. 1b) are shown in Fig. 5.

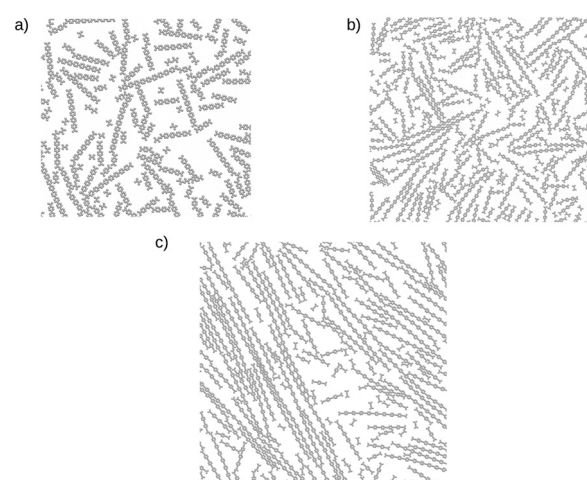


Fig. 3 Results for molecules a) \mathbf{B}_{21} in $\rho^* = 0.257$ at $T^* = 0.1$, b) \mathbf{B}_{31} in $\rho^* = 0.255$ at $T^* = 0.1$ and c) \mathbf{B}_{41} in $\rho^* = 0.251$ at $T^* = 0.1$.

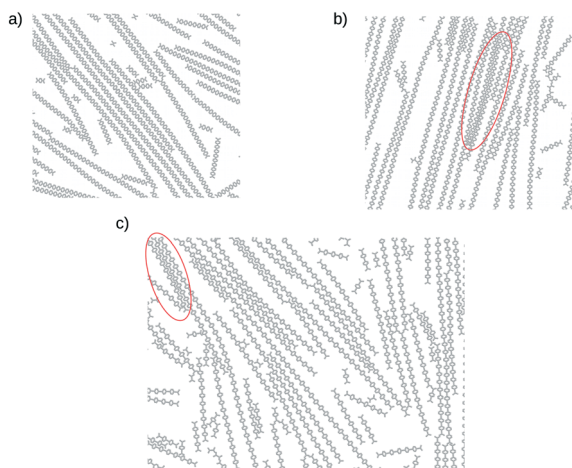


Fig. 4 Results for molecules a) B_{22} in $\rho^* = 0.207$ at $T^* = 0.08$, b) B_{32} in $\rho^* = 0.204$ at $T^* = 0.08$ and c) B_{42} in $\rho^* = 0.2$ at $T^* = 0.08$.

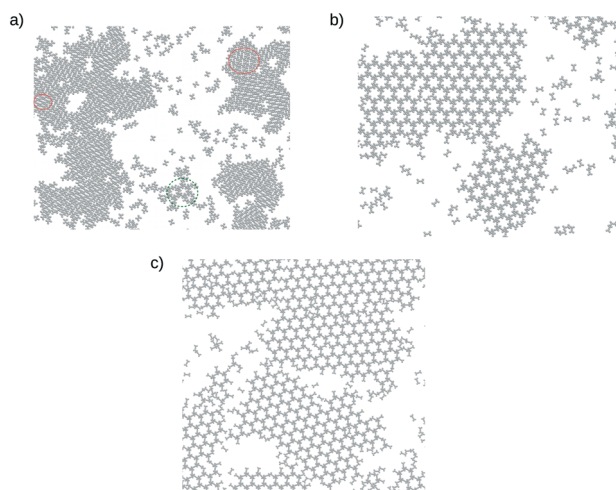


Fig. 5 Results for molecules a) W_{21} in $\rho^* = 0.237$ at $T^* = 0.08$, b) W_{31} in $\rho^* = 0.231$ at $T^* = 0.08$ and c) W_{41} in $\rho^* = 0.227$ at $T^* = 0.08$. Different pores observed in the system W_{21} are marked in red and green.

One can see that for the system consisting of molecules W_{21} , there is a highly ordered, parallel-like network, built of at least two types of pores of different sizes – marked in red in Fig. 5a. We also sometimes observe a formation of smaller clusters – marked in the green dashed line in the Fig. 5a. This structure forms pores of different shape, which are significantly larger than mentioned previously. Even though this structure is very rarely observed in our simulations, the same situation could be the case during experiments.

For a slight elongation of the core length, N_C , in contrast to system W_{21} , we observe the formation of one well ordered phase with small imperfections in its network. It is easy to see that in the case of W_{31} , the structure from the previous system which occurred very rarely is the only one present. This network's pore shape resembles rotated hexagons. The same situation occurs in the system W_{41} . We can clearly see that the change in core length stabilizes this phase.

However, elongation of the arms does not show so apparent an effect as in the case of molecules **B**. Indeed it is easy to see that the supramolecular network built of W_{22} molecules is more pronounced, but is qualitatively the same as for W_{21} . There is also an interesting feature observed in the behavior of this model. The elongation of the core length to $N_C = 3$ and 4, with arms of length $N_A = 2$, causes formation of a Kagomé-like network (Fig. 6). However, this network is rotated, which is due to the nature of the designed direction of interparticle interactions. Another interesting observation is that the parallel-like network almost vanishes and the rotated Kagomé structure starts to dominate in the case of the W_{42} molecule. Moreover, it is apparent that elongation of the core also leads to the stabilization of the formed structures in the system. There are no more observed imperfections in both of the structures. A parallel-like network is formed only by one type of the pores, which was not the case for previously investigated systems. We have also elongated the length of the arms to $N_A = 3$ and we did not observe formation of a Kagomé network for molecules from W_{23} to W_{43} and only a parallel-like network was present. We did not show the results for the sake of brevity. Such an observation allows us to conclude that the elongation of the arm's length means that the phase of lower density is not able to form in the range of investigated core lengths. Because of such promising results, obtained for a yet unknown structure, we have already found the chemical compound which could possibly reflect the phase behavior. To do that, we have already started to prepare experiments in our laboratory, which can confirm our predictions.

As we can see, our model is able to reproduce both experimental and novel supramolecular structures (molecules **W**), hence we wanted to further examine its possibilities. We have checked what frameworks will be formed if we use the molecules of **Y** (Fig. 1c) geometry, but with the active site-terminal arm's segment bonding distance equal to $l = 0.45$. The reason for this is to allow the possibility of three molecules interacting simultaneously

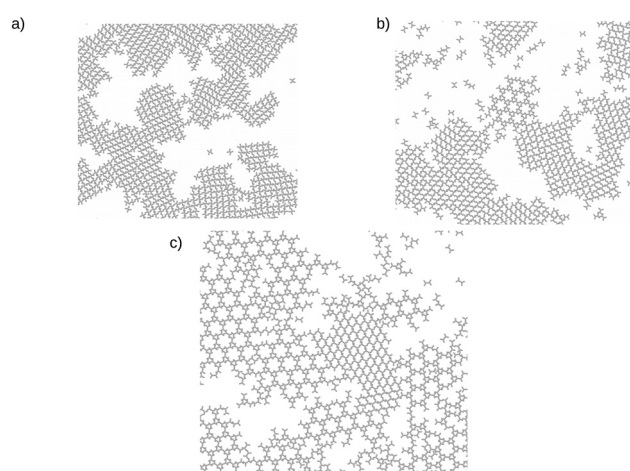


Fig. 6 Results for molecules a) W_{22} in $\rho^* = 0.207$ at $T^* = 0.074$, b) W_{32} in $\rho^* = 0.196$ at $T^* = 0.074$ and c) W_{42} in $\rho^* = 0.18$ at $T^* = 0.074$.

(Fig. 7c and d). In other words, we can assume that the chemical compounds have been substituted with a different chemical group, which has a “wider” interaction zone. It can also reflect interactions of a binary mixture with metal atoms, resulting in a coordination number equal to three. Results for Y_{21} and Y_{41} are shown in Fig. 7a and b, respectively. One can see that for both models, we observe a completely different type of ordering. In the system with molecules Y_{21} , we see the formation of a network of randomly distributed sunflower structures, around which we observe the creation of 12 pores of different sizes to the former one.

Elongation of the core size, $N_C = 4$, causes a completely different, highly ordered structure to be present in the system. We observe a network created by three different kind of pores (see Fig. 7b). Surprisingly, very recently a similar structure have been observed by J. Li *et al.* for 3,3',3'',5,5',5''-benzene-1,3,5-triylhexabenzic acid.⁵⁴ Such a network with different porous sizes can be very useful technologically, for instance in analytical chemistry. Moreover, we can see the similar tendency, as in the case of every other previous model, that the elongation of the core causes formation of better ordered supramolecular networks.

3.2 Application for diverse geometries

We have shown that this model works for various tetrapod molecules. Let us now proceed to a different molecular architecture abbreviated as **V** (Fig. 1d), which has V-shaped particles. It has been proven that molecules of this shape in a mixture with metal atoms form Sierpinski triangle (ST) fractals on solid surfaces. For instance, 1,3-bi(4-pyridyl) benzene with Co atoms creates STs on Au(111).¹¹ Other experimental studies show that it is possible to obtain these frameworks without metal atoms for different active groups, but with the same geometry of particle.^{10,55} It follows from

that that the driving forces for such a phenomenon are the directional interactions and the shape of the molecule.

To check if this is the case, we have constructed V-shape molecules, as shown in Fig. 1d. In this model, we have set the terminal arm's-active site bonding distance to $l = 0.45$, so that three molecules could interact simultaneously, as in one case of tetrapods (**Y**). The results for such a system are shown in Fig. 8a, and one can see that this particular approach also reflects the experimental data of complex structures such as fractals. It is also seen that the formation of up to third-order Sierpinski triangles is possible by our approach. It follows from that that the key factors of such type of self-assembly are the directional interactions and the shape of the template molecule, which can be very helpful for the design of such compounds experimentally.

Besides V-shape molecules, we also show that such an approach is a suitable tool to reflect the behavior of linear molecules, whose architecture is shown in Fig. 1e. As already mentioned, the active sites in these cases were tangentially jointed into the terminal segment of the molecule. The reason for that was to reflect the behavior of a binary mixture consisting of such molecules and metal atoms. By changing the size of the active site, we could mimic the interactions of these tectons with different atoms, resulting in a different coordination number of the supramolecular framework. Fig. 8b shows the structure with square symmetry, with no visible imperfections. This was achieved by changing the bonding distance to the value of $l = 0.6$, with the same $\sigma_a = 0.2$. To obtain the so-called Archimedean tiling and hexagonal network, we have increased the value of the active site size to $\sigma_a = 0.3$ and $\sigma_a = 0.4$, respectively. The results are shown in Fig. 8c and d. The obtained configurations are also in agreement with experimental data.^{8,9} Different lengths of the linear molecules have also been taken into account, but lead to similar results and were omitted for the sake of

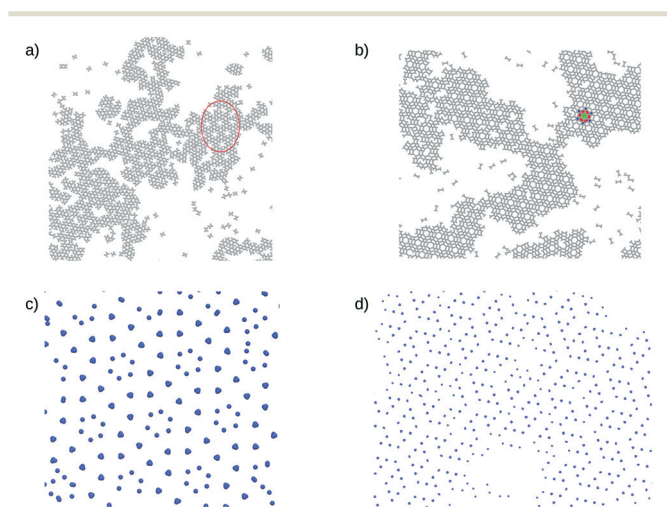


Fig. 7 Results for molecules a) Y_{21} in $\rho^* = 0.24$ at $T^* = 0.116$, b) Y_{41} in $\rho^* = 0.228$ at $T^* = 0.116$; different pore sizes are marked. c) and d) show the configurations formed by “phantom” active sites.

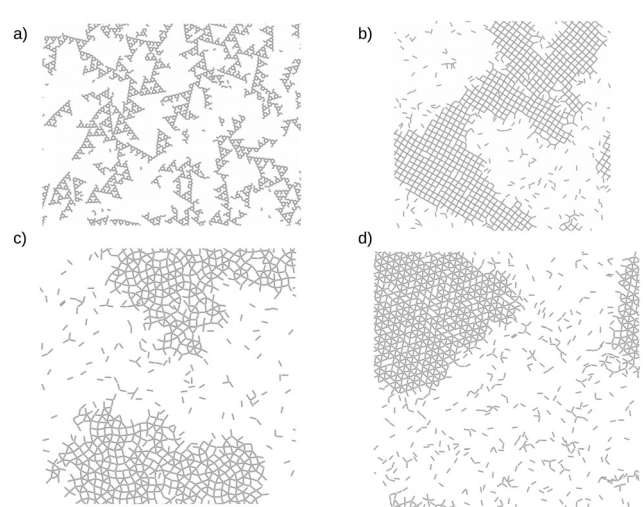


Fig. 8 Results for molecules a) **V** in $\rho^* = 0.17$ at $T^* = 0.1$, b) LIN with $\sigma_a = 0.2\sigma$ in $\rho^* = 0.16$ at $T^* = 0.11$, c) LIN with $\sigma_a = 0.3\sigma$ in $\rho^* = 0.151$ at $T^* = 0.122$ and d) LIN with $\sigma_a = 0.4\sigma$ in $\rho^* = 0.155$ at $T^* = 0.142$.

Paper

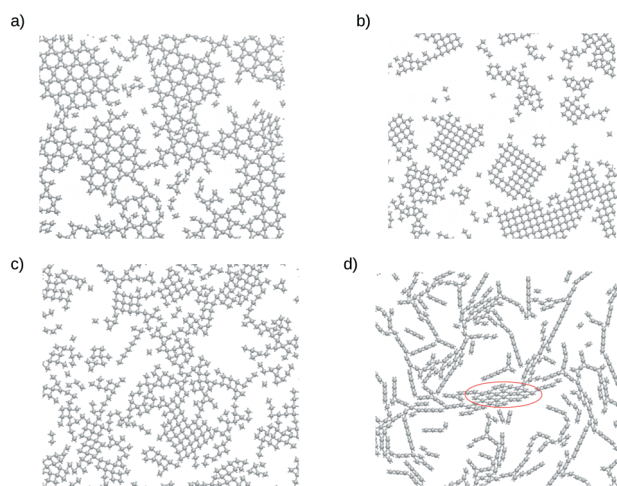


Fig. 9 Results for the decorated disks model obtained in $\rho^* = 0.249$ at $T^* = 0.09$ for molecules with a) $\alpha = 120^\circ$, b) $\alpha = 90^\circ$, c) $\alpha = 105^\circ$, d) $\alpha = 135^\circ$.

brevity. The only observed difference was the pore size of the obtained networks.

Another approach was devoted to mimicking porphyrin or TPE derivatives. In this case we propose the model of decorated disks.^{51,52} We have examined four different systems, where we have changed the angle α between the arms at each side. Fig. 9a shows the results for the molecule with $\alpha = 120^\circ$, which forms a perfect Kagomé lattice, without any visible imperfections. Moreover, it is also shown that very small parts of a brickwall network are also created.

We also computed the systems consisting of decorated disks with $\alpha = 90, 105$, and 135° . Starting from the case shown in Fig. 9b, one can see that for $\alpha = 90^\circ$ we observe formation of a perfect square lattice. Moreover, some additional structures occur, which are similar to the Archimedean tiling as in the case of linear molecules (Fig. 8c). An increase of the side angle to $\alpha = 105^\circ$ results in the formation of similar structures (Fig. 9c). In this system, we also see the square lattice, however with visible imperfections. The pore shape with respect to the previous case is not of an equal size in the entire structure, but rather deformed and sloped, resembling more of a parallelogram shape. Additionally, we observe more smaller clusters in comparison to the previous case of $\alpha = 90^\circ$. A further increase of the angle between arms at one side to $\alpha = 135^\circ$ results mostly in formation of chain-like structures of different sizes. However, one can see that there is also another porous structure, which is marked in red in Fig. 9d.

4 Conclusions

We wanted to propose a simple model which can both reflect and predict the behavior of real experimental systems. Such an approach presented here proves that the molecular architecture and directional interactions are the driving

forces of self-assembly phenomena investigated in the course of our study.

We have constructed several models which were supposed to mimic the behavior of diverse, quite complex organic molecules on solid surfaces. It has been shown that these models, which are very similar to each other in terms of interparticle interactions, can reproduce the behavior of completely different molecular architectures. It follows from this that such an approach can give very helpful insight for both theoreticians and experimentalists. The possibilities of its application seem to be almost unlimited, because as long as one will maintain the geometry of the molecules, the model should be able to work.

The approach can easily be extended to other molecular architectures not investigated in course of this study, such as tripod tectons or any other, which will match the requirements of a particular experimental study of a similar type. We have also checked that this model is compatible with every other molecular simulation method mentioned in the Introduction.^{35–37} However, in our opinion, the advantage of our routine is the implicit facility and speed of calculation employed in the LAMMPS package. Extension to more complicated cases, comprising of mixtures with diverse solvents and surfaces and investigation of 3D systems is currently being thoroughly investigated in our laboratory.

Conflicts of interest

There are no conflicts to declare.

Acknowledgements

This study has been supported by the Polish Ministry of Science and Higher Education, under Grant No. DI2017 001147. Calculations were carried out at the Academic Computer Centre in Gdańsk.

References

- X. Zhang, Q. Zeng and C. Wang, On-surface single molecule synthesis chemistry: a promising bottom-up approach towards functional surfaces, *Nanoscale*, 2013, 5, 8269–8287.
- X. Zhang, Q. Zeng and C. Wang, Molecular templates and nano-reactors: two-dimensional hydrogen bonded supramolecular networks on solid/liquid interfaces, *RSC Adv.*, 2013, 3, 11351–11366.
- R. Gutzler, L. Cardenas, J. Lipton-Duffin, M. El Garah, L. E. Dinca, C. E. Szakacs, C. Fu, M. Gallagher, M. Vondráček, M. Rybachuk, D. F. Perepichka and F. Rosei, Ullmann-type coupling of brominated tetrathienoanthracene on copper and silver, *Nanoscale*, 2014, 6, 2660–2668.
- L. Cardenas, R. Gutzler, J. Lipton-Duffin, C. Fu, J. L. Brusso, L. E. Dinca, M. Vondráček, Y. Fagot-Revurat, D. Malterre, F. Rosei and D. F. Perepichka, Synthesis and electronic structure of a two dimensional π -conjugated polythiophene, *Chem. Sci.*, 2013, 4, 3263–3268.

- 5 Y.-Q. Zhang, T. Lin, B. Cirera, R. Hellwig, C.-A. Palma, Z. Chen, M. Ruben, J. V. Barth and F. Klappenberger, One-dimensionally disordered chiral sorting by racemic tiling in a surface-confined supramolecular assembly of achiral tectons, *Angew. Chem., Int. Ed.*, 2017, **56**(27), 7797–7802.
- 6 J. Ren, E. Larkin, C. Delaney, Y. Song, X. Jin, S. Amirjalayer, A. Bakker, S. Du, H. Gao, Y.-Y. Zhang, S. M. Draper and H. Fuchs, Chemistry of 4-[(4-bromophenyl)ethynyl]pyridine at metal surfaces studied by STM, *Chem. Commun.*, 2018, **54**, 9305–9308.
- 7 D. Ćcija, J. I. Urgel, A. C. Papageorgiou, S. Joshi, W. Auwärter, A. P. Seitsonen, S. Klyatskaya, M. Ruben, S. Fischer, S. Vijayaraghavan, J. Reichert and J. V. Barth, Five-vertex archimedean surface tessellation by lanthanide-directed molecular self-assembly, *Proc. Natl. Acad. Sci. U. S. A.*, 2013, **110**(17), 6678–6681.
- 8 J. I. Urgel, D. Ćcija, G. Lyu, R. Zhang, C.-A. Palma, W. Auwärter, N. Lin and J. V. Barth, Quasicrystallinity expressed in two-dimensional coordination networks, *Nat. Chem.*, 2016, **8**, 657–662, Article.
- 9 U. Schlickum, R. Decker, F. Klappenberger, G. Zoppellaro, S. Klyatskaya, M. Ruben, I. Silanes, A. Arnau, K. Kern, H. Brune and J. V. Barth, Metal-organic honeycomb nanomeshes with tunable cavity size, *Nano Lett.*, 2007, **7**(12), 3813–3817, PMID: 18020476.
- 10 J. Shang, Y. Wang, M. Chen, J. Dai, X. Zhou, J. Kuttner, G. Hilt, X. Shao, J. M. Gottfried and K. Wu, Assembling molecular sierpinski triangle fractals, *Nat. Chem.*, 2015, **7**, 389, Article.
- 11 X. Zhang, G. Gu, N. Li, H. Wang, H. Tang, Y. Zhang, S. Hou and Y. Wang, One-dimensional molecular chains formed by sierpinski triangles on Au(111), *RSC Adv.*, 2018, **8**, 1852–1856.
- 12 J. Liu, T. Lin, Z. Shi, F. Xia, L. Dong, P. N. Liu and N. Lin, Structural transformation of two-dimensional metal-organic coordination networks driven by intrinsic in-plane compression, *J. Am. Chem. Soc.*, 2011, **133**(46), 18760–18766, PMID: 21985163.
- 13 M. Ammon, T. Sander and S. Maier, On-surface synthesis of porous carbon nanoribbons from polymer chains, *J. Am. Chem. Soc.*, 2017, **139**(37), 12976–12984, PMID: 28820266.
- 14 S. Xing, Z. Zhang, X. Fei, W. Zhao, R. Zhang, T. Lin, D. Zhao, H. Ju, H. Xu, J. Fan, J. Zhu, Y.-Q. Ma and Z. Shi, Selective on-surface covalent coupling based on metal-organic coordination template, *Nat. Commun.*, 2019, **10**(1), 70.
- 15 H. Zhou, H. Dang, J.-H. Yi, A. Nanci, A. Rochefort and J. D. Wuest, Frustrated 2d molecular crystallization, *J. Am. Chem. Soc.*, 2007, **129**(45), 13774–13775, PMID: 17948995.
- 16 A. Stannard, J. C. Russell, M. O. Blunt, C. Salesiotis, M. D. C. Giménez-López, N. Taleb, M. Schröder, N. R. Champness, J. P. Garrahan and P. H. Beton, Broken symmetry and the variation of critical properties in the phase behaviour of supramolecular rhombus tilings, *Nat. Chem.*, 2011, **4**, 112–117, Article.
- 17 M. Blunt, X. Lin, M. D. C. Gimenez-Lopez, M. Schröder, N. R. Champness and P. H. Beton, Directing two-dimensional molecular crystallization using guest templates, *Chem. Commun.*, 2008, 2304–2306.
- 18 H. Zhou, T. Maris and J. D. Wuest, Using systematic comparisons of 2d and 3d structures to reveal principles of molecular organization. tetraesters of linear bisophthalic acids, *J. Phys. Chem. C*, 2012, **116**(24), 13052–13062.
- 19 J.-F. Zhao, Y.-B. Li, Z.-Q. Lin, L.-H. Xie, N.-E. Shi, X.-K. Wu, C. Wang and W. Huang, Molecule length directed self-assembly behavior of tetratopic oligomeric phenylene-ethylenes end-capped with carboxylic groups by scanning tunneling microscopy, *J. Phys. Chem. C*, 2010, **114**(21), 9931–9937.
- 20 Z. Shi and N. Lin, Porphyrin-based two-dimensional coordination kagome lattice self-assembled on a Au(111) surface, *J. Am. Chem. Soc.*, 2009, **131**(15), 5376–5377, PMID: 20560634.
- 21 W. Auwärter, D. Ćcija, F. Klappenberger and J. V. Barth, Porphyrins at interfaces, *Nat. Chem.*, 2015, **7**, 105, Review Article.
- 22 T.-Y. Zhou, S.-Q. Xu, Q. Wen, Z.-F. Pang and X. Zhao, One-step construction of two different kinds of pores in a 2d covalent organic framework, *J. Am. Chem. Soc.*, 2014, **136**(45), 15885–15888, PMID: 25360771.
- 23 Z.-F. Pang, S.-Q. Xu, T.-Y. Zhou, R.-R. Liang, T.-G. Zhan and X. Zhao, Construction of covalent organic frameworks bearing three different kinds of pores through the heterostructural mixed linker strategy, *J. Am. Chem. Soc.*, 2016, **138**(14), 4710–4713, PMID: 27015785.
- 24 Y.-P. Mo, X.-H. Liu and D. Wang, Concentration-directed polymorphic surface covalent organic frameworks: Rhombus, parallelogram, and kagome, *ACS Nano*, 2017, **11**(11), 11694–11700, PMID: 29131939.
- 25 X. Peng, L. Cheng, X. Zhu, Y. Geng, F. Zhao, K. Hu, X. Guo, K. Deng and Q. Zeng, Pyridine-induced interfacial structural transformation of tetraphenylethylene derivatives investigated by scanning tunneling microscopy, *Nano Res.*, 2018, **11**, 5823–5834.
- 26 J. F. Dienstmaier, K. Mahata, H. Walch, W. M. Heckl, M. Schmittel and M. Lackinger, On the scalability of supramolecular networks - high packing density vs optimized hydrogen bonds in tricarboxylic acid monolayers, *Langmuir*, 2010, **26**(13), 10708–10716.
- 27 A. Ciesielski, P. J. Szabelski, W. Rzyśko, A. Cadeddu, T. R. Cook, P. J. Stang and P. Samorì, Concentration-dependent supramolecular engineering of hydrogen-bonded nanostructures at surfaces: Predicting self-assembly in 2d, *J. Am. Chem. Soc.*, 2013, **135**(18), 6942–6950, PMID: 23590179.
- 28 F. Silly, Concentration-dependent two-dimensional halogen-bonded self-assembly of 1,3,5-tris(4-iodophenyl)benzene molecules at the solid-liquid interface, *J. Phys. Chem. C*, 2017, **121**(19), 10413–10418.
- 29 J. Shang, Y. Wang, M. Chen, J. Dai, X. Zhou, J. Kuttner, G. Hilt, X. Shao, J. M. Gottfried and K. Wu, Assembling molecular sierpinski triangle fractals, *Nat. Chem.*, 2015, **7**, 389–393, Article.

- 30 Z. Shi and N. Lin, Structural and chemical control in assembly of multicomponent metal-organic coordination networks on a surface, *J. Am. Chem. Soc.*, 2010, **132**(31), 10756–10761, PMID: 20681708.
- 31 Q. Fan, C. Wang, Y. Han, J. Zhu, J. Kuttner, G. Hilt and J. M. Gottfried, Surface-assisted formation, assembly, and dynamics of planar organometallic macrocycles and zigzag shaped polymer chains with C-Cu-C bonds, *ACS Nano*, 2014, **8**(1), 709–718, PMID: 24328267.
- 32 J. I. Urgel, D. Écija, G. Lyu, R. Zhang, C.-A. Palma, W. Auwärter, N. Lin and J. V. Barth, Quasicrystallinity expressed in two-dimensional coordination networks, *Nat. Chem.*, 2016, **8**, 657, Article.
- 33 K. Tahara, C. A. Johnson, T. Fujita, M. Sonoda, F. C. De Schryver, S. De Feyter, M. M. Haley and Y. Tobe, Synthesis of dehydrobenzo[18]annulene derivatives and formation of self-assembled monolayers: Implications of core size on alkyl chain interdigitation, *Langmuir*, 2007, **23**(20), 10190–10197, PMID: 17760473.
- 34 Z. Tao, T. Wang, D. Wu, L. Feng, J. Huang, X. Wu and J. Zhu, Construction of molecular regular tessellations on a cu(111) surface, *Chem. Commun.*, 2018, **54**, 7010–7013.
- 35 D. Nieckarz, W. Rzyśko and P. Szabelski, On-surface self-assembly of tetratopic molecular building blocks, *Phys. Chem. Chem. Phys.*, 2018, **20**, 23363–23377.
- 36 W. Rzyśko, D. Nieckarz and P. Szabelski, Modeling of the 2d self-assembly of tripod-shaped functional molecules with patchy interaction centers, *Adsorption*, 2019, **25**, 75–85.
- 37 T. A. Maula, H. W. Hatch, V. K. Shen, S. Rangarajan and J. Mittal, Designing molecular building blocks for the self-assembly of complex porous networks, *Mol. Syst. Des. Eng.*, 2019, **4**, 644–653.
- 38 S. Whitelam, I. Tamblyn, P. H. Beton and J. P. Garrahan, Random and ordered phases of off-lattice rhombus tiles, *Phys. Rev. Lett.*, 2012, **108**, 035702.
- 39 C. Karner, C. Dellago and E. Bianchi, Design of patchy rhombi: From close-packed tilings to open lattices, *Nano Lett.*, 2019, **19**(11), 7806–7815, PMID: 31580675.
- 40 Ł. Baran, D. Nieckarz, P. Szabelski and W. Rzyśko, Controlling of the 2d self-assembly process by the variation of molecular geometry, *J. Phys. Chem. C*, 2019, **123**(32), 19549–19556.
- 41 Ł. Baran, Influence of the molecular geometry on the formation of the self-assembled structures, *J. Mol. Liq.*, 2019, **294**, 111627.
- 42 C. Vega and E. de Miguel, Surface tension of the most popular models of water by using the test-area simulation method, *J. Chem. Phys.*, 2007, **126**(15), 154707.
- 43 M. El Garah, A. Dianat, A. Cadeddu, R. Gutierrez, M. Cecchini, T. R. Cook, A. Ciesielski, P. J. Stang, G. Cuniberti and P. Samori, Atomically precise prediction of 2d self-assembly of weakly bonded nanostructures: Stm insight into concentration-dependent architectures, *Small*, 2016, **12**(3), 343–350.
- 44 G. Copie, F. Cleri, Y. Makoudi, C. Krzeminski, M. Berthe, F. Cherioux, F. Palmino and B. Grandidier, Surface-induced optimal packing of two-dimensional molecular networks, *Phys. Rev. Lett.*, 2015, **114**, 066101.
- 45 C.-A. Palma, P. Samori and M. Cecchini, Atomistic simulations of 2d bicomponent self-assembly: From molecular recognition to self-healing, *J. Am. Chem. Soc.*, 2010, **132**(50), 17880–17885, PMID: 21114285.
- 46 Y. Zhao and J. Wang, How to obtain high-quality and high-stability interfacial organic layer: Insights from the ptdca self-assembly, *J. Phys. Chem. C*, 2017, **121**(8), 4488–4495.
- 47 W. Rzyśko, J. J. de Pablo and S. Sokołowski, Critical behavior of simple fluids confined by microporous materials, *J. Chem. Phys.*, 2000, **113**(21), 9772–9777.
- 48 W. Rzyśko, A. Patrykiewicz and K. Binder, Phase transitions in a two-dimensional lattice gas model of orientable diatomic molecules. ii. order-disorder transitions of superantiferromagnetic and $c(2 \times 2)_{af}$ phases, *Phys. Rev. B*, 2007, **76**, 195409.
- 49 S. Plimpton, *et al.*, Large-scale atomic/molecular massively parallel simulator, lammmps.sandia.gov, 1995. [Online; accessed 29-April-2019].
- 50 S. Plimpton, Fast parallel algorithms for short-range molecular dynamics, *J. Comput. Phys.*, 1995, **117**(1), 1–19.
- 51 M. Borówko, W. Rzyśko, S. Sokołowski and T. Staszewski, Phase behavior of decorated soft disks in two dimensions, *J. Chem. Phys.*, 2016, **145**(22), 224703.
- 52 Ł. Baran and S. Sokołowski, A comparison of molecular dynamics results for two models of nanoparticles with fixed and mobile ligands in two-dimensions, *Appl. Surf. Sci.*, 2017, **396**, 1343–1351.
- 53 S. Toxvaerd and J. C. Dyre, Communication: Shifted forces in molecular dynamics, *J. Chem. Phys.*, 2011, **134**(8), 081102.
- 54 J. Li, B. Tu, X. Li, C. Ma, C. Chen, W. Duan, X. Xiao and Q. Zeng, The self-assembled flower structures formed by c3-symmetric aromatic carboxylic acids with meta-carboxyl groups, *Chem. Commun.*, 2019, **55**, 11599–11602.
- 55 Y. Mo, T. Chen, J. Dai, K. Wu and D. Wang, On-surface synthesis of highly ordered covalent sierpiński triangle fractals, *J. Am. Chem. Soc.*, 2019, **141**(29), 11378–11382, PMID: 31288514.

PIII

lic. Łukasz Baran
Katedra Chemii Teoretycznej
Instytut Nauk Chemicznych
Wydział Chemii UMCS
Pl. Marii Curie-Skłodowskiej 3
20-031 Lublin

Lublin, 16.05.2022

OŚWIADCZENIE

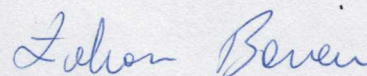
Oświadczam, że mój wkład w niniejszej pracy:

[PIII] Ł. Baran*, W. Rzyśko, "Application of a coarse-grained model for the design of complex supramolecular networks", *Molecular Systems Design & Engineering*, 2020, 5, 484-492.

polegał na przeprowadzeniu symulacji metodą dynamiki molekularnej, napisaniu manuskryptu i przeprowadzeniu analizy części wyników

Udział ten szacuję na 80 %.

lic. Łukasz Baran



PIII

dr hab. Wojciech Rzyśko, prof. UMCS
Katedra Chemii Teoretycznej
Instytut Nauk Chemicznych
Wydział Chemii UMCS
Pl. Marii Curie-Skłodowskiej 3
20-031 Lublin

Lublin, 16.05.2022

OŚWIADCZENIE

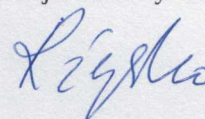
Oświadczam, że mój wkład w niniejszej pracy:

[PIII] Ł. Baran*, W. Rzyśko, "Application of a coarse-grained model for the design of complex supramolecular networks", *Molecular Systems Design & Engineering*, 2020, 5, 484-492.

polegał na koordynowaniu merytorycznym badań i analizie części wyników

Udział ten szacuję na 20 %.

dr hab. Wojciech Rzyśko, prof. UMCS



Cite this: *Mol. Syst. Des. Eng.*, 2021, **6**, 805Received 6th June 2021,
Accepted 13th July 2021

DOI: 10.1039/d1me00068c

rsc.li/molecular-engineering

Variation of interaction zone size for the target design of 2D supramolecular networks†

Łukasz Baran, * Wojciech Rżysko  and Dariusz Tarasewicz

In this study, we have performed extensive coarse-grained molecular dynamics simulations of the self-assembly of tetra-substituted molecules. We have found that such molecules are able to form a variety of structures, depending on the parameters of the employed model. In particular, it has been demonstrated that even slight changes of the interaction zone and the shape of molecules can drastically alter the behavior of investigated systems. We have established the rules governing the formation of the Sierpinski triangles, Archimedean tessellation, Kagomé, and ladder networks. The appearance of Sierpinski triangles is rather surprising, since a majority of papers report the formation of such structures in completely different systems. The only general rule that has been established and proved experimentally is that the so-called “V-shape” molecules are able to order into Sierpinski triangles.

Design, System, Application

The manuscript presents the results of molecular dynamics simulations of the self-assembly of tetrasubstituted molecules. We have demonstrated that even slight changes of the interaction zone and the shape of molecules can drastically alter the behavior of investigated systems. This parameter can be reflected by substitution of diverse chemically active groups. Hence, our results indicate how one can control experimental conditions of the self-assembly process for the target design of supramolecular networks presented herein. Therefore, we believe that the findings presented in this paper can be helpful for scientists working on such systems, as they can help select a building block that is able to create a 2D network with a predefined topology.

1 Introduction

Spontaneous self-assembly processes are ubiquitous in nature. Many biological systems such as phospholipids,¹ RNA² and DNA³ complexes, viruses,⁴ *etc.* undergo self-assembly. Furthermore, Janus (or generally “patchy”) particles with anisotropic interactions also show self-assembly of great importance for materials science,^{5,6} medicine,^{7,8} and other applications. Several organic molecules have been given attention due to their ability to undergo on-surface reactions, which often lead to the formation of products different than those appearing in bulk systems, or they would even not be possible to take place in the bulk. The main objective of this approach is to obtain single nanolayers, which have been proven to be used as membranes for the separation of liquid and gas phases,⁹ in batteries,¹⁰ and in molecular sieves.¹¹

Another interesting behavior of some organic molecules is their assembly into mathematical fractals. There exist several

approaches attempting to fabricate such supramolecular networks. While it is impressive to see that the obtained structures are, for instance, high order Sierpinski triangles, they are often due to the expanded molecular structure of the building blocks.^{12,13} On the other hand, one of the most popular simple precursors being able to form true mathematical fractals, being Sierpinski triangles, are the so-called “V-shaped” molecules. One of the most popular theoretical approaches that have shown the formation of this kind of self-similar network was the lattice Monte Carlo method (l-MC).¹⁴ The predictions stemming from simulations were also proved experimentally.^{15–18} The same authors proposed another molecular architecture that could also possibly form Sierpinski fractals using an identical approach.¹⁹ However, it is well-known that lattice models should be treated as a preliminary method for the investigation of any problem of interest since the lattice type can enforce the formation of structures that correspond to its symmetry and are not necessarily reproducible by other off-lattice methods (or more importantly by experiments).

Due to the multiple possible applications and the variety of different paths of molecular assembly, it is indispensable to find general rules that could lead to the easier design of these kinds of systems. While the synthesis can be tedious

Department of Theoretical Chemistry, Maria Curie Skłodowska University, Lublin, Poland. E-mail: lukasz.baran@poczta.umcs.lublin.pl

† Electronic supplementary information (ESI) available. See DOI: 10.1039/d1me00068c



and costly, computer modelling can be a very convenient substitute for the exploration of problems of interest. Computer simulations can give valuable insight for experimentalists due to the possibility of examination of the influence of multiple factors, such as particle geometry, under different conditions on the self-assembly process in a reasonable time. The most popular methods involve quantum density functional theory,²⁰ classical Monte Carlo^{21–26} and molecular dynamics simulations (MD).^{27,28} In our laboratory, we have proven that the last method can be useful for examination of a variety of molecular geometries, both in one-component systems^{29,30} and in binary mixtures.³¹

In this paper, we report various paths of self-assembly of tetratopic building blocks. We have compared the prediction stemming from I-MC¹⁹ with molecular dynamics and extended the model to different molecular geometries. It was shown in the literature that the precise control over selectivity of on-surface reactions is crucial for the design of desired nanostructures.^{32,33} Here we demonstrate that even slight variations of the size of the interaction zone drastically change the behavior of the systems considered.^{34,35} We have found the rules governing the formation of diverse networks including Sierpinski triangles, Archimedean tessellation, Kagomé, and ladder networks. The last case is of particular importance since it resembles the behavior of liquid crystals which tend to glue due to entropic effects. All of these structures have been characterized by appropriate order parameters.

2 Results and discussion

2.1 Model

The model proposed in this paper has been designed to reflect the geometry of flat and rigid tetra-substituted chemical compounds as shown in Fig. 1. In the structure of molecules, we can distinguish two parts, the core and four arms attached to it, marked as **R** and **A–D**, respectively. We will refer to those as an entire backbone. The angle between neighboring arms has been set to $\theta = 60^\circ$. The influence of the core length, as well as the lengths of arms, has been investigated. Moreover, the terminal segment of each arm has been decorated with the so-called “sticky patch” (red segments in Fig. 1)), which will be referred to as active sites. The size of

every segment forming the entire backbone has been set to σ_b , whereas active sites were five times smaller $\sigma_a = 0.2\sigma_b$. The bonding distance between the neighboring backbone entities has also been set to σ_b , whereas the bonding distance between terminal arms and active sites has been varied between $l = 0.4 \pm 0.04\sigma_b$. Thus, the active sites are, to some extent, embedded into terminal segments to reflect directional interparticle interactions. A detailed description of molecular dynamics simulations can be found in the ESI.†

Fig. 2(a) gives a schematic representation of the interaction zone arising from the above model. Parts b–d of Fig. 2 demonstrate the influence of the bonding distance l on the angular behavior of the employed Lennard-Jones potential. We have estimated that the maximum size of the interaction zone changes with l and is equal to $\alpha = 34.6^\circ$ for $l = 0.36$, $\alpha = 41.4^\circ$ for $l = 0.40\sigma$, and $\alpha = 45.2^\circ$ for $l = 0.44\sigma$.

Kalyuzhnyi and Cummings³⁵ have shown that, due to geometrical constraints, the ranges of the interaction zone α allowing for the connections between two ($30^\circ \leq \alpha < 35.3^\circ$), three ($35.3^\circ \leq \alpha < 45^\circ$), etc. molecules are well defined. However, these authors used a relatively short-ranged square-well potential and the above ranges of α are expected to vary depending on the form of interparticle potential.

In the considered case of the Lennard-Jones potential, the ranges of α are approximately the same, though the cut-off distance between active sites is different. We have found that for distances $l = 0.36\sigma$ and $l = 0.44\sigma$, connections between two and three active sites are possible, respectively. In the case of $l = 0.40\sigma$, the association may involve the formation of bonds between two and three active centers. In our opinion, such a kind of coarse-grained modelling can be mapped on real experimental studies. One should substitute a chemical compound of similar geometry as shown in Fig. 1(c) with groups such as $-\text{OH}$ or $-\text{COOH}$ in single-component systems or alternatively halide groups in a mixture with two-coordinated metal atoms which in both cases allow interactions of two molecules with one another. This case would correspond to the results of $l = 0.36\sigma$ presented in this paper. On the other hand, if one would substitute the same chemical compound with $-\text{B}(\text{OH})_2$ in single-component systems or halide groups in a mixture with three-coordinated metal atoms, one should expect to obtain similar results to those for $l = 0.44\sigma$. The intermediate scenario where two phases may

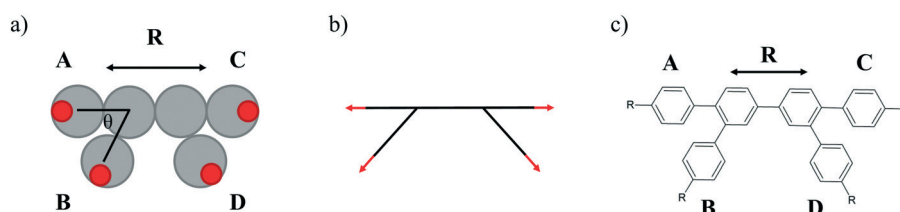
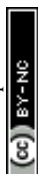


Fig. 1 Model of a tetra-substituted molecule (part a) with **R** and **A–D** being the lengths of the core and the arms, respectively. Silver circles correspond to the segments of the entire backbone, whereas red circles mark the active sites. Part b shows a schematic representation of the molecule from (part a). The example of a chemical compound that can correspond to our model (part c). Notation of **R** and **A–D** is the same as in part (a), and $-\text{R}$ are active sites resulting from the presence of attached functional groups, such as $-\text{CN}$, $\text{B}(\text{OH})_2$, etc.



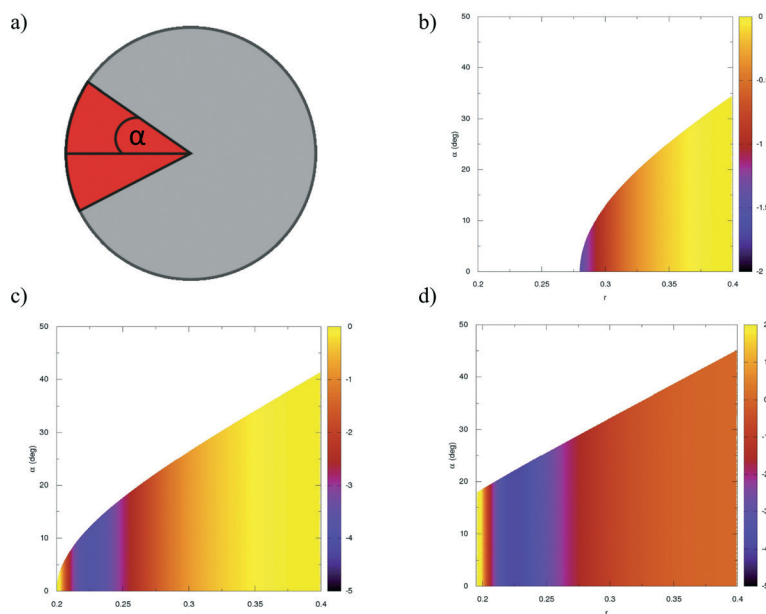


Fig. 2 Schematic representation of the interaction zone (a). Parts (b–d) present the angular dependence of the Lennard-Jones potential with respect to the separation distance between active sites for $l = 0.36\sigma$ (b), $l = 0.4\sigma$ (c), and $l = 0.44\sigma$ (d).

occur, which is most likely the case in experimental studies due to the oscillations of chemical bonds of active groups, can be seen for $l = 0.40\sigma$. In our paper, we have shown the consequences of active zone manipulation on the formation of a variety of self-assembled networks.

All considered systems, summarized in Table 1, can be grouped into five models, abbreviated as **M1–M5**, with different numbers of segments in the arms **A–D**. For each of these models, we have also studied the influence of the core length, **X**, on self-assembly processes.

2.2 The influence of bonding distance on self-assembly

2.2.1 Results for $l = 0.4\sigma$. Let us start with the presentation of results for model **M1**. A typical snapshot for system **R2_M1** is given in Fig. 3(a). In this case, we can see several patterns, schematically drawn in the right-hand side of this panel, showing how the molecules assemble. One can see that one network prevails, which is an isogonal tiling, in which molecules periodically form smaller and bigger triangles. The result for model **R3_M1**, shown in Fig. 3(b) shows that elonga-

tion of the core length **X** leads to the stabilization of this structure and no other patterns can be distinguished. It is also noteworthy that a very similar network was recently obtained by Y. Zhang, *et al.* in the mixture of 1,3-bis(4-pyridyl) benzene molecules and Fe atoms.¹⁸

To better quantify this structure, we have examined the way how the active sites assemble, and the corresponding snapshot can be found in Fig. 3(c). It is clear that connecting the centers of mass of two associated active sites, the 3.4.6.4 Archimedean tessellation is formed. The results for model **R4_M1** are qualitatively the same as for model **R3_M1** and can be found in Fig. S1 in the ESI.† The only difference is the bigger pore size in model **R3_M1**.

All of the observations concerning those networks can be proved by the calculation of several parameters. The first one is the average association number, $\langle N_{\text{asso}} \rangle$, which measures the average number of neighboring molecules within the interaction zone ($r = 0.4\sigma$) of the active sites of a selected molecule. If it takes a value of one it means that two active sites of different molecules associate, *etc.* The changes of this parameter with temperature can be found in Fig. 3(d) and the value at the lowest temperatures is around $\langle N_{\text{asso}} \rangle \approx 0.8$ for all the systems. This result corroborates with the snapshots showing that only two molecules associate. Since this is an average value and there also are non-associated particles present, the value is lowered in comparison with that predicted for the perfect ordering.

Another quantity that we have computed is the cluster distribution function defined so that $\int_0^N P(N_C) dN_C = 1$, where N is the number of active sites. It has been calculated for active sites up to the threshold distance of $r_{\text{cl}} = 0.4\sigma$ and $r_{\text{cl}} = 1.35\sigma$, which are the cut-off distance of the interparticle potential, and the location of the second minimum of the radial

Table 1 The systems investigated in the course of our simulations. **M** marks the models of different molecular architectures, whereas **X** and **A–D** are the numbers of segments in the core and in each of the arms, respectively. In Fig. 1a, model **R2_M2** ($X = 2$, $A–D = 1$) has been shown

Model abbreviation	Full description
RX_M1	$X = 2–4$, $A, C = 0$, $B, D = 1$
RX_M2	$X = 2–4$, $A–D = 1$
RX_M3	$X = 2–4$, $A, C = 1$, $B, D = 2$
RX_M4	$X = 2–4$, $A, C = 2$, $B, D = 1$
RX_M5	$X = 2–4$, $A–D = 2$



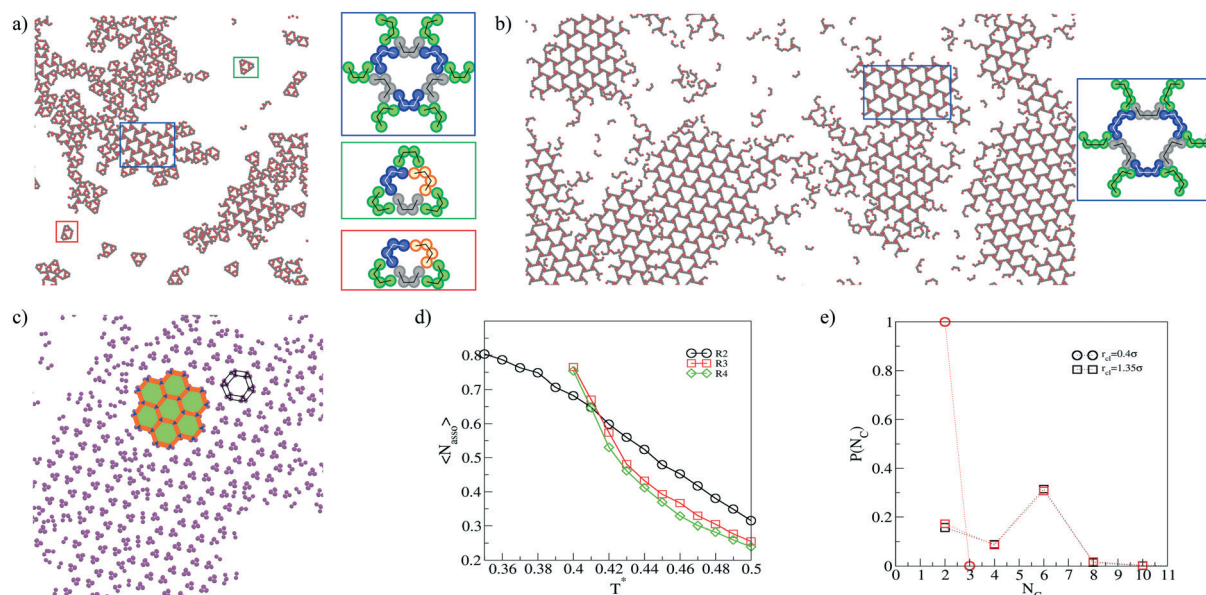


Fig. 3 Fragment of the configurations for models **R2_M1** in $\rho^* = 0.2$, at $T^* = 0.35$ (a) and **R3_M1** in $\rho^* = 0.2$, at $T^* = 0.4$ (b). Schematically drawn association paths are shown on the right-hand sides of these panels. Part c) shows how active sites assemble into Archimedean tessellation. Different polygons are marked by different colors to better show the ordering. The average association number for models **R2–R4_M1** (d). Cluster distribution functions for models **R3_M1** (black symbols) and **R4_M1** (red symbols) for two different threshold distances (e).

distribution function, respectively. The results obtained for models **R3_M1** and **R4_M1** are presented in Fig. 3(e). In model **R3_M1**, the cluster distribution function confirms “visual” observations that only two molecules associate, while in the case of model **R4_M1**, the most probable cluster size is equal to $N_c = 6$. However, there also are clusters with $N_c = 2$ and 4, which appear due to imperfections of the network. In the case of $r_{cl} = 1.35\sigma$, we have computed the center of mass for every cluster found in the system, and these particles form a honeycomb network (see Fig. S1 in the ESI†). The results for the **R4_M1** model are the same and can also be found in the ESI†.

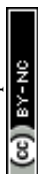
Next, we proceed to the description of model **M2**. A typical snapshot for system **R2_M2** at density $\rho^* = 0.2$ can be found in Fig. 4(a). It has been found that molecules can associate into two different networks, namely into Sierpinski triangles up to the second-order, and into a denser phase. In the former structure, two molecules associate, just the same as in the previously discussed model, while in the latter, two or three active sites associate. As previously mentioned, we have checked the influence of the core length, X and found that in the range of $X = 2-4$ the same tendency occurs (cf. Fig. S2 in the ESI†). The configuration for model **R4_M2** at density $\rho^* = 0.2$ is shown in Fig. 4(b). In this case, however, the amount of dense phase is lower than for smaller core lengths. On the other hand, the elongation of the core does not lead to the preferred formation of Sierpinski triangles of a higher degree. We conclude that at density $\rho^* = 0.2$, the formation of two competing structures is the reason why the system is not able to self-assemble into well-defined bigger clusters.

In all of the systems, we have also checked the influence of the density on self-assembly and found that at lower den-

sities around $\rho^* = 0.12$ there is no qualitative change within the range of $X = 2-4$ (cf. Fig. S2 in the ESI†). On the other hand, at higher densities, around $\rho^* = 0.4$, the formation of only one well-developed ladder-like structure is observed for every **M2** model. A snapshot for the **R4_M2** model, recorded at density $\rho^* = 0.4$, is given in Fig. 4(c), and other examples can be found in Fig. S2 in the ESI†.

To quantify the behavior of the considered systems better, we have computed the distribution of association number for every **M2** model at densities $\rho^* = 0.2$ and $\rho^* = 0.4$. The results, shown in Fig. 4(d), display that at the lower density the most probable is the association involving two molecules ($N_{\text{asso}} = 1$), while at the higher density three active sites associate ($N_{\text{asso}} = 2$). It is also worth mentioning that at density $\rho^* = 0.2$, the maximum of the association distribution increases with the core length. This is consistent with the picture emerging from the snapshots showing that in model **R4_M2** the Sierpinski triangles are the dominating entities. At density $\rho^* = 0.4$, we have observed a higher contribution of well-ordered ladder-like structure of higher density, independent of the core length. The schematic representation of the structure, shown on the right-hand side of Fig. 4(c), shows that two and three molecules can associate to form the network, in agreement with the behavior of the distribution function.

Then, we have examined the behavior of model **M3**. Results for particles **R2_M3** are shown in Fig. 5(a). In this case, the molecules assemble into one and well-defined dense network. Similar to the denser phase observed in model **M2**, two and three active sites can associate and the pattern of the ordering can be found in Fig. 5(b). Clusters of sizes equal to $N_c = 2$ and $N_c = 3$ form lines, arranged vertically in the 2–3–3–2 sequence. We have checked the influence of the core length



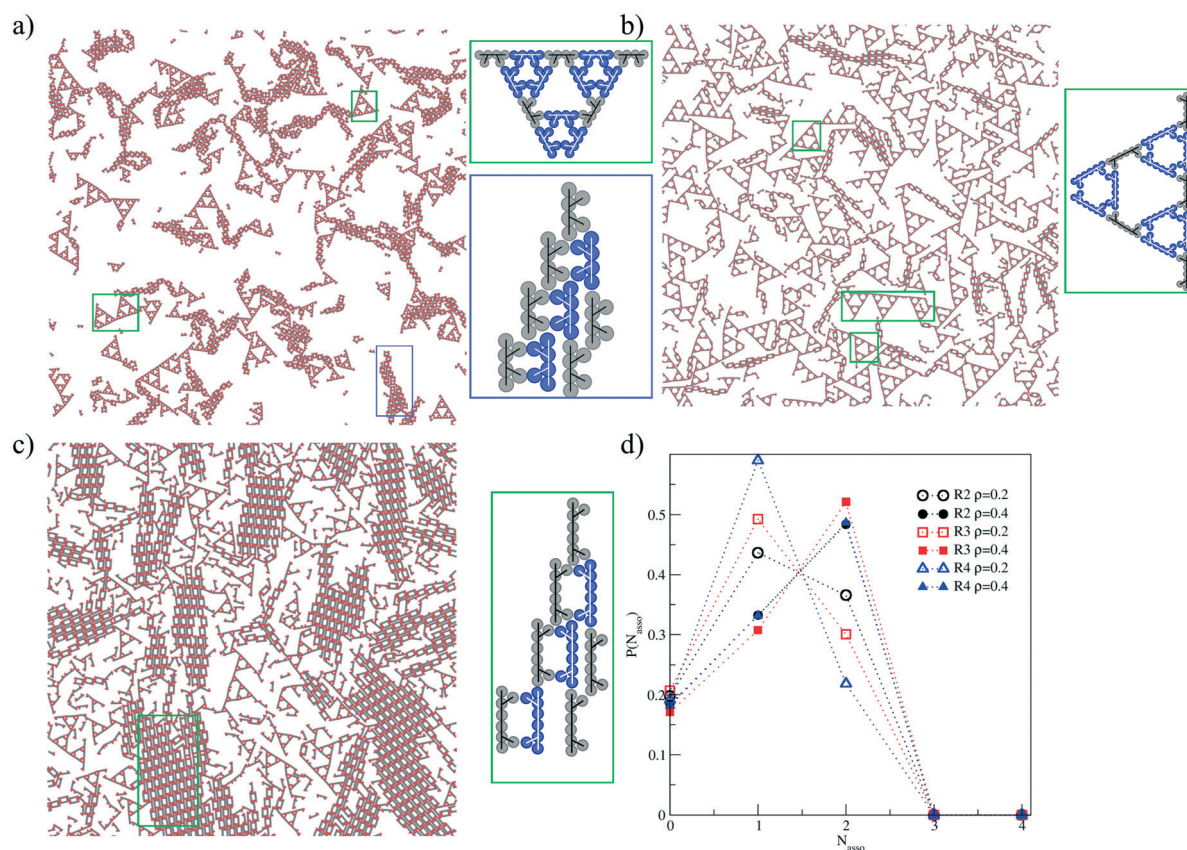


Fig. 4 Configurations for models **R2_M2** in $\rho^* = 0.2$, at $T^* = 0.4$ (a) and **R4_M2** in $\rho^* = 0.2$, at $T^* = 0.4$ (b). Snapshot for model **R4_M2** in $\rho^* = 0.4$, at $T^* = 0.45$ (c). Schematically drawn association paths are shown on the right-hand side of these panels. The distribution of the association number for models **R2-R4_M2** in density $\rho^* = 0.2$, at $T^* = 0.4$ (open symbols) and $\rho^* = 0.4$, at $T^* = 0.45$ (filled symbols) (d).

on the behavior of this model and found qualitatively the same behavior for $X = 2-4$ (cf. Fig. S3 in the ESI†).

Fig. 5(c) gives the results for model **R2_M4**. The structure formed by those particles is very similar to the one formed in the previous case (and to the dense phase in model **M2**). Likewise, one can distinguish two pores of different sizes, and two, as well as three active sites, can assemble. The main difference, however, is on how the latter “atoms” are ordered. Namely the pairs and the triplets are now ordered alternately in lines and form a “zigzag-like” pattern (cf. Fig. 5(d)).

Unlike in model **M3**, elongation of the core length X leads to completely different results. The snapshot for particles **R3_M4** at $\rho^* = 0.2$ and $T^* = 0.4$ is presented in Fig. 5(e). The molecules assemble into an aligned in one direction ladder network. It is rather surprising that these “wires” remain separated and do not glue into a denser structure. From the cluster analysis computed for the segments of the entire backbone, up to the threshold distance taken from the first minimum of the radial distribution function ($r_{cl} = 1.05\sigma$), we have found that the average length of such a wire consists of $\langle N_C \rangle \approx 433 \pm 10$ segments, with the maximum value equal to $N_C = 3357$. It should be noted that the linear system size was equal to $L_x = L_y = 336\sigma$. Thus, the wire length is much larger than the system size. Besides that, the formation of small patches of a dense

phase, with a structure similar to system **R2_M4** is also observed.

In order to check whether the length of these wires is finite or goes to infinity, we have enlarged the system size. It has been found that the average cluster size decreases and is around $\langle N_C \rangle \approx 315 \pm 20$ segments in every case, with the maximum value of $N_C = 4000$, for the linear system size, $L_x = L_y = 469\sigma$ ($N_C = 5800$ for the linear system size, $L_x = L_y = 610\sigma$), and the number of lines of different lengths increased when the system size becomes larger. This means that the wires reach their certain threshold length and they are not growing further upon the increase of the system size.

Another interesting feature is that this structure vanishes when the density becomes high enough. Instead of gluing with another as one could suspect. We have performed simulations for the system in $\rho^* = 0.5$ and in this case, the dense phase prevails at $T^* = 0.5$ (see Fig. S3 in the ESI†). However, it is important to note that at higher temperatures, between $T^* = 0.59 - 0.56$, lines that are glued to the growing dense phase occur, which is not the case for temperatures below $T^* = 0.56$ (cf. Fig. S3 in the ESI†).

In order to quantify this quite unexpected structure, we wanted to see that these lines do not rotate and are arranged in one direction. The parameter that can be used here is the two-dimensional nematic order parameter,³⁶ defined as



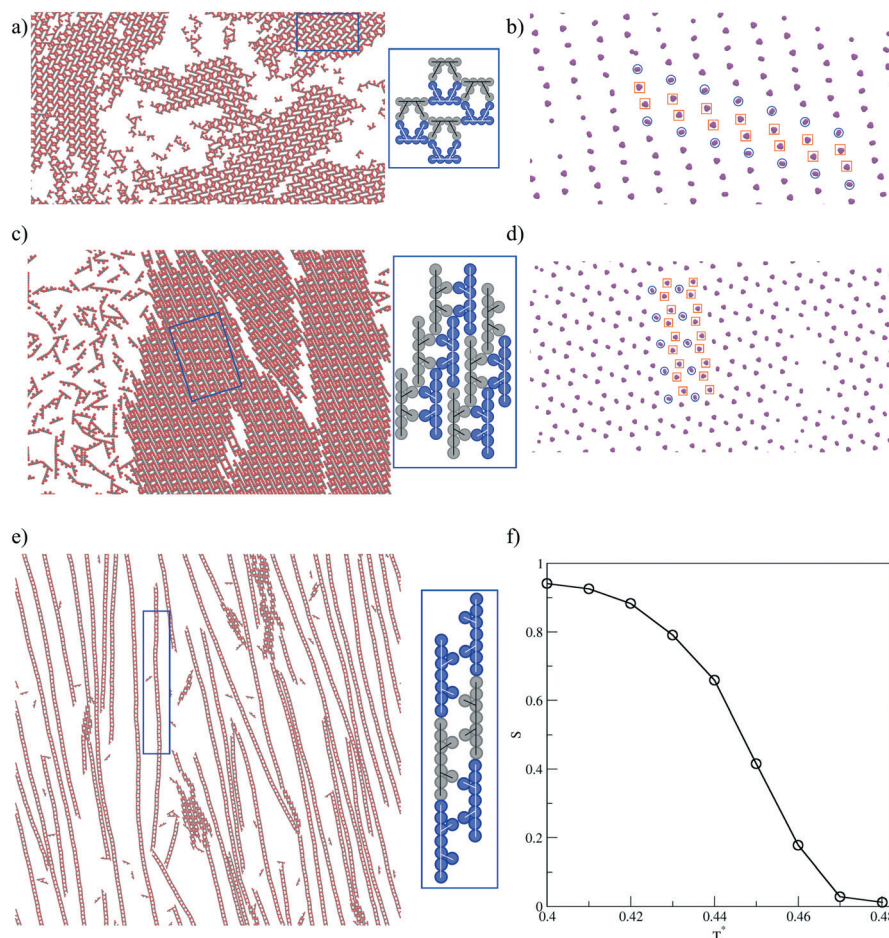


Fig. 5 Fragments of the configurations for models **R2_M3** at $\rho^* = 0.42$ and $T^* = 0.45$ (a) and **R2_M4** at $\rho^* = 0.5$ and $T^* = 0.5$ (c). Parts b) and d) show the locations of active sites for the snapshots shown in parts a) and c), respectively. The configuration for model **R3_M4** at $\rho^* = 0.2$ and $T^* = 0.4$ (e). Part f) displays the temperature changes of the nematic order parameter for model **R3_M4**. Schematically drawn association paths are shown on the right-hand side of panels a), c), and e).

$$Q_{\alpha\beta} = N^{-1} \sum_i^N [2b_{\alpha}(i)b_{\beta}(i) - \delta_{\alpha\beta}] \quad (1)$$

$$\kappa = 2 \frac{\lambda_x^4 + \lambda_y^4}{(\lambda_x^2 + \lambda_y^2)^2} - 1 \quad (2)$$

where $b_{\alpha}(i)$ is the α -th coordinate of the unit vector b , specifying the orientation of the molecule i , and $\delta_{\alpha\beta}$ is the Kronecker delta function. Since the eigenvalues of Q are equal to $\pm S$, the order parameter may be positive or negative. However, the absolute value of S tends to 1 in a perfectly ordered phase, and is expected to vanish in a disordered phase when $N \rightarrow \infty$. In real systems, it is very difficult to reach the value of $|S|$ equal to 1, owing to possible imperfections in the ordered structure, or rotations of differently oriented domains. Fig. 5f shows how the nematic order parameter changes with temperature. At the lowest considered temperature ($T^* = 0.4$) the order parameter reaches the value of about 0.95, allowing us to conclude that the wires are aligned along one direction.

Moreover, to prove that the ladder structure is indeed ordered into straight lines, we have computed the relative shape anisotropy parameter,³⁷ defined as

where λ_x and λ_y are the diagonal eigenvalues of the gyration tensor. This quantity, like the nematic order parameter, takes values between 0 and 1, when the system is spherically symmetric or the molecules lie along a straight line, respectively.

This parameter has been calculated separately for every wire extracted from the cluster analysis, and its value was found to vary between $\kappa = 0.85$ – 0.95 . These values are good enough to prove that the structure consists of nearly straight lines. It is important to note that we have also observed lower values of $\kappa \approx 0.2$, which corresponded to the clusters in which the elements of the ladder network were connected to a more dense phase.

Next, we proceed to the description of the last model **M5**. It has appeared that similar to model **M2**, the molecules associate into Sierpinski triangles and into a more dense phase. In general, the behavior of model **M5** is qualitatively very similar to that found for model **M2**. In particular, the changes of the



structure when the core length, R , and the density are varied remain the same. For the sake of brevity, we have omitted a detailed description of the results in the main text, and the reader is advised to look at Fig. S4 and S5 in the ESI†

2.2.2 Results for $l = 0.36\sigma$ and $l = 0.44\sigma$. Let us start with model **M1** of the increased bonding distance $l = 0.44\sigma$. In this case, three molecules connect and form completely different networks than in the systems with $l = 0.4\sigma$ (cf. Fig. 3). The results for different core lengths R are shown in Fig. 6(a–c). Similar to the systems with the bonding distance $l = 0.4\sigma$, model **R2_M1** does not form any well-defined ordered network. There are several patterns formed by the associating molecules. Likewise in the case of shorter l , the core elongation R leads to the formation of a single dominant network, and a “flower-like” motif appears. At higher temperatures, those small aggregates are randomly connected but do not form a single well-defined network. A decrease in the temperature leads to the condensation of those patterns, as depicted in Fig. 6(b and c). Unfortunately, it is difficult to determine the structure of this ordered network. We have tried to compute the two-dimensional structure factors, which should show the type of ordering,³⁰ but could not obtain statistically relevant results. Therefore, in our opinion, the increase of the system size could lead to the formation of better-ordered larger networks.

Next, we proceed to the description of model **M2**. Since in the case of the bonding length $l = 0.40\sigma$, two different structures were found, we have considered the systems with lower and higher l , to see whether the bonding length affects self-assembly. The results for $l = 0.36\sigma$ are presented in Fig. 7(a). In this case, the molecules form only Sierpinski triangles and no other network can be distinguished. It is also important to note that in comparison with the systems of $l = 0.4\sigma$, the formation of Sierpinski triangles of the third degree with some defects can be observed. Contrary to this, the longer $l = 0.44\sigma$ (Fig. 7b and c) stabilizes a more dense phase and no self-similar structures are observed, both in lower ($\rho^* = 0.2$) and higher densities ($\rho^* = 0.4$). The same tendency remains for different core elongations R (see Fig. S6 in the ESI†).

As previously, we have calculated the distributions of the association numbers for models **R2–R4_M2** with different bond lengths, l and the results are given in Fig. 7(d). We can see that for bond length $l = 0.36\sigma$ the highest value of N_{asso} is equal to 1, confirming that only two molecules connected one to another, and form Sierpinski triangles. On the other hand, for the molecules with bond length $l = 0.44\sigma$, the most probable value of the association number is equal to $N_{\text{asso}} = 2$. One can also observe a peak at $N_{\text{asso}} = 1$, and these results corroborate with the formation of a more dense phase. It is also worth mentioning that the course of the distribution

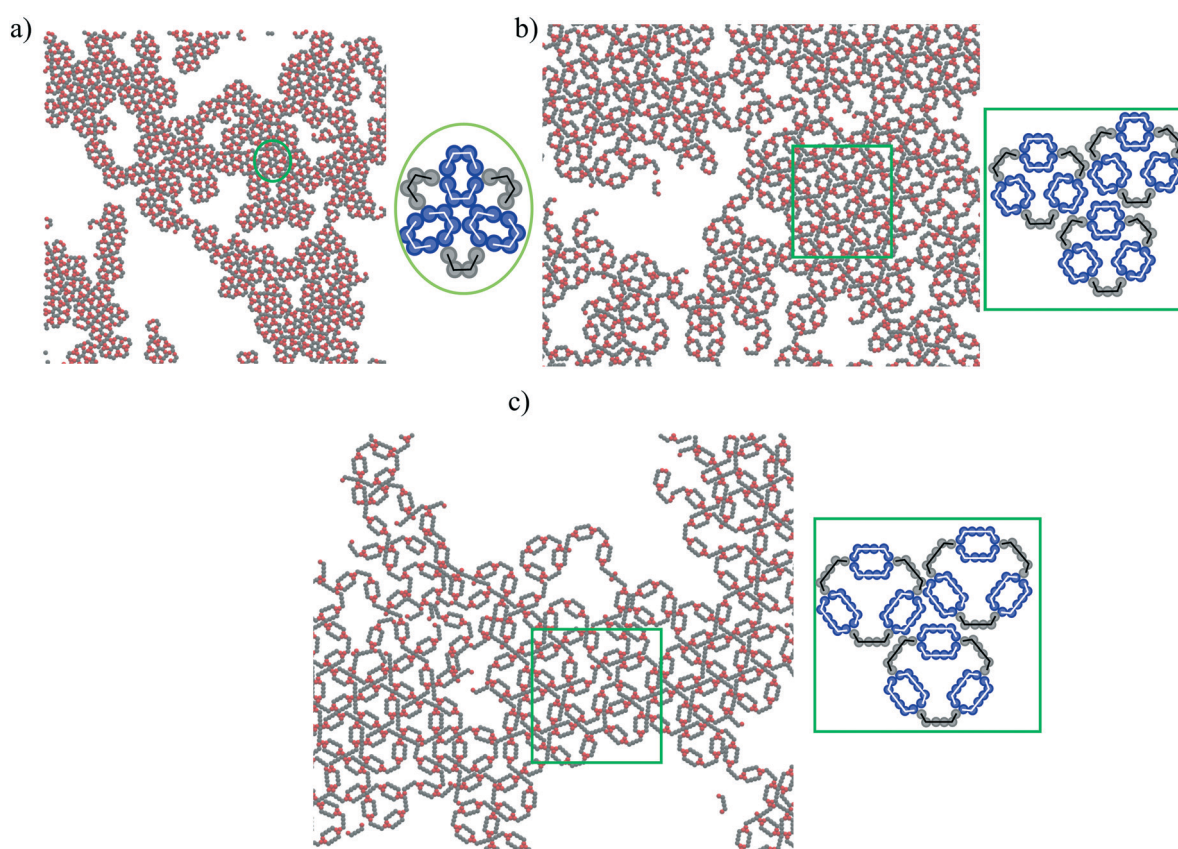


Fig. 6 Parts of the configurations for models **R2_M1** (a), **R3_M1** (b), and **R4_M1** (c) at $\rho^* = 0.4$ and $T^* = 0.42$, and for $l = 0.44\sigma$. Schematically drawn association paths are shown on the right-hand sides of the panels.



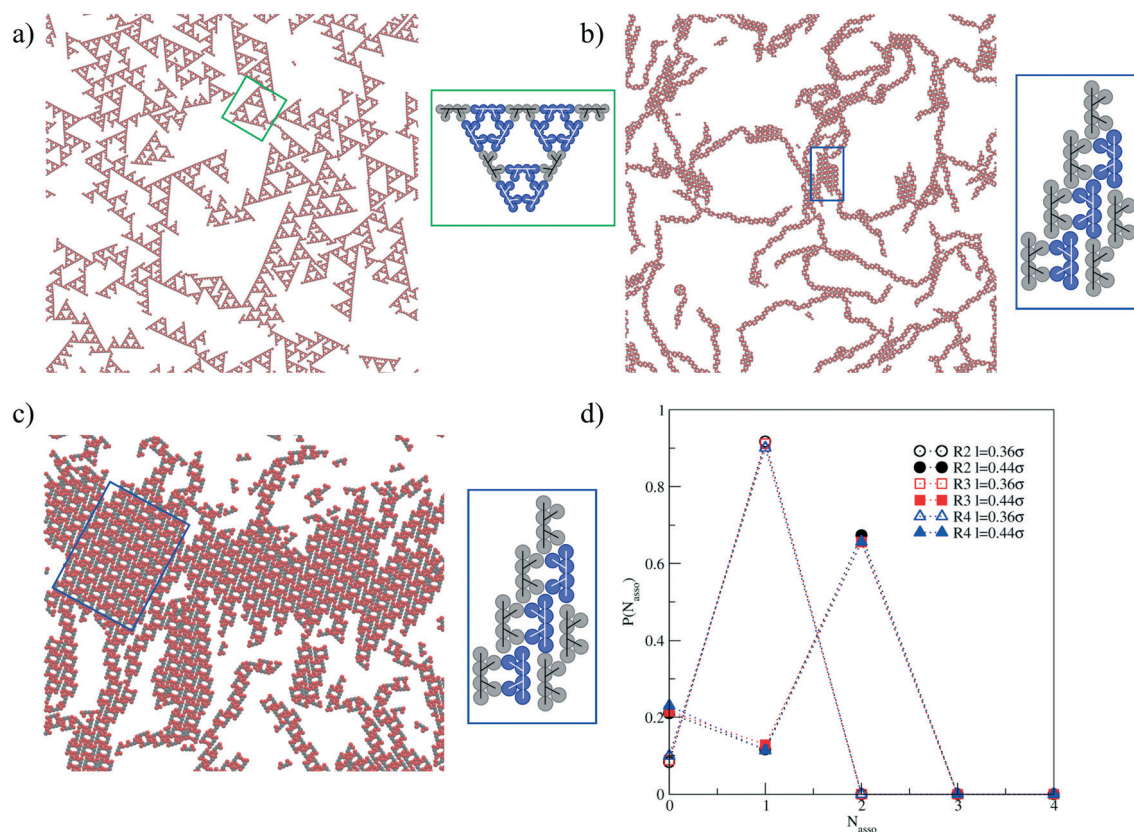


Fig. 7 The configurations for model **R2_M2** at $\rho^* = 0.2$ and $T^* = 0.25$ for $l = 0.36\sigma$ (a) and at $\rho^* = 0.2$ and $T^* = 0.4$ for $l = 0.44\sigma$ (b). The snapshot for model **R2_M2** at $\rho^* = 0.4$ and $T^* = 0.65$ for $l = 0.44\sigma$ (c). Schematically drawn association paths are shown on the right-hand sides of the panels. Distributions of the association number for model **R2-R4_M2** with the density equal to $\rho^* = 0.2$, recorded at $T^* = 0.25$ and using $l = 0.36\sigma$ (open symbols) and recorded at $T^* = 0.50$ with $l = 0.44\sigma$ (filled symbols) (d).

function does not change within the range of the core length values **R2-R4**.

The results for model **M3** with the bond length $l = 0.36\sigma$ can be found in Fig. 8. In the case of $l = 0.40\sigma$, we have observed only one phase, in which the connections of two and three molecules were possible. Now, the results are significantly different (*cf.* Fig. 5(a)). For model **R2_M2** (Fig. 8(a)) one can see a lot of small aggregates that are similar to Sierpinski triangles of the first order. However, we have not observed the formation of a single ordered network. Those small clusters glue randomly and form complex structures.

Contrary to the bonding distance $l = 0.4\sigma$, where the core length **R** did not change qualitatively the structure, for $l = 0.36\sigma$ we observe significant changes. The structure for both **R3_M3** (Fig. 8(b)) and **R4_M3** (Fig. 8(c)) is the same isogonal tiling, which has been previously observed for model **M1** (*cf.* Fig. 3). Likewise, we have examined the arrangement of active sites and this kind of representation reveals similar ordering to the case of model **M1** with $l = 0.4\sigma$. The connection of the centers of mass of two associated active sites results in the formation of 3.4.6.4 Archimedean tessellation in models **R3_M3** (Fig. 8(d)) and **R4_M3**.

These changes of the behavior with the core length are due to the difference in saturation per molecule. For the **R2_M3** model, small clusters are formed by six molecules in

which three tectons have every active site associated. To form a seed, leading to an isogonal tiling, there have to be at least twelve molecules.

The probability of formation of such a group is rather low, and energetically less favorable in this case. On the contrary, in model **R3_M3**, the core elongation leads to a slight mismatch in the direction of association between active sites; hence the formation of small aggregates is energetically less favorable compared to an isogonal tiling. This effect is even better pronounced for model **R4_M3**.

Let us now proceed to model **M4**. For the bond length $l = 0.4\sigma$ we have observed the formation of only one well-defined ordered network, for all systems with different core lengths **R** = 2, 4. Surprisingly, for greater embedment the formation of a similar isogonal tiling, as in models **M1** and **M3** with the same $l = 0.4\sigma$, has been observed (Fig. 9(a)). Nevertheless, it has to be emphasized that in the case of $l = 0.36\sigma$, this structure has not been formed for the core length **R** = 2. However, the arrangement of active sites is quite different than for those isogonal tilings observed previously. Despite the formation of qualitatively the same network if one would connect the center of mass of every two associated active centers, the formation of a structure resembling a Kagomé network can be observed (Fig. 9(b)). For model **R4_M4** (Fig. 9c), similar to **R2_M4**, the more dense



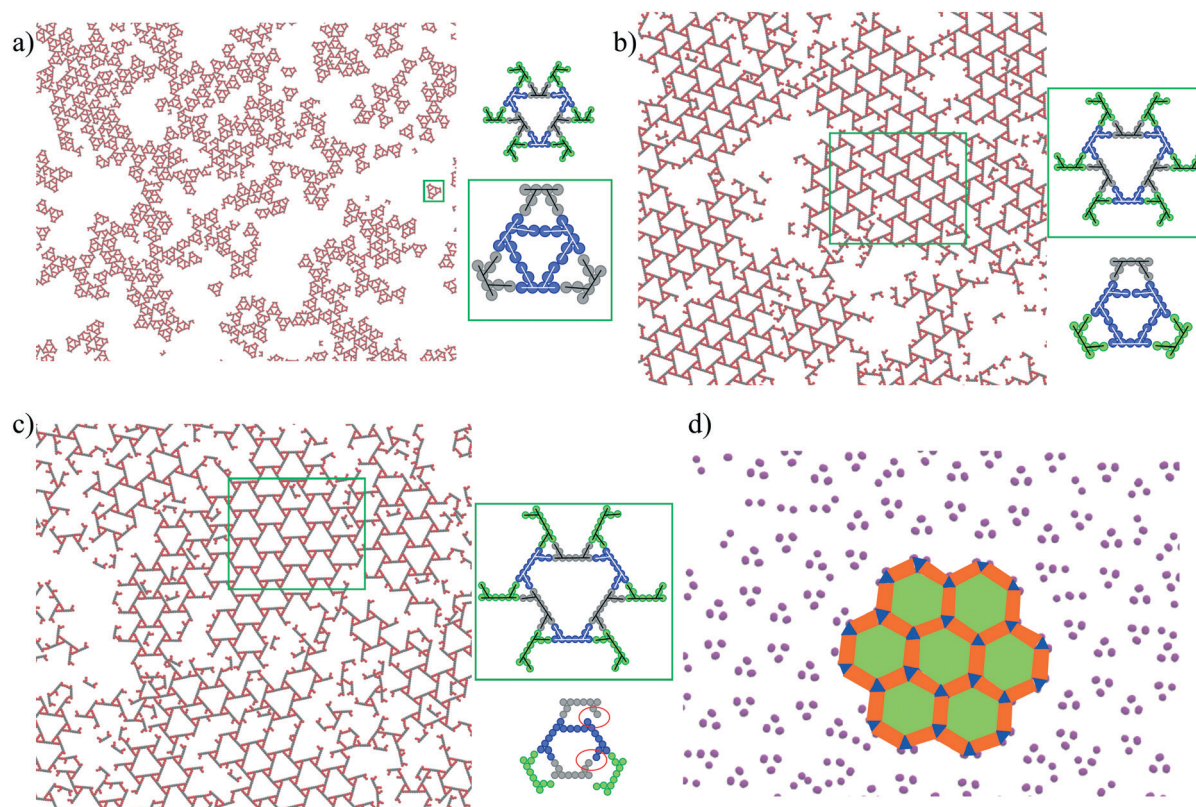


Fig. 8 Parts a), b), and c) present the configurations for models **R2–R4_M3** with $l = 0.36\sigma$, at $\rho^* = 0.2$ and $T^* = 0.28$. Schematically drawn association paths are shown on the right-hand sides of the panels. Part d) shows how the active sites in model **R3_M3** assemble into Archimedean tessellation. Different polygons are marked by different colors to better pronounce the ordering.

phase that has been observed for $l = 0.4\sigma$ has not been formed and an isogonal tiling is the only ordered network. The active site layout is comparable to the **R2_M4** model and has been omitted for the sake of brevity.

For $l = 0.4\sigma$, elongation of the core length leads to the formation of finite one-dimensional wires (ladder network) and a more dense phase. By changing the embedding distance for model **R3_M4** to $l = 0.36\sigma$, two phases are no longer present and the formation of a ladder network is preferred (Fig. 9(d)). The two-dimensional structure factor calculated with respect to the backbone segments, and given in the inset to part (d) of Fig. 9 confirms the alignment of the ladder network along one direction.

On top of that is diffused and the distances in reciprocal space are small which corroborates with the observation that those wires are separated (large distance in real space). Contrary to $l = 0.4\sigma$, the increase of density does not lead to structural changes of the system, and the wires start to glue laterally one to another, instead (Fig. 9(e)). This resembles the behavior of liquid crystals which, even without the presence of attractive interactions, tend to form densely-packed, ordered networks.³⁸ The structure factor calculated for $\rho = 0.5$ is shown in the inset of Fig. 9(e). The wires are aligned along one direction, but the reflexes are not diffused. The distances in the reciprocal space are larger than at lower density, which corroborates with the observation from snapshots.

For every core length **R2–R4** we have geometrically analyzed a possibility to form either isogonal tiling or a ladder network. We have found that due to the architecture of molecules **R2** and **R4** the formation of the former is the only possibility (*cf.* right-hand side of panels (a) and (c) of Fig. 9). We conclude that the reason is an incomplete saturation of possible interparticle interactions in the formation of one-dimensional wires. On the other hand, for **R3** both structures reach the same saturation, and they only differ by the packing fraction of the networks. Therefore, the formation of a denser phase should be preferred.

For the molecules **R3_M4** and with $l = 0.36\sigma$, we have performed cluster analysis which has shown that the linear clusters are nearly two times longer relative to the case of $l = 0.40\sigma$. The average cluster size was estimated to consist of $\langle N_C \rangle = 776 \pm 50$ segments with the maximum value of $N_C = 6687$ (linear system size, $L_x = L_y = 336\sigma$). Similarly, the relative shape anisotropy parameter varied between $\kappa \approx 0.92 \pm 0.05$. However, it has to be emphasized that in this system, no clusters with smaller values have been observed, which in the system with $l = 0.40\sigma$ was caused by the occurrence of the second, more dense phase. On the other hand, an increase of the bonding distance to $l = 0.44\sigma$ results in the formation of a more dense phase in systems at both low ($\rho^* = 0.2$) and high ($\rho^* = 0.5$) densities and the ladder networks have not been observed at all (Fig. 9f).



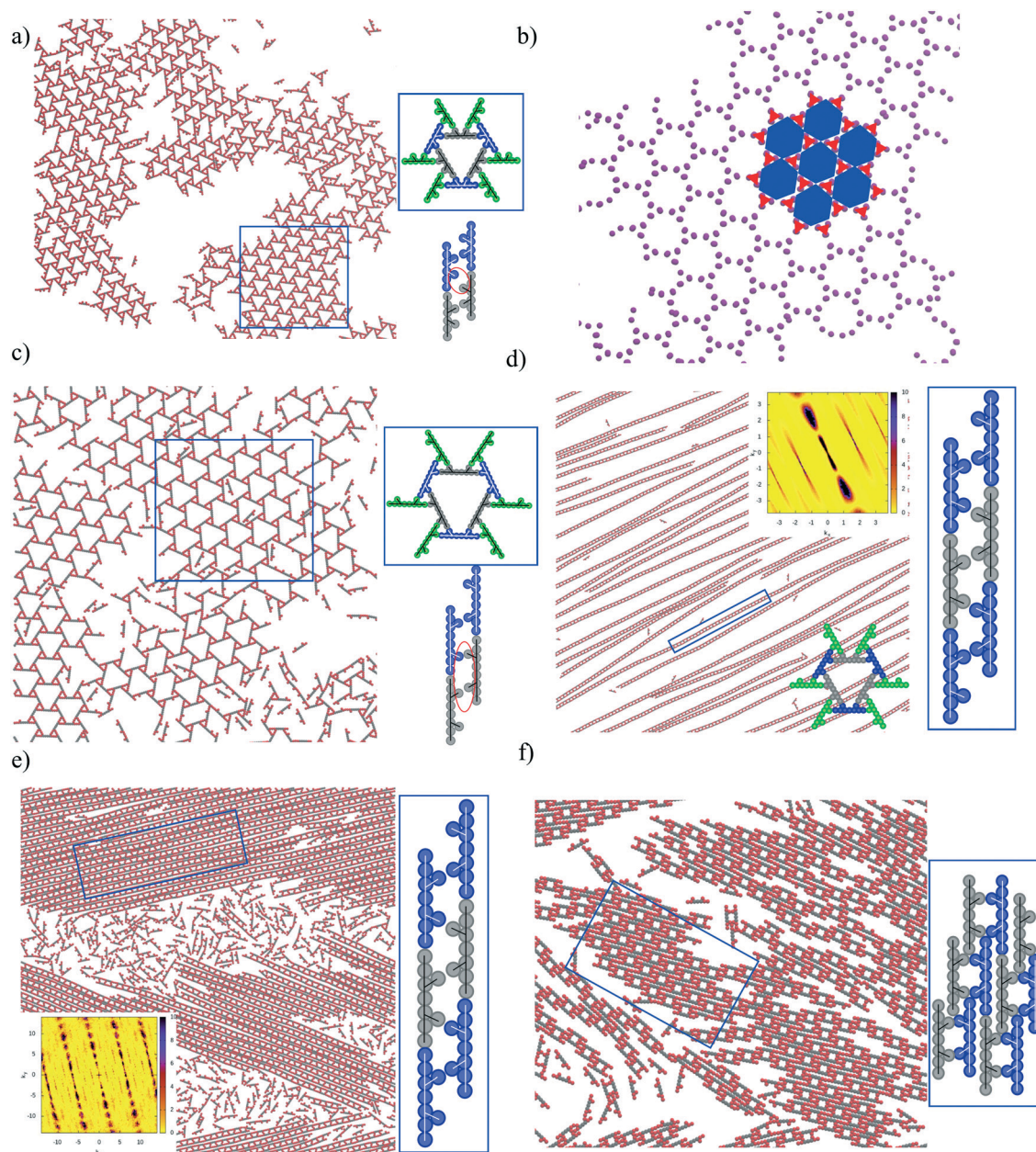
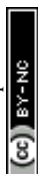


Fig. 9 Fragment of the configuration for model **R2_M4** recorded at $\rho^* = 0.2$ and $T^* = 0.28$ for $l = 0.36\sigma$ (a). Part b) shows how the active sites of model **R2_M4** assemble into a Kagomé-like pattern. Different polygons are marked by different colors to better pronounce the ordering. Part c) shows a part of the configuration for model **R4_M4** recorded at $\rho^* = 0.2$ and $T^* = 0.28$ for $l = 0.36\sigma$. Configurations for model **R3_M4** recorded at $\rho^* = 0.2$ and $T^* = 0.28$ for $l = 0.36\sigma$ (d), at $\rho^* = 0.5$ and $T^* = 0.42$ for $l = 0.36\sigma$ (e), and at $\rho^* = 0.5$ and $T^* = 0.67$ for $l = 0.44\sigma$ (f). 2-D structure factors are shown in the insets to parts (d) and (e). Schematically drawn association paths are shown on the right-hand side of the panels.

Finally, we proceed to the description of the last architecture of the tetrapotic building blocks *i.e.*, model **M5** with bond lengths $l = 0.36\sigma$ and $l = 0.44\sigma$. Similar to model **M2**, the molecules associate into Sierpinski triangles and into a more dense phase. The effects of the elongation of core length **R** as well as the change of density have been found to be the same as in model **M2** (*cf.* Fig. 7). For the sake of brevity, we have omitted the details of analysis in the main text and one should refer to Fig. S7 and S8 in the ESI† for more details.

3 Conclusions

In this study, we have performed extensive coarse-grained molecular dynamics simulations of the self-assembly of tetra-substituted molecules. We have found that they are able to form a variety of different structures depending on the parameters of the employed model. All of these ordered networks have been characterized by cluster analysis, the nematic order parameter, the relative shape anisotropy parameter, and the two-dimensional structure factors.



We have established the following rules depending on the interaction zone α (cf. Fig. 2) and the architecture of tetra-topic molecules. In the case of building blocks with the same numbers of segments in each of the arms (**M2**, **M5**), for $l = 0.4\sigma$, we could distinguish two different networks. Slight changes of the interaction zone allowed us to selectively obtain either Sierpinski triangles ($l = 0.36\sigma$) or a denser phase ($l = 0.44\sigma$) for all core lengths **R**. On the other hand, the molecules with unequal numbers of segments in the arms have demonstrated another tendency. For bond lengths $l = 0.36\sigma$ and $l = 0.40\sigma$ they assemble into isogonal tiling and into a denser phase, respectively. In the former case, it is worth mentioning that the representation of active sites reveals that although those models form qualitatively the same network, geometrical centers of associations form a 3.4.6.4 Archimedean tessellation (**M3**) or Kagomé network (**M4**).

However, there are two exceptions. For model **R2_M3** we have observed the formation of small clusters only, which are similar to the STs of the first-order, whereas the behavior of molecules **R3_M4** is more complex. For the bond length $l = 0.4\sigma$ we have seen the formation of the ladder network and a denser phase. However, the former disappears at high densities. Similar to models **M2**, **M5**, we have been able to selectively obtain each of those networks depending on the bonding distance. Surprisingly, for $l = 0.36\sigma$ we have found that the wires are much longer as compared to the greater jointing distance. Moreover, they are gluing one to another at higher densities, and do not form a denser phase. On the other hand, for the system with $l = 0.44\sigma$, the denser phase is observed even at lower densities, and a ladder network has not been found at all.

Another interesting feature found is that denser phases are qualitatively the same for every model irrespective of their architecture. The connections between molecules are the same; however, the pore sizes are different due to the geometry of investigated models. This observation is better pronounced by the visualization of the active site ordering.

Moreover, we have found that model **M1**, irrespective of the bonding length l , assembled into unique structures compared to other examined systems. For $l = 0.4\sigma$ isogonal tiling, whereas for $l = 0.44\sigma$ a flower-like motif has been found.

Despite the formation of a variety of different structures it has to be emphasized that ordering of tetra-topic molecules into Sierpinski triangles is quite surprising since the majority of the papers report their formation in completely different systems. The only general rule that has been established to date is that the so-called “V-shaped” molecules are able to order into those fractals, and only if three tectons assemble either by hydrogen bonding (B(OH)_2 substitution) or by metal–organic coordination (for instance, $-\text{CN}$ groups with Fe or Ni metal atoms). Here we have shown another possible scheme, together with a proposal on how this kind of model chemical compound could look like (cf. Fig. 1(c)). As already mentioned, if one would substitute it with active groups that would allow two molecules to interact with one another ($-\text{OH}$, COOH , or $-\text{Cl}$ with Fe(II)) it

corresponds to the $l = 0.36\sigma$ case, whereas interactions of three building blocks ($-\text{B(OH)}_2$, or $-\text{Cl}$ with Fe(III)) can reflect results for $l = 0.44\sigma$. On the other hand, the intermediate scenario where two phases occur which is most likely the case in experimental studies due to the oscillations of chemical bonds of active groups can be seen for $l = 0.40\sigma$. Therefore, we believe that our finding may be inspiring for experimentalists.

We have presented a variety of different structures and their analysis. Moreover, we have presented a molecular dynamics model and shown how a slight change of its parameters can drastically change the behavior of systems of interest. We have demonstrated that the possibility of a particular number of molecules that can assemble with one another can determine the formation of completely different structures. As already mentioned, multiple chemically active groups can display diverse behavior depending on the experimental conditions. Therefore, we hope that our observations can be very useful for the better understanding and possibility of selective control of the self-assembly in future experimental studies.

Conflicts of interest

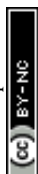
There are no conflicts of interests.

Acknowledgements

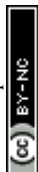
This study has been supported by the Polish Ministry of Science and Higher Education, under Grant No. DI2017 001147 and the research has been supported by the Foundation for Polish Science (FNP).

References

- 1 C. C. Ng, Y.-L. Cheng and P. S. Pennefather, Properties of a self-assembled phospholipid membrane supported on lipobeads, *Biophys. J.*, 2004, **87**, 323–331.
- 2 L. Nasalean, S. Baudrey, N. B. Leontis and L. Jaeger, Controlling RNA self-assembly to form filaments, *Nucleic Acids Res.*, 2006, **34**, 1381–1392.
- 3 J. Won, S. K. Chae, J. H. Kim, H. H. Park, Y. S. Kang and H. S. Kim, Self-assembled DNA composite membranes, *J. Membr. Sci.*, 2005, **249**, 113–117.
- 4 R. F. Garmann, A. M. Goldfain and V. N. Manoharan, Measurements of the self-assembly kinetics of individual viral capsids around their RNA genome, *Proc. Natl. Acad. Sci. U. S. A.*, 2019, **116**, 22485–22490.
- 5 S. R. White, N. R. Sottos, P. H. Geubelle, J. S. Moore, M. R. Kessler, S. R. Sriram, E. N. Brown and S. Viswanathan, Autonomic healing of polymer composites, *Nature*, 2001, **409**, 794–797.
- 6 V. L. Colvin, From opals to optics: Colloidal photonic crystals, *MRS Bull.*, 2001, **26**, 637–641.
- 7 H. Stoyanov, M. Kollosche, S. Risse, R. Waché and G. Kofod, Soft conductive elastomer materials for stretchable



- electronics and voltage controlled artificial muscles, *Adv. Mater.*, 2013, **25**, 578–583.
- 8 M. D. Lima, N. Li, M. Jung de Andrade, S. Fang, J. Oh, G. M. Spinks, M. E. Kozlov, C. S. Haines, D. Suh, J. Foroughi, S. J. Kim, Y. Chen, T. Ware, M. K. Shin, L. D. Machado, A. F. Fonseca, J. D. W. Madden, W. E. Voit, D. S. Galvão and R. H. Baughman, Electrically, chemically, and photonically powered torsional and tensile actuation of hybrid carbon nanotube yarn muscles, *Science*, 2012, **338**, 928–932.
 - 9 C. Zhang, B.-H. Wu, M.-Q. Ma, Z. Wang and Z.-K. Xu, Ultrathin metal/covalent-organic framework membranes towards ultimate separation, *Chem. Soc. Rev.*, 2019, **48**, 3811–3841.
 - 10 S. Wang, Q. Wang, P. Shao, Y. Han, X. Gao, L. Ma, S. Yuan, X. Ma, J. Zhou, X. Feng and B. Wang, Exfoliation of covalent organic frameworks into few-layer redox-active nanosheets as cathode materials for lithium-ion batteries, *J. Am. Chem. Soc.*, 2017, **139**, 4258–4261.
 - 11 G. Li, K. Zhang and T. Tsuru, Two-dimensional covalent organic framework (COF) membranes fabricated via the assembly of exfoliated COF nanosheets, *ACS Appl. Mater. Interfaces*, 2017, **9**, 8433–8436.
 - 12 L. Wang, R. Liu, J. Gu, B. Song, H. Wang, X. Jiang, K. Zhang, X. Han, X.-Q. Hao, S. Bai, M. Wang, X. Li, B. Xu and X. Li, Self-assembly of supramolecular fractals from generation 1 to 5, *J. Am. Chem. Soc.*, 2018, **140**, 14087–14096.
 - 13 Z. Jiang, D. Liu, M. Chen, J. Wang, H. Zhao, Y. Li, Z. Zhang, T. Xie, F. Wang, X. Li, G. R. Newkome and P. Wang, Assembling shape-persistent high-order Sierpiński triangular fractals, *iScience*, 2020, **23**(5), 101064.
 - 14 D. Nieckarz and P. Szabelski, Simulation of the self-assembly of simple molecular bricks into Sierpiński triangles, *Chem. Commun.*, 2014, **50**, 6843–6845.
 - 15 J. Shang, Y. Wang, M. Chen, J. Dai, X. Zhou, J. Kuttner, G. Hilt, X. Shao, J. M. Gottfried and K. Wu, Assembling molecular Sierpiński triangle fractals, *Nat. Chem.*, 2015, **7**, 389–393.
 - 16 Y. Mo, T. Chen, J. Dai, K. Wu and D. Wang, On-surface synthesis of highly ordered covalent Sierpiński triangle fractals, *J. Am. Chem. Soc.*, 2019, **141**, 11378–11382.
 - 17 C. Li, X. Zhang, N. Li, Y. Wang, J. Yang, G. Gu, Y. Zhang, S. Hou, L. Peng, K. Wu, D. Nieckarz, P. Szabelski, H. Tang and Y. Wang, Construction of Sierpiński triangles up to the fifth order, *J. Am. Chem. Soc.*, 2017, **139**, 13749–13753.
 - 18 Y. Zhang, X. Zhang, Y. Li, S. Zhao, S. Hou, K. Wu and Y. Wang, Packing Sierpiński triangles into two-dimensional crystals, *J. Am. Chem. Soc.*, 2020, **142**, 17928–17932.
 - 19 D. Nieckarz and P. Szabelski, Chiral and fractal: from simple design rules to complex supramolecular constructs, *Chem. Commun.*, 2016, **52**, 11642–11645.
 - 20 A. Rochefort and J. D. Wuest, Interaction of substituted aromatic compounds with graphene, *Langmuir*, 2009, **25**, 210–215.
 - 21 A. Ibenskas and E. E. Tornau, Modeling of ribbon and oblique structures of benzene-1,3,5-triyl-tribenzoic acid, *J. Phys. Chem. C*, 2020, **124**, 18650–18659.
 - 22 C. Karner, C. Dellago and E. Bianchi, Design of patchy rhombi: From close-packed tilings to open lattices, *Nano Lett.*, 2019, **19**, 7806–7815.
 - 23 C. Karner, C. Dellago and E. Bianchi, Hierarchical self-assembly of patchy colloidal platelets, *Soft Matter*, 2020, **16**, 2774–2785.
 - 24 A. Ibenskas, M. Šimėnas, K. J. Kizlaitis and E. E. Tornau, Pinwheel structures of deprotonated trimesic acid on Ag(111): Model and simulations, *J. Phys. Chem. C*, 2020, **124**, 11212–11220.
 - 25 A. I. Fadeeva, V. A. Gorbunov, P. V. Stishenko, S. S. Akimenko and A. V. Myshlyavtsev, Melting of Fe-terephthalate layers on Cu(100) surface with randomly distributed point defects, *Appl. Surf. Sci.*, 2021, **545**, 148989.
 - 26 J. Lisiecki and P. Szabelski, Designing 2d covalent networks with lattice Monte Carlo simulations: precursor self-assembly, *Phys. Chem. Chem. Phys.*, 2021, **23**, 5780–5796.
 - 27 C.-A. Palma, P. Samori and M. Cecchini, Atomistic simulations of 2d bicomponent self-assembly: From molecular recognition to self-healing, *J. Am. Chem. Soc.*, 2010, **132**, 17880–17885.
 - 28 Y. Zhao and J. Wang, How to obtain high-quality and high stability interfacial organic layer: Insights from the pteda self-assembly, *J. Phys. Chem. C*, 2017, **121**, 4488–4495.
 - 29 Ł. Baran and W. Rzyśko, Application of a coarse-grained model for the design of complex supramolecular networks, *Mol. Syst. Des. Eng.*, 2020, **5**, 484–492.
 - 30 Ł. Baran, D. Nieckarz, P. Szabelski and W. Rzyśko, Controlling of the 2d self-assembly process by the variation of molecular geometry, *J. Phys. Chem. C*, 2019, **123**, 19549–19556.
 - 31 Ł. Baran, W. Rzyśko and S. Szajnar, Archimedean tessellation found by the variation of building blocks' and linkers' geometry: In silico investigations, *J. Phys. Chem. C*, 2020, **124**, 20101–20108.
 - 32 S. Xing, Z. Zhang, X. Fei, W. Zhao, R. Zhang, T. Lin, D. Zhao, H. Ju, H. Xu, J. Fan, J. Zhu, Y.-q. Ma and Z. Shi, Selective on surface covalent coupling based on metal-organic coordination template, *Nat. Commun.*, 2019, **10**, 70.
 - 33 S. Xing, Z. Zhang, H. Liang, B. Sun, H. Xu, J. Fan, Y.-q. Ma and Z. Shi, On-surface cascade reaction based on successive debromination via metal-organic coordination template, *Langmuir*, 2020, **36**, 6286–6291.
 - 34 W. Rzyśko, S. Sokołowski and T. Staszewski, Monte Carlo simulations of a model two-dimensional, two-patch colloidal particles, *J. Chem. Phys.*, 2015, **143**, 064509.
 - 35 Y. V. Kalyuzhnyi and P. T. Cummings, Two-patch colloidal model with re-entrant phase behaviour, *J. Chem. Phys.*, 2013, **139**, 104905.
 - 36 D. Frenkel and R. Eppenga, Evidence for algebraic orientational order in a two-dimensional hard-core nematic, *Phys. Rev. A: At., Mol., Opt. Phys.*, 1985, **31**, 1776–1787.
 - 37 D. N. Theodorou and U. W. Suter, Shape of unperturbed linear polymers: polypropylene, *Macromolecules*, 1985, **18**, 1206–1214.
 - 38 P. Bolhuis and D. Frenkel, Tracing the phase boundaries of hard spherocylinders, *J. Chem. Phys.*, 1997, **106**, 666–687.



PIV

lic. Łukasz Baran
Katedra Chemii Teoretycznej
Instytut Nauk Chemicznych
Wydział Chemii UMCS
Pl. Marii Curie-Skłodowskiej 3
20-031 Lublin

Lublin, 16.05.2022

OŚWIADCZENIE


Oświadczam, że mój wkład w niniejszej pracy:

[PIV] **Ł. Baran***, W. Rżysko, D. Tarasewicz, "Variation of interaction zone size for the target design of 2D supramolecular networks", *Molecular Systems Design & Engineering*, 2020, **6**, 805-816.

polegał na przeprowadzeniu części symulacji metodą dynamiki molekularnej, napisaniu manuskryptu i przeprowadzeniu analizy części wyników

Udział ten szacuję na 70 %.

lic. Łukasz Baran



PIV

dr hab. Wojciech Rzyśko, prof. UMCS
Katedra Chemii Teoretycznej
Instytut Nauk Chemicznych
Wydział Chemii UMCS
Pl. Marii Curie-Skłodowskiej 3
20-031 Lublin

Lublin, 16.05.2022

OŚWIADCZENIE

Oświadczam, że mój wkład w niniejszej pracy:

[PIV] **Ł. Baran***, W. Rzyśko, D. Tarasewicz, "Variation of interaction zone size for the target design of 2D supramolecular networks", *Molecular Systems Design & Engineering*, 2020, **6**, 805-816.

polegał na koordynowaniu merytorycznym badań i analizie części wyników

Udział ten szacuję na 20 %.

dr hab. Wojciech Rzyśko, prof. UMCS



PIV

mgr Dariusz Tarasewicz
Katedra Chemii Teoretycznej
Instytut Nauk Chemicznych
Wydział Chemii UMCS
Pl. Marii Curie-Skłodowskiej 3
20-031 Lublin

Lublin, 13.05.2022

OŚWIADCZENIE

Oświadczam, że mój wkład w niniejszej pracy:

[PIV] **Ł. Baran***, W. Rżysko, D. Tarasewicz, "Variation of interaction zone size for the target design of 2D supramolecular networks", *Molecular Systems Design & Engineering*, 2020, **6**, 805-816.

polegał na wykonaniu części symulacji komputerowych.

Udział ten szacuję na 10 %.

mgr Dariusz Tarasewicz



Coarse-Grained Modeling of On-Surface Self-Assembly of Mixtures Comprising Di-Substituted Polyphenyl-Like Compounds and Metal Atoms of Different Sizes

Lukasz Baran*

Cite This: *ACS Omega* 2021, 6, 25193–25200

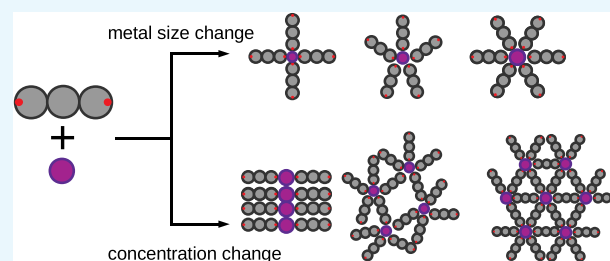
Read Online

ACCESS |

Metrics & More

Article Recommendations

ABSTRACT: We use coarse-grained molecular dynamics simulations to investigate the phase behavior of binary mixtures of di-substituted polyphenyl-like compounds and metal atoms of different sizes. We have estimated the possible on-surface behavior that could be useful for the target design of particular ordered networks. We have found that due to the variation of system conditions, we can observe the formation of the parallel, square, and triangular networks, Archimedean tessellation, and “spaghetti wires.” All of these structures have been characterized by various order parameters.



1. INTRODUCTION

Fabrication of two-dimensional materials attracts considerable attention, owing to their possibility to exhibit different features from their bulk counterparts. This field has begun with the discovery of graphene and characterization of its properties, especially in the electronic field.¹ From this date, a variety of different two-dimensional (2D) materials have been synthesized, and two main routes have been established. The first one is a top-down approach that benefits from the general knowledge of the three-dimensional (3D) materials such as covalent or metal-organic frameworks (COFs and MOFs, respectively) and is supposed to exfoliate a layered crystal due to applied external forces to form a single layer of the smallest thickness as possible. The second protocol is a bottom-up approach, which can be applied on the surfaces such as highly oriented pyrolytic graphite (HOPG) or coinage metals (Au, Ag, Cu) or in the air/water or liquid/liquid interfaces. The obtained single nanolayers have already been used as membranes for separation in both liquid and gas phases,² batteries,³ molecular sieves,⁴ and insulin delivery.⁵

The on-surface synthesis performed either in ultrahigh vacuum or liquid conditions generally has proven to be the successful and most conventional routine for the preparation of well-ordered networks. To date, a variety of compounds of different geometry have been investigated, and it has been found that they can form small clusters⁶ up to extended porous structures,⁷ as well as Kagomé patterns,^{8,9} rhombus tilings,¹⁰ and five-vertex Archimedean tessellations.^{11,12} The latter is particularly interesting since it has been obtained in a mixture of dicyanide polyphenyl compounds with rare-earth metal

atoms, whereas the first reports of such structures appeared in alloy particles¹³ or chalcogenides.¹⁴

In this paper, we wanted to further explore the conditions on how di-substituted polyphenyl-like (linker) molecules behave with mixtures of metal atoms. Unlike in the references,^{11,12} we have changed not only the mixture concentration but also the metal atom sizes. For this purpose, we have designed a coarse-grained model and performed comprehensive molecular dynamics simulations. We believe that the protocol used in the course of this study can give a very helpful insight for the experimentalists owing to the fact that computer modeling is a very convenient substitute to the exploration of problems of interest and can reasonably complement experimental findings. Although there are other methods that have been widely used such as quantum density functional theory¹⁵ or classical Monte Carlo,^{16–21} we have already proven that the approach used in our laboratory can be useful for examination of similar systems of interest both in one-component systems and binary mixtures.^{22–24}

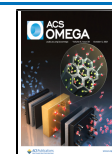
2. METHODS

In this paper, the geometry of the linear linker molecules has been devoted to reflecting the behavior of di-substituted

Received: June 1, 2021

Accepted: September 8, 2021

Published: September 21, 2021



polyphenyl compounds, as shown in Figure 1. In its structure, each of the gray segments mimicked one phenyl group,

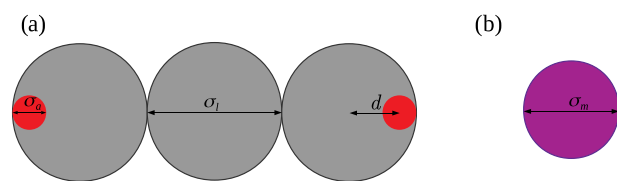


Figure 1. Model of the linker molecule (a) and metal atom (b). Gray circles correspond to the segments of the linear linker, whereas the red ones pertain to the active sites. For the description of parameters used in the model, confer the text.

whereas red entities were the active interaction centers. The size of every linker's segment has been set to $\sigma_l = \sigma$, while the active sites have been five times smaller, $\sigma_a = 0.2\sigma_l$. The segments in the former have been tangentially jointed with one another; therefore, the bonding distance has been set to σ_l . The active sites have been entirely embedded into both terminal units of the linear linker, and the bonding distance has been abbreviated as $d = 0.36\sigma_l$. In our previous paper, we have already shown that both the size and the bonding distance d can provide structures of 3- to 6-fold symmetries.²² This approach, however, lacks the possibility to change the concentration of the mixtures since the second component has been treated implicitly. Therefore, we wanted to fill this gap, and metal atoms in our simulations have been treated explicitly, and their size varied between $\sigma_m = 0.5 - 1.0\sigma_l$.

In molecular dynamics simulations, all of the objects have been treated as flat and rigid objects, and all of the necessary bonds have been maintained by harmonic binding potentials

$$u_{ll} = k_{ll}(r - \sigma_{ll})^2 \quad (1)$$

and

$$u_{al} = k_{al}(r - d)^2 \quad (2)$$

Likewise, all of the necessary angles have been preserved

$$u_{ll}(\theta_{ll}) = k_{\theta}(\theta_{ll} - \theta_{0,ll})^2 \quad (3)$$

and

$$u_{al}(\theta_{al}) = k_{\theta}(\theta_{al} - \theta_{0,al})^2 \quad (4)$$

The interparticle potential employed in our simulations was (12,6) Lennard-Jones potential, which has been appropriately shifted to ensure the continuity of both the potential and of its first derivative^{25,26}

$$U_{SF} = \begin{cases} U_{LJ}(r) - U_{LJ}(r_{cut}) + U'_{LJ}(r_{cut})(r - r_{cut}) & r < r_{cut} \\ 0 & \text{otherwise} \end{cases} \quad (5)$$

where $U_{LJ}(r) = 4\epsilon_{ij}[(\sigma_{ij}/r)^{12} - (\sigma_{ij}/r)^6]$ and $U'_{LJ}(r_{cut})$ is the first derivative of $U_{LJ}(r)$ at $r = r_{cut}$.

The Lennard-Jones potential parameters, $\sigma_l = \sigma$ and $\epsilon_{ll} = \epsilon$, have been set to be the units of length and energy, respectively. The reduced time and temperature are equal to $\tau^* = t\sqrt{\epsilon/m\sigma^2}$ and $T^* = kT/\epsilon_{ll}$, respectively. The number density has been defined as $\rho^* = \frac{R\sigma_c^2 + N_m\sigma_m^2}{L_x L_y}$, where R and N_m

are the number of segments in the linear linker and metal "atoms," respectively. Moreover, we define the binary mixture composition as $\chi = \frac{N_l}{N_{tot}}$, where N_l is the number of linker molecules and $N_{tot} = N_l + N_m$. It has been varied in the range of $\chi = 0.25 - 0.83$.

The energies of the linker–linker and the linker–active site interactions have been set to $\epsilon_{ll} = \epsilon_{aa} = \epsilon$ and $\epsilon_{ma} = 5.0\epsilon$. The linker-site diameter and the energy of the linker-site interactions have been set to $\sigma_{al} = (\sigma_a + \sigma_l)/2$ and $\epsilon_{al} = \epsilon$, respectively. The cutoff distance of the interactions between the active site and the metal atom has been set to $r_{cut,ma} = 2\sigma_{ma}$, whereas the remaining ones are $r_{cut,ij} = \sigma_{ij}$ where $ij = aa, al, ll, lm,$ and mm . This has been done to assume that the only attraction in the system is due to the metal-organic coordination, whereas the remaining are the soft-core interactions. We did not use any solvent explicitly, but rather by means of presented interparticle potential, we modeled the system so that the interactions other than the active site-metal atoms are screened due to the solvent presence. The harmonic potential constants $k_{al} \equiv k_{ll}$ have been set to $1000\epsilon/\sigma^2$ and $k_{\theta} = 1000\epsilon/(\text{rad})^2$. Such high values of harmonic constants have been set to reduce the range of fluctuations and, in consequence, to maintain the rigidity of the assumed geometries.

All of the molecular dynamics simulations have been performed in the NVT ensemble, using LAMMPS simulation package.^{27,28} The velocity Verlet integration scheme has been used with the reduced time step of the order of $t = 0.001\tau$. The number of linker molecules and metal atoms varied from 1600 to 8000 and 1600 to 4800, respectively. However, one has to note that the total number of atoms varied, depending on the concentration. This amount is sufficient for most of the self-assembly systems, which is simultaneously large enough to form ordered networks and small enough to form those structures in a reasonable time frame.

The simulation scheme involved preliminary runs in the NPT ensemble to establish the desired density. Next, equilibration runs for 5×10^6 times steps using Berendsen thermostat,²⁹ with the damping constant equal to $\tau_B = 10\tau$ have been performed. Further equilibration for 5×10^7 as well as production runs have been performed using Nosé–Hoover chain algorithm,³⁰ with the damping constant equal to $\tau_{NH} = 10\tau$ and the number of chains set to $N_{chain} = 3$. Every system has been cooled down from temperatures where we did not observe any order, up to the point where self-assembled networks have been distinct. The temperature grid was set to $\Delta T^* = 0.01$.

3. RESULTS AND DISCUSSION

Let us start from the description of the binary mixture with metal atoms 2-fold smaller than the diameter of core's segments, i.e., $\sigma_m = 0.5\sigma$. The results for the system with an equal amount of linker and metal entities ($\chi = 0.5$) can be found in Figure 2a. One can see the formation of a network with square symmetry with distinct imperfections in its structure. If one increases the number of linker molecules three times ($\chi = 0.75$), the formation of a nearly perfect square lattice can be observed, as it has been shown in Figure 2b. To better understand the development of this network, we wanted to investigate the arrangement of metal atoms. In part (c) of Figure 2, we can see their layout for the mixture composition $\chi = 0.5$. In this case, two atoms tend to glue with one another,

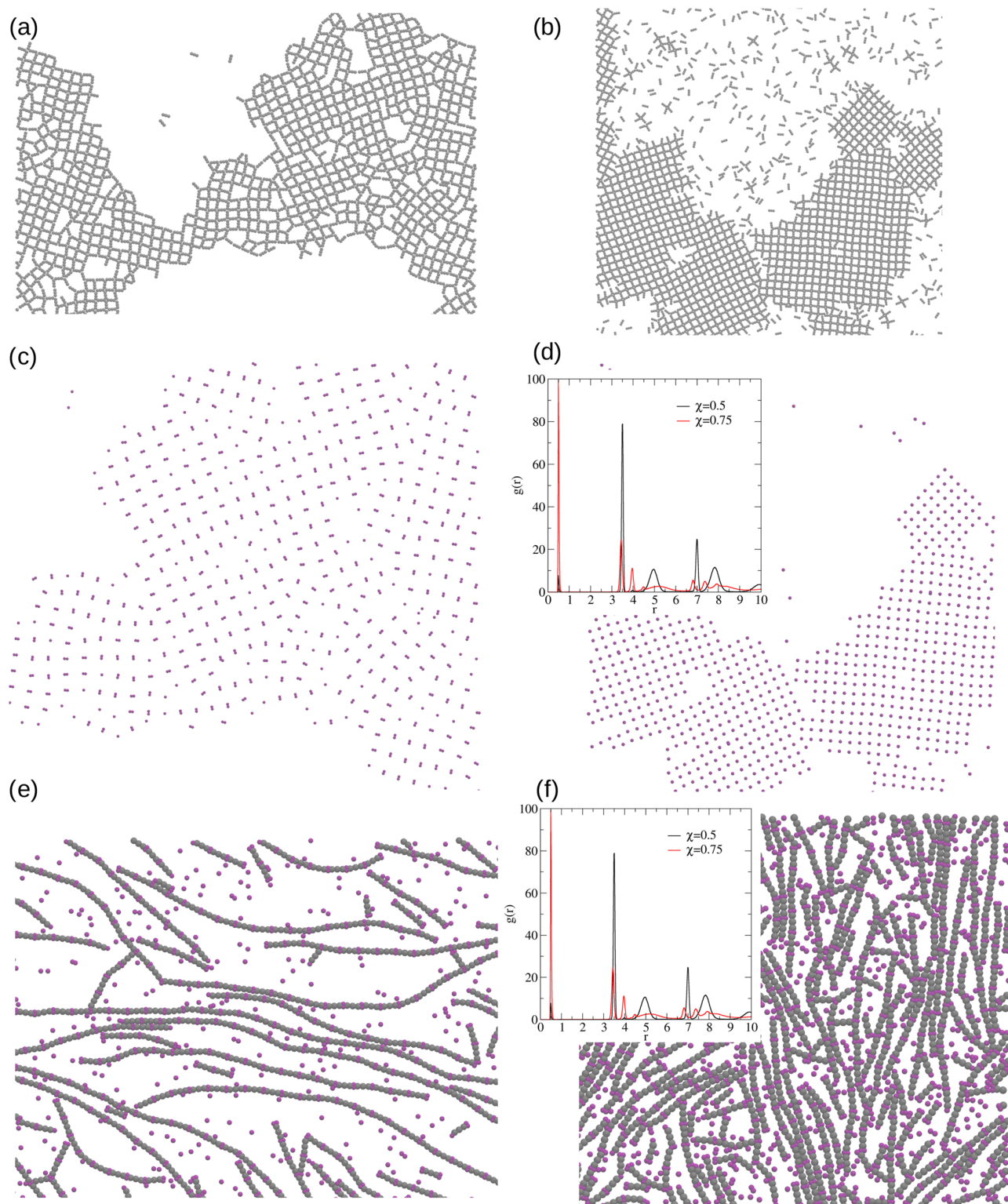


Figure 2. Fragment of the configurations for linker molecules (a, b) and metal atoms of size $\sigma_m = 0.5\sigma$ (c, d) for $\chi = 0.5$ (a, b) and $\chi = 0.75$ (c, d) mixture compositions in $\rho^* = 0.2$ at $T^* = 0.3$. Fragment of the configurations for $\chi = 0.25$ in $\rho^* = 0.2$ at $T^* = 0.3$ (e) and in $\rho^* = 0.5$ at $T^* = 0.4$ (f). The insets to part (d) and (f) display the radial distribution function calculated with respect to metal atoms.

despite their soft-core interactions. On the contrary, for $\chi = 0.75$, metal atoms are entirely separated (cf. Figure 2d).

To verify if observations from snapshots are correct, we have calculated the radial distribution function with respect to metal atoms, which can be found in the inset to Figure 2d. For the

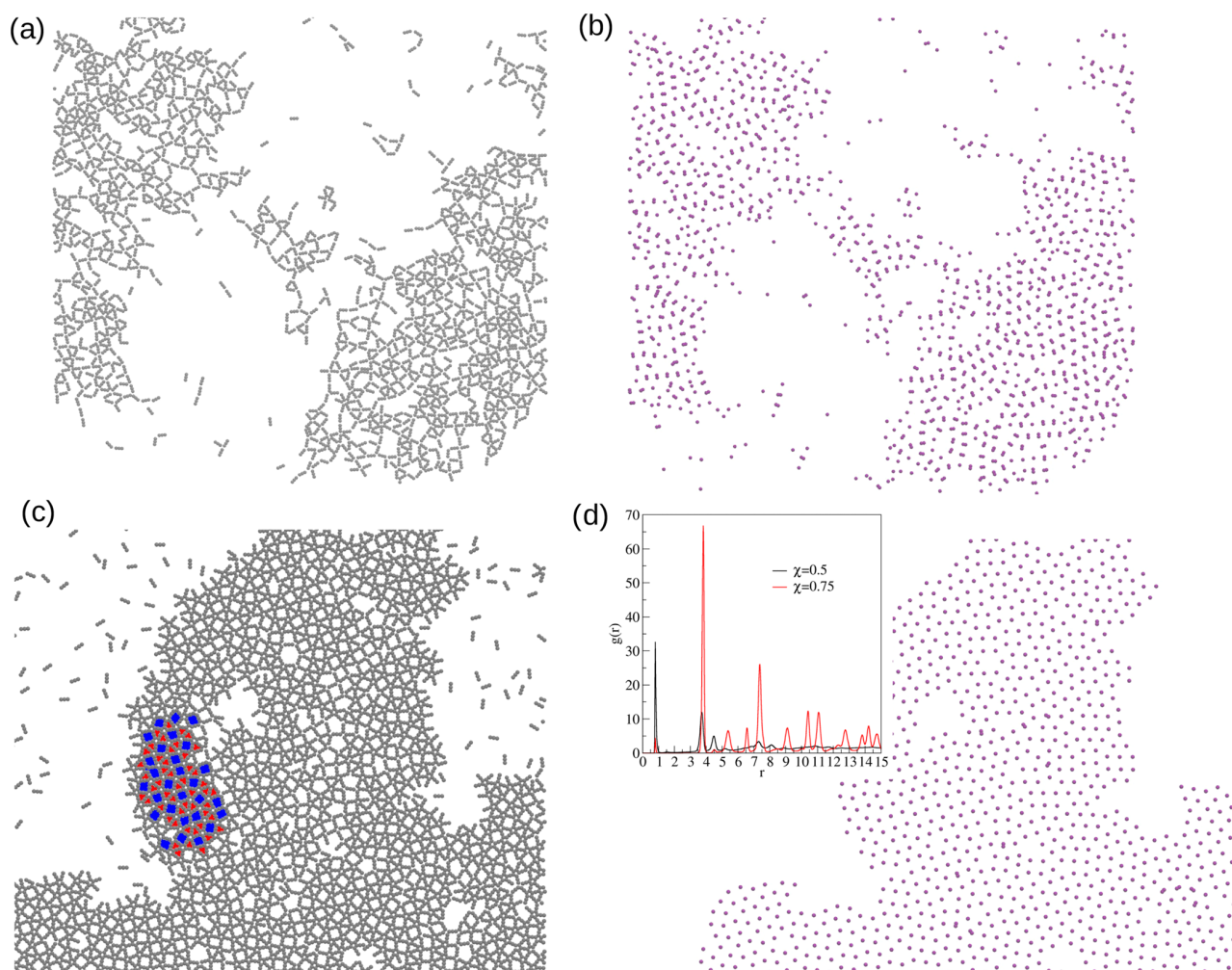


Figure 3. Fragment of the configurations for linker molecules (a, c) and metal atoms of size $\sigma_m = 0.8\sigma$ (b, d) for mixture compositions $\chi = 0.5$ in $\rho^* = 0.2$ at $T^* = 0.4$ (a, c) and $\chi = 0.75$ in $\rho^* = 0.2$ at $T^* = 0.3$ (b, d). The inset to part (d) displays the radial distribution function calculated with respect to metal atoms.

smaller molar fraction $\chi = 0.5$, the most prominent peak is around $r \approx 0.5$, which means that those entities are glued one to another. On the other hand, for higher $\chi = 0.75$, this peak almost vanished, and the most prominent distance is around $r \approx 3.5$. Moreover, we have computed the number of dimers in both cases, which is approximately 90 and 5% for mixture compositions $\chi = 0.5$ and 0.75 , respectively.

Another quantity that we used to characterize the formation of a highly ordered, square network was the two-dimensional bond-orientational order parameter (BOOP), calculated with respect to metal atoms, which is defined as³¹

$$Q_k^{2D} = \frac{1}{N_{\text{bond}}} \left| \sum_i \sum_{i \neq j} \exp(ki\phi_{ij}) \right| \quad (6)$$

where i runs over all metal atoms of the system, j runs over all neighbors of i , ϕ_{ij} denotes the angle between the bond connecting particles i and j and an arbitrary but fixed reference axis, N_{bond} denotes the number of bonds in the system, and $k = 2, 3, 4, 5, 6$. For the square network, we have assumed that two metal atoms are neighbors if their distance is less than 3.8σ , which is the second minimum extracted from the radial

distribution function (cf. inset to Figure 2d). The bond-orientational order parameter can take the values between 0 and 1 for the disordered and the ordered structures of a particular symmetry, respectively.

To corroborate the observations from snapshots and radial distribution function, we have calculated this parameter for the aforementioned mixture compositions. In the first case, i.e., $\chi = 0.5$, the 2D BOOP is approximately $Q_4 = 0.202 \pm 0.05$, which indicates that there is an order to some extent, however, the presence of imperfections in the network is noticeable, which in consequence decreases its value. On the other hand, for the composition $\chi = 0.75$, this parameter takes a value of $Q_4 = 0.915 \pm 0.03$, which corresponds to a nearly perfect structure of 4-fold symmetry. This analysis demonstrates that the increase in the number of linker molecules in the system stabilizes the formation of a square network.

We have also examined the mixture composition of $\chi = 0.25$, which means that there are 3-fold more metal atoms than linker molecules. In this case, we have found that the formation of “spaghetti-like” strings (cf. Figure 2e). Similarly, as in the case of $\chi = 0.5$, metal atoms are gluing one to another and are forming “dimers”. An increase of the density does not lead to the increase of order in the system, and those strings do not

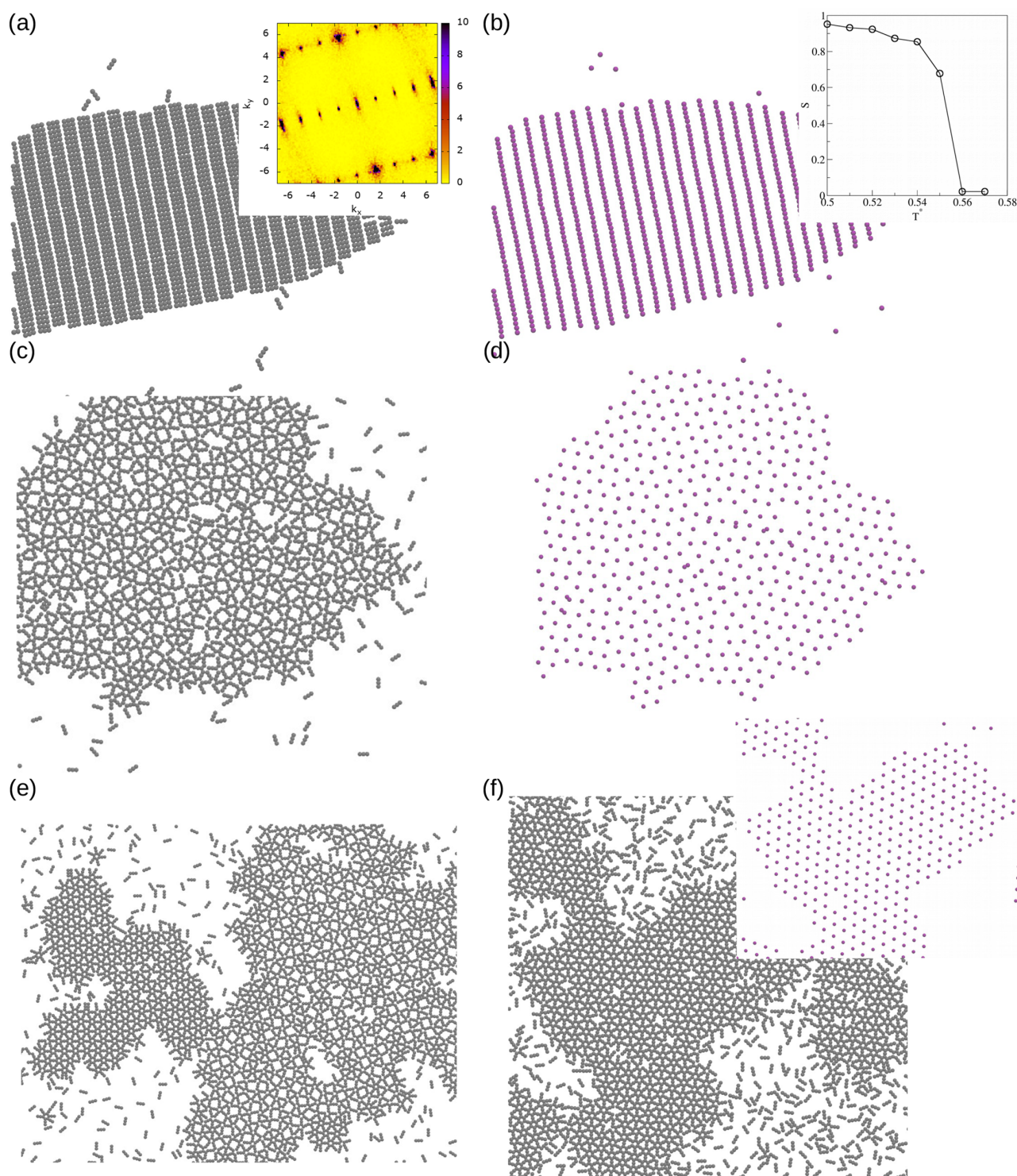


Figure 4. Fragment of the configurations for linker molecules (a, c) and metal atoms of size $\sigma_m = 1.0\sigma$ (b, d) for mixture compositions $\chi = 0.5$ in $\rho^* = 0.2$ at $T^* = 0.5$ (a, b) and $\chi = 0.75$ in $\rho^* = 0.2$ at $T^* = 0.4$ (c, d). The insets to part (a) and (b) show the 2D structure factor and relation of nematic order parameter with respect to the temperature, respectively. Parts (e) and (f) display the snapshots for the systems $\chi = 0.83$ in $\rho^* = 0.2$ at $T^* = 0.3$ and $\chi = 0.83$ in $\rho^* = 0.4$ at $T^* = 0.4$, respectively. The inset to part (f) displays the arrangement of metal atoms in this system.

start to align in one direction (cf. Figure 2f). The radial distribution function calculated with respect to metal atoms shown in the inset to Figure 2f shows that the most prominent peak is around $r \approx 0.5$, which confirms that metals tend to form dimers. Moreover, we have computed the number of

dimers in both cases, which is approximately 63 and 53% for the densities $\rho^* = 0.2$ and 0.5 , respectively.

Next, we proceed to the description of a binary mixture with metal atoms of size equal to $\sigma_m = 0.8\sigma$. The results for $\chi = 0.5$ can be found in Figure 3a. One can see that we are not able to

distinguish any network of a particular symmetry. Linker molecules connect with metal atoms quite randomly, and multiple pore shapes can be observed. The arrangement of metal atoms as shown in Figure 3b shows that for this mixture composition, they tend to glue one to another and form dimers, as for smaller metal sizes. As previously, it leads to the disturbance in the formation of any ordered network.

The results for the system with mixture composition $\chi = 0.75$ can be found in Figure 3c. In this case also, the formation of multiple pore shapes can be observed; however, this pattern resembles the $3^2.4.3.4$ Archimedean tiling with several visible imperfections. For better visualization, we have colored the particular polygons belonging to this semiregular tessellation. The arrangement of metal atoms, as shown in Figure 3d, shows that they are separated, as it has been observed in a previous case (cf. Figure 2). The radial distribution function inserted to part (d) of this figure corroborates with the observations from the snapshots. Likewise, as for smaller σ_m we have evaluated the average amount of dimers in the system, which is approximately 73% ($\chi = 0.5$) and 4% ($\chi = 0.75$). We conclude that the increase of the number of linker molecules leads to the stabilization of ordered networks of a particular symmetry.

Similarly, as for the previous metal size, we have examined the mixture composition of $\chi = 0.25$. The formation of similar spaghetti stripes has been found, as in the case of $\sigma_m = 0.5\sigma$. The results have been omitted for the sake of brevity.

Let us proceed to the description of a binary mixture with metal atoms of size equal to $\sigma_m = 1.0\sigma$. The results for the system with mixture composition $\chi = 0.5$ can be found in Figure 4a. In this case, we can see the formation of a network with both positional and orientational order. To prove the former, we have calculated the two-dimensional structure factor²⁴ with respect to linker molecules, which can be found in the inset to Figure 4a. Moreover, to demonstrate the orientational order, we have calculated the nematic order parameter³² with respect to linker molecules, defined as

$$Q_{\alpha\beta} = N^{-1} \sum_i^N [2b_\alpha(i)b_\beta(i) - \delta_{\alpha\beta}] \quad (7)$$

where $b_\alpha(i)$ is the α -th coordinate of the unit vector b , specifying the orientation of the molecule i , and $\delta_{\alpha\beta}$ is the Kronecker delta function. The corresponding eigenvalues of Q are $\pm S$. This function takes values between 0 and 1 in disordered and perfectly ordered phases, respectively. In real systems, it is very difficult to reach the value of S equal to 1, owing to the possible imperfections of the ordered structure or rotation of differently oriented domains.

One can see that for this structure, the value of this order parameter is around $S \approx 0.95$ in the lowest temperatures. This value proves the formation of a highly ordered network of a single orientation. The temperature relation of this quantity also indicates that the structure remains until $T^* = 0.56$.

The results for the system with mixture composition $\chi = 0.75$ can be found in Figure 4c. We can see the formation of similar $3^2.4.3.4$ Archimedean tiling, as for smaller metal size. It is noteworthy that this structure has more visible imperfections compared to the previous case.

Further increase of linker molecules in relation to metal atoms, i.e., $\chi = 0.83$, not only leads to the formation of $3^2.4.3.4$ Archimedean tiling but also a network with triangular symmetry can be observed. An increase in the density of the system shows that the semiregular tessellation vanished, and

the latter structure is only present. The BOOP for this network takes high values and is around $Q_6 = 0.96$. This indicates that the Archimedean tessellation in this system is not a stable structure, and the formation of a triangular network is favored. However, it is worth mentioning that the same situation can be observed in experiments, where the formation of various different patterns can be observed, and the determination of which of them is thermodynamically stable is not so trivial.

Finally, we proceed to the examination of the system with the mixture composition of $\chi = 0.25$. Surprisingly, we do not observe the formation of spaghetti wires, as for previous cases, but the parallel network remains. The only effect that the increase of the number of metal atoms caused is that there are two differently ordered domains in the system. In this case, due to the observation of two differently oriented domains, the nematic order parameter takes values around $S \approx 0.55$. However, it is worth mentioning that if one would compute this quantity separately for each of those clusters, the situation would reflect the one observed in Figure 4a. The corresponding snapshots have been omitted for the sake of brevity.

4. CONCLUSIONS

In this paper, we have investigated the phase behavior of binary mixtures of di-substituted polyphenyl-like molecules and metal atoms. We considered the influence of metal atoms' size and the mixture composition of the self-assembly behavior. To deepen our discussion, we summarize the results in a more systematic way. In Figure 5, we present the overview of the structures observed for the systems with different metal atom sizes σ_m and mixture compositions χ .

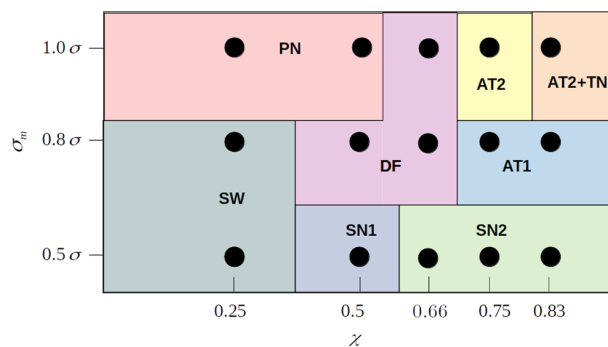


Figure 5. Schematic overview of structures formed in the binary mixtures investigated in this study. Black circles refer to simulation results; structure boundaries are drawn arbitrarily to guide the eye.

We have found that for $\sigma_m = 0.5\sigma$, depending on the mixture composition χ , the formation of two distinct networks can occur, which are spaghetti wires (SW) (cf. Figure 2e,f) and a nearly perfect square network (SN2) (cf. Figure 2b). The imperfect square structure (SN1) (cf. Figure 2a) is quite similar to SN2, but due to the concentration χ , the metal atoms form dimers, which in consequence, result in the deterioration of the formed square lattice. We conclude that the mixture composition below a certain amount of linker molecules enforces gluing metal atoms with one another, which may lead to a bigger amount of possible orientations on how linker molecules can interact with them. This corroborates with the observation that a nearly perfect square network SN1 is formed

in higher linker concentrations due to the separation of metal atoms.

An increase of metal size to $\sigma_m = 0.8\sigma$ leads to the formation of similar spaghetti wires as for $\sigma = 0.5\sigma$; however, the ordered network is completely different. We have observed the development of 3².4.3.4 Archimedean tessellation (AT1) for the mixture concentrations of $\chi = 0.75$ and above (cf. Figure 3c). Similarly, as for the previous case, the formation of the ordered network was only possible if the mixture composition enforced the separation of metal atoms.

For the further increase to $\sigma_m = 1.0\sigma$, we observe the occurrence of a parallel network (PN) for mixture composition of $\chi = 0.25$ and 0.5 (cf. Figure 4a). In higher concentrations of linker molecules, we can see two different types of ordered structures. The first one is similar to 3².4.3.4 Archimedean tessellation; however, we observe significant imperfections in its structure (AT2) (cf. Figure 4c), and the second is a nearly perfect triangular lattice (TN) (cf. Figure 4f).

The general conclusions which can be extracted from our simulations are as follows: (i) the increase of metal atom size, σ_m , changes its maximum coordination number due to the geometric effects. (ii) the mixture composition can “change” the maximum coordination number of the metal atom owing to the possibility of soft-interactive “gluing” with one another. This, in consequence, leads to the deterioration of the observed ordered structures.

Based on our observations, we can estimate the possible on-surface behavior of di-substituted polyphenyl-like compounds with metal atoms in different conditions. We have shown the possible paths on how molecules can assemble. We believe that those findings can be very useful for experimentalists to design future experimental conditions for a target development of particular networks of interest.

AUTHOR INFORMATION

Corresponding Author

Lukasz Baran – Department of Theoretical Chemistry, Maria Curie Skłodowska University, 20-031 Lublin, Poland;
 ● orcid.org/0000-0003-1777-1998; Email: lukasz.baran@poczta.umcs.lublin.pl

Complete contact information is available at:
<https://pubs.acs.org/10.1021/acsomega.1c02857>

Notes

The author declares no competing financial interest.

ACKNOWLEDGMENTS

This study has been supported by the Polish Ministry of Science and Higher Education under Grant No. DI2017 001147, and the research has been supported by the Foundation for Polish Science (FNP).

REFERENCES

- (1) Novoselov, K. S.; Geim, A. K.; Morozov, S. V.; Jiang, D.; Zhang, Y.; Dubonos, S. V.; Grigorieva, I. V.; Firsov, A. A. Electric Field Effect in Atomically Thin Carbon Films. *Science* **2004**, *306*, 666–669.
- (2) Zhang, C.; Wu, B.-H.; Ma, M.-Q.; Wang, Z.; Xu, Z.-K. Ultrathin metal/covalent-organic framework membranes towards ultimate separation. *Chem. Soc. Rev.* **2019**, *48*, 3811–3841.
- (3) Wang, S.; Wang, Q.; Shao, P.; Han, Y.; Gao, X.; Ma, L.; Yuan, S.; Ma, X.; Zhou, J.; Feng, X.; Wang, B. Exfoliation of Covalent Organic Frameworks into Few-Layer Redox-Active Nanosheets as Cathode

Materials for Lithium-Ion Batteries. *J. Am. Chem. Soc.* **2017**, *139*, 4258–4261.

- (4) Li, G.; Zhang, K.; Tsuru, T. Two-Dimensional Covalent Organic Framework (COF) Membranes Fabricated via the Assembly of Exfoliated COF Nanosheets. *ACS Applied Materials & Interfaces* **2017**, *9*, 8433–8436.

- (5) Benyettou, F.; et al. In vivo oral insulin delivery via covalent organic frameworks. *Chem. Sci.* **2021**, *12*, 6037–6047.

- (6) Heim, D.; Seufert, K.; Auwärter, W.; Aurisicchio, C.; Fabbro, C.; Bonifazi, D.; Barth, J. V. Surface-Assisted Assembly of Discrete Porphyrin-Based Cyclic Supramolecules. *Nano Lett.* **2010**, *10*, 122–128.

- (7) Kudernac, T.; Lei, S.; Elemans, J. A. A. W.; de Feyter, S. Two-dimensional supramolecular self-assembly: nanoporous networks on surfaces. *Chem. Soc. Rev.* **2009**, *38*, 402–421.

- (8) Ren, J.; Larkin, E.; Delaney, C.; Song, Y.; Jin, X.; Amirjalayer, S.; Bakker, A.; Du, S.; Gao, H.; Zhang, Y.-Y.; Draper, S. M.; Fuchs, H. Chemistry of 4-[(4-bromophenyl)ethynyl]pyridine at metal surfaces studied by STM. *Chem. Commun.* **2018**, *54*, 9305–9308.

- (9) Zhou, H.; Dang, H.; Yi, J.-H.; Nanci, A.; Rochefort, A.; Wuest, J. D. Frustrated 2D Molecular Crystallization. *J. Am. Chem. Soc.* **2007**, *129*, 13774–13775.

- (10) Stannard, A.; Russell, J. C.; Blunt, M. O.; Salesiotis, C.; Giménez-López, M. dC.; Taleb, N.; Schröder, M.; Champness, N. R.; Garrahan, J. P.; Beton, P. H. Broken symmetry and the variation of critical properties in the phase behaviour of supramolecular rhombus tilings. *Nat. Chem.* **2012**, *4*, 112–117.

- (11) Ćija, D.; Urgel, J. I.; Papageorgiou, A. C.; Joshi, S.; Auwärter, W.; Seitsonen, A. P.; Klyatskaya, S.; Ruben, M.; Fischer, S.; Vijayaraghavan, S.; Reichert, J.; Barth, J. V. Five-vertex Archimedean surface tessellation by lanthanide-directed molecular self-assembly. *Proc. Natl. Acad. Sci. U.S.A.* **2013**, *110*, 6678–6681.

- (12) Urgel, J. I.; Ćija, D.; Lyu, G.; Zhang, R.; Palma, C.-A.; Auwärter, W.; Lin, N.; Barth, J. V. Quasicrystallinity expressed in two-dimensional coordination networks. *Nat. Chem.* **2016**, *8*, 657–662.

- (13) Chen, H.; Li, D. X.; Kuo, K. H. New type of two-dimensional quasicrystal with twelvefold rotational symmetry. *Phys. Rev. Lett.* **1988**, *60*, 1645–1648.

- (14) Conrad, M.; Krumeich, F.; Harbrecht, B. A Dodecagonal Quasicrystalline Chalcogenide. *Angew. Chem., Int. Ed.* **1998**, *37*, 1383–1386.

- (15) Rochefort, A.; Wuest, J. D. Interaction of Substituted Aromatic Compounds with Graphene. *Langmuir* **2009**, *25*, 210–215.

- (16) Ibenskas, A.; Tornau, E. E. Modeling of Ribbon and Oblique Structures of Benzene-1,3,5-triyl-tribenzoic Acid. *J. Phys. Chem. C* **2020**, *124*, 18650–18659.

- (17) Karner, C.; Dellago, C.; Bianchi, E. Design of Patchy Rhombi: From Close-Packed Tilings to Open Lattices. *Nano Lett.* **2019**, *19*, 7806–7815.

- (18) Karner, C.; Dellago, C.; Bianchi, E. Hierarchical self-assembly of patchy colloidal platelets. *Soft Matter* **2020**, *16*, 2774–2785.

- (19) Ibenskas, A.; Šimėnas, M.; Kizlaitis, K. J.; Tornau, E. E. Pinwheel Structures of Deprotonated Trimesic Acid on Ag(111): Model and Simulations. *J. Phys. Chem. C* **2020**, *124*, 11212–11220.

- (20) Fadeeva, A. I.; Gorbunov, V. A.; Stishenko, P. V.; Akimenko, S. S.; Myshlyavtsev, A. V. Melting of Fe-terephthalate layers on Cu(100) surface with randomly distributed point defects. *Appl. Surf. Sci.* **2021**, *545*, No. 148989.

- (21) Lisiecki, J.; Szabelski, P. Designing 2D covalent networks with lattice Monte Carlo simulations: precursor self-assembly. *Phys. Chem. Chem. Phys.* **2021**, *23*, 5780–5796.

- (22) Baran, Ł.; Rzyśko, W. Application of a coarse-grained model for the design of complex supramolecular networks. *Mol. Syst. Des. Eng.* **2020**, *5*, 484–492.

- (23) Baran, Ł.; Rzyśko, W.; Szajnar, S. Archimedean Tessellation Found by the Variation of Building Blocks’ and Linkers’ Geometry: In Silico Investigations. *J. Phys. Chem. C* **2020**, *124*, 20101–20108.

- (24) Baran, E.; Nieckarz, D.; Szabelski, P.; Rżysko, W. Controlling of the 2D Self-Assembly Process by the Variation of Molecular Geometry. *J. Phys. Chem. C* **2019**, *123*, 19549–19556.
- (25) Toxvaerd, S.; Dyre, J. C. Communication: Shifted forces in molecular dynamics. *J. Chem. Phys.* **2011**, *134*, No. 081102.
- (26) Allen, M. P.; Tildesley, D. J. *Computer Simulation of Liquids*, 2nd ed.; Oxford University Press: Oxford, 2017; p 640.
- (27) Plimpton, S. et al. Large-scale Atomic/Molecular Massively Parallel Simulator lammmps.sandia.gov, 1995 (accessed April 29, 2019).
- (28) Plimpton, S. Fast Parallel Algorithms for Short-Range Molecular Dynamics. *J. Comput. Phys.* **1995**, *117*, 1–19.
- (29) Berendsen, H. J. C.; Postma, J. P. M.; van Gunsteren, W. F.; DiNola, A.; Haak, J. R. Molecular dynamics with coupling to an external bath. *J. Chem. Phys.* **1984**, *81*, 3684–3690.
- (30) Martyna, G. J.; Klein, M. L.; Tuckerman, M. Nosé-Hoover chains: The canonical ensemble via continuous dynamics. *J. Chem. Phys.* **1992**, *97*, 2635–2643.
- (31) Weber, H.; Marx, D.; Binder, K. Melting transition in two dimensions: A finite-size scaling analysis of bond-orientational order in hard disks. *Phys. Rev. B* **1995**, *51*, 14636–14651.
- (32) Frenkel, D.; Eppenga, R. Evidence for algebraic orientational order in a two-dimensional hard-core nematic. *Phys. Rev. A* **1985**, *31*, 1776–1787.

Archimedean Tessellation Found by the Variation of Building Blocks' and Linkers' Geometry: In Silico Investigations

Łukasz Baran,* Wojciech Rżysko, and Sebastian Szajnar

Cite This: *J. Phys. Chem. C* 2020, 124, 20101–20108

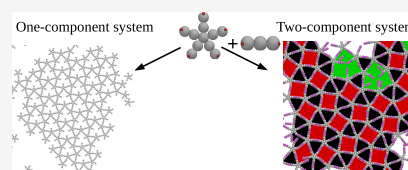
Read Online

ACCESS |

Metrics & More

Article Recommendations

ABSTRACT: We use molecular dynamics simulations to investigate the behavior of multivalent molecules in a single-component system and in binary mixtures in various compositions. In this study, we have found that, depending on the molecule's and the linkers' geometry, we can control the pore size and observe the formation of novel ordered structures. We have found that, in the mixture of a pentavalent molecule and linear linker, the Archimedean tiling has been formed, which has not been the case in the single-component system. We have concluded that, for this case, the mobility of the linker is the driving force. The ordered networks have been characterized by the order parameters, such as theoretically evaluated diffraction patterns or bond-orientational order parameter. Moreover, in one case, the inspection of the voids' arrangement has been utilized.



INTRODUCTION

Synthesis of organic molecules of different shapes that possess the ability to self-assemble into ordered structures on well-defined substrates is a newly developing field of research. The confinement template is often necessary to initiate a chemical reaction that would be impossible to perform in the bulk. Hence, on-surface self-assembly can be considered as a type of chemistry that complements present synthetic capabilities. The geometry of molecules varies from isotropic linear,^{1,2} tritopic,^{3,4} tetratopic,^{5,6} hexatopic,⁷ and many other combinations, including anisotropic chemical compounds within previously mentioned.⁸

Apart from the shape of the building blocks, the directionality of interparticle interactions, owing to the presence of diverse active groups, is also crucial for the development of predefined self-assembled networks. It has been shown that the molecules with the same geometry, but with different substitutions, can form completely different ordered structures.⁴ Many other factors, such as the solvent affinity to the chemical compound,⁹ substrate nature, and symmetry^{10,11} and the presence of the second component,^{12,13} may influence the formation of supramolecular networks. The reviews concerning such effects can be found in refs 14–16.

The multiplicity of factors affecting self-assembly processes makes it necessary to establish rules that would allow the formation of predefined molecular structures. In this aspect, molecular modeling comes as an efficient and cheap way, which can support and give a better insight into experimental investigations. The most commonly used simulation technique is the molecular dynamics method, where two main models have been considered, that is, an all-atom representation and coarse-grained modeling. The former methodology, due to the use of more realistic force fields, allows for the evaluation and

comparison of calculated properties, such as the strength of the interparticle interactions, with the experimental data.^{17,18} On the other hand, however, it is not able to study collective phenomena properly due to the limitation in the system size and it is computationally more expensive. The coarse-grained modeling comes with help to this issue. It is a well-known and used technique, which allows for the determination of structural properties as well as mechanical and dynamical properties of investigated materials. In this kind of methodology, Monte Carlo^{19–21} simulations have been widely used.

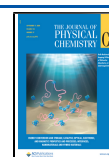
In our previous papers,^{22–24} we have presented using molecular dynamics simulations that our coarse-grained model is also able to predict supramolecular networks from various molecular geometries and directionality of interparticle interactions. In this paper, however, except for the investigation of single-component systems, we have also performed comprehensive simulations for a binary mixture that is able both to reflect very well experimental data and to predict novel structures, not observed experimentally, for this kind of mixture. We have also characterized the obtained structures by the calculated diffraction patterns and by the bond orientational order parameters. Analysis of the voids' arrangement has also been performed.

The paper is organized as follows. In the next section, we present our model, and then we proceed to the results for both

Received: June 6, 2020

Revised: August 19, 2020

Published: August 20, 2020



a one-component system of tetra-, penta-, and hexatopic building blocks. Next, we describe their mixture with linear and V-shape molecules. We also consider the influence of the mixture composition. Finally, we conclude our findings.

MODEL AND SIMULATION DETAILS

As previously mentioned, the model presented in this work was similar to the one used in our previous papers;^{22–24} however, we wanted to extend its possibilities into the investigation of different molecular shapes involving tetra-, penta-, and hexavalent (primary molecules) chemical compounds in single-component systems and in binary mixtures.

All of the molecules used in the course of our simulations are shown in Figure 1, and they were treated as flat, rigid bodies.

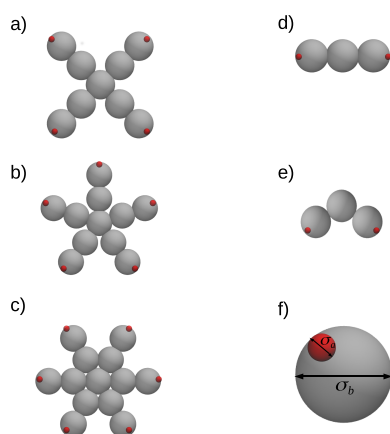


Figure 1. Models of molecules used in the course of our simulations, that is, (a) tetra-valent, (b) penta-valent, and (c) hexa-valent molecules. Linear and V-shape molecules have been shown in parts (d) and (e), respectively. Part (f) explains the parameters of the model used. Silver circles correspond to the segments of the entire backbone, whereas the red ones pertain to the active sites.

In the structure of models shown in parts a–c of Figure 1, two main features can be distinguished, namely, the core and the arms. In the former, the segments have been distributed on the vertices of regular polygons, that is, on a square, pentagon, and hexagon with a central atom inside each of them. The latter segments have been tangentially grafted into each of the vertexes of particular polygons. For the linear and V-shape molecules shown in parts d and e of Figure 1, only the core can be distinguished. One has to note that we will refer to them as linkers since we only investigate them in mixtures with multivalent molecules. The sizes of the segments forming core and arms have been set the same and equal to σ_b for every molecule. Owing to that, we will not distinguish them one from another and will refer to them as components of the backbone. The bonding distance between particular entities in the main structure has been also assumed to be equal to σ_b .

The active sites, each of the diameter σ_a , have been entirely embedded into terminal arm's (core) segment for polygon (linear and V-shape) molecules, and the bonding distance has been defined as l . The inclusion has been performed in order to ensure the directionality of interparticle interactions.

To ensure bonding distances between particular entities in the molecules, we have used harmonic binding potentials:

$$u_{bb} = k_{bb}(r - \sigma_{bb})^2 \quad (1)$$

and

$$u_{ab} = k_{ab}(r - \sigma_{ab})^2 \quad (2)$$

In a similar manner, all of the necessary angles have also been maintained by an application of angular-harmonic potential:

$$u_{bb}(\theta_{bb}) = k_{\theta}(\theta_{bb} - \theta_{0,bb})^2 \quad (3)$$

and

$$u_{ab}(\theta_{ab}) = k_{\theta}(\theta_{ab} - \theta_{0,ab})^2 \quad (4)$$

The interparticle potential employed in our simulations was (12,6) Lennard-Jones potential, which has been appropriately shifted to ensure its continuity:²⁵

$$U_{SF} = \begin{cases} U_{LJ}(r) - U_{LJ}(r_{cut}) + U'_{LJ}(r_{cut})(r - r_{cut}) & r < r_{cut} \\ 0 & \text{otherwise} \end{cases} \quad (5)$$

where $U_{LJ}(r) = 4\epsilon_{kl}[(\sigma_{kl}/r)^{12} - (\sigma_{kl}/r)^6]$ and $U'_{LJ}(r_{cut})$ is the first derivative of $U_{LJ}(r)$ at $r = r_{cut}$.

The Lennard-Jones potential parameters, $\sigma_b \equiv \sigma$ and $\epsilon_{bb} \equiv \epsilon$, have been set to be the units of length and energy, respectively.

The reduced time and temperature are equal to $\tau^* = t\sqrt{\epsilon/m\sigma^2}$ and $T^* = kT/\epsilon_{bb}$, respectively. The number density has been defined as $\rho^* = \frac{X^* \sigma_b + Y^* \sigma_a}{L_x^* L_y^*}$, where X and Y means the number

of segments in the main framework and the number of active sites, respectively. In the case of binary mixtures, we define the mole fraction of $\chi = N_p/N_t$ and total number of molecules $N_t = N_p + N_l$, where N_p and N_l means the number of primary and linker molecules, respectively. In the simulations, the mass of the segments and active sites has been set to the unity, whereas their diameters differed. The segment's diameters in the main framework were equal and set to $\sigma_b = \sigma$, while the active sites were five times smaller $\sigma_a = 0.2\sigma$. The latter, as mentioned previously, has been done in order to ensure the directionality of interparticle interactions and to allow only single association due to the size of the active site and the range of interparticle potential. The active site-terminal arm (core) segment bonding distance was set to $l = 0.36\sigma$.

The energies of the backbone-backbone and the backbone-active site interactions have been set to $\epsilon_{bb} = \epsilon$ and $\epsilon_{aa} = 5.0\epsilon$ for a single-component system. In the case of binary mixture, we only allowed for a mixed association, namely, $\epsilon_{aa} = 5.0\epsilon$ for active sites of molecules of different geometries, whereas $\epsilon_{aa} = \epsilon$ in the case of the same type. It is noteworthy to say that this kind of screened interparticle interaction can be reflected by the use of particular chemically active groups as well as a particular solvent, which allow only this kind of mixed association in the system. In spite of that, we did not add any solvent molecules explicitly but rather refer to our coarse-grained model as it would have an implicit solvent owing to the defined interparticle interactions.

The backbone-site diameter and the energy of the backbone-site interactions have been set to $\sigma_{ab} = (\sigma_a + \sigma_b)/2$ and $\epsilon_{ab} = \epsilon$, respectively. The cutoff distance of the interactions between two active sites has been set to $r_{cut, aa} = 2\sigma_{aa}$ in a single-component system. In the case of a binary mixture, the cutoff distance has been set to $r_{cut, aa} = 2\sigma_{aa}$ for active sites for molecules of different geometries, whereas for the same type, $r_{cut, aa} = \sigma_{aa}$. Additionally, we have set $r_{cut, ij} = \sigma_{ij}$

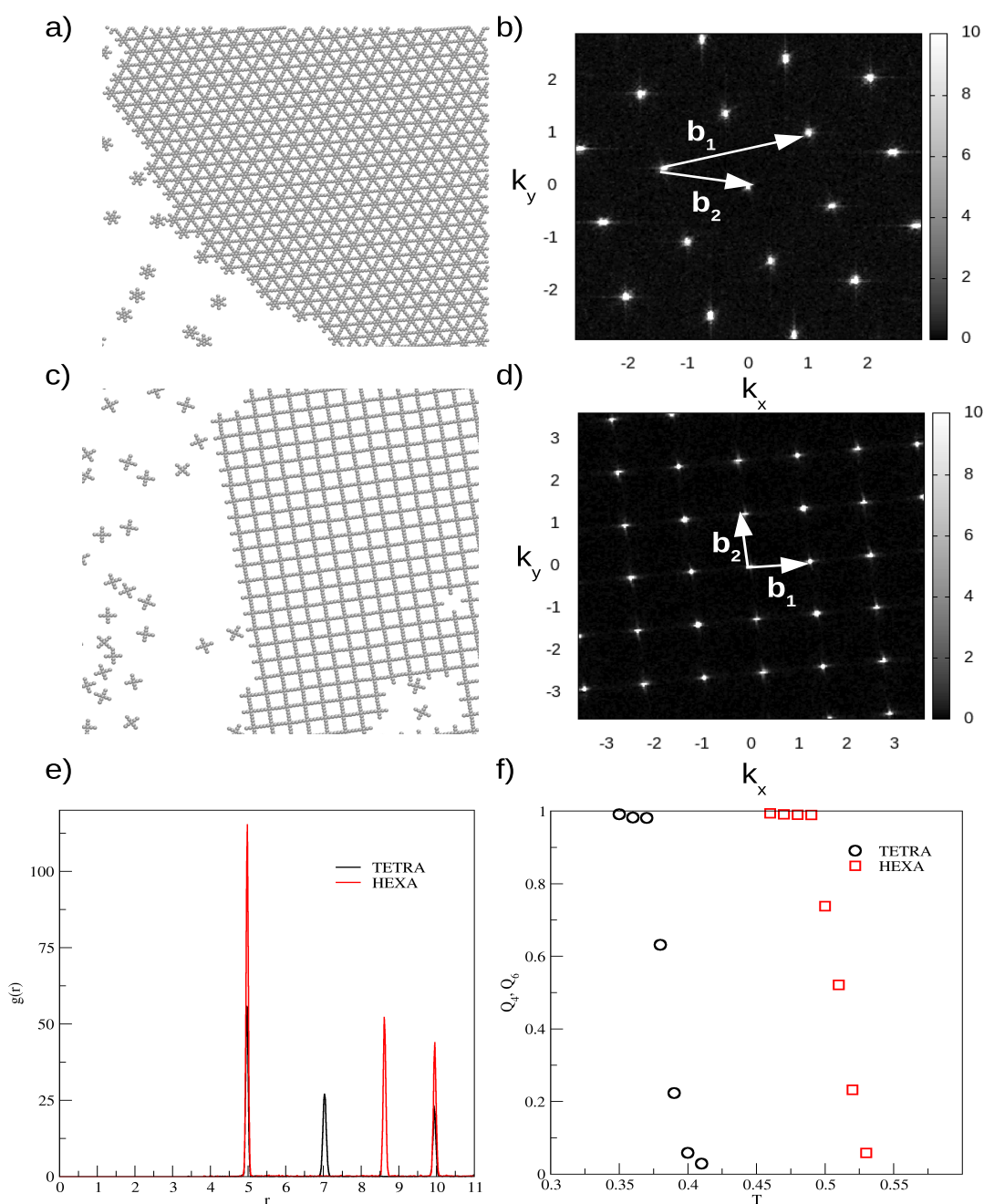


Figure 2. (a, c) Fragments of the configurations, (b, d) the corresponding diffraction patterns for their central atoms, (e) the radial distribution functions calculated with respect to central atoms, and (f) temperature relation of BOOP for (a) hexavalent molecules at $T^* = 0.46$ in $\rho^* = 0.2$ and (c) tetravalent molecules at $T^* = 0.37$ in $\rho^* = 0.216$. k_x and k_y are wave vectors of the 2D structure factor.

where $ij = ab, bb$. This has been done in order to assume that the only attraction in the system is due to the association between active sites, whereas the remaining are the soft-core interactions. The harmonic potential constants $k_{bb} \equiv k_{ab}$ have been set to $1000\epsilon/\sigma^2$ and $k_\theta = 1000\epsilon/(\text{radian})^2$. Such high values of harmonic constants have been set to reduce the range of fluctuations and, in consequence, to maintain the rigidity of the assumed geometries.

All of the molecular dynamics simulations have been performed in the NVT ensemble, using LAMMPS simulation package.^{26,27} The velocity Verlet integration scheme has been used with the reduced time step of the order of $t = 0.001\tau$. The

number of molecules varied from $N_p = 1600$ in the single-component system up to $N_p = 900$ and $N_l = 5400$ for a binary mixture. One has to note, however, that the total number of “atoms” varied depending on the molecular architecture and the mole fraction of a mixture.

The simulation scheme involved preliminary runs in the NPT ensemble to establish the desired density. Next, equilibration runs for 5×10^6 time steps using the Berendsen²⁸ thermostat with the damping constant equal to $\tau_B = 10\tau$ have been performed. The further equilibration for 5×10^7 as well as production runs have been performed using the Nosé–Hoover chain algorithm, with the damping constant equal to

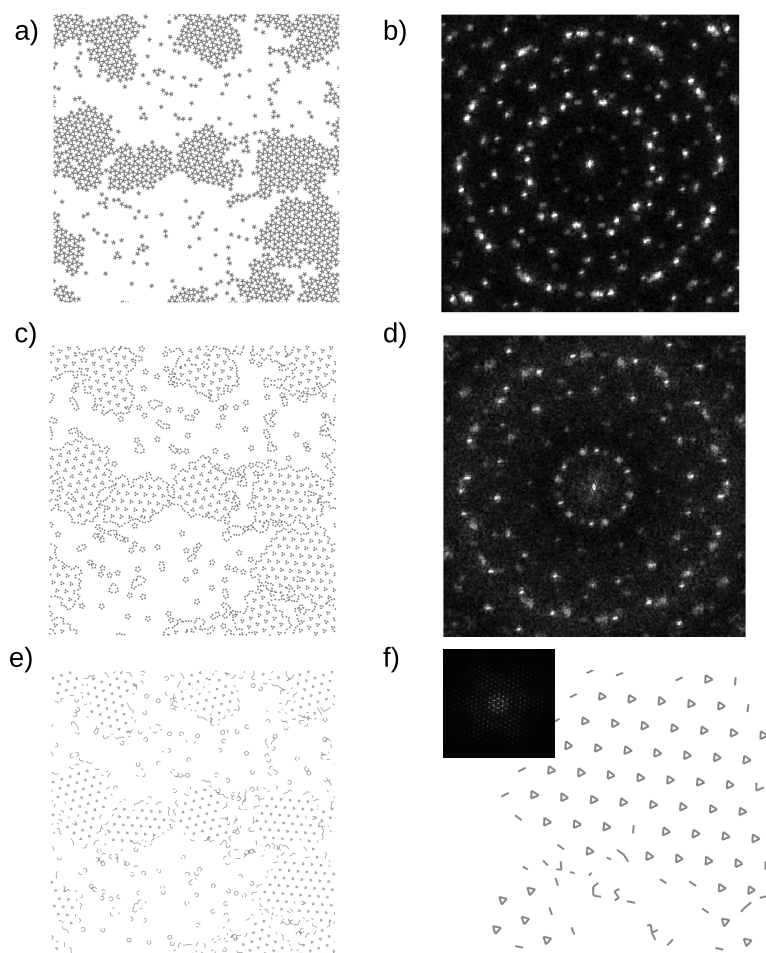


Figure 3. Results obtained for pentavalent molecules at $T^* = 0.33$ in $\rho^* = 0.2$. Configuration of (a) the system and (b) the corresponding diffraction pattern with respect to the central atom. (c, d) Configuration of the system for (c) non-associated terminal segments and (d) the corresponding diffraction pattern. Part (e) represents different graphical representations of part (c) (see the text). Part (f) shows the magnified fragment and its diffraction pattern in the inset.

$\tau_{\text{HN}} = 10\tau$ and the number of chains set to $N_{\text{chain}} = 3$. Each system has been slowly cooled down from temperatures where we observed no order to the point, where the self-assembly process appeared. The temperature grid was fixed as set to be $\Delta T = 0.01$.

RESULTS AND DISCUSSION

The discussion begins with the presentation of results obtained in single-component systems for molecules shown in Figure 1a–c. The obtained structures that can be seen in Figure 2 demonstrate the influence of predefined molecular architectures on the formation of self-assembled networks. One can see that, in the case of hexavalent (part a) and tetravalent (part c) molecules, networks formed by them are not surprising and exhibit hexagonal and square symmetry, respectively. In the former case, the chemical compound, which corresponds to its symmetry is, for instance, benzenehexol. This compound indeed forms the same type of lattice when deposited on the Cu(111) substrate.⁷ In the latter, however, symmetrical tetraphenylene chemical compounds²⁹ or porphyrins³⁰ can be modeled employing this molecular geometry. In such a case, they also tend to form self-assembled networks of square symmetry.

To prove that we have highly ordered, two-dimensional structures, we have computed the 2D bond-orientational order parameter (BOOP) with respect to the central atom of a core, according to the definition of Weber et al.³¹ It has been defined as

$$Q_k^{2D} = \frac{1}{N_{\text{bond}}} \sum_i \sum_j \exp(ki\phi_{ij}) \quad (6)$$

where i runs over all molecules in the system, j runs over all nearest neighbors of i , ϕ_{ij} indicates the angle between the bond connecting particles i and j and an arbitrary but fixed reference axis, N_{bond} is the number of bonds in the system, and $k = 2, 3, 4, 5, 6$. The maximum distance between two connected central atoms has been taken as equal to the position of the first minimum of radial distribution function for each of the molecules. The bond-orientational order parameter can take the values between 0 and 1 for the disordered and the ordered structures of a particular symmetry, respectively.

The radial distribution functions with respect to the central atom are shown in Figure 2e. One can see that, for both systems, the first maximum is around $r \approx 5$ and is related to the side distances. The next maxima are connected with diagonal distances. Next, we have computed the 2D BOOP and found

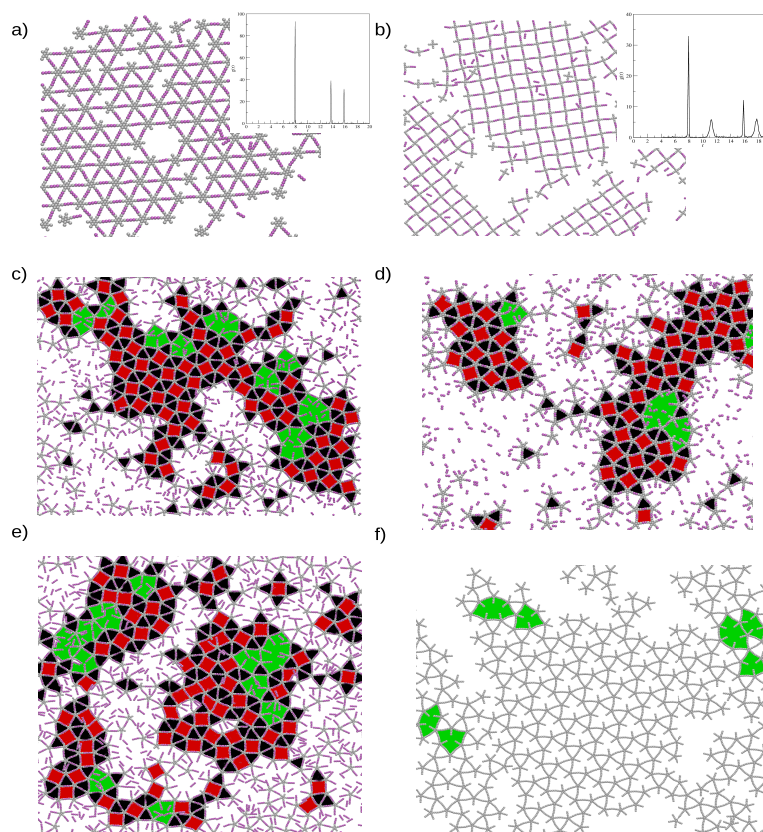


Figure 4. Fragments of the configurations of mixtures of different primary molecules with linear linkers for (a) hexavalent molecules ($T^* = 0.28$, $\rho^* = 0.18$, and $\chi = 0.33$), (b) tetravalent molecules ($T^* = 0.26$, $\rho^* = 0.2$, and $\chi = 0.2$), (c–e) pentavalent molecules ($T^* = 0.24$, $\rho^* = 0.3$, and $\chi = 0.2$). Part (f) shows the fragment of configuration for a one-component system of pentavalent molecules with elongated arms at $T^* = 0.2$ and $\rho^* = 0.2$. Insets of parts (a) and (b) show the radial distribution function calculated with respect to the central segment of primary molecule. Silver and purple segments correspond to the X-valent molecule and linear molecules, respectively. Particular polygons belonging to this network are colored in red (squares) and black (triangles). The reminiscence of the one-component system is marked in green.

out that they were equal to $Q_6^{2D} = 0.96$ and $Q_4^{2D} = 0.98$ for hexagonal and square lattices, respectively. It means that highly ordered structures, without any visible imperfections, have been constructed. The temperature changes of the 2D BOOP are also shown in Figure 2f. Here, we can see that, depending on the number of association sites, the temperature of the phase transition is shifted. It is a well-known fact that, with the increase of interaction energy, which in our case is related to the valency of the primary molecule, the transition temperature also increases. The rough estimation of the ratio of transition temperatures between hexa- and tetravalent molecules is approximately equal to about 1.4. We can recall that the ratio of transition temperatures in the 2D Ising model on a triangular and a square lattice is equal to about 1.6.³²

To further prove the existence of highly ordered networks, we have calculated 2D structure factors (see Figure 2b,d), which confirm our findings. Moreover, we have marked the vectors, \mathbf{b}_1 , \mathbf{b}_2 , in the reciprocal space, which are related to the characteristic distances in the system. The transformation of those into real space vectors, \mathbf{a}_1 , \mathbf{a}_2 , and calculation of their length, a , allows a direct comparison with radial distribution function, which is in a perfect agreement in our case. However, it is noteworthy that, even though the structure factors show the long-range ordering, since it is a 2D system, in fact it is a quasi-long range order.³³

Next, we proceed to the description of the pentavalent molecule. Part of the configuration shown in Figure 3a is completely different than in the previously considered cases. For this system, we have also computed the 2D BOOP; however, its value was $Q_k^{2D} \approx 0$ for each k . The calculation of the 2D structure factor, with respect to the central segment, also did not give us an answer on what type of ordered structure it is. Then, we have decided to distinguish the terminal segment of the arms, which is not associated with any segment of another molecule. In other words, we wanted to analyze the voids' ordering. The part of the configuration obtained by this approach is shown in Figure 3c. Due to this kind of representation, we can see that the non-associated segments form triangles, which are ordered into a hexagonal network. For this purpose, we have computed the corresponding 2D structure factor (see Figure 3d). In this case, the diffraction pattern is not significantly different than the one shown for central segments. However, it can be seen that the system is ordered in hexagonal arrays but of different orientations. To prove this statement, we have employed the procedure described by us,²⁴ which involved analysis of only fragments of configurations. The difference was that we represented the triangles by means of bonds between each of the "atoms", which are not associated with anything. The threshold radius was taken from the first minimum of the radial distribution function and was equal to $r = 2.8$. The result for

the entire system can be found in Figure 3e, whereas the magnified fragment is shown in Figure 3f. One can see that, due to such a graphical representation, the voids are indeed ordered in a hexagonal structure, which has been established by the calculation of the corresponding diffraction pattern, shown in the inset of Figure 3f.

Let us now proceed to the description of a binary mixture involving the aforementioned primary molecules with the linear and V-shape linkers, shown in Figure 1d,e, respectively. All of these systems have been investigated within a range of densities $\rho^* = (0.1, 0.3)$ and mole fractions $\chi = (0.143, 0.5)$. In the case of the mixture of hexavalent and linear molecules, we did not observe any structural changes in comparison to the single-component system. The primary molecules and the linkers connect alternately and, in effect, only “elongate” the arms of the hexavalent molecules. The system orders into a hexagonal structure but with larger distances between the molecules (see Figure 4a). This observation has been confirmed by the behavior of the radial distribution function computed with respect to the central segment of the primary molecule (see the inset of Figure 4a). The first maximum is located at $r \approx 8$, while it appeared at $r \approx 5$ in the single-component system (cf. Figure 2e). Quite similar effects have been observed for the mixtures with the mole fraction between $\chi = 0.5$ and $\chi = 0.143$. Another difference was that the hexagonal network had slight imperfections in its structure such as voids or trapped molecules inside the framework. The latter effect is more pronounced when the mole fraction of the primary molecules is lower. In this case, similar to single-component systems, we have computed the 2D BOOP, for which the Q_6^{2D} parameter also reached a rather high values, up to about $Q_6^{2D} = 0.782$. The structure presented here comply with experimental data shown recently by Lu et al.¹² These authors have obtained quite similar 2D networks based on the Schiff base reaction between hexa(4-formylphenyl)benzene (primary molecule) and *p*-phenylenediamine (linker).

Similar observations concern the mixture of tetravalent and linear molecules within the same range of mole fractions (see Figure 4b). The radial distribution function, calculated with respect to the central segment of the primary molecule, shown in the inset of Figure 4b, shows the first maximum to be around $r \approx 8$, which is larger than in the single-component system (cf. Figure 2e). Quite similar effects have been observed for the mixtures with the mole fraction between $\chi = 0.5$ and $\chi = 0.143$. This means that the presence of a linker resulted in the formation of slightly bigger pores. However, one additional feature is noteworthy. The assembled square network is slightly “folded” in comparison to the single-component system (cf. Figure 2c). In addition to that, the 2D BOOP has been calculated. We have found out that, as in the previous case of Q_6^{2D} , the Q_4^{2D} parameter, due to the imperfections in the system, is lower in comparison to the one-component system and reaches the value of $Q_4^{2D} = 0.689$.

The structure formed in a mixture of a pentavalent and linear molecule is completely different in comparison to the one-component system. One can see in Figure 4c that the new structure reminds the $3^2.4.3.4$ Archimedean tilings,³⁴ which have been previously found in the mixture of linear molecules with metal atoms.^{35,36} Particular polygons belonging to this network are colored in red (squares) and black (triangles). In addition, another interesting feature in the structure can be seen, namely, the presence of defects, which remind pores formed in a single-component system (green color). This

structure have been found in the mixtures with the mole fraction between $\chi = 0.5$ and $\chi = 0.143$ and densities from $\rho^* = 0.1$ to $\rho^* = 0.3$; however, we present only the most representative results below.

We wanted to check what is the reason for the formation of Archimedean tessellation. For this purpose, we have performed additional simulations for shorter and longer linkers and their lengths were equal to two and four segments, respectively. The results are presented in Figure 4d,e. One can see that there is no qualitative difference between obtained structures, so our conclusion is that the length of the linker does not affect the formation of such an ordered phase. Another aspect, which we wanted to take into account, is whether this particular network is connected with the presence of the second component or due to the increased intermolecular separation distance between two molecules. To check that, we have elongated each of the arms by two segments and performed simulations in the one-component system for molecules of this geometry. It has been done in order to match the intermolecular distance between two molecules in a mixture (cf. Figure 4e) and the one-component system. The results can be found in Figure 4f, which shows qualitatively the same network as the one formed for shorter arms (cf. Figure 3a). This result means that the Archimedean tiling is formed strictly due to the presence of the second component. Interestingly, a quite obvious conclusion concerning the length of interparticle distance that determines the obtained structure, which has been already reported,³⁷ is not always entirely correct. In this case, the linkers' mobility drives the self-assembly of the Archimedean tiling-like network in the system instead.

Finally, we have investigated the mixture of the hexavalent molecule with V-shape molecules. In this case, we have obtained a completely different structure in comparison to the one-component system. Within this self-assembled network, two main features can be seen, that is, a formation of “flower-like” and rhombus pores, colored in green and red in Figure 5a,

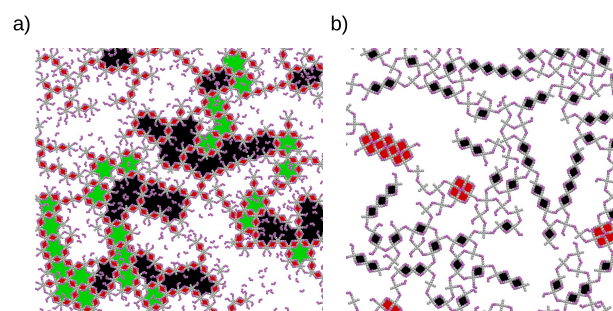


Figure 5. Fragments of the configurations of mixtures of different primary molecules with V-shape tectons for (a) hexavalent molecules ($T^* = 0.24$, $\rho^* = 0.298$, and $\chi = 0.2$) and (b) tetravalent molecules ($T^* = 0.22$, $\rho^* = 0.2$, and $\chi = 0.2$). Silver and purple segments correspond to the X-valent molecule and V-shape molecules, respectively.

respectively. In the case of the latter, it is noteworthy that they also form chains. Moreover, defects in the self-assembled network are also observed and result from merging of several “flower-like” pores into a larger pore (black pore in Figure 5a). This result is also consistent with the experimental data presented elsewhere.¹²

In the case of tetravalent molecules, we observe that the main tendency is to form a gel structure, of chain-like

networks, consisted of rhombus pores, marked in black in Figure 5b. However, one interesting feature is that these chains tend to “glue” one to another by non-interaction sides. One has to note that this structure is very rarely observed and could be more pronounced in higher densities. The increase of mole fraction does not lead to any appreciable changes in results. The results for pentavalent molecules have been omitted owing to the fact that we did not obtain any structure but only gel-like disordered networks.

CONCLUSIONS

In this work, we have shown how the single-component system of molecules with four, five, and six active interaction sites, constructed on the regular polygons, can self-assemble. Furthermore, mixtures of various compositions have been considered. Moreover, we have characterized chosen structures by diverse quantities, such as the bond-orientational order parameters, the structure factors, and the image analysis.

The self-assembled structures composed in single-component systems are consistent with the symmetry of molecules, except for pentavalent ones. Closer inspection of pores has shown that they are ordered into a hexagonal network. In the first trial, order parameters failed to describe that because of the presence of clusters of different sizes and orientations.

Another, and probably the most interesting feature found by us, is that, depending on the molecular geometry of both the linker and the primary molecule, we can (i) control the pore size or (ii) observe novel structures. In the latter case, we conclude that the linker’s mobility is the driving force for the formation of ordered networks (cf. Figure 4c–f).

We have pointed out that the extension of the previously proposed models,^{22–24} which both are consistent with experimental data and can predict novel supramolecular networks. We have proven that our approach can be applied to different geometries and model mixtures, which may explain experimental results. We hope that this paper can be helpful for further design of chemical compounds and will give a better insight into on-surface self-assembly phenomena.

AUTHOR INFORMATION

Corresponding Author

Lukasz Baran – Department of Theoretical Chemistry, Institute of Chemical Sciences, Faculty of Chemistry, Maria Curie-Skłodowska University in Lublin, Lublin 20-031, Poland; orcid.org/0000-0003-1777-1998; Email: lukasz.baran@poczta.umcs.lublin.pl

Authors

Wojciech Rzyśko – Department of Theoretical Chemistry, Institute of Chemical Sciences, Faculty of Chemistry, Maria Curie-Skłodowska University in Lublin, Lublin 20-031, Poland; orcid.org/0000-0001-9806-6056

Sebastian Szajnar – Department of Theoretical Chemistry, Institute of Chemical Sciences, Faculty of Chemistry, Maria Curie-Skłodowska University in Lublin, Lublin 20-031, Poland

Complete contact information is available at: <https://pubs.acs.org/10.1021/acs.jpcc.0c05137>

Notes

The authors declare no competing financial interest.

ACKNOWLEDGMENTS

This study has been supported by the Polish Ministry of Science and Higher Education under grant no. D12017 001147, and the research has been supported by the Foundation for Polish Science (FNP).

REFERENCES

- (1) Zhang, Y.-Q.; Lin, T.; Cirera, B.; Hellwig, R.; Palma, C.-A.; Chen, Z.; Ruben, M.; Barth, J. V.; Klappenberger, F. One-Dimensionally Disordered Chiral Sorting by Racemic Tiling in a Surface-Confined Supramolecular Assembly of Achiral Tectons. *Angew. Chem., Int. Ed.* **2017**, *56*, 7797.
- (2) Ren, J.; Larkin, E.; Delaney, C.; Song, Y.; Jin, X.; Amirjalayer, S.; Bakker, A.; Du, S.; Gao, H.; Zhang, Y.-Y.; et al. Chemistry of 4-[(4-bromophenyl)ethynyl]pyridine at metal surfaces studied by STM. *Chem. Commun.* **2018**, *54*, 9305.
- (3) Liu, J.; Lin, T.; Shi, Z.; Xia, F.; Dong, L.; Liu, P. N.; Lin, N. Structural Transformation of Two-Dimensional Metal-Organic Coordination Networks Driven by Intrinsic In-Plane Compression. *J. Am. Chem. Soc.* **2011**, *133*, 18760–18766.
- (4) Ammon, M.; Sander, T.; Maier, S. On-Surface Synthesis of Porous Carbon Nanoribbons from Polymer Chains. *J. Am. Chem. Soc.* **2017**, *139*, 12976–12984.
- (5) Xing, S.; Zhang, Z.; Fei, X.; Zhao, W.; Zhang, R.; Lin, T.; Zhao, D.; Ju, H.; Xu, H.; Fan, J.; et al. Selective on-surface covalent coupling based on metal-organic coordination template. *Nat. Commun.* **2019**, *10*, 70.
- (6) Zhou, H.; Dang, H.; Yi, J.-H.; Nanci, A.; Rochefort, A.; Wuest, J. D. Frustrated 2D Molecular Crystallization. *J. Am. Chem. Soc.* **2007**, *129*, 13774.
- (7) Zhang, R.; Liu, J.; Gao, Y.; Hua, M.; Xia, B.; Knecht, P.; Papageorgiou, A. C.; Reichert, J.; Barth, J. V.; Xu, H.; et al. On-surface Synthesis of a Semiconducting 2D Metal-Organic Framework Cu₃(C₆O₆) Exhibiting Dispersive Electronic Bands. *Angew. Chem. Int. Ed.* **2020**, *132*, 2691.
- (8) Liang, R.-R.; Xu, S.-Q.; Zhang, L.; Ru-Han, A.; Chen, P.; Cui, F.-Z.; Qi, Q.-Y.; Sun, J.; Zhao, X. Rational design of crystalline two-dimensional frameworks with highly complicated topological structures. *Nat. Commun.* **2019**, *10*, 4609.
- (9) Cebula, I.; Smith, E. F.; Gimenez-Lopez, M. D. C.; Yang, S.; Schröder, M.; Champness, N. R.; Beton, P. H. Packing of Isophthalate Tetracarboxylic Acids on Au(111): Rows and Disordered Herringbone Structures. *J. Phys. Chem. C* **2013**, *117*, 18381.
- (10) Gutzler, R.; Cardenas, L.; Lipton-Duffin, J.; El Garah, M.; Dinca, L. E.; Szakacs, C. E.; Fu, C.; Gallagher, M.; Vondráček, M.; Rybachuk, M.; et al. Ullmann-type coupling of brominated tetrathienoanthracene on copper and silver. *Nanoscale* **2014**, *6*, 2660.
- (11) Cardenas, L.; Gutzler, R.; Lipton-Duffin, J.; Fu, C.; Brusso, J. L.; Dinca, L. E.; Vondráček, M.; Fagot-Revurat, Y.; Malterre, D.; Rosei, F.; et al. Synthesis and electronic structure of a two dimensional π -conjugated polythiophene. *Chem. Sci.* **2013**, *4*, 3263–3268.
- (12) Lu, C.; Li, Y.; Wang, L.-M.; Yan, H.-J.; Chen, L.; Wang, D. Rational design of two-dimensional covalent tilings using a C₆-symmetric building block via on-surface Schiff base reaction. *Chem. Commun.* **2019**, *55*, 1326.
- (13) Ascherl, L.; Sick, T.; Margraf, J. T.; Lapidus, S. H.; Calik, M.; Hettstedt, C.; Karaghiosoff, K.; Döblinger, M.; Clark, T.; Chapman, K. W.; et al. Molecular docking sites designed for the generation of highly crystalline covalent organic frameworks. *Nat. Chem.* **2016**, *8*, 310.
- (14) Cui, D.; Perepichka, D. F.; MacLeod, J. M.; Rosei, F. Surface-confined single-layer covalent organic frameworks: design, synthesis and application. *Chem. Soc. Rev.* **2020**, *2020*.
- (15) Clair, S.; de Oteyza, D. G. Controlling a Chemical Coupling Reaction on a Surface: Tools and Strategies for On-Surface Synthesis. *Chem. Rev.* **2019**, *119*, 4717.

- (16) Dong, L.; Gao, Z.; Lin, N. Self-assembly of metal-organic coordination structures on surfaces. *Prog. Surf. Sci.* **2016**, *91*, 101–135.
- (17) Palma, C.-A.; Samori, P.; Cecchini, M. Atomistic Simulations of 2D Bicomponent Self-Assembly: From Molecular Recognition to Self-Healing. *J. Am. Chem. Soc.* **2010**, *132*, 17880.
- (18) Zhao, Y.; Wang, J. How To Obtain High-Quality and High-Stability Interfacial Organic Layer: Insights from the PTCDA Self-Assembly. *J. Phys. Chem. C* **2017**, *121*, 4488.
- (19) Fadeeva, A. I.; Gorbunov, V. A.; Stishenko, P. V.; Myshlyavtsev, A. V. Model of FeTerephthalate Ordering on Cu(100). *J. Phys. Chem. C* **2019**, *123*, 17265.
- (20) Karner, C.; Dellago, C.; Bianchi, E. Hierarchical self-assembly of patchy colloidal platelets. *Soft Matter* **2020**, *16*, 2774.
- (21) Karner, C.; Dellago, C.; Bianchi, E. Design of Patchy Rhombi: From Close-Packed Tilings to Open Lattices. *Nano Lett.* **2019**, *19*, 7806.
- (22) Baran, L. Influence of the molecular geometry on the formation of the self-assembled structures. *J. Mol. Liq.* **2019**, *294*, 111627.
- (23) Baran, L.; Rzyśko, W. Application of a coarse-grained model for the design of complex supramolecular networks. *Mol. Syst. Des. Eng.* **2020**, *5*, 484.
- (24) Baran, L.; Nieckarz, D.; Szabelski, P.; Rzyśko, W. Controlling of the 2D Self-Assembly Process by the Variation of Molecular Geometry. *J. Phys. Chem. C* **2019**, *123*, 19549.
- (25) Toxvaerd, S.; Dyre, J. C. Communication: Shifted forces in molecular dynamics. *J. Chem. Phys.* **2011**, *134*, No. 081102.
- (26) Plimpton, S. *LAMMPS Molecular Dynamics Simulator*; lammmps.sandia.gov, 1995; [Online; accessed 29-April-2019].
- (27) Plimpton, S. Fast Parallel Algorithms for Short-Range Molecular Dynamics. *J. Comput. Phys.* **1995**, *117*, 1–19.
- (28) Berendsen, H. J. C.; Postma, J. P. M.; van Gunsteren, W. F.; DiNola, A.; Haak, J. R. Molecular dynamics with coupling to an external bath. *J. Chem. Phys.* **1984**, *81*, 3684.
- (29) Zhou, T.-Y.; Xu, S.-Q.; Wen, Q.; Pang, Z.-F.; Zhao, X. One-Step Construction of Two Different Kinds of Pores in a 2D Covalent Organic Framework. *J. Am. Chem. Soc.* **2014**, *136*, 15885.
- (30) Liu, Q.-Y.; Jia, Q.-Y.; Zhu, J.-Q.; Shao, Q.; Fan, J.-F.; Wang, D.-M.; Yin, Y.-S. Highly ordered arrangement of meso-tetrakis(4-aminophenyl)porphyrin in self-assembled nanoaggregates via hydrogen bonding. *Chin. Chem. Lett.* **2014**, *25*, 752–756.
- (31) Weber, H.; Marx, D.; Binder, K. Melting transition in two dimensions: A finite-size scaling analysis of bond-orientational order in hard disks. *Phys. Rev. B* **1995**, *51*, 14636.
- (32) Newell, G. F. Crystal Statistics of a Two-Dimensional Triangular Ising Lattice. *Phys. Rev.* **1950**, *79*, 876.
- (33) Mermin, N. D.; Wagner, H. Absence of Ferromagnetism or Antiferromagnetism in One- or Two-Dimensional Isotropic Heisenberg Models. *Phys. Rev. Lett.* **1966**, *17*, 1133.
- (34) Matsushita, Y.; Takano, A.; Hayashida, K.; Asari, T.; Noro, A. Hierarchical nanophase-separated structures created by precisely-designed polymers with complexity. *Polymer* **2009**, *50*, 2191–2203.
- (35) Ēcija, D.; Urgel, J. I.; Papageorgiou, A. C.; Joshi, S.; Auwärter, W.; Seitsonen, A. P.; Klyatskaya, S.; Ruben, M.; Fischer, S.; Vijayaraghavan, S.; et al. Five-vertex Archimedean surface tessellation by lanthanide-directed molecular self-assembly. *Proc. Natl. Acad. Sci. U. S. A.* **2013**, *110*, 6678.
- (36) Urgel, J. I.; Ēcija, D.; Lyu, G.; Zhang, R.; Palma, C.-A.; Auwärter, W.; Lin, N.; Barth, J. V. Quasicrystallinity expressed in two-dimensional coordination networks. *Nat. Chem.* **2016**, *8*, 657.
- (37) Stannard, A.; Russell, J. C.; Blunt, M. O.; Salesiotis, C.; Giménez-López, M. d. C.; Taleb, N.; Schröder, M.; Champness, N. R.; Garrahan, J. P.; Beton, P. H. Broken symmetry and the variation of critical properties in the phase behaviour of supramolecular rhombus tilings. *Nat. Chem.* **2012**, *4*, 112.

lic. Łukasz Baran
Katedra Chemii Teoretycznej
Instytut Nauk Chemicznych
Wydział Chemii UMCS
Pl. Marii Curie-Skłodowskiej 3
20-031 Lublin

Lublin, 16.05.2022

OŚWIADCZENIE


Oświadczam, że mój wkład w niniejszej pracy:

[PVI] **Ł. Baran***, W. Rżysko, S. Szajnar, "Archimedean Tessellation Found by the Variation of Building Blocks' and Linkers' Geometry: In Silico Investigations", *Journal of Physical Chemistry C*, 2020, **124**, 20101-20108.

polegał na przeprowadzeniu części symulacji metodą dynamiki molekularnej, napisaniu manuskryptu i przeprowadzeniu analizy części wyników

Udział ten szacuję na 34 %.

lic. Łukasz Baran



PVI

dr hab. Wojciech Rzyśko, prof. UMCS
Katedra Chemii Teoretycznej
Instytut Nauk Chemicznych
Wydział Chemii UMCS
Pl. Marii Curie-Skłodowskiej 3
20-031 Lublin

Lublin, 16.05.2022

OŚWIADCZENIE

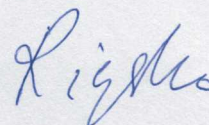
Oświadczam, że mój wkład w niniejszej pracy:

[PVI] Ł. Baran*, W. Rzyśko, S. Szajnar, "Archimedean Tessellation Found by the Variation of Building Blocks' and Linkers' Geometry: In Silico Investigations", *Journal of Physical Chemistry C*, 2020, **124**, 20101-20108.

polegał na koordynowaniu merytorycznym badań, przeprowadzeniu części symulacji i analizie wyników

Udział ten szacuję na 33 %.

dr hab. Wojciech Rzyśko, prof. UMCS



lic. Sebastian Szajnar
Katedra Chemii Teoretycznej
Instytut Nauk Chemicznych
Wydział Chemii UMCS
Pl. Marii Curie-Skłodowskiej 3
20-031 Lublin

Lublin, 16.05.2022

OŚWIADCZENIE

Oświadczam, że mój wkład w niniejszej pracy:

[PVI] **L. Baran***, W. Rzyśko, S. Szajnar, "Archimedean Tessellation Found by the Variation of Building Blocks' and Linkers' Geometry: In Silico Investigations", Journal of Physical Chemistry C, 2020, **124**, 20101-20108.

polegał na wykonaniu części symulacji komputerowych.

Udział ten szacuję na 33 %.

Sebastian Szajnar
lic. Sebastian Szajnar



Simulations of the 2D self-assembly of tripod-shaped building blocks

Łukasz Baran*, Wojciech Rżysko and Edyta Słyk

Full Research Paper

Open Access

Address:

Department for Theoretical Chemistry, Institute of Chemical Sciences,
Faculty of Chemistry, Maria Curie-Skłodowska University in Lublin,
Poland.

Email:

Łukasz Baran* - lukasz.baran@poczta.umcs.lublin.pl

* Corresponding author

Keywords:

2D materials; coarse-grained model; molecular simulations;
self-assembly; structural characterization; tripod building blocks

Beilstein J. Nanotechnol. **2020**, *11*, 884–890.

doi:10.3762/bjnano.11.73

Received: 06 January 2020

Accepted: 26 May 2020

Published: 08 June 2020

Associate Editor: S. A. Claridge

© 2020 Baran et al.; licensee Beilstein-Institut.

License and terms: see end of document.

Abstract

We introduce a molecular dynamics (MD) coarse-grained model for the description of tripod building blocks. This model has been used by us already for linear, V-shape, and tetrapod molecules. We wanted to further extend its possibilities to trifunctional molecules to prove its versatility. For the chosen systems we have also compared the MD results with Monte Carlo results on a triangular lattice. We have shown that the constraints present in the latter method can enforce the formation of completely different structures, not reproducible with off-lattice simulations. In addition to that, we have characterized the obtained structures regarding various parameters such as theoretical diffraction pattern and average association number.

Introduction

On-surface synthesis is a newly developing field in chemistry that aims at making use of solid surfaces as a confinement template to initiate chemical reactions. It can be thought of as an extension of heterogeneous catalysis where the initial precursors, the intermediate state, and the final supramolecular network all remain in an adsorbed state. Complex self-assembled structures are essential for many problems in the chemical industry such as gas storage, chemical sensing, and drug delivery [1-3]. Thus, this field has very recently gained particular interest in both experimental and theoretical studies, which was followed by a vast amount of papers devoted to investigating these phenome-

na. Thanks to this research, several factors have been established that can help to control the self-assembly process, such as precursor design [4,5], substrate nature and symmetry [6,7], type of solvent and its concentration, and thermodynamic conditions. The knowledge of the influence of these variables is crucial to reduce time, cost, and effort regarding the preparation of networks with predefined structural properties.

There are various molecules that possess the ability to self-assemble on solid surfaces. One of the most interesting types are building blocks of linear [8-12], V-shape [13,14], tripod

[15,16], tetrapod [17-21], and hexapod [22] architecture. Also, a lot of effort has been put into the investigation of the mixtures [23-25] and the guest-induced self-assembly [26] of aforementioned particles. An important aspect of the on-surface synthesis is that a lot of these chemical reactions are impossible to be performed in bulk. This is mainly because the substrate reduces the number of rotational and translational degrees of freedom of the admolecules. As a consequence, intermolecular contacts occur that stabilize the interactions between the particles.

To investigate such phenomena in more detail, a proper methodology for the development of complex structures is of particular interest. However, the properties of these structures are hard to predict due to the high number of possible parameters that influence their formation. Thus, it is necessary to use computer modeling, which allows for a versatile examination of various thermodynamic conditions in acceptable time frames. Additionally, it is also a convenient tool to vary multiple factors such as the shape of the molecules, and the type of solvent and substrate. The insight gained from the simulations can lead to valuable conclusions, which can be further explored and proved by experimental studies.

To date, there are two main approaches that can complement the results obtained in experiments. The first one involves the use of all-atom simulations by molecular dynamics (MD) [27-30]. Even though these models are able to compare explicitly the quantities measured in experiments, the possibilities in the prediction of structural properties are limited due to the complex form of the employed interparticle potentials used in the empirical force field, such as Amber99sb [31,32] or MMFF94 [33]. It follows that it is only possible to investigate tens of molecules in total in a reasonable time. The second approach involves the use of simple coarse-grained models, which have been shown to reflect already existing experimental data and to predict new structures, which have not been observed yet. Simulations for this kind of models have been performed using lattice [34,35] and off-lattice [36-38] Monte Carlo simulations, or MD simulations [37,39]. Regarding the latter, we have very recently shown that this methodology is suitable for the representation of tetrapod molecules with different directions of interparticle interactions [37,39], as well as for linear, V-shape, and tetraphenylethylene derivatives [40].

In this work, we want to show that the possibilities of our MD coarse-grained model are not limited to these geometries but can also be used for tripod molecules. In addition to that, we have also compared the results with Monte Carlo results on a triangular lattice (l-MC). We have shown that not for every system the results obtained from both methods agree. Obviously, the latter method is not always an adequate tool for the

investigation of molecules of this type, due to the constraints present on the lattice, which might enforce the formation of structures congruent with the lattice symmetry. Moreover, we have characterized the obtained structures regarding various structural parameters such as structure factor and distribution of association number.

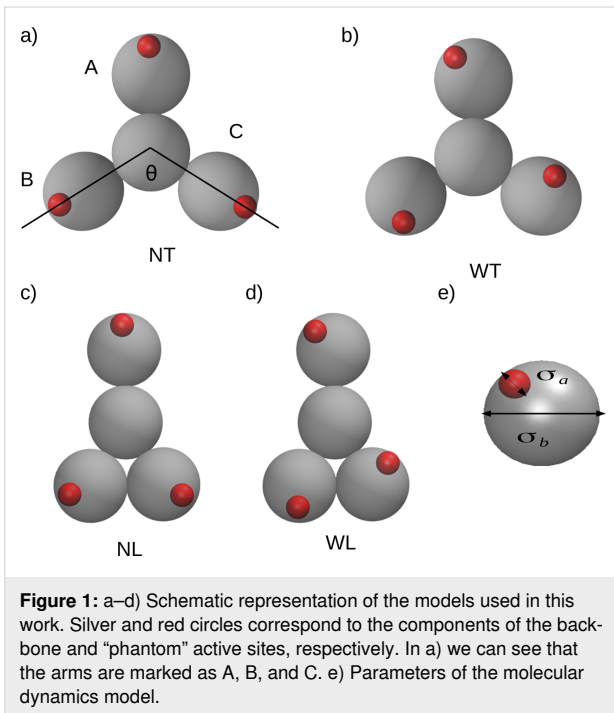
The outline of this paper is as follows. In the next section, we describe our model and simulation details used in the course of our study. Then, we present the results of our simulations, which show various structures, depending on the molecular architecture, and their characterization. Finally, we briefly summarise our findings.

Model and Simulation Details

In this paper, we have used the same approach as in [37,39,40], which is a coarse-grained MD model, now extended to describe the behavior of tripod building blocks. One of the examples of chemical compounds with this molecular geometry is benzene-1,3,5-tricarboxylic acid, more commonly known as trimesic acid. In our investigations, every molecule was treated as a flat and rigid object. The molecules were modeled with one center segment to which three arms are attached. The beads are of equal size σ_b , so we will not distinguish them, but rather refer to them as the components of the entire backbone. The length of each of the arms has been changed in the course of the simulations to investigate also asymmetrical molecules. The three lengths of the arms are denominated **A**, **B**, and **C** as shown in Figure 1a. From the chemical point of view, the length of the arms and the chemical nature of the “active” groups can be controlled by the use of different substituents, for instance, a different number of connected phenyl groups [18,19]. To simplify the notation, we will refer to every model as **MABC**, where **M** means the name of the model and **A**, **B**, and **C** are the length of each arm. As shown in Figure 1a, we have marked the angle θ between arms **B** and **C**. This angle has been set for the models **NT** and **WT** to $\theta = 120^\circ$ and to $\theta = 60^\circ$ for the models **NL** and **WL**. One has to note that for the latter models we can not reproduce the counterparts in the Monte Carlo simulations on a triangular lattice. The active sites, each of size σ_a , which are supposed to reflect directional interactions are grafted onto the terminal segment of each arm and the bonding distance between them is abbreviated as l .

To ensure the distances between particular beads and active sites in the MD simulations we have used the harmonic binding potentials

$$u_{bb} = k_{bb} (r - \sigma_{bb}) \quad (1)$$



and

$$u_{ab} = k_{ab} (r - \sigma_{ab}). \quad (2)$$

The same approach has been used to maintain small fluctuations of the angles:

$$u_{bb}(\theta_{bb}) = k_{\theta} (\theta_{bb} - \theta_{0,bb}), \quad (3)$$

$$u_{ab}(\theta_{ab}) = k_{\theta} (\theta_{ab} - \theta_{0,ab}). \quad (4)$$

The interparticle potential used was the Lennard-Jones 12,6 potential, which was shifted in such way that potential and forces are continuous at the cut-off distance [41]:

$$U_{SF} = \begin{cases} U_{LJ}(r) - U_{LJ}(r_{cut}) + U'_{LJ}(r_{cut})(r - r_{cut}) & r < r_{cut} \\ 0 & \text{otherwise} \end{cases}. \quad (5)$$

where $U_{LJ}(r) = 4\epsilon_{kl}[(\sigma_{kl}/r)^{12} - (\sigma_{kl}/r)^6]$, and $U'_{LJ}(r_{cut})$ is the first derivative of $U_{LJ}(r)$ at $r = r_{cut}$. The backbone Lennard-Jones parameters $\sigma = \sigma_b$ and $\epsilon = \epsilon_{bb}$ have been set to be the units of length and energy, respectively. Reduced temperature and timestep have been defined as $T^* = kT/\epsilon$ and $\tau^* = t\sqrt{\epsilon/m\sigma^2}$, respectively. The number density is equal to

$$\rho^* = \frac{(A + B + C + 1) \cdot \sigma_b^2 + 3 \cdot \sigma_a^2}{L_x \cdot L_y}.$$

The mass of backbone constituents as well as of the active sites were set to unity, their diameters were set to $\sigma_b = 1.0$ and $\sigma_a = 0.2$. The distance between active site and the terminal segment of the arm segment was set to $l = 0.5$, which ensures that three tripod molecules can associate simultaneously. The energies of the backbone–backbone and backbone–site interactions were set to $\epsilon_{bb} = \epsilon_{ab} = 1.0\epsilon$, while $\epsilon_{aa} = 4.0\epsilon$. Briefly, these parameters were chosen so that no other interactions were taken into account, except the highly directional interparticle interactions, which can mimic, for instance, the association of carboxylic acid groups.

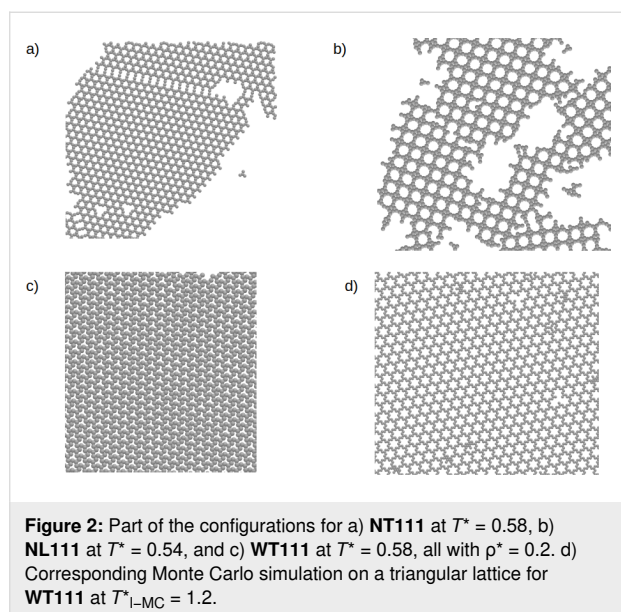
The diameters of pairs were calculated from the mixing rule $\sigma_{kl} = (\sigma_k + \sigma_l)/2$, where $k, l = a, b$. The cut-off distance for active sites were set to $r_{cut,aa} = 2.5\sigma_{aa}$, while the remaining were set to $r_{cut,ij} = \sigma_{ij}$, where $i, j = ab, bb$. The latter means that the only attraction in the system is due to the interactions between active sites. The harmonic potential constants are equal to $k_{bb} \equiv k_{ab} = 1000\epsilon/\sigma^2$ and $k_{\theta} = 1000\epsilon/\text{rad}^2$.

All MD simulations have been performed in the *NVT* ensemble with the LAMMPS simulation package [42,43]. The standard velocity-Verlet integration scheme has been used with a reduced timestep of $t^* = 0.002\tau$. To maintain a constant temperature, the system has been preliminarily equilibrated with a Berendsen thermostat for $5 \cdot 10^6$ simulation steps and after that, we have switched to the Nosé–Hoover chains scheme for further equilibration for at least $5 \cdot 10^7$ simulation steps. The parameters of the latter thermostat were as follows: number of chains $N_{chain} = 3$ and dampening constant $\tau_{NH} = 10\tau$. The system was slowly cooled down from disordered systems to the point where self-assembled structures appeared using a temperature grid of $\Delta T^* = 0.01$.

In the Monte Carlo simulations, we have assumed that one segment can occupy only one vertex of a triangular lattice and the interaction energy between terminal arm segments is taken into account only if the neighboring arms are collinear ($\rightarrow \leftarrow$), resulting in $\epsilon = -1$ energy contribution. One has to take into account that in this method we do not need smaller active sites as in the case of MD. To explicitly compare temperatures from both methods, we have multiplied the temperatures of lattice systems by ϵ_{aa} , and abbreviated it as T^*_{I-MC} . The total amount of molecules was set to 2500 for both methods. However, it is important to highlight that the total number of atoms were different depending on the tripod geometry.

Results and Discussion

We start our discussion with the presentation of the results for the models **M111**, in which every arm consists of only one bead. Parts of the configurations are shown in Figure 2. One can see in Figure 2a and Figure 2c that, depending on the direction of interparticle interactions, we observe qualitatively different structures. For model **NT111** (Figure 2a) the formation of hexagonal pores is observed. It is interesting that aside from well-defined porous networks, we observe small defects, which are artifacts of the cooling process. These can also be observed very often in experiments.



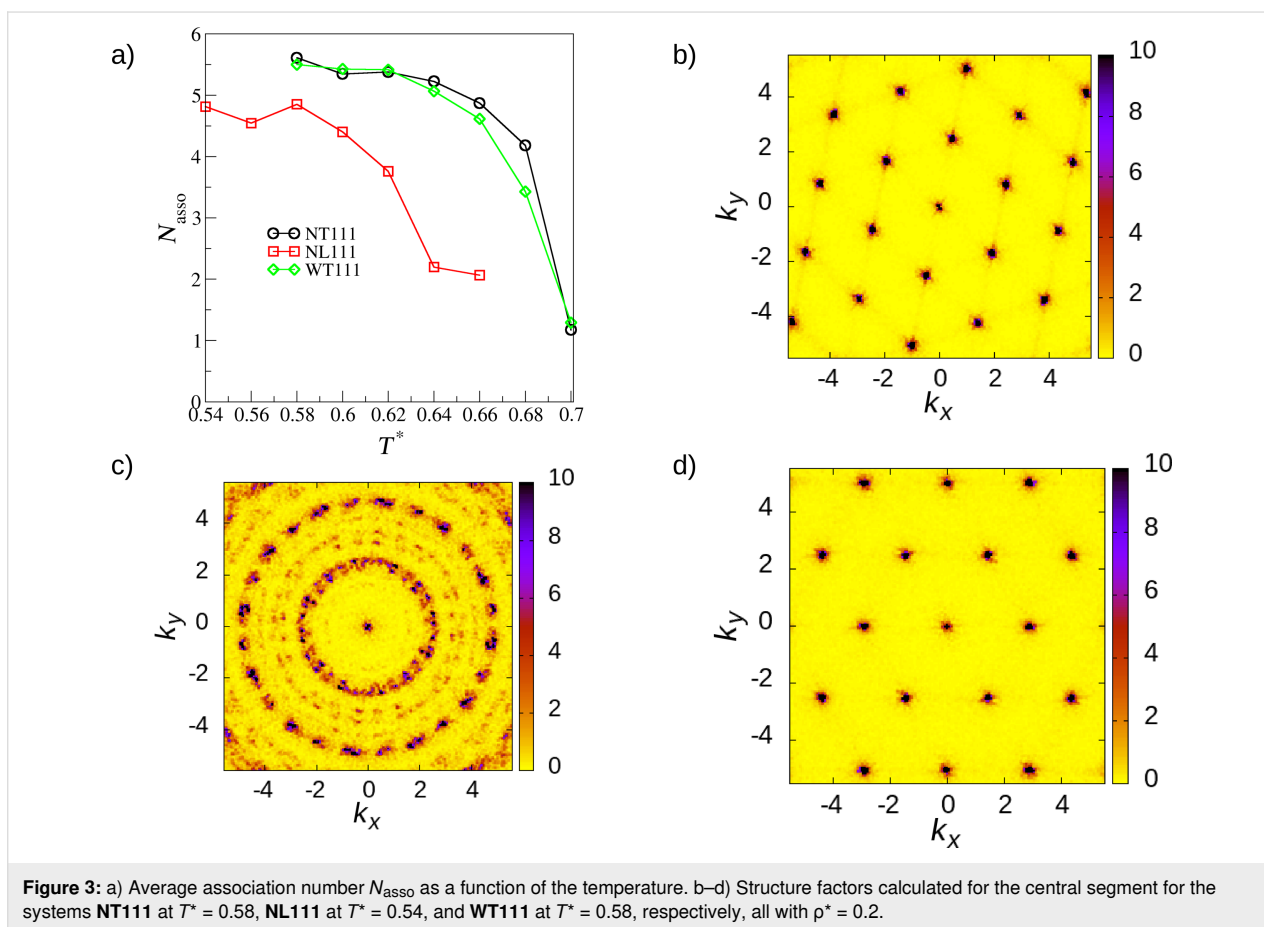
For model **WT111** (Figure 2c) the formation of a different structure occurs. Also, there is only one aggregate built of almost all molecules in the system. It is surprising that for this case the structure reminds of a honeycomb structure, which is the product of the homotactic polycondensation of 1,3-benzene diboronic acid on a HOPG surface [44]. In addition to these MD results, we have performed l-MC simulations. The results for model **NT111** agree with the MD results. However, the situation is different for **WT111**. The configuration obtained with the l-MC method is clearly different from its MD counterpart. It shows a flower-like structure, instead of a closely packed honeycomb network (Figure 2d). This particular result highlights the problem that the lattice type can enforce the formation of structures that are congruent with its symmetry and not necessarily reproducible by other off-lattice methods. Another aspect that has to be taken into account in such analysis is that even if the methods agree with each other or even with experimental data, the l-MC method idealizes obtained structures due to the limited amount of possible arrangements. This has been already observed by us in the case of tetratopic molecules,

which assembled into Kagomé and brickwall networks [39]. In Figure 1b one can see the results for molecule **NL111**, which forms a square-like pattern. It shows that even the directions of interparticle interactions are the same as for **NT111**. The change of the angle θ is a key factor that changes the behavior of molecules of this type.

To characterize the structures presented in Figure 1 we have computed the average association number, N_{asso} , and the structure factors with respect to the central segment. N_{asso} takes values from 0 to 6, where 0 means that no molecules have interacted and 6 means that all molecules are associated. The structure factor shows the symmetry of the obtained functions. This parameter corresponds to the neutron scattering patterns in the experimental results. The results of our analysis can be found in Figure 3. One can see in Figure 3a that the ordering starts at relatively high temperatures (cf. Figure 2), around $T^* = 0.62$ – 0.64 . Nevertheless, by cooling down the systems we can obtain larger clusters, which is a well-known fact.

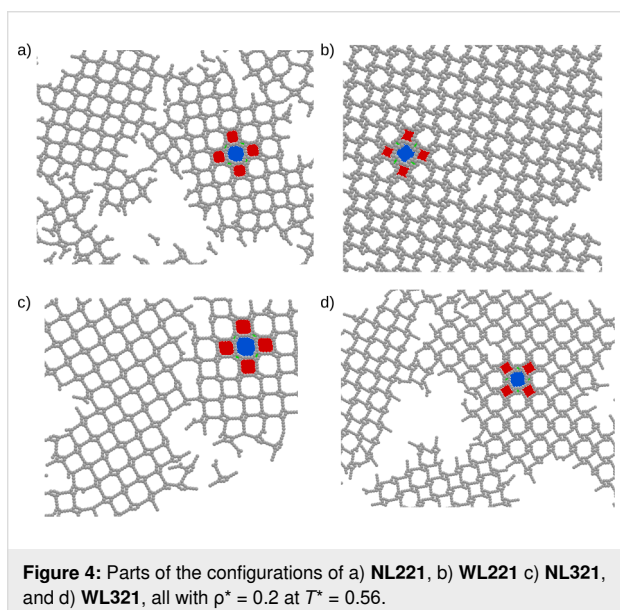
In Figure 3b–d diffraction patterns for the systems **NT111**, **NL111**, and **WT111** are shown. It is very interesting that even though the networks of **NT111** and **WT111** are completely different, the structure factor shows hexagonal symmetry for both. In the case of molecule **NL111** we see a diffused diffraction pattern, which means that there are a lot of differently oriented clusters in the system. We have very recently shown that this issue can lead to the wrong interpretation of results [39]. One of the possible solutions to that is to take a fragment of the configuration and to compute diffraction pattern (or any other orientation-dependent function) from that. Unfortunately, in this particular case, the number of molecules, hence also the number of central segments, was too low to obtain satisfactory statistics.

Let us now proceed to asymmetrical tripod building blocks. Figure 4 shows parts of the configurations of **NL221** (Figure 4a), **WL221** (Figure 4b), **NL321** (Figure 4c), and **WL321** (Figure 4). One can see that for these molecules with $\theta = 60^\circ$ all formed networks have square symmetry, similar to that observed in Figure 2b. The only difference between them is due to the direction of the interparticle interactions between the models **NL** and **WL**, which causes a rotation of the square lattice for the latter. It is also interesting that there are three distinguishable pore sizes in every system, marked in color in Figure 4. Structures of this type can be of particular interest for the selective deposition of guest molecules of different size. Another possible application can be found in analytical chemistry and, particularly, in chromatography, where such porous networks can be used as molecular sieves. The fact that there is no distinct difference between the direction of interparticle



interactions or the architecture within the molecules with $\theta = 60^\circ$ leads us to the conclusion that the key factor for the arrangement of this type of molecules is not the architecture itself but the aforementioned angle between the arms **B** and **C**.

To characterize these networks we have again computed the average association number, which can be found in Figure 5a. Again, the ordering transition occurs at relatively high temperatures, that is $T^* = 0.60$ – 0.62 .



The next investigated molecules are **NT311** and **NL311**. Parts of the configurations are shown in Figure 6. **NL311** also forms a square lattice. This result proves our previous conclusion on what is a key factor for the development of these networks. For **NT311** we see a coexistence of two ordered networks, one with parallel structures and one with structures resembling a ship’s-wheel. These results agree with those from the l-MC method. Again, we have characterized these structures and computed the average association number, which can be found in Figure 5b.

Conclusion

We have shown MD simulation results of the self-assembly of different models of tripod building blocks. We have characterized the self-assembled structures regarding different structural parameters such as theoretical diffraction patterns and average association number. We have found that for molecules with $\theta = 60^\circ$ the key factor is the angle itself rather than the direction of interparticle interactions or molecular architecture.

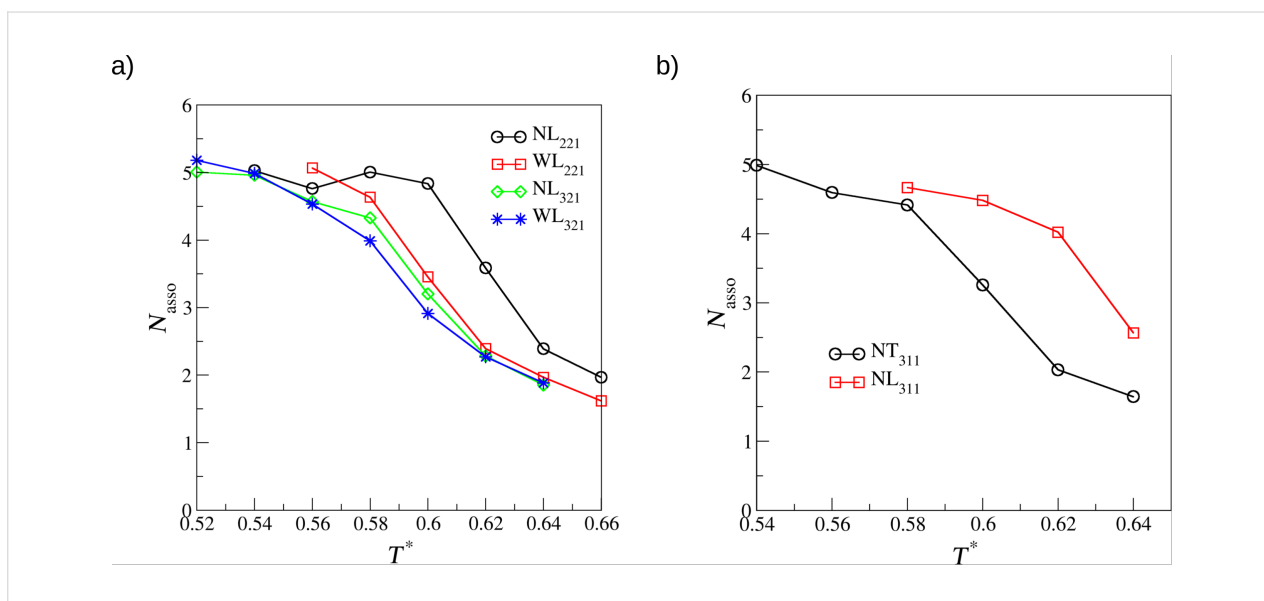


Figure 5: a, b) Average association number, N_{asso} , as a function of the temperature for the molecules given in the legends.

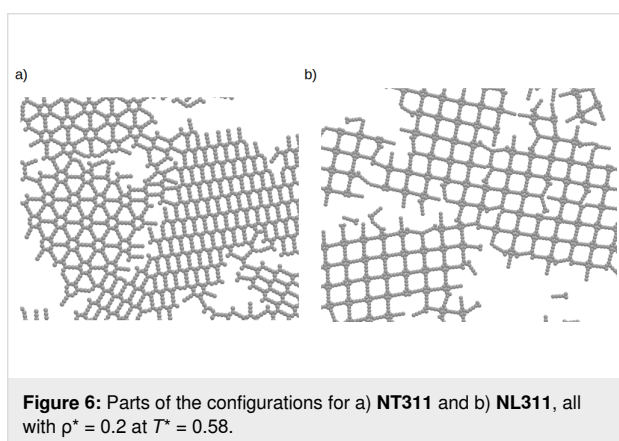


Figure 6: Parts of the configurations for a) **NT311** and b) **NL311**, all with $\rho^* = 0.2$ at $T^* = 0.58$.

Unfortunately, in the case of tectons with $\theta = 120^\circ$, we can not find a general rule for the prediction of predefined networks. One can see from our simulations that the formed networks highly depend on both the interparticle interactions and the molecular architecture. The sensitivity of the aforementioned variables shows us that simplified approaches are of particular importance because they allow us to examine systems under different conditions more effectively than experiments would do. This is mainly associated to reduced cost and time efforts of the coarse-grained model. Moreover, we have shown that the lattice symmetry in Monte Carlo simulations can enforce the formation of structures, which are not reproducible with off-lattice simulations.

Acknowledgements

Calculations were carried out at the Academic Computer Centre in Gdansk.

ORCID® iDs

Lukasz Baran - <https://orcid.org/0000-0003-1777-1998>

Wojciech Rzyśko - <https://orcid.org/0000-0001-9806-6056>

Edyta Słyk - <https://orcid.org/0000-0003-0993-2683>

References

- Das, S.; Heasman, P.; Ben, T.; Qiu, S. *Chem. Rev.* **2017**, *117*, 1515–1563. doi:10.1021/acs.chemrev.6b00439
- Tong, M.; Lan, Y.; Yang, Q.; Zhong, C. *Chem. Eng. Sci.* **2017**, *168*, 456–464. doi:10.1016/j.ces.2017.05.004
- Beuerle, F.; Gole, B. *Angew. Chem., Int. Ed.* **2018**, *57*, 4850–4878. doi:10.1002/anie.201710190
- Zhang, X.; Zeng, Q.; Wang, C. *Nanoscale* **2013**, *5*, 8269–8287. doi:10.1039/c3nr01611k
- Zhang, X.; Zeng, Q.; Wang, C. *RSC Adv.* **2013**, *3*, 11351–11366. doi:10.1039/c3ra40473k
- Gutzler, R.; Cardenas, L.; Lipton-Duffin, J.; El Garah, M.; Dinca, L. E.; Szakacs, C. E.; Fu, C.; Gallagher, M.; Vondráček, M.; Rybachuk, M.; Perepichka, D. F.; Rosei, F. *Nanoscale* **2014**, *6*, 2660–2668. doi:10.1039/c3nr05710k
- Cardenas, L.; Gutzler, R.; Lipton-Duffin, J.; Fu, C.; Brusso, J. L.; Dinca, L. E.; Vondráček, M.; Fagot-Reverat, Y.; Malterre, D.; Rosei, F.; Perepichka, D. F. *Chem. Sci.* **2013**, *4*, 3263–3268. doi:10.1039/c3sc50800e
- Zhang, Y.-Q.; Lin, T.; Cirera, B.; Hellwig, R.; Palma, C.-A.; Chen, Z.; Ruben, M.; Barth, J. V.; Klappenberger, F. *Angew. Chem., Int. Ed.* **2017**, *56*, 7797–7802. doi:10.1002/anie.201702771
- Ren, J.; Larkin, E.; Delaney, C.; Song, Y.; Jin, X.; Amirjalayer, S.; Bakker, A.; Du, S.; Gao, H.; Zhang, Y.-Y.; Draper, S. M.; Fuchs, H. *Chem. Commun.* **2018**, *54*, 9305–9308. doi:10.1039/c8cc03986k
- Écija, D.; Urgel, J. I.; Papageorgiou, A. C.; Joshi, S.; Auwärter, W.; Seitsonen, A. P.; Klyatskaya, S.; Ruben, M.; Fischer, S.; Vijayaraghavan, S.; Reichert, J.; Barth, J. V. *Proc. Natl. Acad. Sci. U. S. A.* **2013**, *110*, 6678–6681. doi:10.1073/pnas.1222713110

11. Urgel, J. I.; Écija, D.; Lyu, G.; Zhang, R.; Palma, C.-A.; Auwärter, W.; Lin, N.; Barth, J. V. *Nat. Chem.* **2016**, *8*, 657–662. doi:10.1038/nchem.2507
12. Schlickum, U.; Decker, R.; Klappenberger, F.; Zoppellaro, G.; Klyatskaya, S.; Ruben, M.; Silanes, I.; Arnau, A.; Kern, K.; Brune, H.; Barth, J. V. *Nano Lett.* **2007**, *7*, 3813–3817. doi:10.1021/nl072466m
13. Shang, J.; Wang, Y.; Chen, M.; Dai, J.; Zhou, X.; Kuttner, J.; Hilt, G.; Shao, X.; Gottfried, J. M.; Wu, K. *Nat. Chem.* **2015**, *7*, 389–393. doi:10.1038/nchem.2211
14. Zhang, X.; Gu, G.; Li, N.; Wang, H.; Tang, H.; Zhang, Y.; Hou, S.; Wang, Y. *RSC Adv.* **2018**, *8*, 1852–1856. doi:10.1039/c7ra11825b
15. Liu, J.; Lin, T.; Shi, Z.; Xia, F.; Dong, L.; Liu, P. N.; Lin, N. *J. Am. Chem. Soc.* **2011**, *133*, 18760–18766. doi:10.1021/ja2056193
16. Ammon, M.; Sander, T.; Maier, S. *J. Am. Chem. Soc.* **2017**, *139*, 12976–12984. doi:10.1021/jacs.7b04783
17. Xing, S.; Zhang, Z.; Fei, X.; Zhao, W.; Zhang, R.; Lin, T.; Zhao, D.; Ju, H.; Xu, H.; Fan, J.; Zhu, J.; Ma, Y.-q.; Shi, Z. *Nat. Commun.* **2019**, *10*, 70. doi:10.1038/s41467-018-07933-0
18. Zhou, H.; Dang, H.; Yi, J.-H.; Nanci, A.; Rochefort, A.; Wuest, J. D. *J. Am. Chem. Soc.* **2007**, *129*, 13774–13775. doi:10.1021/ja0742535
19. Stannard, A.; Russell, J. C.; Blunt, M. O.; Salesiotis, C.; Giménez-López, M. d. C.; Taleb, N.; Schröder, M.; Champness, N. R.; Garrahan, J. P.; Beton, P. H. *Nat. Chem.* **2012**, *4*, 112–117. doi:10.1038/nchem.1199
20. Zhou, H.; Maris, T.; Wuest, J. D. *J. Phys. Chem. C* **2012**, *116*, 13052–13062. doi:10.1021/jp300029z
21. Zhao, J.-F.; Li, Y.-B.; Lin, Z.-Q.; Xie, L.-H.; Shi, N.-E.; Wu, X.-K.; Wang, C.; Huang, W. *J. Phys. Chem. C* **2010**, *114*, 9931–9937. doi:10.1021/jp1022482
22. Lu, C.; Li, Y.; Wang, L.-M.; Yan, H.-J.; Chen, L.; Wang, D. *Chem. Commun.* **2019**, *55*, 1326–1329. doi:10.1039/c8cc08801b
23. Ascherl, L.; Sick, T.; Margraf, J. T.; Lapidus, S. H.; Calik, M.; Hettstedt, C.; Karaghiosoff, K.; Döblinger, M.; Clark, T.; Chapman, K. W.; Auras, F.; Bein, T. *Nat. Chem.* **2016**, *8*, 310–316. doi:10.1038/nchem.2444
24. Dalapati, S.; Jin, E.; Addicoat, M.; Heine, T.; Jiang, D. *J. Am. Chem. Soc.* **2016**, *138*, 5797–5800. doi:10.1021/jacs.6b02700
25. Dong, W.-L.; Li, S.-Y.; Yue, J.-Y.; Wang, C.; Wang, D.; Wan, L.-J. *Phys. Chem. Chem. Phys.* **2016**, *18*, 17356–17359. doi:10.1039/c6cp01804a
26. Blunt, M.; Lin, X.; Gimenez-Lopez, M. d. C.; Schröder, M.; Champness, N. R.; Beton, P. H. *Chem. Commun.* **2008**, 2304–2306. doi:10.1039/b801267a
27. El Garah, M.; Dianat, A.; Cadeddu, A.; Gutierrez, R.; Cecchini, M.; Cook, T. R.; Ciesielski, A.; Stang, P. J.; Cuniberti, G.; Samori, P. *Small* **2016**, *12*, 343–350. doi:10.1002/sml.201502957
28. Copie, G.; Cleri, F.; Makoudi, Y.; Krzeminski, C.; Berthe, M.; Cherioux, F.; Palmino, F.; Grandidier, B. *Phys. Rev. Lett.* **2015**, *114*, 066101. doi:10.1103/physrevlett.114.066101
29. Palma, C.-A.; Samori, P.; Cecchini, M. *J. Am. Chem. Soc.* **2010**, *132*, 17880–17885. doi:10.1021/ja107882e
30. Zhao, Y.; Wang, J. *J. Phys. Chem. C* **2017**, *121*, 4488–4495. doi:10.1021/acs.jpcc.7b00606
31. Guy, A. T.; Piggot, T. J.; Khalid, S. *Biophys. J.* **2012**, *103*, 1028–1036. doi:10.1016/j.bpj.2012.08.012
32. Sorin, E. J.; Pande, V. S. *Biophys. J.* **2005**, *88*, 2472–2493. doi:10.1529/biophysj.104.051938
33. Halgren, T. A. *J. Comput. Chem.* **1996**, *17*, 490–519. doi:10.1002/(sici)1096-987x(199604)17:5<490::aid-jcc1>3.0.co;2-p
34. Szabelski, P.; Rzyzko, W.; Niecekarz, D. *J. Phys. Chem. C* **2016**, *120*, 13139–13147. doi:10.1021/acs.jpcc.6b03842
35. Szabelski, P.; Rzyzko, W.; Pańczyk, T.; Ghijssens, E.; Tahara, K.; Tobe, Y.; De Feyter, S. *RSC Adv.* **2013**, *3*, 25159–25165. doi:10.1039/c3ra45342a
36. Maula, T. A.; Hatch, H. W.; Shen, V. K.; Rangarajan, S.; Mittal, J. *Mol. Syst. Des. Eng.* **2019**, *4*, 644–653. doi:10.1039/c9me00006b
37. Baran, Ł. *J. Mol. Liq.* **2019**, *294*, 111627. doi:10.1016/j.molliq.2019.111627
38. Karner, C.; Dellago, C.; Bianchi, E. *Nano Lett.* **2019**, *19*, 7806–7815. doi:10.1021/acs.nanolett.9b02829
39. Baran, Ł.; Niecekarz, D.; Szabelski, P.; Rzyzko, W. *J. Phys. Chem. C* **2019**, *123*, 19549–19556. doi:10.1021/acs.jpcc.9b04108
40. Baran, Ł.; Rzyzko, W. *Mol. Syst. Des. Eng.* **2020**, *5*, 484–492. doi:10.1039/c9me00122k
41. Toxvaerd, S.; Dyre, J. C. *J. Chem. Phys.* **2011**, *134*, 081102. doi:10.1063/1.3558787
42. LAMMPS Molecular Dynamics Simulator; <https://lammps.sandia.gov/>. (accessed 2020-05-26).
43. Plimpton, S. *J. Comput. Phys.* **1995**, *117*, 1–19. doi:10.1006/jcph.1995.1039
44. Cui, D.; Fang, Y.; MacLean, O.; Perepichka, D. F.; Rosei, F.; Clair, S. *Chem. Commun.* **2019**, *55*, 13586–13589. doi:10.1039/c9cc05674b

License and Terms

This is an Open Access article under the terms of the Creative Commons Attribution License (<http://creativecommons.org/licenses/by/4.0>). Please note that the reuse, redistribution and reproduction in particular requires that the authors and source are credited.

The license is subject to the *Beilstein Journal of Nanotechnology* terms and conditions: (<https://www.beilstein-journals.org/bjnano>)

The definitive version of this article is the electronic one which can be found at: doi:10.3762/bjnano.11.73

PVII

lic. Łukasz Baran
Katedra Chemii Teoretycznej
Instytut Nauk Chemicznych
Wydział Chemii UMCS
Pl. Marii Curie-Skłodowskiej 3
20-031 Lublin

Lublin, 16.05.2022

OŚWIADCZENIE

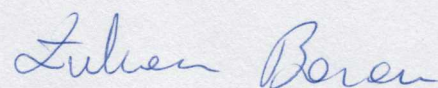
Oświadczam, że mój wkład w niniejszej pracy:

[PVII] **Ł. Baran***, W. Rżysko, E. Słyk, "Simulations of the 2D self-assembly of tripod-shaped building blocks", Beilstein Journal of Nanotechnology, 2020, **11**, 884-890.

polegał na przeprowadzeniu symulacji metodą dynamiki molekularnej, napisaniu manuskryptu i przeprowadzeniu analizy części wyników

Udział ten szacuję na 60 %.

lic. Łukasz Baran



PVII

dr hab. Wojciech Rzyśko, prof. UMCS
Katedra Chemii Teoretycznej
Instytut Nauk Chemicznych
Wydział Chemii UMCS
Pl. Marii Curie-Skłodowskiej 3
20-031 Lublin

Lublin, 16.05.2022

OŚWIADCZENIE

Oświadczam, że mój wkład w niniejszej pracy:

[PVII] Ł. Baran*, W. Rzyśko, E. Słyk, "Simulations of the 2D self-assembly of tripod-shaped building blocks", Beilstein Journal of Nanotechnology, 2020, **11**, 884-890.

polegał na koordynowaniu merytorycznym badań i analizie wyników

Udział ten szacuję na 25 %.

dr hab. Wojciech Rzyśko, prof. UMCS



dr Edyta Słyk
Katedra Chemii Teoretycznej
Instytut Nauk Chemicznych
Wydział Chemii UMCS
Pl. Marii Curie-Skłodowskiej 3
20-031 Lublin

Lublin, 15.05.2022

OŚWIADCZENIE

Oświadczam, że mój wkład w niniejszej pracy:

[PVII] **Ł. Baran***, W. Rzyśko, E. Słyk, "Simulations of the 2D self-assembly of tripod-shaped building blocks", Beilstein Journal of Nanotechnology, 2020, **11**, 884-890.

polegał na wykonaniu części symulacji komputerowych i analizie części wyników.

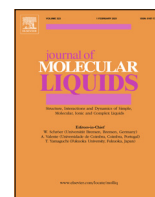
Udział ten szacuję na 15 %.

Edyta Słyk
dr Edyta Słyk



Contents lists available at ScienceDirect

Journal of Molecular Liquids

journal homepage: www.elsevier.com/locate/molliq

Influence of the substitution position in the tetratopic building blocks on the self-assembly process



Łukasz Baran^{a,*}, Konrad Dyk^b, Daniel Michael Kamiński^b, Marek Stankevič^c, Wojciech Rzyśko^a, Dariusz Tarasewicz^a, Tomasz Zientarski^d

^a Department of Theoretical Chemistry, Institute of Chemical Sciences, Faculty of Chemistry, Maria Curie-Skłodowska University in Lublin, Poland

^b Department of General and Coordination Chemistry and Crystallography, Institute of Chemical Sciences, Faculty of Chemistry, Maria Curie-Skłodowska University in Lublin, Poland

^c Department of Organic Chemistry, Institute of Chemical Sciences, Faculty of Chemistry, Maria Curie-Skłodowska University in Lublin, Poland

^d Department of Computer Science, Faculty of Electrical Engineering and Computer Science, Lublin University of Technology, Poland

ARTICLE INFO

Article history:

Received 6 April 2021

Revised 16 June 2021

Accepted 20 July 2021

Available online 22 July 2021

Keywords:

Self-assembly

Molecular simulations

Supramolecular chemistry

ABSTRACT

Self-assembled structures formed by chemical compounds with allowed internal rotations can form various ordered phases depending on the conformation. Using classical molecular dynamics and quantum calculations for tetraphenyl derivatives with different substitutions in X and Y positions (either hydroxyl or carboxyl group), we have investigated the formation of ordered structures depending on the substitution and molecular conformation. Our paper shows that certain functional groups have a big impact on the self-assembly process. We have found that those molecules can form different phases among which the most interesting seems to be Archimedean tiling. The obtained ordered networks have been characterized by radial distribution functions, cluster analysis, and two-dimensional structure factors.

© 2021 Elsevier B.V. All rights reserved.

1. Introduction

Fabrication of self-assembled supramolecular networks with predefined parameters have aroused great interest due to its possible application in developing new materials. Spatial confinement has been widely used to generate 1D and 2D ordered structures. The dimensionality of a structure highly depends on the geometry and the arrangement of binding groups of precursors possessing the ability to self-assemble at the solid–fluid interface [1–8]. It has also been reported that the solvent affinities to the active groups of particular chemical compounds can influence the formation of diverse ordered phases [9]. On the other hand, for one solvent, the formation of either porous or highly packed network can be observed depending on the concentration of the compound [10,11]. Therefore, it is possible to position functional entities over specific areas and, in consequence, to tune desired properties of the obtained nanostructure. Possible applications of such materials involve optics and electronics [12], gas storage, or more generally, in nanotechnology [13].

Spontaneous self-assembly process is often driven by highly directional van der Waals forces [14], metal–ligand coordination [15,16], halogen [17] or hydrogen [18,19] bonding interactions.

Among them, weak and reversible non-covalent bonding seems to be the most effective for the design of self-assembled networks. Due to their weak bond strength, once aggregated, the sum of these small interactions energy results in materials with self-healing properties [20].

Another aspect which has to be taken into account is the nature of a particular substrate. The on-surface synthesis has been mainly performed on coinage metal substrates (Ag, Au, Cu) or highly-oriented pyrolytic graphite (HOPG). The type of substrate can affect the reactivity of precursors, the reaction pathway, and its selectivity [21,22]. In general, the on-surface phase behavior depends on the relative strengths and ranges of adatom–adatom and adatom–substrate attractions. Besides that, crystallographic orientation is also an important factor governing the reactivity of on-surface reactions. It has been shown that depending on the surface index, the self-assembly process can be either exhibited or inhibited. For instance, in the case of dibromo-bianthryl, the reaction on Cu(111) leads to the formation of 1D nanoribbons whereas on Cu(110) intermolecular coupling is completely prevented [23].

Within this plethora of possible factors influencing the self-assembly process it is reasonable to employ strategies allowing for the direct explanation of the system's behavior. The most powerful approach is to combine experimental results with the *in silico* investigations. The latter involve all-atom [24,25] and coarse grained molecular dynamics [26–28] or Monte Carlo simulations [29–32].

* Corresponding author.

E-mail address: lukasz.baran@poczta.umcs.lublin.pl (Ł. Baran).

In this work, we investigated the influence of substitution pattern of two substituents, namely hydroxyl -OH and carboxyl -COOH groups on the self-assembly process. Moreover, we have taken into account two possible conformations which those molecules can possess. The first compound, abbreviated later as **M1** has been already investigated experimentally in our group [33].

The main intention of MD computer simulations was to obtain a preliminary insight into their possible on-surface behavior. This aspect is being studied in our laboratory for compounds M1 and these systematic studies could show us which derivatives could be of potential interest to be studied experimentally as well. To further justify our decision, the synthesis of these kinds of compounds takes significantly more time and can be much more expensive compared to those theoretical investigations. In our future work, when we will aim to obtain UHV-STM images on different substrates such as HOPG and Au(111). Then, we will perform more detailed theoretical investigations aimed at the parametrization of our forcefields since we will be able to compare with the experimental results explicitly. Moreover, we will be able to extract the influence of the model's parameters on the phase behavior of the system. To date, we have found out that depending on the position of active centers, the formation of different ordered networks can be observed. It has to be emphasized that at this stage our intention was to quantify the obtained results only qualitatively and to show the influence of the chemical structure of chemical compounds of interest.

The remainder of this work is as follows. In Section 2, we describe the model and simulation details. In Section 3 we present the results obtained for different molecular models. Ultimately in Section 4, we conclude on our results.

2. Model and simulation details

The model proposed by us has been designed to reflect the on-surface behavior of tetra-substituted aromatic chemical compounds. The schematic representation is shown in Fig. 1 a and will be referred to as "zigzag". In our approach, we have distinguished -CH groups (gray circles) which form benzene rings. Each of the aromatic rings is substituted by either -OH or -COOH group in which each of the atoms has been distinguished. The position of those functional groups is marked as X and Y. One has to note that, unlike the X substitution, which is always on the same carbon atom, the latter has been changed and those atoms are marked as C_{a-c}. Another feature of our model is the addition of "phantom" atom in the middle of the aromatic ring (yellow star). This trick has been done in order to maintain the rigidity and flatness of benzene rings. We also considered another conformation of these molecules (Fig. 1 b), which will be referred to as "V-shape".

In this case, we did not consider a wall explicitly and we have performed all of the studies in a two-dimensional system, instead. We are familiar with the aspect that the surface can change the behavior of the system of interest. It has to be emphasized, however, that the most important factor is the ratio between the surface unit cell and the size/shape of the compound of interest. If the molecule is "big enough" the compound does not "feel" the surface's geometry and therefore the compound-surface interactions are averaged which in consequence can be modelled as a "flat wall" (e.g. (9, 3) Lennard-Jones potential) or as a simple 2D simulations (as in our paper). As already mentioned in the previous section, we plan to perform such experimental studies in our laboratory to estimate the possible influence of this parameter on the self-assembly process.

We are aware that there are plenty of parametrized molecular dynamics force fields, such as OPLS [34] or MMFF [35], which potentially would be also useful for the description of the behavior of chemical compounds of interest. Our intention, however, was to extend the investigations performed already in our laboratory, where one "atom" was thought of as an entire benzene ring and substitution has never been considered explicitly [26–28]. By the latter we mean that the directional interparticle interactions have been modelled by the form of potential or "active phantom site". Another argument was that we wanted our model to be as simple as possible, yet able to investigate the topology of supramolecular networks (dihedrals, partial charges, etc., which are present in more realistic force fields have not been included). It has to be emphasized that at this stage we are not able to compare any properties measured experimentally, such as the strength of interparticle interactions but, on the other hand, we are able to study collective phenomena such as phase transitions.

To ensure bonding distances between particular entities in the molecules, we have used harmonic binding potentials

$$u_{kl} = k_{kl}(r - r_{0,kl})^2 \quad (1)$$

In a similar manner, all of necessary angles have also been maintained by an application of angular-harmonic potential

$$u_{kl}(\theta_{kl}) = k_{\theta}(\theta_{kl} - \theta_{0,kl})^2 \quad (2)$$

The interparticle potential employed in our simulations was (12,6) Lennard-Jones potential, which have been appropriately shifted to ensure its continuity [36]

$$U_{SF} = \begin{cases} U_{IJ}(r) - U_{IJ}(r_{cut}) + U'_{IJ}(r_{cut})(r - r_{cut}) & r < r_{cut} \\ 0 & \text{otherwise} \end{cases} \quad (3)$$

where $U_{IJ}(r) = 4\epsilon_{kl}[(\sigma_{kl}/r)^{12} - (\sigma_{kl}/r)^6]$, $U'_{IJ}(r_{cut})$ is the first derivative of $U_{IJ}(r)$ at $r = r_{cut}$, and $k, l = CH, C, O, H$.

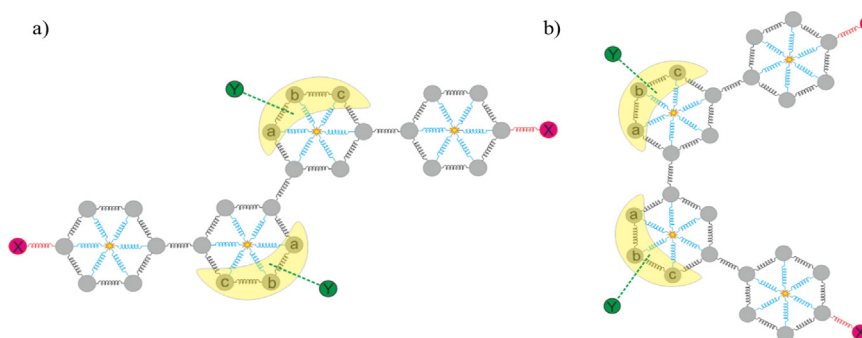


Fig. 1. Schematic representation of model chemical compounds: "zigzag" (a) and "V-shape" (b), used in the course of our study. X and Y refer to the position -OH or -COOH active groups substitution. In the latter, it has to be emphasized that the position changed on carbon atoms, which are marked as C_{a-c}. -CH groups are marked on silver, yellow star is a "phantom" molecule in the middle of the aromatic ring (cf. text), and springs are related to the bonds (harmonic potentials).

The Lennard-Jones potential parameters, $\sigma_{CH} \equiv \sigma$ and $\varepsilon_{CH-CH} \equiv \varepsilon$, have been set to be the units of length and energy, respectively. The reduced time and temperature are equal to $\tau^* = t\sqrt{\varepsilon/m\sigma^2}$, $T^* = kT/\varepsilon_{CH}$. The number density has been defined as $\rho^* = N_{tot} * \sigma_{kl}/(L_x * L_y)$, where $N_{tot} = N_{CH} + N_C + N_O + N_H$. The sizes of all entities was set to σ . The only attractive force in the system was due to the interactions between O-H atoms and the energies was $\varepsilon_{OH} = 5\varepsilon$ and cut off distance was $r_{cut_{OH}} = 2\sigma$. In the remaining cases, the ε_{kl} and the cut off distance was set to be unity. Since we were not interested in the dynamic processes in the system, we have set the mass also to unity. The harmonic potential constants $k_{kl} = 1000\varepsilon/\sigma^2$ and $k_\theta = 1000\varepsilon/(rad)^2$.

All of the molecular dynamics simulations have been performed in the NVT ensemble, using LAMMPS simulation package [37,38]. The velocity Verlet integration scheme has been used with the reduced time step of the order of $t = 0.001\tau$. The number of molecules varied from $N = 900$ to $N = 2500$. However, the total number of “atoms” varied depending on the used model and system size. This amount is sufficient for most of the self-assembly systems which is large enough to form ordered networks, but small enough to form those structures in a reasonable time frame.

The simulation scheme involved preliminary runs in the *NPT* ensemble to establish the desired density. Next, equilibration runs for 5×10^6 time steps using the Berendsen [39] thermostat with damping constant equal to $\tau_B = 10\tau$ have been performed. The further equilibration for 5×10^7 , as well as production runs have been performed using Nosé-Hoover chains algorithm [40], with the damping constant equal to $\tau_{HN} = 10\tau$ and the number of chains set to $N_{chain} = 3$. Each system has been slowly cooled down from temperatures where we observed no order to the point where the self-assembly process appeared. The temperature grid was fixed and set to be $\Delta T = 0.01$.

In addition to molecular dynamics simulations, we have performed density functional theory (DFT) and second-order Møller-Plesset perturbation theory (MP2) calculations with different basis sets, calculated in the Gaussian16 program [41]. The calculations were repeated for every 10° rotation step around the central bond of each of the molecules in the gaseous state without intermolecular interactions. Details of the calculations are presented in [33]. The main purpose of this additional calculations was to estimate the energy difference of two planar conformations (“V-shape” and “zigzag”).

3. Results

We begin with the presentation of models considered in the course of our paper, which can be found in Table 1. For each of these models, we have performed full geometry optimization for every state following the procedure described in the previous section. The results obtained from quantum calculations are presented in Table 2. The energy difference is calculated based on energies of each of two contrary conformations (“V-shape” and “zigzag”) in the ground state. One can see that the value of ΔE is always positive. This means that for every considered model the “zigzag” conformation is more favorable. Due to high energy difference, comparable with the medium value range of hydrogen bonds [42] for models **M1** and **M4**, we did not consider the “V-shape” conformations.

Let us start with the description of results obtained for molecules in “zigzag” conformation. In the models presented in Fig. 2 a-c we show the structures formed in the systems built of molecules **M1-M3**, respectively. On the right side of each of these panels, we have shown the schematic representation of observed networks. For the system **M1** we have also displayed different pos-

sible association path, which is not present in our simulations. For each schematic representation we have distinguished the molecules on blue and silver. We believe that this kind of visualization should improve understanding of how the molecules connect.

Molecules **M1** form only one ordered network (Fig. 2a), whereas molecules **M2** and **M3** form three that can be distinguished. For the system **M1** structure is dense and only two hydroxyl groups of the same type of different molecules associate. The latter can be proven from the analysis of radial distribution functions shown in Fig. 3 a-c. This function has been calculated with respect to the X and Y oxygen atoms (cf. Fig. 1). One can see from those functions that there are only connections of X – X and Y – Y in the first coordination shell, with the maximum in $r \approx 1.6 \pm 0.05$ for both types. The distance for the “mixed” correlation of X – Y oxygen atoms is around $r \approx 4.2 \pm 0.05$. To further characterize that only two hydroxyl groups associate which is consistent with our observation from the snapshots, we have performed the cluster analysis. This parameter has been calculated for the oxygen atoms up to the threshold distance equal to $r = 2.5$. This distance has been taken from the aforementioned radial distribution functions and is the most distant separation length of the first coordination shell for any pair correlation function. The average cluster size was approximately $ACS = 2$. Moreover, to prove that the structure is well defined and possesses a pseudo-long-range order [43], we have calculated two-dimensional structure factor which can be found in the Fig. 3 d.

As we have already mentioned, models **M2** (Fig. 3 and **M3** (Fig. 2c) form three ordered networks which can be distinguished. Contrary to the model **M1**, in the molecules **M2** the most pronounced correlations are due to the “mixed” connections of X – Y oxygen atoms with the maximum in $r \approx 1.9 \pm 0.05$. This indeed corroborates with the observations from the snapshots. The remaining X – X and Y – Y associations are approximately fivefold less likely than the mixing ones and their peaks are diffused. Those connections can be explained by the occurrence of the less dense network, marked in the orange circle in Fig. 2b. The cluster analysis counted up to the threshold distance $r = 2.5$ shows us that $CS = 2$, $CS = 3$ and $CS = 4$ exist with equal probability and the average cluster size is approximately $ACS = 3.01$. Those results can lead us to the conclusion that the amount of two dense phases (black and green circles in Fig. 2b) and porous structure (orange circle in Fig. 2b) is approximately the same. It has to be emphasized that the $CS = 3$ as well as some part of $CS = 2$ are connected with defects and network boundaries present in the system of interest.

In the case of model **M3** the first two ordered networks marked in the green and black on the right panel of Fig. 2c are qualitatively the same at the first glance. However, a deeper inspection of the oxygen arrangement of hydroxyl groups shows us that they slightly differ one from another. In the former, the molecules are packed in a slightly more dense network relative to the latter. Only due to the alternating coloring of **M3** molecules one can distinguish the connections. The third network (orange circle of Fig. 2c) is similar to the corresponding one formed by molecules **M2**. From the radial distribution functions for this model we can see that the most dominant connections are X – X with the maxima around $r \approx 1.1 \pm 0.05$ and “mixed” X – Y correlations with two sharp peaks around $r \approx 1.9 \pm 0.05$ and $r \approx 2.15 \pm 0.05$, respectively. The Y – Y connections are over ten times less likely than the most prominent X – X correlations. This suggests that the porous network is rarely observed, which corresponds to the snapshots. The cluster analysis performed in the same manner as previously shows that the most probable cluster size is $CS = 4$. $CS = 2$ and $CS = 3$ are less likely but of equal probability. The average cluster size is approximately $ACS = 3.31$. Those results suggest us that

Table 1
Structural formula along with name of the chemical compounds investigated in our work with corresponding abbreviations.

Model abbreviation		
M1	M2	M3
5,5'-Bis(4-hydroxyphenyl)-2,2'-dihydroxy-1,1'-biphenyl	5,5'-Bis(4-hydroxyphenyl)-3,3'-dihydroxy-1,1'-biphenyl	3,3'-Bis(4-hydroxyphenyl)-4,4'-dihydroxy-1,1'-biphenyl
M4	M5	M6
5,5'-Bis(4-carboxyphenyl)-2,2'-dihydroxy-1,1'-biphenyl	5,5'-Bis(4-carboxyphenyl)-3,3'-dihydroxy-1,1'-biphenyl	3,3'-Bis(4-carboxyphenyl)-4,4'-dihydroxy-1,1'-biphenyl
M7		M2 "V-shape"
5,5'-Bis(4-carboxyphenyl)-1,1'-biphenyl-3,3'-dicarboxylic acid		

Table 2
Energy difference between "V-shape" and "zigzag" conformations for each of the models, $\Delta E = E_V - E_Z$, obtained from quantum calculations.

Model	M1	M2	M3	M4	M5	M6	M7
ΔE [kcal/mol]	8.218	0.084	0.094	8.199	0.022	0.046	0.602

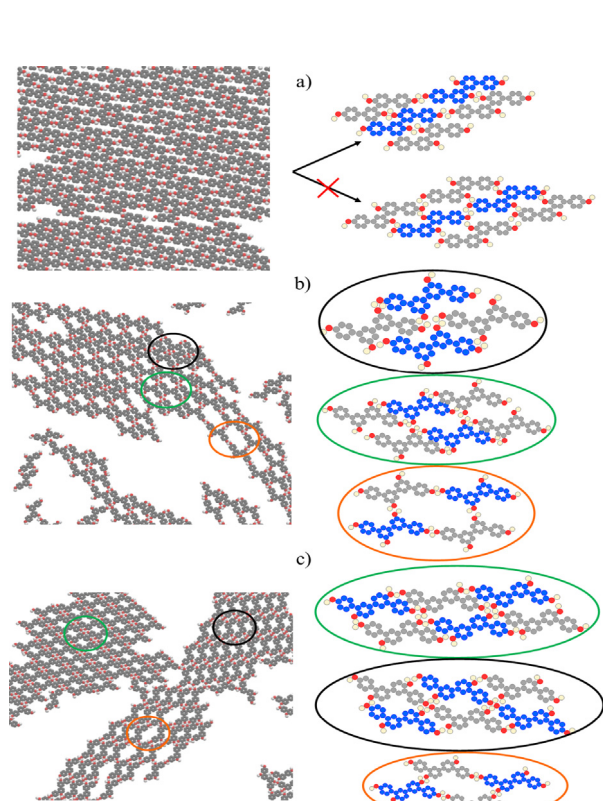


Fig. 2. Part a, b, c presents fragments of configurations obtained for models **M1**, **M2** and **M3** in $\rho^* = 0.2$ at $T^* = 1.0$, respectively. Right hand side shows schematic representation of obtained ordered networks. Alternating coloring is performed for visualization purposes only.

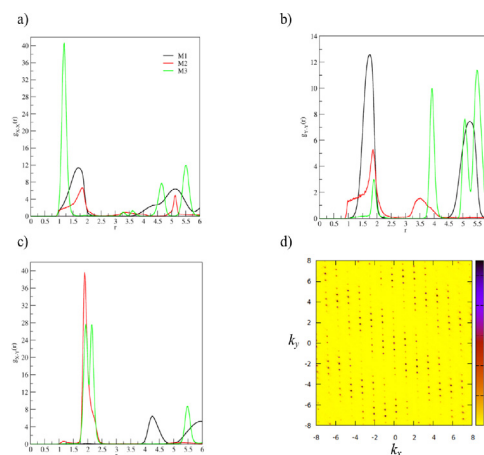


Fig. 3. Part a, b, c presents radial distribution functions calculated with respect to oxygen atoms for models **M1**, **M2** and **M3** in $\rho^* = 0.2$ at $T^* = 1.0$, respectively. Part d is a two-dimensional structure factor for model **M1** calculated in the same conditions.

the most probable networks are dense structures (marked by black and orange circles in Fig. 2c), however boundaries of the aggregates as well as rarely observed porous network play also a key role.

We can clearly see that the change in substitution of central (Y) -OH groups can lead to the formation of completely different structures. Therefore, we wanted to further check the influence of change in substitution of Y position while the X position is now a carboxyl group -COOH. The results for models **M4-M6** can be found in Fig. 4 a-c, respectively. As previously, on the right-hand side of each panel we have shown the schematic representation of each ordered network. Due to the formation of only one structure for every **M4-M6** molecule, we have also shown other

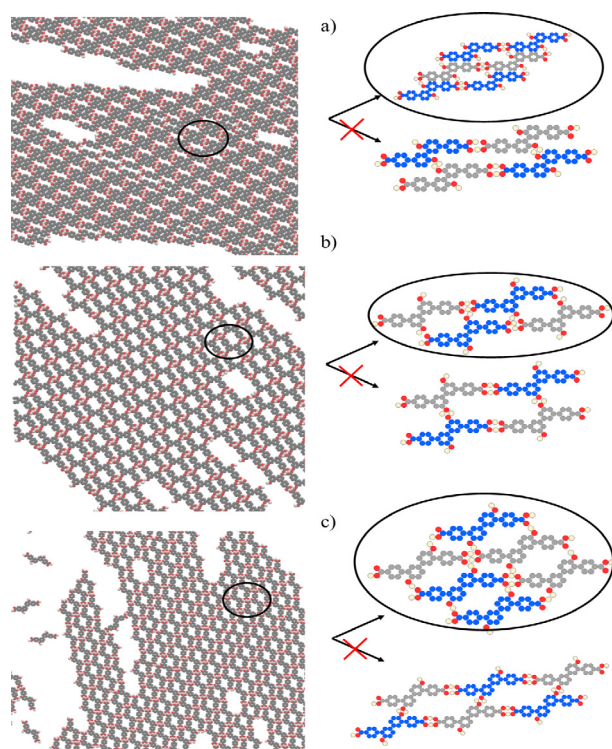


Fig. 4. Part a, b, c presents fragments of configurations obtained for models **M4**, **M5** and **M6** in $\rho^* = 0.2$ at $T^* = 1.3$, respectively. Right-hand side shows schematic representation of obtained ordered networks. Alternating coloring is performed for visualization purposes only.

possible paths on how molecules could connect which are not forbidden yet they have not been observed in our simulations. We can clearly see the different behavior caused by the substitution of -COOH group in the X position for every considered case. The molecules **M4-M6** form only one ordered network which previously was only the case in the **M1** model. From the snapshots, we can see that there is no huge difference caused by the change of substitution's position Y.

As previously, we have performed the same analysis for every model **M4-M6** to better quantify the observed supramolecular networks. From radial distribution functions presented in Fig. 5 a-c we can see that for every considered model there are only correlations

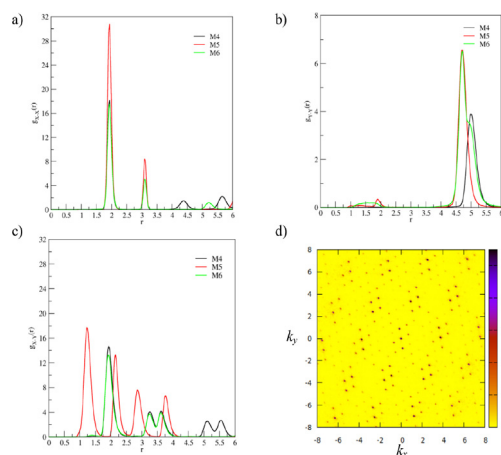


Fig. 5. Part a, b, c presents radial distribution functions calculated with respect to oxygen atoms for models **M4**, **M5** and **M6** in $\rho^* = 0.2$ at $T^* = 1.3$, respectively. Part d is a two-dimensional structure factor for model **M4** calculated in the same conditions.

for X – X and “mixed” X – Y oxygens of -OH and -COOH groups in the first coordination shell. The Y – Y connections in similar separation distance are negligible and are present due to imperfections in the lattice structure. However, the Y – Y correlations are in more distant interparticle separations around $r \approx 4.5 - 5.5$ and are due to the “indirect” association, which is consistent with the snapshots and is well-pronounced on magnified networks on the right-hand side of every panel in Fig. 4. One has to note that the probability of those connections is four to six times lower than the aforementioned ones. In the models **M4** and **M6** the most probable separation distance is around $r \approx 1.95 \pm 0.05$ for both X – X and X – Y correlations. For the model **M5**, while the distance of X – X association is the same as for **M4** and **M6**, the distribution function of X – Y connections is different. We can observe in the Fig. 5 c that the first maxima is around $r \approx 1.2 \pm 0.05$ and the second coordination shell is around $r \approx 2.2$. This is indeed consistent with the obtained structure (cf. Fig. 4 b) where one can see that oxygens from both carboxyl and hydroxyl groups are nearly “glued” one to another.

In addition to pair correlation functions, we have performed cluster analysis in the same manner as for models **M1-M3**. For models **M4-M6** the most probable cluster size is CS = 6 and the average cluster size is in the range of ACS = $4.9 - 5.2 \pm 0.2$. The latter value means that there are some imperfections in the structure, as well as its boundaries decreases the average value.

While it is not clearly visible from the snapshots that those structures differ, the differences are better pronounced due to the analysis we have performed. One can see that all of the distances as well as type of correlations and cluster sizes changed in the comparison with previous models, that is **M1-M3**. This shows that the substitution by a certain functional group has a significant impact on the self-assembly process. Therefore, we wanted to further check the influence of the four -COOH carboxyl groups

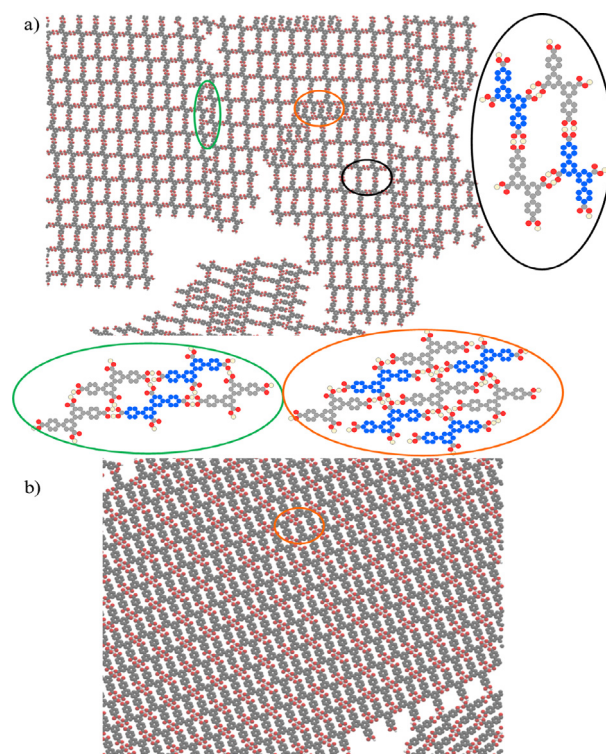


Fig. 6. Part a and b presents fragments of configurations obtained for model **M7** in $\rho^* = 0.2$ at $T^* = 1.3$ and $\rho^* = 0.4$ at $T^* = 1.6$ respectively. The right-hand side shows a schematic representation of obtained ordered networks. Alternating coloring is performed for visualization purposes only.

and substituted them in the X and Y positions, as it can be seen in Fig. 1 and we abbreviated this model as **M7**. The results for this chemical compound can be found in Fig. 6. Part a is shown in the density $\rho^* = 0.2$ and one can see that three different networks can be distinguished. Schematically drawn, magnified structures can be found below and on the right-hand side of panel a. Part b on the other hand shows the higher density, $\rho^* = 0.4$, where all of the networks vanished except the dense phase, shown in orange circle.

In Fig. 7 one can see the radial distribution functions calculated with respect to the oxygen atoms of the carboxyl group. In the density $\rho^* = 0.2$, we can observe mainly X – X and Y – Y correlations around $r \approx 2 \pm 0.05$ in the first coordination shell, which corresponds to the phase marked in the black circle of Fig. 6 a. Mixed X – Y association is nearly five times less probable and is due to the defects and rarely observed two remaining structures (orange and green circles of Fig. 6 a). This corroborates with the observation from the snapshots. In the density, $\rho^* = 0.4$ correlations extracted from the radial distribution functions confirm that only a dense phase has been formed. There are only associations of Y – Y and X – Y oxygen atoms around $r \approx 2 \pm 0.05$. If any of those two remaining phases would occur, the X – X correlations should also be observed. In part d of Fig. 7, due to the well-defined ordered structure of the dense phase, the two-dimensional structure factor has been shown.

Let us now proceed to another conformation, which we will refer to as “V-shape”. As mentioned before, due to the energy computation extracted from quantum calculations, we will not consider every model that was in the “zigzag” conformation. The results for model **M2** can be found in Fig. 8 a. One can see multiple of different pore types, where we can not distinguish any particular ordered network. On the right-hand side of this figure, we have schematically drawn one of the possible configurations. We did not show any distribution analysis owing to the difficulty in their interpretation.

In part b of Fig. 8, we can see the configuration obtained for the “V-shape” conformation of model **M3**. There are two different networks that can be distinguished, that is a dominant dense phase marked in the orange circle and a rarely observed isogonal tiling marked as a black square in this figure. Moreover, in the latter, we have examined the arrangement of the oxygen atoms, which form 3.4.6.4 Archimedean tessellation. This representation has been done as follows, we have separated the two nearest associated oxygen atoms and computed their center of mass. Afterward, those

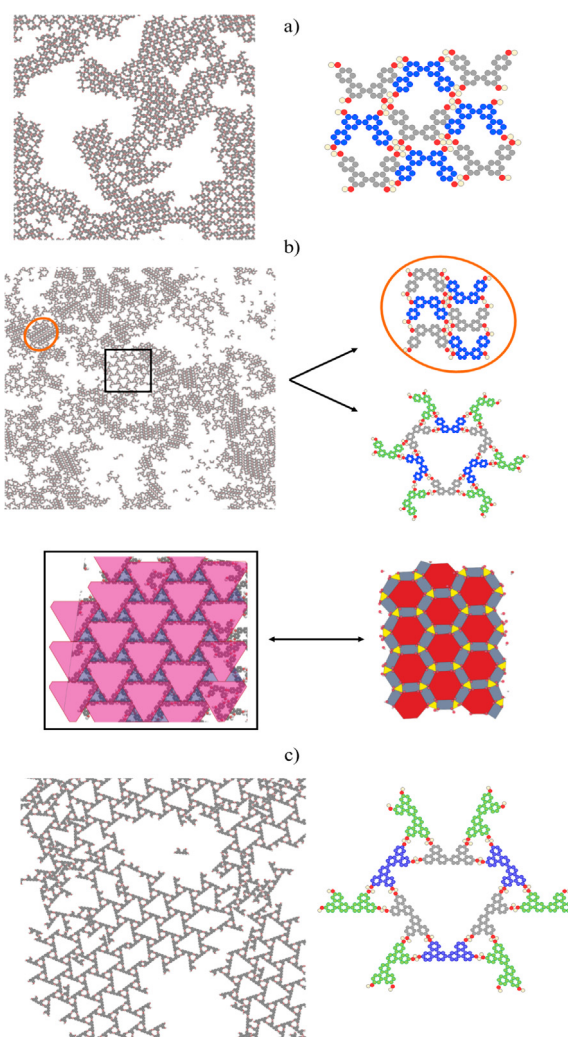


Fig. 8. Part a shows the configuration for system of **M2** “V-shape” conformation in $\rho^* = 0.3$, at $T^* = 0.8$. On the right-hand side of this panel we show one of the possible paths on how molecules connect. Part b in the clockwise order shows the configuration for system of **M3** “V-shape” conformation in $\rho^* = 0.25$, at $T^* = 0.8$, two types of schematically drawn structures in the system, oxygen atoms representation with different polygons colored, the magnified fragment of isogonal structure. Part c shows a configuration for elongated **M3** “V-shape” conformation (cf. text) in $\rho^* = 0.15$ at $T^* = 0.8$. On the right-hand side of panel c there is a schematic representation of an isogonal network. Alternating coloring is performed for visualization purposes only.

center mass has been connected which results in the formation of the aforementioned structure. It has to be emphasized that depending on the system size built of **M3** “V-shape” molecules we observe that its increase does not result in the vanishing of the latter structure. We have performed the cluster analysis for this system according to the previous procedure and we have obtained a distribution of CS = 2, 3, 4. While the CS = 4 is related to the dense phase, the other values are both connected with isogonal tiling and defects, boundaries, etc.

Owing to the formation of quite an unusual, isogonal structure we performed additional simulations for elongated molecules. This means that we have substituted the Y position with carboxyphenyl groups. The results can be found in Fig. 8 c. One can see that the formation of an isogonal network is preferred. On the right-hand side, we can see a schematic representation of this structure. It has to be emphasized that oxygen representation for these molecules shows the same results and Archimedean tessellation has been formed. We can conclude that the formation of this structure

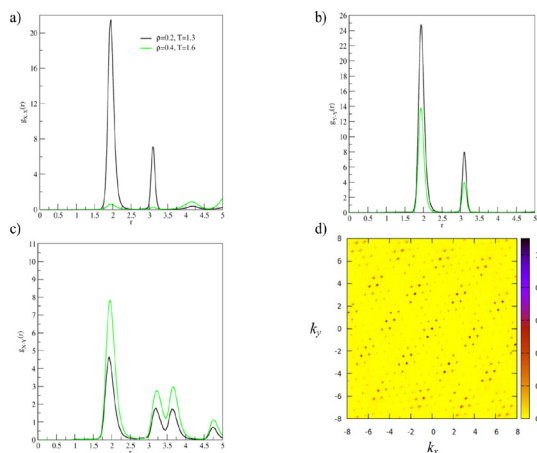


Fig. 7. Part a, b, c presents radial distribution functions calculated with respect to oxygen atoms for model **M7** in $\rho^* = 0.2$ at $T^* = 1.3$ and $\rho^* = 0.4$ at $T^* = 1.6$, respectively. Part d is a two-dimensional structure factor for model **M7** calculated in $\rho^* = 0.4$ at $T^* = 1.6$.

is connected with the elongation of the molecule in *Y* substitution position. In this case, since we obtained an isogonal network, the cluster analysis has shown that the probability of $CS = 2$ is around 0.85 ± 0.05 with the average cluster size $ACS = 2.12 \pm 0.02$, which confirms that this phase is dominant in this system. The latter value corroborates with the observation from snapshots, where one can see that there are some imperfections in the lattice.

The next models considered by us are **M5-M7** in “V-shape” conformations results for which can be found in Fig. 9 a-c, respectively. In panel a of this Figure we can find that majority of the system forms one well-defined ordered dense structure which is marked by a green circle on the right-hand side of this part. Moreover, we can distinguish another possible path on how molecules associate with one another, marked by a red circle. From the cluster analysis we find that the most probable cluster size is $CS = 5$ and $CS = 6$ with the average cluster size $ACS = 4.6$ which corroborates with snapshots. For the perfect dense structure, the cluster size should be equal to $CS = 6$. However, the simulations as shown in Fig. 9 a show a lot of imperfections and boundary effects are also well pronounced which causes a decrease of the cluster size probability and its average value.

Results for **M6** “V-shape” molecule, as shown in Fig. 9 b display a similar triangular pattern that has been found in the previous case. However, contrary to the **M5** “V-shape” conformation, this

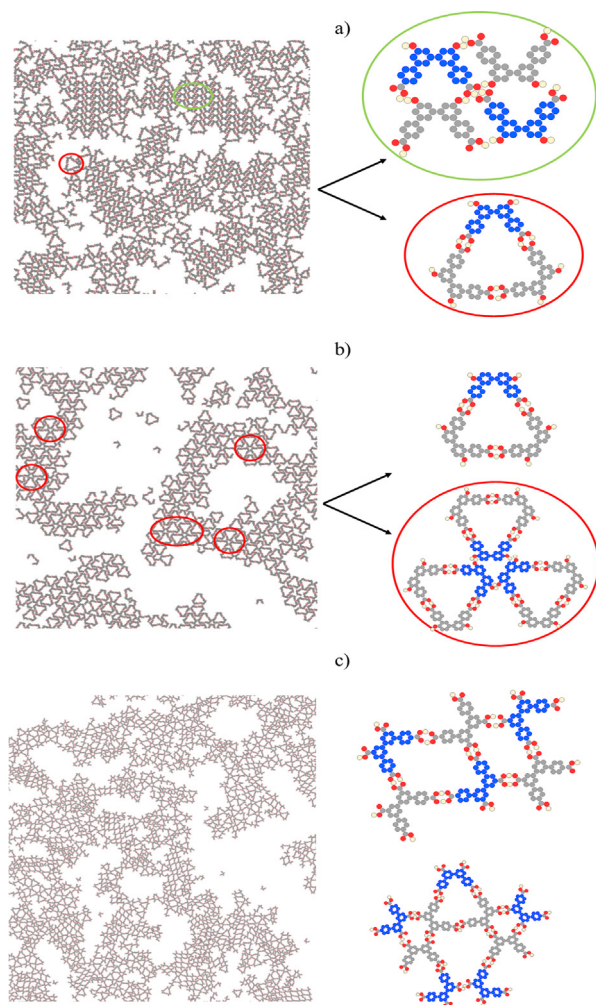


Fig. 9. Parts a, b, c show the configuration for system of **M5-M7** “V-shape” conformations, respectively in $\rho^* = 0.2$, at $T^* = 1.0$ (**M6,M7**) and in $\rho^* = 0.3$, at $T^* = 1.0$ (**M5**). On the right hand side of panels a-c we show two of possible paths on how molecules connect.

structure occupies the entire system. This can be proven by cluster analysis which shows that there is an equivalent probability of cluster size equal to $CS = 2$ and $CS = 4$. One can find it surprising that the average cluster size is around $ACS = 3.96$. While we present two possible paths on how molecules can associate on the right-hand side of panel b, the most probable value is $CS = 5$. This can be explained by the lateral association of differently rotated, consecutive triangles. While there is indeed an approach for the molecules to form a more regular network, it is hard to obtain due to the huge amount of possible connections. The triangles are associated in a quite random pattern which corresponds to the snapshots.

Ultimately, we present the results for **M7** molecule in “V-shape” conformation. The results can be found in Fig. 9 c. There is no obvious structure that can be distinguished and a variety of different pores are formed which means that the system is degenerated. There are several energetically equivalent paths, two of which we have schematically presented on the right-hand side of this panel. From the cluster analysis, we see that the most probable size is $CS = 4$ with an average around $ACS = 3.65$ which proves our observation.

4. Conclusions

In this paper, we have presented both quantum calculations and classical molecular dynamics simulations for real chemical compounds of tetra-substituted aromatic alcohols and carboxylic acids. We have found out from quantum calculations that for certain models only one of the conformation is favorable due to the high energy difference between “V-shape” and “zigzag” conformations.

For models with “zigzag” conformations substituted with hydroxyl groups both in *X* and *Y* positions (**M1-M3**) only in the case of the first chemical compound we observe one ordered phase. For the remaining ones, there are existing three well-defined networks. Contrary to the previous cases, the substitution of carboxylic groups in *X* positions leads to the formation of one supramolecular network for every model which differed one from another. However, if one substitutes both *X* and *Y* positions with -COOH groups, as in the **M2** model, the formation of three ordered networks in lower density is observed again whereas in the higher density one structure remains.

We postulate that not only position but the type of functional group can change the behavior of the system. Furthermore, the occurrence of carboxylic substitution increases the the temperature of the formation of ordered phases.

Concerning the “V-shape” conformation, we did not examine two models where the energy difference was of an order of hydrogen bond energy. For the remaining cases we have found that only few models, i.e. **M3, M5** are able to form ordered networks. The rest of compounds in this conformation are highly degenerated and they can not form single (or more) ordered networks due to the many possible paths on how molecules are able to connect.

The main aim of our manuscript was to consider various possible paths on how the molecules **M1-M7** can self-assemble in different conformations. We have shown that most of the cases exhibit polydomain structures. We are aware of the limitations presented herein and we suggest several protocols, which could allow us to solve this issue, that will be studied in the future in our laboratory. Those methods involve: (i) change of the system size which has been taken into account only for one particular case (**M3-V_shape**), (ii) consequent heating/cooling down of the considered system, (iii) parallel tempering method, and (iv) the usage of collective moves. The latter strategy, however, requires the usage of Monte Carlo simulations.

The majority of the structures formed by the **M1-M7** molecules form voids of different shapes and sizes. Due to this aspect, we believe that those structures might find an application for selective adsorption or chromatography of molecules of different sizes (such as coronene or other polycyclic aromatic hydrocarbons). This aspect also will be studied in our laboratory in the future.

CRedit authorship contribution statement

Łukasz Baran: Conceptualization, Methodology, Software. **Konrad Dyk:** Software, Visualization. **Daniel Michael Kamiński:** Software, Visualization. **Marek Stankevič:** Software, Visualization. **Wojciech Rzyśko:** Conceptualization, Methodology, Software. **Dariusz Tarasiewicz:** Software, Visualization. **Tomasz Zientarski:** Software, Visualization.

Declaration of Competing Interest

The authors declare that they have no known competing financial interests or personal relationships that could have appeared to influence the work reported in this paper.

Acknowledgments

This study has been supported by the Polish Ministry of Science and Higher Education, under Grant No. DI2017 001147 and the research has been supported by the Foundation for Polish Science (FNP).

References

- Y.-Q. Zhang, T. Lin, B. Cirera, R. Hellwig, C.-A. Palma, Z. Chen, M. Ruben, J.V. Barth, F. Klappenberger, One-dimensionally disordered chiral sorting by racemic tiling in a surface-confined supramolecular assembly of achiral tectons, *Angew. Chem. Int. Ed.* 56 (2017) 7797–7802.
- J. Ren, E. Larkin, C. Delaney, Y. Song, X. Jin, S. Amirjalayer, A. Bakker, S. Du, H. Gao, Y.-Y. Zhang, S.M. Draper, H. Fuchs, Chemistry of 4-[(4-bromophenyl)ethynyl]pyridine at metal surfaces studied by STM, *Chem. Commun.* 54 (2018) 9305–9308.
- F. Ishiwari, G. Nascimbeni, E. Sauter, H. Tago, Y. Shoji, S. Fujii, M. Kiguchi, T. Tada, M. Zharnikov, E. Zojer, T. Fukushima, Triptycene tripods for the formation of highly uniform and densely packed self-assembled monolayers with controlled molecular orientation, *J. Am. Chem. Soc.* 141 (2019) 5995–6005, PMID: 30869881.
- M. Sánchez-Molina, A. Díaz, E. Sauter, M. Zharnikov, J.M. López-Romero, Tripod-shaped molecules: Synthesis and immobilization on Au(111) substrates, *Appl. Surf. Sci.* 470 (2019) 259–268.
- V. Rohnacher, F.S. Benneckendorf, M. Münch, E. Sauter, A. Asyuda, M.-M. Barf, J.-N. Tisserant, S. Hillebrandt, F. Rominger, D. Jänsch, J. Freudenberg, W. Kowalsky, W. Jaegermann, U.H.F. Bunz, A. Pucci, M. Zharnikov, K. Müllen, Functionalized tetrapodal diazatriptycenes for electrostatic dipole engineering in n-type organic thin film transistors, *Adv. Mater. Technol.* n/a (2021) 2000300.
- S. Xing, Z. Zhang, X. Fei, W. Zhao, R. Zhang, T. Lin, D. Zhao, H. Ju, H. Xu, J. Fan, J. Zhu, Y.-Q. Ma, Z. Shi, Selective on-surface covalent coupling based on metal-organic coordination template, *Nature Commun.* 10 (2019) 70.
- M. Ammon, T. Sander, S. Maier, On-surface synthesis of porous carbon nanoribbons from polymer chains, *J. Am. Chem. Soc.* 139 (2017) 12976–12984, PMID: 28820266.
- R.-R. Liang, S.-Q. Xu, L. Zhang, R.-H. A. P. Chen, F.-Z. Cui, Q.-Y. Qi, J. Sun, X. Zhao, Rational design of crystalline two-dimensional frameworks with highly complicated topological structures, *Nature Commun.* 10 (2019) 4609.
- I. Cebula, E.F. Smith, M.D.C. Gimenez-Lopez, S. Yang, M. Schröder, N.R. Champness, P.H. Beton, Packing of isophthalate tetracarboxylic acids on Au(111): Rows and disordered herringbone structures, *J. Phys. Chem. C* 117 (2013) 18381–18385, PMID: 24163714.
- F. Silly, Concentration-dependent two-dimensional halogen-bonded self-assembly of 1,3,5-tris(4-iodophenyl)benzene molecules at the solid-liquid interface, *J. Phys. Chem. C* 121 (2017) 10413–10418.
- A. Ciesielski, P.J. Szabelski, W. Rzyśko, A. Cadeddu, T.R. Cook, P.J. Stang, P. Samorì, Concentration-dependent supramolecular engineering of hydrogen-bonded nanostructures at surfaces: Predicting self-assembly in 2d, *J. Am. Chem. Soc.* 135 (2013) 6942–6950, PMID: 23590179.
- S.A. DiBenedetto, A. Facchetti, M.A. Ratner, T.J. Marks, Molecular self-assembled monolayers and multilayers for organic and unconventional inorganic thin-film transistor applications, *Adv. Mater.* 21 (2009) 1407–1433.
- J.V. Barth, G. Costantini, K. Kern, Engineering atomic and molecular nanostructures at surfaces, *Nature* 437 (2005) 671–679.
- K. Tahara, C.A. Johnson, T. Fujita, M. Sonoda, F.C. De Schryver, S. De Feyter, M. M. Haley, Y. Tobe, Synthesis of dehydrobenzo[18]annulene derivatives and formation of self-assembled monolayers: Implications of core size on alkyl chain interdigitation, *Langmuir* 23 (2007) 10190–10197, PMID: 17760473.
- Z. Shi, N. Lin, Structural and chemical control in assembly of multicomponent metal-organic coordination networks on a surface, *J. Am. Chem. Soc.* 132 (2010) 10756–10761, PMID: 20681708.
- J.I. Urgel, D. Ēcija, G. Lyu, R. Zhang, C.-A. Palma, W. Auwärter, N. Lin, J.V. Barth, Quasicrystallinity expressed in two-dimensional coordination networks, *Nature Chem.* 8 (2016) 657–662.
- J. Shang, Y. Wang, M. Chen, J. Dai, X. Zhou, J. Kuttner, G. Hilt, X. Shao, J.M. Gottfried, K. Wu, Assembling molecular Sierpinski triangle fractals, *Nature Chem.* 7 (2015) 389–393.
- A. Ciesielski, A. Cadeddu, C.-A. Palma, A. Gorczyński, V. Patroniak, M. Cecchini, P. Samorì, Self-templating 2d supramolecular networks: a new avenue to reach control over a bilayer formation, *Nanoscale* 3 (2011) 4125–4129.
- J.F. Dienstmaier, K. Mahata, H. Walch, W.M. Heckl, M. Schmittel, M. Lackinger, On the scalability of supramolecular networks – high packing density vs optimized hydrogen bonds in tricarboxylic acid monolayers, *Langmuir* 26 (2010) 10708–10716, PMID: 20536167.
- P. Samorì, K. Müllen, J. Rabe, Molecular-scale tracking of the self-healing of polycrystalline monolayers at the solid-liquid interface, *Adv. Mater.* 16 (2004) 1761–1765.
- L. Cardenas, R. Gutzler, J. Lipton-Duffin, C. Fu, J.L. Brusso, L.E. Dinca, M. Vondráček, Y. Fagot-Revurat, D. Malterre, F. Rosei, D.F. Perepichka, Synthesis and electronic structure of a two dimensional π -conjugated polythiophene, *Chem. Sci.* 4 (2013) 3263–3268.
- R. Gutzler, L. Cardenas, J. Lipton-Duffin, M. El Garah, L.E. Dinca, C.E. Szakacs, C. Fu, M. Gallagher, M. Vondráček, M. Rybachuk, D.F. Perepichka, F. Rosei, Ullmann-type coupling of brominated tetrathienoanthracene on copper and silver, *Nanoscale* 6 (2014) 2660–2668.
- K.A. Simonov, N.A. Vinogradov, A.S. Vinogradov, A.V. Generalov, E.M. Zagrebina, G.I. Svirskiy, A.A. Cafolla, T. Carpy, J.P. Cunniffe, T. Taketsugu, A. Lyalin, N. Märtensson, A.B. Preobrajenski, From graphene nanoribbons on Cu(111) to nanographene on Cu(110): Critical role of substrate structure in the bottom-up fabrication strategy, *ACS Nano* 9 (2015) 8997–9011, PMID: 26301684.
- C.-A. Palma, P. Samorì, M. Cecchini, Atomistic simulations of 2d bicomponent self-assembly: From molecular recognition to self-healing, *J. Am. Chem. Soc.* 132 (2010) 17880–17885, PMID: 21114285.
- Y. Zhao, J. Wang, How to obtain high-quality and high-stability interfacial organic layer: Insights from the ptcda self-assembly, *J. Phys. Chem. C* 121 (2017) 4488–4495.
- Ł. Baran, W. Rzyśko, Application of a coarse-grained model for the design of complex supramolecular networks, *Mol. Syst. Des. Eng.* 5 (2020) 484–492.
- Ł. Baran, D. Nieckarz, P. Szabelski, W. Rzyśko, Controlling of the 2d self-assembly process by the variation of molecular geometry, *J. Phys. Chem. C* 123 (2019) 19549–19556.
- Ł. Baran, W. Rzyśko, S. Szajnar, Archimedean tessellation found by the variation of building blocks' and linkers' geometry: In silico investigations, *J. Phys. Chem. C* 124 (2020) 20101–20108.
- A.I. Fadeeva, V.A. Gorbunov, P.V. Stishenko, A.V. Myshlyavtsev, Model of ferreththalate ordering on Cu(100), *J. Phys. Chem. C* 123 (2019) 17265–17272.
- C. Karner, C. Dellago, E. Bianchi, Hierarchical self-assembly of patchy colloidal platelets, *Soft Matter* 16 (2020) 2774–2785.
- C. Karner, C. Dellago, E. Bianchi, Design of patchy rhombi: From close-packed tilings to open lattices, *Nano Lett.* 19 (2019) 7806–7815, PMID: 31580675.
- A. Ibenskas, M. Šimėnas, K.J. Kizlaitis, E.E. Tornau, Pinwheel structures of deprotonated trimelic acid on Ag(111): Model and simulations, *J. Phys. Chem. C* 124 (2020) 11212–11220.
- K. Dyk, Ł. Baran, W. Rzyśko, M. Stankevič, D.M. Kamiński, Interplay between the crystal stability and the energy of the molecular conformation, *CrystEngComm* (2021).
- W.L. Jorgensen, J. Tirado-Rives, The OPLS [optimized potentials for liquid simulations] potential functions for proteins, energy minimizations for crystals of cyclic peptides and crambin, *J. Am. Chem. Soc.* 110 (1988) 1657–1666, PMID: 27557051.
- T.A. Halgren, Merck molecular force field. I. basis, form, scope, parameterization, and performance of mmff94, *J. Comput. Chem.* 17 (1996) 490–519.
- S. Toxvaerd, J.C. Dyre, Communication: Shifted forces in molecular dynamics, *J. Chem. Phys.* 134 (2011) 081102.
- Steve Plimpton et al., Large-scale atomic/molecular massively parallel simulator, *lammmps.sandia.gov*, 1995. [Online; accessed 29-April-2019].
- S. Plimpton, Fast parallel algorithms for short-range molecular dynamics, *J. Comput. Phys.* 117 (1995) 1–19.
- H.J.C. Berendsen, J.P.M. Postma, W.F. van Gunsteren, A. DiNola, J.R. Haak, Molecular dynamics with coupling to an external bath, *J. Chem. Phys.* 81 (1984) 3684–3690.
- G.J. Martyna, M.L. Klein, M. Tuckerman, Nosé–Hoover chains: The canonical ensemble via continuous dynamics, *J. Chem. Phys.* 97 (1992) 2635–2643.
- M.J. Frisch, G.W. Trucks, H.B. Schlegel, G.E. Scuseria, M.A. Robb, J.R. Cheeseman, G. Scalmani, V. Barone, G.A. Petersson, H. Nakatsuji, X. Li, M. Caricato, A.V. Marenich, J. Bloino, B.G. Janesko, R. Gomperts, B. Mennucci, H.P. Hratchian, J.V.

PVIII

Ortiz, A.F. Izmaylov, J.L. Sonnenberg, D. Williams-Young, F. Ding, F. Lipparini, F. Egidi, J. Goings, B. Peng, A. Petrone, T. Henderson, D. Ranasinghe, V.G. Zakrzewski, J. Gao, N. Rega, G. Zheng, W. Liang, M. Hada, M. Ehara, K. Toyota, R. Fukuda, J. Hasegawa, M. Ishida, T. Nakajima, Y. Honda, O. Kitao, H. Nakai, T. Vreven, K. Throssell, J.A. Montgomery, Jr., J.E. Peralta, F. Ogliaro, M.J. Bearpark, J.J. Heyd, E.N. Brothers, K.N. Kudin, V.N. Staroverov, T.A. Keith, R. Kobayashi, J. Normand, K. Raghavachari, A.P. Rendell, J.C. Burant, S.S. Iyengar, J. Tomasi, M. Cossi, J.M. Millam, M. Klene, C. Adamo, R. Cammi, J.W. Ochterski, R.

L. Martin, K. Morokuma, O. Farkas, J.B. Foresman, D.J. Fox, Gaussian 16 Revision B.01, 2016. Gaussian Inc., Wallingford CT.

- [42] T. Steiner, *The hydrogen bond in the solid state*, *Angew. Chem. Int. Ed.* **41** (2002) 48–76.
- [43] N.D. Mermin, H. Wagner, *Absence of ferromagnetism or antiferromagnetism in one- or two-dimensional isotropic heisenberg models*, *Phys. Rev. Lett.* **17** (1966) 1133–1136.

PVIII

lic. Łukasz Baran
Katedra Chemii Teoretycznej
Instytut Nauk Chemicznych
Wydział Chemii UMCS
Pl. Marii Curie-Skłodowskiej 3
20-031 Lublin

Lublin, 16.05.2022

OŚWIADCZENIE

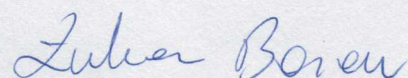
Oświadczam, że mój wkład w niniejszej pracy:

[PVIII] **Ł. Baran***, K. Dyk, D. M. Kamiński, M. Stankevič, W. Rżysko, D. Tarasewicz, T. Zientarski,
“Influence of the substitution position in the tetratopic building blocks on the self-assembly process”,
Journal of Molecular Liquids, 2022, **346**, 117074.

polegał na przeprowadzeniu części symulacji metodą dynamiki molekularnej, napisaniu manuskryptu i przeprowadzeniu analizy części wyników

Udział ten szacuję na 35 %.

lic. Łukasz Baran



PVIII

mgr Konrad Dyk
Katedra Chemii Ogólnej, Koordynacyjnej i Krystalografii
Instytut Nauk Chemicznych
Wydział Chemii UMCS
Pl. Marii Curie-Skłodowskiej 3
20-031 Lublin

Lublin, 15.05.2022

OŚWIADCZENIE

Oświadczam, że mój wkład w niniejszej pracy:

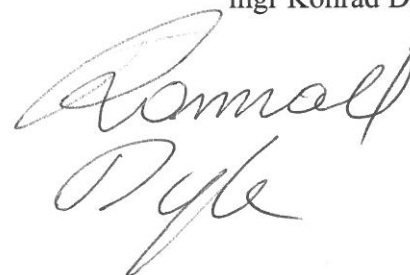
[PVIII] **Ł. Baran***, K. Dyk, D. M. Kamiński, M. Stankevič, W. Rżysko, D. Tarasewicz, T. Zientarski,
“Influence of the substitution position in the tetratopic building blocks on the self-assembly process”,
Journal of Molecular Liquids, 2022, **346**, 117074.

polegał na

- przeprowadzeniu obliczeń kwantowo-mechanicznych
 - analizowaniu otrzymanych wyników

Udział ten szacuję na 35%.

mgr Konrad Dyk



PVIII

dr hab. Daniel Kamiński, prof. UMCS
Katedra Chemii Ogólnej, Koordynacyjnej i Krystalografii
Instytut Nauk Chemicznych
Wydział Chemii UMCS
Pl. Marii Curie-Skłodowskiej 3
20-031 Lublin

Lublin, 13.05.2022

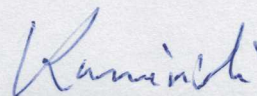
OŚWIADCZENIE

Oświadczam, że mój wkład w niniejszej pracy:

[PVIII] **Ł. Baran***, K. Dyk, D. M. Kamiński, M. Stankevič, W. Rżysko, D. Tarasewicz, T. Zientarski,
“Influence of the substitution position in the tetratopic building blocks on the self-assembly process”,
Journal of Molecular Liquids, 2022, **346**, 117074.

polegał na wykonaniu części obliczeń.

Udział ten szacuję na 5 %.



dr hab. Daniel Kamiński, prof. UMCS

PVIII

dr hab. Marek Stankevič, prof. UMCS
Katedra Chemii Organicznej
Instytut Nauk Chemicznych
Wydział Chemii UMCS
Pl. Marii Curie-Skłodowskiej 3
20-031 Lublin

Lublin, 16.05.2022

OŚWIADCZENIE

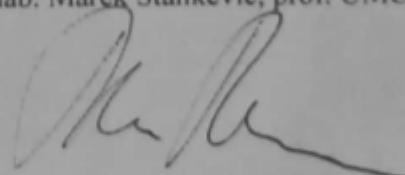
Oświadczam, że mój wkład w niniejszej pracy:

[PVIII] **L. Baran***, K. Dyk, D. M. Kamiński, M. Stankevič, W. Rżysko, D. Tarasewicz, T. Zientarski,
“Influence of the substitution position in the tetratopic building blocks on the self-assembly process”,
Journal of Molecular Liquids, 2022, **346**, 117074.

polegał na analizie części otrzymanych wyników

Udział ten szacuję na 10 %.

dr hab. Marek Stankevič, prof. UMCS



PVIII

dr hab. Wojciech Rzyśko, prof. UMCS
Katedra Chemii Teoretycznej
Instytut Nauk Chemicznych
Wydział Chemii UMCS
Pl. Marii Curie-Skłodowskiej 3
20-031 Lublin

Lublin, 16.05.2022

OŚWIADCZENIE


Oświadczam, że mój wkład w niniejszej pracy:

[PVIII] **Ł. Baran***, K. Dyk, D. M. Kamiński, M. Stankevič, W. Rzyśko, D. Tarasewicz, T. Zientarski,
“Influence of the substitution position in the tetratopic building blocks on the self-assembly process”,
Journal of Molecular Liquids, 2022, **346**, 117074.

polegał na koordynowaniu merytorycznym badań

Udział ten szacuję na 5 %.

dr hab. Wojciech Rzyśko, prof. UMCS



PVIII

mgr Dariusz Tarasewicz
Katedra Chemii Teoretycznej
Instytut Nauk Chemicznych
Wydział Chemii UMCS
Pl. Marii Curie-Skłodowskiej 3
20-031 Lublin

Lublin, 13.05.2022

OŚWIADCZENIE

Oświadczam, że mój wkład w niniejszej pracy:

[PVIII] **Ł. Baran***, K. Dyk, D. M. Kamiński, M. Stankevič, W. Rżysko, D. Tarasewicz, T. Zientarski,
“Influence of the substitution position in the tetrapic building blocks on the self-assembly process”,
Journal of Molecular Liquids, 2022, **346**, 117074.

polegał na wykonaniu części symulacji komputerowych

Udział ten szacuję na 5 %.

mgr Dariusz Tarasewicz

Dariusz Tarasewicz

PVIII

dr hab. Tomasz Zientarski, prof. Uczelni
Katedra Informatyki
Wydział Elektrotechniki i Informatyki Politechniki Lubelskiej
ul. Nadbystrzycka 36B
20-618 Lublin

Lublin, 15.05.2022

OŚWIADCZENIE

Oświadczam, że mój wkład w niniejszej pracy:

[PVIII] **Ł. Baran***, K. Dyk, D. M. Kamiński, M. Stankevič, W. Rżysko, D. Tarasewicz, T. Zientarski,
“Influence of the substitution position in the tetratopic building blocks on the self-assembly process”,
Journal of Molecular Liquids, 2022, **346**, 117074.

polegał na

wykonaniu części obliczeń numerycznych.

Udział ten szacuję na 5%.



dr hab. Tomasz Zientarski, prof. Uczelni